Centre for Hydrogeology
and Geothermics (CHYN)
University of Neuchâtel

Numerical simulations and uncertainty analysis for assessing spatial and temporal dynamics in alluvial river-aquifer systems:

An application in the context of the 3rd Rhône River Correction

Ph.D. thesis presented to the Faculty of Science of the University of Neuchâtel
to satisfy the requirements for the degree of Doctor of Philosophy in Science

Guillaume Gianni

Thesis defense date: 27.10.2017
Public defense date: 08.12.2017

Ph.D. Thesis evaluation committee:
Prof. Dr. Philip Brunner, University of Neuchâtel (Director of the thesis)
Prof. Dr. Pierre Perrochet, University of Neuchâtel (Co-director)
Prof. Dr. Mario Schirmer, University of Neuchâtel / Eawag
Prof. Dr. Philippe Renard, University of Neuchâtel
Prof. Dr. Jan Fleckenstein, University of Bayreuth

UNIVERSITÉ DE NEUCHÂTEL

Faculté des Sciences
Secrétariat-décanat de Faculté
Rue Emile-Argand 11
2000 Neuchâtel – Suisse
Tél : + 41 (0)32 718 21 00
E-mail : secretariat.sciences@unine.ch

IMPRIMATUR POUR THESE DE DOCTORAT

La Faculté des sciences de l'Université de Neuchâtel autorise l'impression de la présente thèse soutenue par

Monsieur Guillaume A. GIANNI

Titre:

"Numerical simulations and uncertainty analysis for assessing spatial and temporal dynamics in alluvial river-aquifer systems: an application in the context of the 3rd Rhône River Correction"

sur le rapport des membres du jury composé comme suit:

- Prof. Philip Brunner, directeur de thèse, UniNE
- Prof. Pierre Perrochet, UniNE
- Prof. ass. Philippe Renard, UniNE
- Prof. ass. Mario Schirmer, UniNE
- Prof. Jan Fleckenstein, Helmholtz, Centre for Environmental Research, Allemagne

Neuchâtel, le 22 décembre 2017

Le Doyen, Prof. R. Bshary

Summary

Characterizing river-groundwater interactions in alluvial aquifers is essential when forecasting the impact of river management strategies, such as river restorations, on the overall water resources distribution and dynamics. Therefore, the development of methods and calibration approaches that allow for better identification of the spatial and temporal characteristics of the hydraulic properties of the aquifer and the riverbed are required. Moreover, the analysis of commonly made assumptions, such as constant hydraulic properties of the streambed, isotropy of the aquifer hydraulic conductivity and steady-state calibration, is important in order to identify potential biases in predictions and related uncertainties.

Chapter 1 introduces the relevant concepts and methods as well as the framework, i.e. the 3rd Rhône River Correction, and the purpose of the Ph.D. thesis.

Chapter 2 presents a method that assesses the temporal variations of the hydraulic properties of the riverbed. The method is based on the inversion of a numerical convolution between an aquifer unit step response and stream stage variations. Calibrations against successive time series of observed water table variations allow to estimate the transience in the riverbed properties. A synthetic analysis demonstrated the robustness of the method and its application to field data pointed out the influence of climatic events on the transience in riverbed hydraulic properties.

Chapter 3 aims at understanding how simplifications in modeling practice regarding horizontal isotropy of the aquifer hydraulic conductivity affect the estimated uncertainty of predictions. It is demonstrated that assuming isotropy or fixed anisotropy may cause the predictive uncertainty of the water table elevation to be underestimated. Then, by taking into account the uncertainty in aquifer anisotropy, it is shown that calibration against transient data allows to achieve a better estimation of the aquifer and riverbed hydraulic parameters and to reduce the predictive uncertainty of water table elevations.

Chapter 4 presents the model forecasting and related uncertainty of the water table elevation in the area of Sion (Switzerland) in the framework of the modifications projected by the 3rd Rhône River Correction. Furthermore, the predictive uncertainty related to model calibration is complemented by scenario modeling taking into account the uncertainties in the future state of the Rhône riverbed hydraulic properties and geomorphologies. The results show that although the calibration process can significantly reduce the predictive uncertainty, the uncertainty in the future elevation of the water table, related to potential variations in the hydraulic properties of the Rhône riverbed, remains important.

Chapter 5 summarizes the results of the studies and provides recommendations and perspectives regarding hydrogeological modeling approaches in general and in the framework of 3rd Rhône River Correction.

Keywords

Surface water and groundwater interactions
Riverbed
Numerical modeling
Parameter estimation
Predictive uncertainty
3rd Rhône River Correction

Résumé

La caractérisation de l'interaction entre les rivières et les eaux souterraines pour des aquifères alluviaux est essentielle afin d'anticiper l'impact des stratégies de gestion de rivière, comme le sont les restaurations de rivières, sur l'ensemble de la ressource en eau et sur sa dynamique. De ce fait, le développement de méthodes et d'approches de calibration permettant une meilleure caractérisation et estimation des paramètres hydrauliques des aquifères et des lits de rivière est nécessaire. De plus, l'analyse d'hypothèses communes, telles que la constance des propriétés hydrauliques des lits de rivière, l'isotropie de la conductivité hydraulique de l'aquifère ou encore la calibration en régime permanent, est indispensable afin d'identifier des biais potentiels dans les prévisions et leurs incertitudes.

Le *chapitre 1* introduit les concepts pertinents, les méthodes, le cadre de recherche, c.-à-d. la 3e Correction du Rhône, ainsi que le but de la thèse doctorale.

Le *chapitre 2* présente une méthode qui permet d'évaluer le caractère transitoire des propriétés hydrauliques de lits de rivière. La méthode est basée sur l'inversion d'une convolution numérique entre les variations de niveau de la rivière et la réponse unitaire, en terme de variation de la surface piézométrique, de l'aquifère. L'estimation du caractère transitoire des propriétés hydrauliques du lit de la rivière est obtenue par des calibrations utilisant des séries temporelles successives de charges hydrauliques. Une analyse synthétique a démontré la fiabilité de la méthode et son application à des données réelles de terrain a permis d'indiquer l'influence d'événements climatiques sur le caractère transitoire des propriétés hydrauliques.

Le *chapitre 3* analyse les conséquences sur l'estimation de l'incertitude de la prévision de l'hypothèse communément faite sur l'isotropie de la conductivité hydraulique de l'aquifère. Il est démontré que les présupposés sur l'isotropie de l'aquifère peuvent causer une sous-estimation de l'incertitude des prévisions sur l'élévation de la surface piézométrique. De plus, il est démontré que la calibration transitoire, en comparaison à celle en régime permanent, permet une meilleure estimation des paramètres hydrauliques de l'aquifère et du lit de la rivière et ainsi de réduire l'incertitude de la prévision.

Le *chapitre 4* présente les prévisions sur l'élévation de la surface piézométrique et leurs incertitudes dans la région de Sion (Suisse) dans le cadre des modifications projetées par la 3e Correction du Rhône. Ce faisant, l'incertitude de la prévision liée à la calibration du modèle numérique hydrogéologique est complétée par la prise en compte, via la modélisation de scénarios, de l'incertitude sur les futures propriétés hydrauliques et géomorphologiques du lit du Rhône. Les résultats montrent que bien que le processus de calibration réduit de manière importante l'incertitude de la prévision, l'incertitude sur l'élévation future de la surface piézométrique, liée au potentielles variations des propriétés hydrauliques du lit du Rhône reste importante.

Le chapitre 5 résume les résultats des études présentées, fournis des recommandations quant aux approches de modélisations hydrogéologiques d'une manière générale et dans le cadre de la 3e Correction du Rhône.

Mots clés

Interactions entre les eaux de surface et les eaux souterraines
Lit de rivière
Modélisation numérique
Estimation de paramètres
Incertitude de la prévision
3e Correction du Rhône

Preface

Since the beginning, I have been interested and motivated in doing this Ph.D. thesis because of its stimulating framework embracing fundamental and applied research. The present document synthesizes the outcomes of the research I have carried out with the objective of solving a specific river-groundwater management issue, raised by the 3rd Rhône River Correction project, as well as developing generally applicable methods.

In doing so, the present document describes a new method of identification of the transience in streambed hydraulic properties that has been recently published in the journal Water Resources Research. In the same token, modeling and forecasting of the future water table of the Rhône alluvial aquifer in the area of Sion was the center of gravity for further investigations. In particular, analysis of the process of model calibration and predictive uncertainty for anisotropic alluvial aquifer using head observations has been carried out and the results are presented in the following chapters. Finally, the development and the calibration of a three-dimensional transient model of the study site has been performed. The quantification of the predictive uncertainty through linear and scenario modeling analysis have been carried out and the results have been discussed in order to anticipate future site developments.

More generally, I am delighted to mention that this exciting experience of pursuing fundamental and applied research was possible and, day after day, enriched through everybody's experiences and contributions. At the Center for Hydrogeology and Geothermics of Neuchâtel, I was able to be involved in many interdisciplinary side projects and tasks: from providing training for bachelor and master students in geology, hydrogeology and groundwater modeling to managing projects concerning wetlands of national importance in Switzerland in collaboration with several consulting firms and cantons. This ideal framework enhanced my experience and opened my mind to all different aspects of environmental issues, knowledge sharing, and project management.

In short, through the investigations pursued during my Ph.D. thesis and through the reading of hundreds of papers and books I have improved my scientific knowledge in groundwater modeling and river-groundwater interaction, and above all, I hope I have used it and brought my contribution to the specific projects I have been involved in and to the worldwide research community.

Acknowledgements

First, I would like to express my sincere gratitude to my supervisor Prof. Dr. Philip Brunner for the continuous and infallible support of my studies and research. His guidance expressed through his vast knowledge, motivation, and patience, helped me all along these years. I hope other motivated students will have the privilege to pursue their research under his supervision and mentorship.
I am grateful to the other persons responsible for my project: Prof. Dr. Pierre Perrochet who has always been present to respond to my questions and Alexandre Vogel who has provided us with his appreciations.
I am thankful to the other jury members of my Ph.D. thesis, namely Prof. Dr. Mario Schirmer, Prof. Dr. Jan Fleckenstein and Prof. Dr. Philippe Renard for their interesting comments and questions.
My sincere thanks go to Dr. John Doherty who provided me with an in-depth understanding of state-of-the-art groundwater modeling calibration and parameter/prediction uncertainty analysis.
Concerning the publication of the method for the identification of the transience in streambed hydraulic properties, I would like to thank Dr. Ben O'Connor and the two anonymous reviewers for their helpful comments and suggestions. The data used in this paper were also generously provided by the 3rd Rhône River Correction project.
I thank my fellow officemates, the master students that I supervised, the helpful technicians and the many people from the Centre for Hydrogeology and Geothermics of Neuchâtel for their supports, the interesting discussions that we had and will continue to have in the future and for the moments of relaxation we shared together.

Table of Contents

Chapter 1

1. Introduction

Providing good quality water in sufficient quantity and protecting populations and infrastructures from flood events are essential. In addition, holding back or reducing the eco-environmental pressure is also important for sustainable society growth and prosperity. In Switzerland (Canton of Valais, **Figure 1.1**), the Rhône Valley groundwater is extracted mainly from a shallow alluvial aquifer and exploited for drinking water supplies, irrigation of agricultural crops and many industrial applications. Meanwhile, the Rhône River, upstream Lake Geneva, flowing through the valley has been, over the years, channelized and elevated levees constrain its dynamics, intending to protect people and infrastructures in the valley from flooding. However, this regulation of the Rhône River emerged as not being sustainable, both in terms of flood protection and in terms of preservation of ecosystems [*Canton du Valais*, 2014; 2016]. Therefore, modifications of the Rhône River cross-section have been planned and a global analysis of the consequences of the project, namely the 3rd Rhône River Correction, on the groundwater and surface-water interactions, has been pursued.

River-groundwater systems are transient and controlled by both aquifer geology and river hydrogeomorphology. Improving the understanding of the interactions between surface water and groundwater is crucial for a sustainable management of the water and ecological resources, as well as implementing and controlling river regulations and restorations [*Fisher et al.*, 1998; *Hynes*, 1983; *Krause et al.*, 2014; *Ward*, 1999]. The complexity of these environmental systems is explicitly recognized by contemporary researchers, which underline the heterogeneous, transient and scale-dependent nature of these systems [*Partington et al.*, 2017; Ward et al., 2001; *Wiens*, 1999; *Winter et al.*, 1998]. Over the years, consciousness has been gained that integrated management of surface and ground waters is essential for the sustainable exploitation of our environment [*Boulton and Hancock*, 2006; *Brunner and Simmons*, 2012; *Sophocleous*, 2002; *Winter et al.*, 1998]. Consequently, projects altering one of these systems components, whether surface water or groundwater, should encompass investigations of the consequences on the water resources as a whole.

1.1. River regulation

Over the last 250 years, and in much of the world (e.g. the Mississippi, the Missouri in the United States; the Rhine, the Danube, the Vistula in Europe), large rivers corridors have been subjected to important human-induced changes. Most of these man-made changes have been related to economic developments, such as land reclamation, navigation, fish production, or hydro-engineering [*Antipa*, 1932; *Benke*, 1990; *Bridge and Demicco*, 2008; *Brookes*, 1985; *Charlton*, 2008b; *Duckson*, 1990; *Petts*, 1989; *Ward et al.*, 2001]. However, the ecosystems and water quality have often been negatively impacted by human development by-products. River channels, characterized by dynamic interaction with their alluvial plain, have been regulated by straightening of their courses and artificial constraints (dykes, levees, dams, revetments etc.) [*Babinski*, 1992; *Dynesius and Nilsson*, 1994; *Hallberg et al.*, 1979; *Nilsson et al.*, 2005; *Wu*, 2007] in order to protect riparian human development from flood events [*Dister et al.*, 1990; *Toth et al.*, 1993]. In Switzerland, 22 % of the watercourses (14'000 Km of the 65'000 Km) has undergone important modifications (Straightening, correction, channelization, dredging, snagging, etc.) in order to protect infrastructures, peoples, and agriculture from flood events and/or facilitate transportation and enable power production. **Figure 1.2** shows the modification undergone by the Rhine River over the last century. As a consequence, the biodiversity associated with the natural fluvial dynamics, geomorphology and river-groundwater interaction (lotic, lentic and riparian) has been drastically reduced.

Figure 1.1: Canton of Valais (Switzerland) and its inhabitable areas. The blue line represents the Rhône River, the red dots represent the major cities of the canton of Valais and the green dashed lines rectangle locates the study area of Sion (Swiss Atlas, Geography Institute of Lausanne University).

The upper Rhône River (Canton of Valais) has not been an exception. The first (1863 – 1928) and second (1930 – 1960) Rhône River Corrections (regulations) were achieved for flood control and land reclamation. Along its course, the Rhône River has been channelized by dams. Over these periods, observation and analysis of the sedimentation and drainage capacity of the Rhône River showed that the delivery ratio to the Lake Geneva is about 10% of the total amount of sediments generated by the Rhône Valley. This value is close to the average value of 5% for sediment delivery ratio in large drainage basins [*Walling and Webb*, 1983]. Consequently, the constant increase of the elevation of the Rhône riverbed and the ageing and weakened by time embankments render less effective the protection of the valley from flooding. The recent storm event of October 2000 (100-year flood event), which resulted in the partial flooding of the valley due to a levee failure, confirmed the necessity, already ratified in the previous month by the Great Conseil of the Canton of Valais, of implementing modern floodplain protection.
From an environmental point of view, the Rhône River is considered as denatured and part of its ecosystemic services have been severely affected. Therefore, following the recommendations of the Swiss Confederation [*Conseil fédéral suisse*, 1991, 2017] on watercourses alterations, the modifications defined in the 3rd Rhône River Correction project are intended to increase the Rhône River ecological condition by integrating river restoration measures.

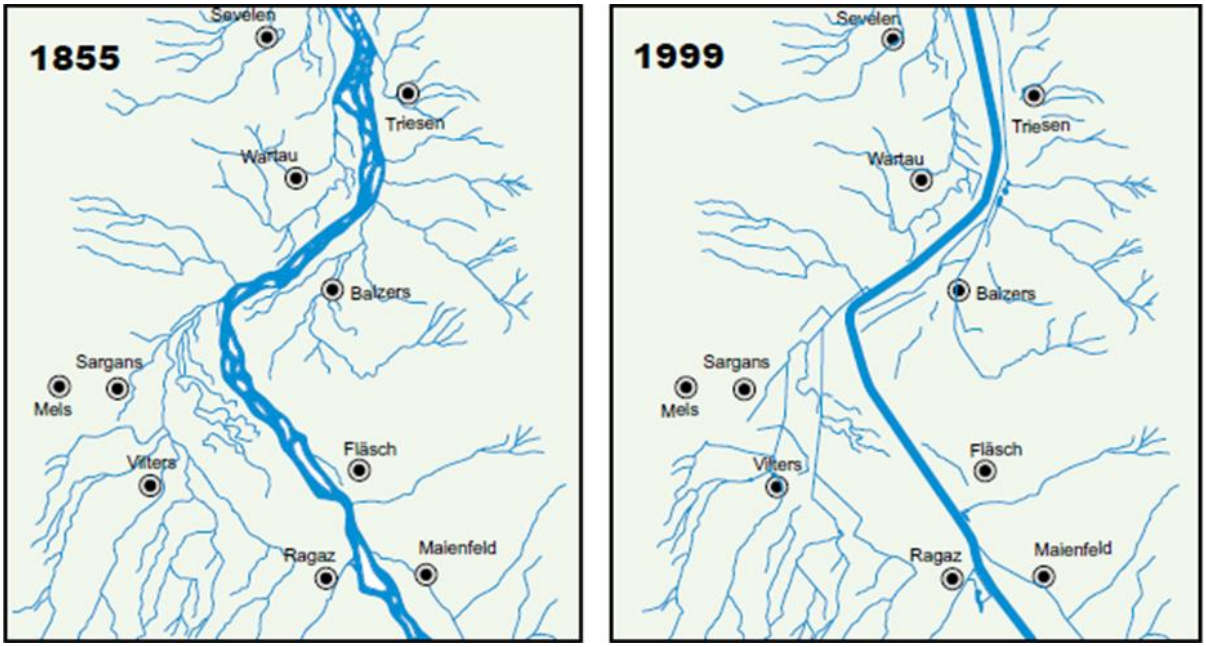

Figure 1.2: Changes of the Alpin Rhine geomorphology between 1855 (Dufour Map) and 1999, between Lanquart and Buchs [*Internationalen Regierungskommission Alpenrhein*, 2000].

1.2. River restoration

The term "river restoration" suggests an attempt to return the river to its original condition, i.e. prior any alteration, regarding its physical, chemical and biological properties. However, *Stanford et al.* [1996] pointed out the limitations of this objective due, in general, to the little knowledge of these original conditions. In a more pragmatic sense, river restoration can be defined as a human intervention that creates a river corridor that is self-regulating and integrated within its landscape [*Charlton*, 2008a; Ward et al., 2001].

Firsts documented stream restoration projects were realized in the 1970s on small rivers and were focused on the rehabilitation of selected river sections and design of stream habitat for natural biota [*Gore*, 1985; *Gore and Petts*, 1989; *Newbury and Gaboury*, 1993]. Small stream restorations included deflectors, weirs, boulders, logs, and other woody debris [*Gore and Shields*, 1995; *Shields and Smith*, 1992]. These structures protect fish from high current velocities and predation. At the end of the 1980s, restoration projects of large rivers in populated areas and high channel erosion potential were initiated [*De Waal et al.*, 1995; *Gore and Petts*, 1989; *Kern*, 1992]. Artificial construction of gravel bars habitats was attempted, in order to enhance the poor hydro-geomorphology of regulated rivers. Some results with respect to increasing biodiversity could be observed. However, the sustainability of these constructions was impacted by erosion or sand aggradation during high flows [*Miller et al.*, 1983].

At the beginning of the 1990s, the first water reclamation process results, in high population density area, demonstrated that the negative impact of human development can be minimized [*Douglas and McCreanor*, 1990; *Lelek and Köhler*, 1990; *Romano et al.*, 1992]. *Kern* [1992] proposed to restore floodplain hydrology by excavating breaches in levees at predefined river reaches during floods. Building new levees more distant from the river than the current levees can permit the flooding of defined areas, partly restoring ecological values of the floodplain [*Bayley*, 1991; *Galat et al.*, 1998; *Welcomme*, 1989]. In 1992, the restoration project of the 69 km of the Kissimmee River (Florida, United States) was authorized by the Congress and sponsored by the U.S. Army Corps of Engineers [*Chen et al.*, 2016]. Meanwhile, in Europe, many restoration projects were planned. Amongst them, the Danube in Germany, Austria and Romania [*Buijse et al.*, 2002; *Kern*, 1992; *Schiemer et al.*, 1999]; the Rhône in France [*Nougier et al.*, 2015]; the Rhine in Switzerland, Germany, France, Luxembourg and Netherland

[*Simons et al.*, 2001; *Verweij*, 2017]; the Mersey in England [*Bannister et al.*, 2005] or the Skjern in Denmark [*Kristensena et al.*, 2014] can be cited. The project of the 3rd Rhône River Correction in the canton of Valais (Switzerland) was decided in 2000 [*Canton du Valais*, 2014; 2016].
Currently, feedbacks of their implementations, as well as their current or projected results in terms of biodiversity and hyporheic zone dynamics, are being investigated [*Buijse et al.*, 2002; *Januschke and Verdonschot*, 2016; *Kristensena et al.*, 2014; *Meuli and Edmaier*, 2017; *Wondzell et al.*, 2009]. In general, it could be affirmed that the success of river restoration projects resides in a landscape approach at the catchment scale that re-establishes functional processes of natural river-aquifer systems [*Schiemer et al.*, 1999; *Ward et al*., 2001]. In many cases, this approach is technically implemented by widening the imposed cross-section of the river or by restoring flows inside arms [*Schiemer et al.*, 1999]. Accordingly, the *International Commission for the Protection of the Rhine* [2001] published the flood defense action, which combines flood protection with ecological improvements. Finally, with growing acceptance of the importance of interaction between the surface water and the groundwater [*European Commission*, 2000; *Sophocleous*, 2002; *Winter et al.*, 1998], river restoration entered in a new integrated and multidisciplinary water management framework [*European Commission*, 2008; *International Commission for the Protection of the Rhine*, 2001; *OFEFP et al.*, 2003].

1.3. 3rd Rhône River Correction

The term "Correction" is employed in the framework of the Rhône River management (Valais, Switzerland) for government supported actions of both river regulation, which modified the Rhône River and its alluvial plain over the last 150 years (1st and 2nd Rhône River Corrections [*Pasche*, 2002; *Torrenté and Kalbermatten*, 1964]) and for the combined flood protection-restoration project that started in 2000, namely the 3rd Rhône River Correction. This 3rd major modification of the Rhône River consists of classical river regulation measures, such as levees reinforcements, and restoration oriented measures, such as river cross-sections widening. Risk related to flood events of the Rhône River in the valley (Overflow or dam burst), as well as the space necessary for the river management and the achievement of the 3rd Rhône River Correction's objectives have been defined in the Sector Plan approved by the State Council of Valais in June 2006 [*Canton du Valais*, 2006]. The river correction is performed at the catchment scale, from the Rhône headwaters to the Lake Geneva, in order to consider every processes and thus to maintain flood protection and achieve ecological improvement [*Alexander and Allan*, 2007; *Roni et al.*, 2002; *Speed et al.*, 2016; *Ward et al.*, 2001].
The 3rd Rhone River Correction project presents 3 types of measures:

- **Lowering** of the riverbed in infrastructures constrained areas such as city crossing, for example along the crossing of the city of Sion.
- **Targeted enlargements** of the river cross-section of two to three times the current width. These important enlargements are essential for the security of the valley during major flood events. Moreover, they will foster the development of specific biotopes and socio-economic activities.
- **Safe enlargements** of the river cross-section of 1.5 to 1.6 times the current width along the major part of its course. This enlargement corresponds to the regime width, within which the frequent floods occurring every 2 to 5 years, on average, do not allow the growth of hardwood vegetation.

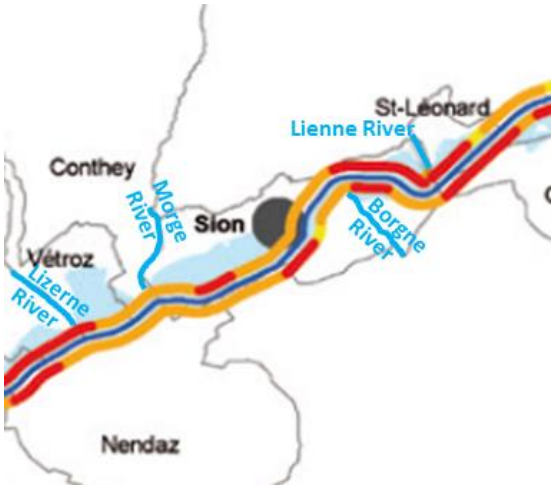

Figure 1.3: The discharge capacity of the Rhône River in the study zone [*Canton du Valais*, 2016], located in **Figure 1.1**. *Blue lines* represent the major rivers. *Light Blue areas* represent inundation zones. The red, orange and yellow lines along both sides of the Rhône River showed its hydraulic capacity: *Red*: inferior to Q_{100min}; *Orange*: between Q_{100min} and $Q_{100cible}$; *Yellow*: superior to $Q_{100cible}$.

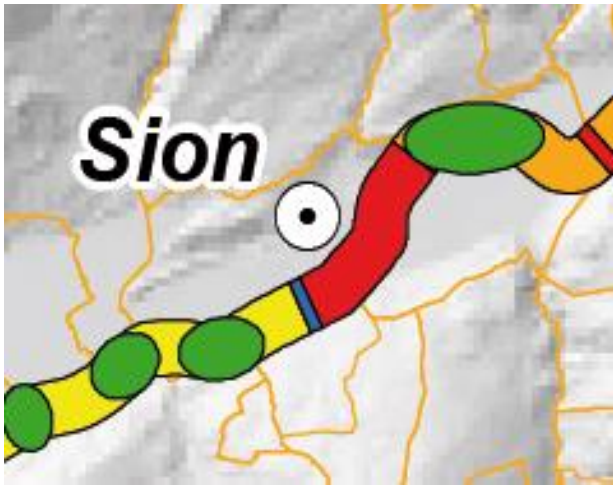

Figure 1.4: 3rd Rhône River Correction measures [*Canton du Valais*, 2016]. The colored areas superimposed on the Rhône River are *Blue*: No modification; *Red*: Lowering of the riverbed; *Yellow*: Enlargement of the river cross-section; *Orange*: Lowering and Enlargement; *Green*: Targeted Enlargement. The *Orange lines* represent the limits of the communes and the *Background map* is a hillshade of the Swiss Alti3D Digital Elevation Model.

From a security point of view, enlargements are considered an optimal solution because of their robustness and their ability to discharge floodwaters with smaller water stage increases. Lower water stages also reduce the risk of flooding the tributaries and canals in the plain. From an environmental and water quality point of view, enlargements allow the formation of gravel bars which may promote hyporheic circulations and create new habitats [*Louisoder*, 2012].

The study area represents the priority measure of Sion-Vétroz and extends from the Lienne River (upstream) to the Lizerne River (downstream). The city of Sion, capital of the canton of Valais, constitutes a major stake in the study zone. In the present state, the Rhône River has a discharge capacity below the estimations for 100-years flood discharges minimum value Q_{100min} and higher target value $Q_{100cible}$, which is between 1120 and 1200 m^3/s in the study zone [*GEI-MPS*, 2011] (**Figure 1.3**).

In the study area, the management plan [*Canton du Valais*, 2016] of the 3rd Rhône River Correction presents the 3 types of solutions aforementioned (**Figure 1.4**).

- **Lowering** of the riverbed will mainly occur along the crossing of the city of Sion, for which no cross-section widening is possible due to the urbanized area.
- **Targeted enlargements** are mainly located upstream of the mouths of the Borgne River and the Morge River. The important widening upstream of the mouth of the Borgne River will allow the Rhône River to deposit some of its sediments (which will be extracted) and thus to ensure the durability of the deepening along the crossing of Sion.
- **Safe enlargements** in the rest of the area (between 80 and 90 m) provide protection against flooding and an enhancement of the ecological state of the reaches supported by expected formation of alternate bars and diversified habitats.

Concerning the general evolution of the surrounding water table following the modifications of the Rhône riverbed, *Rovina + Partner AG* [2009] has estimated that lowering the Rhône River stage will lead to a lowering of the surrounding water table. Lowering of the water table may lead to settlement in fine-grained soils, which could damage the existing structures.

Table 1.1: Overview of possible negative consequences following variations of the water table.

Increase of water table	Decrease of water table
- Water infiltration in underground infrastructures and facilities. - Ground surfaces flooding. - Asphyxia of plants roots. - Deterioration of the water quality due to the leaching of contaminated sites.	- Land subsidence/settlement. - Decreased efficiency or drying up of wells. - Reduction of water in streams, irrigation channels, and lakes. - Decreased humidity of the shallow subsurface (impact on wetlands and crops).

The decrease in pore-water pressure results in equivalent increases in effective stress which may lead to the compression and settlement of soils, wall cracks and ground fissures [*Budhu*, 2011; *Conway*, 2016; *Galloway and Burbey*, 2011; *GéoVal Ingénieurs-Géologues SA*, 2010; *Li et al.*, 2014]. In the alluvial dejection cones areas, such as the dejection cone of the Borgne River (**Figure 1.3**), the predominance of coarser materials makes the ground less sensitive to changes in the water table. Conversely, the Vissigen area (neighborhood of the city of Sion) is constituted of fine-grained soils that may present a risk. However, *GéoVal Ingénieurs-Géologues SA* [2010] has estimated that a lowering of the water table would not have a detrimental effect on the building. Nevertheless, if not anticipated, both decrease and increase of the water table elevation can cause substantial damage to underground and surface structures, crops, water facilities and communication channels (**Table 1.1**).
Water table lowering is of particular concern, as recovering groundwater and treating land subsidence through artificial recharge can be a difficult task. Furthermore, modifications of the groundwater flow and water table elevation in the presence of contaminated sites can affect the quality of water through leaching of chemical components into the groundwater. In order to anticipate the aforementioned situations, the forecast of the future water table elevation based on sound analysis and modeling of the interaction between the river and its alluvial aquifer is necessary.

1.4. State of the art of river and alluvial aquifer interaction conceptualization

Over the last 30 years, interest in the interaction between surface water and groundwater as well as the recognition of its importance in sustainable water resources management have continuously gained in significance [*Fleckenstein et al.*, 2010; *Sophocleous*, 2002; *Winter et al.*, 1998; *Woessner*, 2000]. Legal guidelines, such as the EU Water Framework Directive – integrated river basin management for Europe, followed this unifying approach [*European Parliament*, 2000]. Similarly, in Switzerland, the federal law on water protection [*Conseil fédéral suisse*, 1991, 2017] stipulates that "the interactions between surface water and groundwater shall be maintained as much as possible" (Art. 37 2-b).
Kalbus et al. [2006] published a comprehensive review of the different methods used to estimate surface water-groundwater interactions. More recently, *Fleckenstein et al.* [2010] put forward the advances and novelties in measurement methods. Seepage meters and natural tracers (e.g. heat) are used extensively for estimation of water fluxes at the interface between a surface water body and the underlying aquifer [*Cook et al.*, 2008; *Landon et al.*, 2001; *Rosenberry et al.*, 2008; *Rosenberry et al.*, 2013].

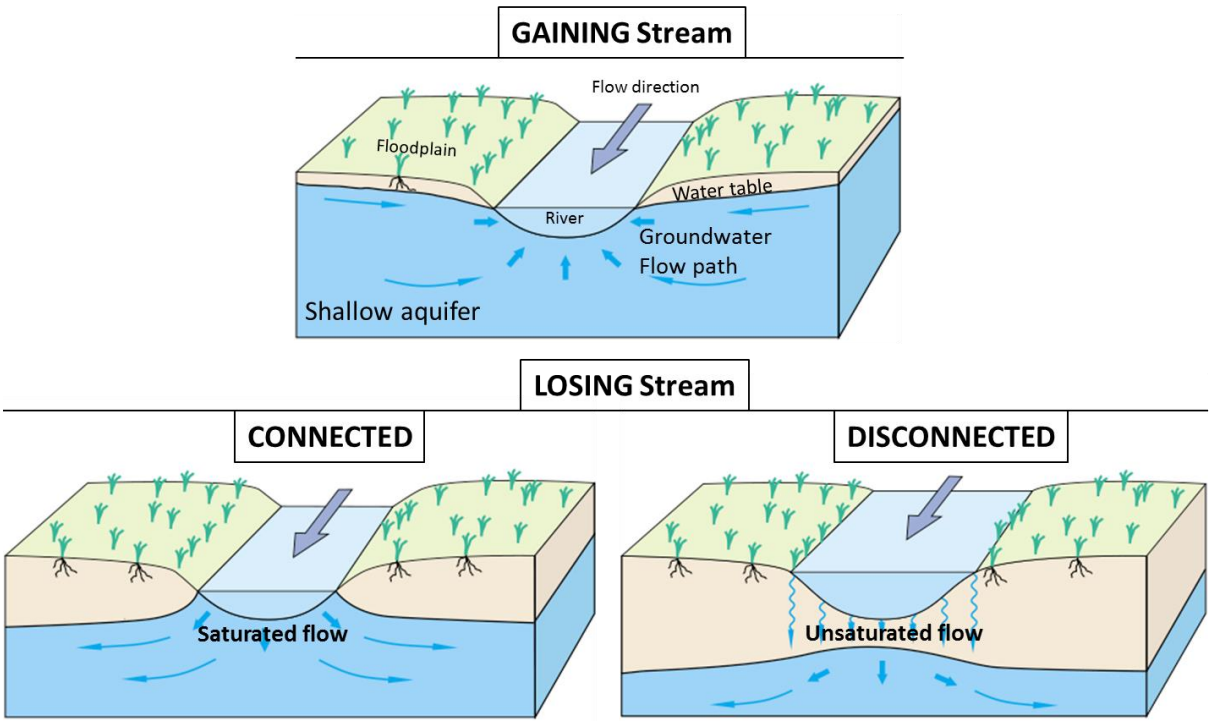

Figure 1.5: A schematized cross-section of gaining and losing river aquifer system. In a gaining stream, the groundwater infiltrates the stream and conversely for a losing stream (Figures from *Winter et al*., [1998]).

The recent development of distributed temperature sensing has allowed acquisition of data at increased spatial and temporal resolutions [*Mwakanyamale et al.*, 2012; *Slater et al.*, 2010; *Westhoff et al.*, 2010]. Physical (laboratory flume systems) and numerical (Coupled surface water-groundwater process based codes) modeling have allowed analyzing the influence of surface water bodies hydro-geomorphology [*Cardenas*, 2010; *Fox et al.*, 2014; *Fox et al.*, 2016; *Trauth et al.*, 2015]. In the next paragraphs, the components (aquifer, river, and riverbed) and interactions (hyporheic zone) of the surface water and groundwater bodies are succinctly described in the context of river-alluvial aquifer systems.

Alluvial aquifers are natural water-bearing aggregations of sediments composed of gravel, sand, silt, and clay. Sedimentological processes, influenced by river dynamics, structure alluvial aquifers by laying material in their channel and on their floodplain [*Partington et al.*, 2017]. The river flowing across the aquifer can exfiltrate (gaining stream) or infiltrate (losing stream, connected or disconnected) the groundwater (**Figure 1.5**). Due to the influence of river hydrodynamic on sediment deposits, alluvial aquifers can present significant degrees of anisotropy both horizontally and vertically. Also, alluvial aquifers constitute major water resources due to their favorable hydraulic properties, shallowness and recharge that endowed them with the ability to yield large amounts of groundwater. When hydraulically connected with surface water (rivers, lakes), quantitative or qualitative variations of water resources or hydraulics properties of one of the system components, surface water or groundwater system, may affect the whole water resources [*Winter et al.*, 1998].

River flow results from inland precipitation drainage through overland flow (over the land surface), interflow (Vadose zone component of river flow) and baseflow (Groundwater component of river flow). These components are dependent on the size, geometry and nature of the drained areas and on the weather conditions. Consequently, an increase of the river stage can be caused by rain in the river watershed or by ice/snow melt due to warmer temperatures.

Groundwater flow is recharged by water from precipitations that infiltrate the subsurface and percolate through the vadose zone (soil moisture) until the water table (pressure head equal to the atmospheric pressure).

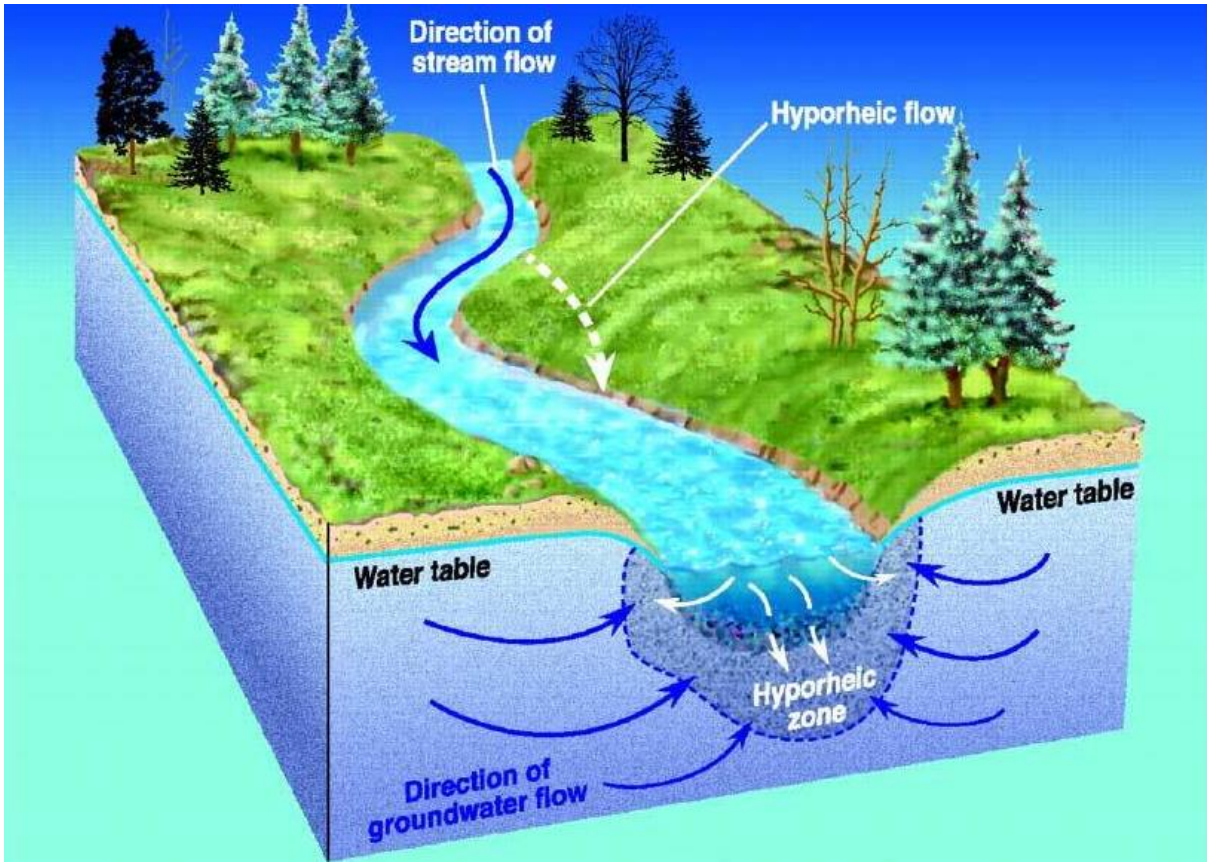

Figure 1.6: Schematized hyporheic zone and exchange fluxes [*Alley et al.*, 2002].

For losing streams, water from the river infiltrates the aquifer through the riverbed. This infiltration can occur under saturated or unsaturated conditions [*Brunner et al.*, 2009, 2011] (**Figure 1.5**) and is influenced by the heterogeneity of the streambed hydraulic properties [*Irvine et al.*, 2012, 2015; *Schilling et al.*, 2017]. Variations of the river stage can saturate or desaturate the part of the aquifer adjacent to the riverbank by infiltration of water from the stream into the unsaturated part of the riverbanks (riverbank storage). The decrease of the river stage causes the stored water to return to the river flow. Rapid increases in the river stage are usually caused by storm precipitations; rapid snow melts; or, as it is the case in the study area, releases of water from upstream reservoirs used to generate electricity, also called hydropeaking. Resulting from the interaction between groundwater and surface water, a particular zone adjacent to the river is referred to as the hyporheic zone (**Figure 1.6**) [*Ward*, 2016].

The definition of the hyporheic zone varies from hydraulic, biologic or chemical perspectives. However, based on the local origin of the water, it can be defined as the zone of mixing between river water and groundwater. This zone is commonly maintained by the flow of river water through a relatively short portion of its adjacent banks and bed [*Winter et al.*, 1998]. The hyporheic zone is generally characterized by an enhanced biogeochemical activity [*Boano et al.*, 2010; *Boano et al.*, 2014; *Briggs et al.*, 2014]. The geometry and the dynamics of the hyporheic zone are affected by both the hydraulic regime of the river and the hydro-geomorphological properties of the riverbed.

The riverbed controls the interaction between river water and groundwater [*Constantz*, 2016; *Partington et al.*, 2017; *Sujay et al.*, 2017] (**Figure 1.7**). The riverbed can be defined by its hydraulic properties and its geomorphology. Both will influence the interaction between the river and the groundwater [*Kasahara and Wondzell*, 2003; *Sujay et al.*, 2017; *Ward et al.*, 2012].

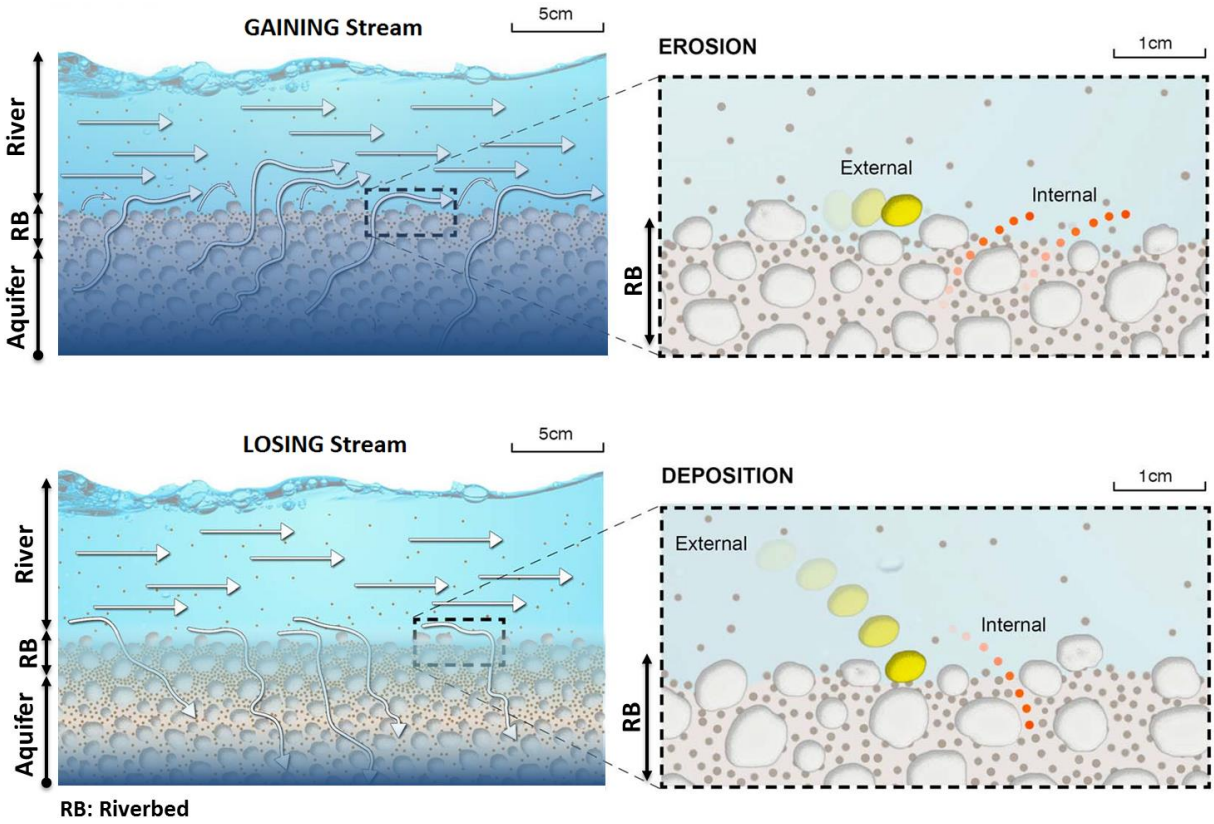

Figure 1.7: Schematized longitudinal section of the river aquifer system (left) and related erosion/deposition of riverbed sediments (right). Sedimentological processes affecting the very top of the riverbed are designed as external erosion/deposition and those penetrating the riverbed are designed as internal erosion/deposition [*Partington et al.* 2017].

In a natural state, channel geomorphology and hydraulic properties are evolving according to the capacity of the river flow to erode its substratum and to deposit its sediment load (**Figure 1.7**, [*de Almeida and Rodriguez*, 2011; *Dong et al.*, 2012; *Partington et al.*, 2017; *Schalchli*, 1992]). These complex erosion/deposition processes, related to the river dynamics, are often transient [*Fette et al.*, 2005; *Genereux et al.*, 2008; *Hatch et al.*, 2010]. River geometry can reach a pseudo-steady state when the stream is able to develop a channel, which is able to carry its normal flow, or when fixed and maintained human-made limits are imposed. However, riverbed hydraulic properties can still be highly transient according to river sediment load and climatic events [*Gianni et al.*, 2016; *Levy et al.*, 2011; *Wu et al.*, 2015]. Nevertheless, natural channels can exhibit different morphologies and channel transformations can be dramatic in response to changes in discharge and sediment load. In temperate environments, it is bankfull discharges, for which the channel is completely filled [*Knighton*, 1998], occurring with 1- to 2-years frequency that are the main agents that shape channels and determine stream morphology [*Andrews*, 1980; *Carling*, 1988; *Heritage et al.*, 2001; *Leopold and Wolman*, 1957; *Wolman and Miller*, 1960]. In the case of regulated rivers for which levees constrain laterally the river flow, as it is the case for the Rhône River, the streambed section, constantly flooded, do not show diversified morphology, due to the insufficient width of the cross-section, and the bottom of the riverbed is relatively flat. However, widening of its cross-section, as it is planned by the 3rd Rhône River Correction project, is expected to generate, over the time, a riverbed composed of alternate bars, as it is the case, for example, for reaches of the Rhine River (**Figure 1.8**).

Figure 1.8: The Rhine River between Triessen and Buchs, (Left) and next to Feldkirch (Right), Switzerland.

Bars are accumulations of sediment within the channel. Adjacent to these bars the flowing cross-section is deepened, i.e. pools, and the transition between each bar is marked by a step or riffle. More explicitly, pools are depressions in the riverbed, and riffles are areas of relatively shallow and fast flow [*Charlton*, 2008c]. In the context of the 3rd Rhône River Correction, assessment of the consequences of the project on the groundwater must take into account the hydraulic properties of the alluvial aquifer, those of the riverbed, including its morphology and transience. Also, the limitation of the current methods for streambed hydraulic properties estimation, such as seepage meters, permeameters or laboratory measurements [*Landon et al.*, 2001; *Rosenberry and Pitlick*, 2009; *Rosenberry et al.*, 2008], which have the disadvantage of yielding only point values, being time-consuming, expensive and not possible in large rivers can be pointed out.

Therefore, a method based on hydraulic variations of the river and aquifer that would provide an estimation of the hydraulic properties of the riverbed, which is a key component in the interaction between rivers and aquifers, would be valuable. Moreover, being based on hydraulic heads that can easily be measured continuously, this approach could support the identification of transience in the riverbed hydraulic properties. Furthermore, the influence and possible bias in predictive uncertainty caused by not taking into account the potential uncertainty in the value of the horizontal anisotropy of alluvial aquifers has not been investigated. Therefore, using analytic and numerical approaches the present work will tend to fill these gaps.

1.5. Hydrogeological modeling

Qualitative and quantitative analysis of groundwater dynamics in river-alluvial aquifer systems is essential to anticipate consequences of climate change and human activities. Hydrogeological processes occur across a vast range of spatiotemporal scales. Moreover, we cannot completely know head distribution in space and time, thus hydrogeological models are fundamental tools to synthesize the current knowledge in a quantitative framework and to interpolate this knowledge according to the mathematical description of the appropriate

processes. Whether it is to model a real system, which will undergo new a management strategy or to simulate processes in a hypothetical system, models help to assess and demonstrate if a particular management strategy could lead to particular unwanted consequences [*Anderson et al.*, 2015]. In summary, hydrogeological models can be used for synthesizing information; conceptualizing and understanding groundwater systems; the estimation of parameters and related uncertainties; the understanding of present hydrogeological states; and the prediction of future ones. Two main types of mathematical models exist: analytical and numerical models. Analytical models provide closed-form solutions. They can be solved rapidly using hand calculator or computer program [*MATLAB*, 2014] for the dependent variable. In the study of the Rhône riverbed transience (*Chapter 2*), a method based on an analytical model has been developed for a rapid identification of riverbed conductance variations. However, analytical models require generally a high level of simplification of the real world and caution must be taken to ensure that these simplifications do not significantly bias the predictions.

Numerical models allow simulating complex spatiotemporal conditions, i.e. complex geometries, hydrologic stresses, system parameterization and parameters transience, thanks to the flexibility provided by finite-difference and finite-element methods (*Chapter 3* and *Chapter 4*). Hydrogeological numerical models calculate the water table elevation at every nodes of the designed mesh according to the imposed parameters in a broad sense, i.e. material properties, hydraulic stresses (surface water and groundwater) and boundaries geometry. Those parameters can be estimated from the distribution of the water table elevations. This process is called inversion (manual history matching or automated parameters estimation) and is an essential step for the support of model forecasting [*Wang and Anderson*, 1995]. This topic will be discussed later in this section.

Physically based models [*Brunner and Simmons*, 2012], such as FEFLOW, developed by DHI [*Diersch*, 2014], or HydroGeoSphere, developed by Aquanty, use mathematical representations of natural processes to calculate the groundwater fluxes q and heads h within the model domain. Groundwater flow is controlled by the gradient of heads that set water into motion from high hydraulic heads to lower hydraulic heads, and the hydraulic conductivity K of the media in which the water is flowing that regulate the intensity of the flow. The governing equation, derived from groundwater flow (Darcy's law [*Darcy*, 1856]) through a representative elementary volume, which characterizes the transient (time t) hydrogeological process for a confined (specific storage S_s [-]) aquifer in a three-dimensional Cartesian coordinate system (pair-wise perpendicular axes x, y, z) is:

$$\frac{\partial q_x}{\partial x} + \frac{\partial q_y}{\partial y} + \frac{\partial q_z}{\partial z} - W = -S_s \frac{\partial h}{\partial t} \qquad \textbf{1.1}$$

with,

$$q_i = -K_i \frac{\partial h}{\partial i} \qquad \textbf{1.2}$$

where W is a source/sink term, q_x, q_y and q_z are the groundwater flux along the axes x, y and z respectively (in **equation 1.2** the subscript i can be replaced by x, y or z) and ∂ is the partial derivative notation. For steady state systems, **equation 1.1** is simplified by setting $\partial h/\partial t = 0$, thus the right member is equal to 0. For two-dimensional systems, the z axes is dropped and thus **equation 1.1** is simplified by setting $\partial q_z/\partial z = 0$. When the aquifer is unconfined, the specific storage is replaced by the specific yield S_y. To solve these equations at each node of the mesh, the numerical model requires boundary conditions, i.e. specified values of heads or fluxes around or inside the model domain. For a transient simulation (time-dependent) initial heads distribution (at the beginning of the simulation) are also required.

Generally, prior to the use of a numerical model as a predictor of future system states, it is expected that the model went through calibration. Calibration of a model means that the model

reproduces historical data, i.e. observations and measurements done in the past, for example, the water table elevation in different piezometers located in the model domain and at a certain time. When errors between simulated and observed values are deemed too high, the model parameters, that the modeler assumed to be responsible for these discrepancies, are changed in order to decrease these errors. The values that a parameter is allowed to take during the calibration process are limited by the modeler according to his/her expert knowledge (range of values that the modeler consider acceptable for a certain parameter, according to his/her knowledge of the study site). Finally, the model is considered to be calibrated when it is given a set of parameters that satisfies both historical measurements and expert knowledge. However, based on Bayes theory, the uncertainty in the values of the parameters that have been estimated through the calibration process, and thus in predictions made by the model, remains:

$$f_{(k|h)} = \frac{f_{(h|k)} \cdot f_k}{\int_{-\infty}^{+\infty} f_{(h|k)} \cdot f_k} \qquad \textbf{1.3}$$

where $f_{(k|h)}$ is, in term of calibration process, the posterior probability density function of the estimated model parameter set k (i.e. all parameters values estimated during the calibration process are represented in the vector k) and in Bayesian terms, it is the conditional probability density function of k based on the observation data set h. f_k is the prior probability density function of k which express expert knowledge and $f_{(h|k)}$ is the likelihood function or the probability density function of the observation dataset h based on the values of the parameter set k. In the context of the calibration process, this term is related to the probability distribution of the measurement error of the observed values. Bayes **equation 1.3** demonstrates that uncertainties are present before and after the calibration process and that decrease of these uncertainties may or may not be significant. Therefore, the success of a calibration process is not defined solely by the decrease of the discrepancies between simulated and observed values but also by the reduction of the uncertainties of the estimated parameters and predictions in question.

In hydrogeological modeling, uncertainties are resulting from several factors. Errors in measurements used as calibration data are one obvious factor. Sensitivity analysis can delineate this uncertainty when the measurement error is defined. However, another source of uncertainty is related to the model structural error. The selection of a particular code, process and the definition of the parameter set, qualitatively (parameters that are included or not in the model) and quantitatively (spatial distribution of the parameters) can generate an important source of error that cannot always be fully evaluated, but that should be taken into account. Finally, errors in model prediction can be influenced by the uncertainty in future conditions, such as hydraulic stresses and variations in the hydrogeological properties of the system. Predictions using scenario modeling approaches can frame this uncertainty. Nevertheless, limitations in the estimation of the uncertainty remain with so-called "Unknown unknowns" that represent unanticipated future stresses and properties variations.

In the present work, the modeling strategy has been defined following the guidelines of *Anderson et al.* [2015] and the calibration and uncertainty analysis were realized using the theory and codes developed by *Doherty* [2015]. The calibration approach is based on gradient method (Gauss-Levenberg-Marquardt) and tends to minimize an objective function defined as the sum of squared weighted errors between simulated and observed values. Non-uniqueness due to ill-posed problems, characterized by the fact that calibration data can be matched with simulated data generated using different values for the estimated parameters, is tackled using regularization methods. The regularization approaches employed are based on parameters combinations achieved through singular value decomposition (Reduction of the number of parameters) and the addition of expert knowledge and parameter constraints achieved through Tikhonov regularization (Increase of the number of observations). The sensitivity matrix

(Jacobian matrix) calculated for the temporary linearization of the problem and the probability distributions of measurement noise and parameters values expressed by covariance matrices (assuming Gaussian distribution) are employed for pre- and post-calibration parameter and forecast linear uncertainty and error analysis.
In a nutshell, for complex natural systems, numerical models are indispensable tools to assess variations of the water table and their associated uncertainties overall the study area. In the framework of the 3rd Rhône River Correction two-dimensional steady-state isotropic models have been built [*Glenz*, 2013]. However, as suggested in the previous section, rivers associated to alluvial aquifers are subject to transience in the hydraulic properties of their riverbeds. Furthermore, vertical gradients generated by partially penetrating hydraulic features, such as the Rhône River, its tributaries and the drainage network should be considered regarding the design of the numerical model. Finally, the surrounding alluvial aquifer can be subjected to a horizontal anisotropy of its hydraulic conductivity that may control the water table elevation distribution and dynamics throughout the domain. Previous approaches did not consider these issues. It is therefore essential to explore them and to assess their importance and influence in the context of river-alluvial aquifer model prediction and more specifically for the project of the 3rd Rhône River Correction. In order to investigate these issues, the Cantonal Office for the Rhône River Construction (OCCR3) supported the present work in the framework of the 3rd Rhône River Correction in the priority area of Sion-Vétroz (Mandate MR0565).

1.6. Structure of the thesis

The present work aims at analyzing the *Influence of fluvial morphology on the interaction between surface water and groundwater: 3rd Rhône Correction in Sion* (the title of the mandate MR0565).
Therefore, the framework of the research, i.e. the 3rd Rhône River Correction, has been defined as being an investigation of the surface water and groundwater interaction in the case of an alluvial aquifer, i.e. the Rhône River alluvial aquifer. Also, the influence of the fluvial morphology is understood as the hydrogeological and morphological properties of the riverbed and their influences on groundwater. In line with the objectives of the project of the 3rd Rhône River Correction, the focus of the research is on the impact of the Rhône River stage alterations on the water table elevation in the alluvial aquifer surrounding the river in the area of Sion. Finally, as introduced in the previous section, research has been carried out using analytical and numerical modeling approaches based on current and projected hydraulic and geomorphologic properties of the Rhône River.
From the above description and decomposition of the project aims, the problem has been decomposed into three axes, corresponding to the following *Chapters 2* to *4*:

- A new method, based on the inversion of a convolution using an analytical formula, is developed in order to identify transience in the riverbed conductance. The required dataset is comprised of variations of the river stage and water table.
- The bias in model predictive uncertainty introduced by not taking into account potential uncertainty in the value of the horizontal anisotropy of alluvial aquifers during the calibration process is assessed. Parameters identifiability and reduction of the predictive uncertainty using steady-state and transient calibrations are then investigated.
- These investigations are followed by the actual modeling, calibration, and prediction of the water table elevation for the area of Sion. The predictive uncertainty is calculated using linear uncertainty analysis based on the model calibration and using scenario modeling based on different hydraulic and geomorphologic (alternate bars) properties of the Rhône riverbed.

1.7. References

Alexander, G. G., and J. D. Allan (2007), Ecological success in stream restoration: Case studies from the midwestern United States, *Environmental Management*, *40*(2), 245-255.

Alley, W. M., R. W. Healy, J. W. LaBaugh, and T. E. Reilly (2002), Hydrology – Flow and storage in groundwater systems, *Science*, *296*, 1985-1990.

Anderson, M. P., W. W. Woessner, and R. J. Hunt (2015), *Applied Groundwater Modeling*, Second ed., 563 pp., Elsevier.

Andrews, E. D. (1980), Effective and Bankfull Discharges of Streams in the Yampa River Basin, Colorado and Wyoming, *J Hydrol*, *46*(3-4), 311-330.

Antipa, G. (1932), Les principes de l'amélioration de la productivité du bas Danube. Académie Roumaine, Bucharest,, *Bulletin de la section scientifique*, *XV(3-4)*, 1-19.

Babinski, Z. (1992), Hydromorphological Consequences of Regulating the Lower Vistula, Poland, *Regul River*, *7*(4), 337-348.

Bannister, N., J. Mant, and M. Janes (2005), A Review of Catchment Scale River Restoration Projects in the UK, *Environment Agency, UK*.

Bayley, P. B. (1991), The flood pulse advantage and the restoration of river-floodplain systems, *Regul. Rivers Res. Manage.*, *6*, 75-86.

Benke, A. C. (1990), A Perspective on America Vanishing Streams, *J N Am Benthol Soc*, *9*(1), 77-88.

Boano, F., A. Demaria, R. Revelli, and L. Ridolfi (2010), Biogeochemical zonation due to intrameander hyporheic flow, *Water Resour Res*, *46*.

Boano, F., J. W. Harvey, A. Marion, A. I. Packman, R. Revelli, L. Ridolfi, and A. Worman (2014), Hyporheic flow and transport processes: Mechanisms, models, and biogeochemical implications, *Rev Geophys*, *52*(4), 603-679.

Boulton, A. J., and P. J. Hancock (2006), Rivers as groundwater-dependent ecosystems: a review of degrees of dependency, riverine processes and management implications, *Aust J Bot*, *54*(2), 133-144.

Bridge, J. S., and R. V. Demicco (2008), Rivers, alluvial plains, and fans, in *Earth Surface Processes, Landforms and Sediment Deposits*, edited by J. S. Bridge and R. V. Demicco, pp. 365-462, Cambridge University Press.

Briggs, M. A., L. K. Lautz, and D. K. Hare (2014), Residence time control on hot moments of net nitrate production and uptake in the hyporheic zone, *Hydrol Process*, *28*(11), 3741-3751.

Brookes, A. (1985), River Channelization - Traditional Engineering Methods, Physical Consequences and Alternative Practices, *Prog Phys Geog*, *9*(1), 44-73.

Brunner, P., P. G. Cook and C. T. Simmons (2009), Hydrogeologic controls on disconnection between surface water and groundwater, *Water Resour Res*, *45*.

Brunner, P., P. G. Cook and C. T. Simmons (2011), Disconnected Surface Water and Groundwater: From Theory to Practice, *Ground Water*, *49(4)*, 460-467.

Brunner, P., and C. T. Simmons (2012), HydroGeoSphere: A Fully Integrated, Physically Based Hydrological Model, *Ground Water*, *50*(2), 170-176.

Budhu, M. (2011), Earth Fissure Formation from the Mechanics of Groundwater Pumping, *Int J Geomech*, *11*(1), 1-11.

Buijse, A. D., H. Coops, M. Staras, L. H. Jans, G. J. Van Geest, R. E. Grift, B. W. Ibelings, W. Oosterberg, and F. C. J. M. Roozen (2002), Restoration strategies for river floodplains along large lowland rivers in Europe, *Freshwater Biol*, *47*(4), 889-907.

Canton du Valais (2006), Plan sectoriel 3ème correction du Rhône, 51 p.

Canton du Valais (2014), Rapport d'impact sur l'environnement, 1er étape, 164 p.

Canton du Valais (2016), Plan d'aménagement (PA-R3) - Rapport de synthèse, 103 p.

Cardenas, M. B. (2010), Lessons from and assessment of Boussinesq aquifer modeling of a large fluvial island in a dam-regulated river, *Adv Water Resour*, *33*(11), 1359-1366.
Carling, P. (1988), The Concept of Dominant Discharge Applied to 2 Gravel-Bed Streams in Relation to Channel Stability Thresholds, *Earth Surf Processes*, *13*(4), 355-367.
Charlton, R. (2008a), The Fluvial System, in *Fundamentals of Fluvial Geomorphology*, edited by R. Charlton, pp. 10-20, Taylor & Francis Group.
Charlton, R. (2008b), Managing River Channels, in *Fundamentals of Fluvial Geomorphology*, edited by R. Charlton, pp. 177-200, Taylor & Francis Group.
Charlton, R. (2008c), Channel Form and Behaviour, in *Fundamentals of Fluvial Geomorpology*, edited by R. Charlton, pp. 117-156, Taylor & Francis Group.
Chen, X., D. B. Wang, F. Q. Tian, and M. Sivapalan (2016), From channelization to restoration: Sociohydrologic modeling with changing community preferences in the Kissimmee River Basin, Florida, *Water Resour Res*, *52*(2), 1227-1244.
Conseil fédéral suisse (1991, 2017), Loi fédérale sur l'aménagement des cours d'eau, 6 p.
Constantz, J. (2016), Streambeds merit recognition as a scientific discipline, *Wires-Water*, *3*(1), 13-18.
Conway, B. D. (2016), Land subsidence and earth fissures in south-central and southern Arizona, USA, *Hydrogeol J*, *24*(3), 649-655.
Cook, P. G., C. Wood, T. White, C. T. Simmons, T. Fass, and P. Brunner (2008), Groundwater inflow to a shallow, poorly-mixed wetland estimated from a mass balance of radon, *J Hydrol*, *354*(1-4), 213-226.
Darcy, H. (1856), Les Fontaines Publiques de la ville Dijon, *Dalmont, Paris*.
de Almeida, G. A. M., and J. F. Rodriguez (2011), Understanding pool-riffle dynamics through continuous morphological simulations, *Water Resour Res*, *47*.
De Waal, L. C., A. R. G. Large, C. J. Gippel, and P. M. Wade (1995), River and floodpain rehabilitation in Western Europe: opportunities and constraints, *Archiv für Hydrobiologie*, *101*, 679-693.
Diersch, H.-J. G. (2014), *FEFLOW Finite Element Modeling of Flow, Mass and Heat Transport in Porous and Fractured Media*, Springer.
Dister, E., D. Gomer, P. Obrdlik, P. Petermann, and Schneider E. (1990), Water management and ecological perspective of the Upper Rhine's floodplains, *Regul. Rivers Res. Manage.*, *5*, 1-15.
Doherty, J. (2015), *Calibration and Uncertainty Analysis for Complex Environmental Models*, first ed., 227 pp., Watermark Numerical Computing.
Dong, W. H., X. H. Chen, Z. W. Wang, G. X. Ou, and C. Liu (2012), Comparison of vertical hydraulic conductivity in a streambed-point bar system of a gaining stream, *J Hydrol*, *450*, 9-16.
Douglas, D. J., and J. McCreanor (1990), The Big River, Co Louth, Ireland: a case study in recovery, *Ann Limnol-Int J Lim*, *26*(1), 73-79.
Duckson, D. W. (1990), Historical Change of Large Alluvial Rivers - Western-Europe - Petts,Ge, Moller,H, Roux,Al, *Prof Geogr*, *42*(4), 507-508.
Dynesius, M., and C. Nilsson (1994), Fragmentation and Flow Regulation of River Systems in the Northern 3rd of the World, *Science*, *266*(5186), 753-762.
European Commission (2000), EU Water Framework Directive, *Office for Official Publications of the European Communities (OJ L 327)*.
European Commission (2008), Groundwater Protection in Europe - The New Groundwater Directive - Consolidating the EU Regulatory Framework, *Office for Official Publications of the European Communities*.
European Parliament (2000), EU Water Framework Directive, *Official Journal of the European Communities*.

Fette, M., R. Kipfer, C. J. Schubert, E. Hoehn, and B. Wehrli (2005), Assessing river-groundwater exchange in the regulated Rhone River (Switzerland) using stable isotopes and geochemical tracers, *Applied Geochemistry*, *20*(4), 701-712.

Fisher, S. G., N. B. Grimm, E. Marti, R. M. Holmes, and J. B. Jones (1998), Material spiraling in stream corridors: A telescoping ecosystem model, *Ecosystems*, *1*(1), 19-34.

Fleckenstein, J. H., S. Krause, D. M. Hannah, and F. Boano (2010), Groundwater-surface water interactions: New methods and models to improve understanding of processes and dynamics, *Adv Water Resour*, *33*(11), 1291-1295.

Fox, A., F. Boano, and S. Arnon (2014), Impact of losing and gaining streamflow conditions on hyporheic exchange fluxes induced by dune- shaped bed forms, *Water Resour Res*, *50*(3), 1895-1907.

Fox, A., G. Laube, C. Schmidt, J. H. Fleckenstein, and S. Arnon (2016), The effect of losing and gaining flow conditions on hyporheic exchange in heterogeneous streambeds, *Water Resour Res*, *52*(9), 7460-7477.

Galat, D. L., et al. (1998), Flooding to restore connectivity of regulated, large-river wetlands - Natural and controlled flooding as complementary processes along the lower Missouri River, *Bioscience*, *48*(9), 721-733.

Galloway, D. L., and T. J. Burbey (2011), Review: Regional land subsidence accompanying groundwater extraction, *Hydrogeol J*, *19*(8), 1459-1486.

GEI-MPS (2011), 3ème Correction du Rhône - Mesure Prioritaire du Plan d'Aménagement - Traversée urbaine du Rhône à Sion, *Département des transports, de l'équipement et de l'environnement - Service des routes et des cours d'eau - Canton du Valais*, 117 p.

Genereux, D. P., S. Leahy, H. Mitasova, C. D. Kennedy, and D. R. Corbett (2008), Spatial and temporal variability of streambed hydraulic conductivity in West Bear Creek, North Carolina, USA, *Journal of Hydrology*, *358*(3-4), 332-353.

GéoVal Ingénieurs-Géologues SA (2010), Faisabilité de l'abaissement du lit du fleuve à travers Sion, 23 p.

Gianni, G., J. Richon, P. Perrochet, A. Vogel, and P. Brunner (2016), Rapid identification of transience in streambed conductance by inversion of floodwave responses, *Water Resour Res*, *52*(4), 2647-2658.

Glenz, D. (2013), Inverse Modeling of Groundwater Flow in Rhone Alluvial Aquifer, Impact of the Third Rhone Correction, 172 p.

Gore, J. A. (1985), The Restoration of Rivers and Streams: Theories and Experience, *Butterworth Publ., Boston, MA*.

Gore, J. A., and G. E. Petts (1989), *Alternatives in regulated river management*, 344 p. pp., CRC Press, Boca Raton, Fla.

Gore, J. A., and F. D. Shields (1995), Can Large Rivers Be Restored, *Bioscience*, *45*(3), 142-152.

Hallberg, G. R., J. M. Harbaugh, and P. M. Witinok (1979), Changes in the Channel Area of the Missouri River in Iowa, 1879-1976, *Iowa Geological Survey, Special Report Series Number 1. Iowa Geological Survey, Iowa City, IA*.

Hatch, C. E., A. T. Fisher, C. R. Ruehl, and G. Stemler (2010), Spatial and temporal variations in streambed hydraulic conductivity quantified with time-series thermal methods, *Journal of Hydrology*, *389*(3-4), 276-288.

Heritage, G. L., L. J. Broadhurst, and A. L. Birkhead (2001), The influence of contemporary flow regime on the geomorphology of the Sabie River, South Africa, *Geomorphology*, *38*(3-4), 197-211.

Hynes, H. B. N. (1983), Groundwater and Stream Ecology, *Hydrobiologia*, *100*, 93-99.

International Commission for the Protection of the Rhine (2001), Rhine 2020 - Program on the sustainable development of the Rhine, *ICPR, Koblenz, Germany. www.ikst.org*.

Internationalen Regierungskommission Alpenrhein (2000), Grundwasserhaushalt Alpenrhein. Grundwassermodellierung für den Abschnitt Landquart bis Bodensee, 15 p.

Irvine, D. J., P. Brunner, H. J. H. Franssen, and C. T. Simmons (2012), Heterogeneous or homogeneous? Implications of simplifying heterogeneous streambeds in models of losing streams, *Journal of Hydrology*, 424, 16-23.

Irvine, D. J., R. H. Cranswick, C. T. Simmons, M. A. Shanafield, and L. K. Lautz (2015), The effect of streambed heterogeneity on groundwater-surface water exchange fluxes inferred from temperature time series, *Water Resour Res*, *51*(1).

Januschke, K., and R. C. M. Verdonschot (2016), Effects of river restoration on riparian ground beetles (Coleoptera: Carabidae) in Europe, *Hydrobiologia*, *769*(1), 93-104.

Kalbus, E., F. Reinstorf, and M. Schirmer (2006), Measuring methods for groundwater - surface water interactions: a review, *Hydrol Earth Syst Sc*, *10*(6), 873-887.

Kasahara, T., and S. M. Wondzell (2003), Geomorphic controls on hyporheic exchange flow in mountain streams, *Water Resour Res*, *39*(1).

Kern, K. (1992), Restoration of lowland rivers: the German experience, in *Lowland Floodplain Rivers*, edited by P. A. Carling and G. E. Petts, pp. 279-297, John Wiley and Sons, Chichester, UK.

Knighton, D. (1998), Fluvial Forms and Processes: A New Perspective, *Hodder Arnold*, 383 p.

Krause, S., F. Boano, M. O. Cuthbert, J. H. Fleckenstein, and J. Lewandowski (2014), Understanding process dynamics at aquifer-surface water interfaces: An introduction to the special section on new modeling approaches and novel experimental technologies, *Water Resour Res*, *50*(2), 1847-1855.

Kristensena, E. A., B. Kronvang, P. Wiberg-Larsen, H. Thodsen, C. Nielsen, E. Amor, N. Friberg, M. L. Pedersen, and A. Baattrup-Pedersen (2014), 10 years after the largest river restoration project in Northern Europe: Hydromorphological changes on multiple scales in River Skjern, *Ecol Eng*, *66*, 141-149.

Landon, M. K., D. L. Rus, and F. E. Harvey (2001), Comparison of instream methods for measuring hydraulic conductivity in sandy streambeds, *Ground Water*, *39*(6), 870-885.

Lelek, A., and C. Köhler (1990), Restoration of fish communities of the Rhine River two years after a heavy pollution wave, *River Res Appl*, *5*(1), 57-66.

Leopold, L. B., and M. G. Wolman (1957), River Channel Patterns: Braided, Meandering and Straight., *United States Geological Survey Professional Paper 282B*.

Levy, J., M. D. Birck, S. Mutiti, K. C. Kilroy, B. Windeler, O. Idris, and L. N. Allen (2011), The impact of storm events on a riverbed system and its hydraulic conductivity at a site of induced infiltration, *Journal of Environmental Management*, *92*(8), 1960-1971.

Li, Y. Q., Z. L. Hu, T. Q. Weng, J. Fonseca, and X. D. Zhang (2014), Experimental study on the vertical deformation of sand caused by cyclic withdrawal and recharging of groundwater, *Eng Geol*, *183*, 247-253.

Louisoder, G. (2012), Studie zum Gewässerpflegeplan Mühltal, *Natureprojekt*.

MATLAB (2014), *8.3.0.532 (R2014a)*, The MathWorks Inc., Natick, Massachusetts.

Meuli, K., and K. Edmaier (2017), Valoriser les cours d'eaux et les lacs - Pour l'être humain et pour la nature, *Office fédéral de l'environement (OFEV) - Confédération suisse*.

Miller, A. C., R. H. King, and J. E. Glover (1983), Design of a gravel habitat for the Tombigbee River near Columbus, Mississippi., *US Army Engineer Waterways Experiment Station, Vicksburg, MS*.

Mwakanyamale, K., L. Slater, F. Day-Lewis, M. Elwaseif, and C. Johnson (2012), Spatially variable stage-driven groundwater-surface water interaction inferred from time-frequency analysis of distributed temperature sensing data, *Geophys Res Lett*, *39*.

Newbury, R. W., and M. N. Gaboury (1993), Stream Analysis and Fish Habitat Design, *Newbury Hydraulics Ltd., Gibson, BC*.

Nilsson, C., C. A. Reidy, M. Dynesius, and C. Revenga (2005), Fragmentation and flow regulation of the world's large river systems, *Science, 308*(5720), 405-408.

Nougier, S., C. Bleuze, P. Debères, S. Forestier, J. Lesueur, and M. Alison (2015), SDAGE Rapport Environnemental Rhône-Méditerranée, *Agence de l'eau, Rhône Méditerranée Corse*.

OFEFP, OFEG, OFAG, and ODT (2003), Idées directrices - Cours d'eau suisses - Pour une politique de gestion durable de nos eaux, *Office fédéral de l'environement (OFEV) - Confédération suisse*, 12.

Partington, D., R. Therrien, C. T. Simmons, and P. Brunner (2017), Blueprint for a coupled model of sedimentology, hydrology, and hydrogeology in streambeds, *Rev Geophys*.

Pasche, L. (2002), travaux de correction des cours d'eau en Valais et dans la région de Conthey (1860-1900). Extrait de : Inondations de 1868 et émergence de la politique de correction des eaux et de reboisement dans les Alpes suisses au cours du XIXème siècle, *Mémoire de licence, Université de Lausanne*, p. 225-246.

Petts, G. E. (1989), Perspectives for ecological management of regulated rivers, in *Alternatives in Regulated River Management*, edited by J. A. Gore and G. E. Petts, pp. 3-26, CRC Press, Boca Raton, FL.

Romano, P., R. Ranzani, and F. Tecchiati (1992), Water Reclamation of the Po River in the Turin Area, *Water Sci Technol*, *26*(9-11), 2579-2582.

Roni, P., T. J. Beechie, R. E. Bilby, F. E. Leonetti, M. M. Pollock, and G. R. Pess (2002), A review of stream restoration techniques and a hierarchical strategy for prioritizing restoration in Pacific northwest watersheds, *N Am J Fish Manage*, *22*(1), 1-20.

Rosenberry, D. O., and J. Pitlick (2009), Local-scale variability of seepage and hydraulic conductivity in a shallow gravel-bed river, *Hydrol Process*, *23*(23), 3306-3318.

Rosenberry, D. O., J. W. LaBaugh, and Geological Survey (U.S.) (2008), *Field techniques for estimating water fluxes between surface water and ground water*, iv, 128 p. pp., U.S. Geological Survey, Reston, Va.

Rosenberry, D. O., R. W. Sheibley, S. E. Cox, F. W. Simonds, and D. L. Naftz (2013), Temporal variability of exchange between groundwater and surface water based on high-frequency direct measurements of seepage at the sediment- water interface, *Water Resour Res*, *49*(5), 2975-2986.

Rovina + Partner AG (2009), Beurteilung der GW-Beeinträchtigungen auf Stufe Generelles Projekt, 48 p.

Schalchli, U. (1992), The Clogging of Coarse Gravel River Beds by Fine Sediment, *Hydrobiologia*, *235*, 189-197.

Schiemer, F., C. Baumgartner, and K. Tockner (1999), Restoration of floodplain rivers: The 'Danube restoration project', *Regul River*, *15*(1-3), 231-244.

Schilling, O. S., D. J. Irvine, H. J. H. Franssen, P. Brunner (2017), Estimating the Spatial Extent of Unsaturated Zones in Heterogeneous River-Aquifer Systems, *Water Resour Res*.

Shields, F. D., and R. H. Smith (1992), Effects of Large Woody Debris Removal on Physical Characteristics of a Sand-Bed River, *Aquat Conserv*, *2*(2), 145-163.

Simons, J. H. E. J., C. Bakker, M. H. I. Schropp, L. H. Jans, F. R. Kok, and R. E. Grift (2001), Man-made secondary channels along the River Rhine (the Netherlands); results of post-project monitoring, *Regul River*, *17*(4-5), 473-491.

Slater, L. D., D. Ntarlagiannis, F. D. Day-Lewis, K. Mwakanyamale, R. J. Versteeg, A. Ward, C. Strickland, C. D. Johnson, and J. W. Lane (2010), Use of electrical imaging and distributed temperature sensing methods to characterize surface water-groundwater exchange regulating uranium transport at the Hanford 300 Area, Washington, *Water Resour Res*, *46*.

Sophocleous, M. (2002), Interactions between groundwater and surface water: the state of the science (vol 10, pg 52, 2002), *Hydrogeol J*, *10*(2), 348-348.
Speed, R., et al. (2016), River Restoration: A Strategic Approach to Planning and Management, *UNESCO*, 202 p.
Stanford, J. A., J. V. Ward, W. J. Liss, C. A. Frissell, R. N. Williams, J. A. Lichatowich, and C. C. Coutant (1996), A general protocol for restoration of regulated rivers, *Regul River*, *12*(4-5), 391-413.
Sujay, R. N., P. C. Deka, and C. Sudheer (2017), Significance of streambed hydraulic conductivity in stream-aquifer interaction - A systematic review of fundamentals and recent research (vol 578, pg 256, 2016), *Sci Total Environ*, *578*, 256-256.
Torrenté, C., and A. Kalbermatten (1964), La correction du Rhône en amont du lac Léman, 135 p.
Toth, L. A., J. T. B. Obeysekera, W. A. Perkins, and M. K. Loftin (1993), Flow Regulation and Restoration of Florida Kissimmee River, *Regul River*, *8*(1-2), 155-166.
Trauth, N., C. Schmidt, M. Vieweg, S. E. Oswald, and J. H. Fleckenstein (2015), Hydraulic controls of in-stream gravel bar hyporheic exchange and reactions, *Water Resour Res*, *51*(4), 2243-2263.
Verweij, M. (2017), The remarkable restoration of the Rhine: plural rationalities in regional water politics, *Water International*, *42*(2), 207-221.
Walling, D. E., and B. W. Webb (1983), Patterns of sediment yield, in *Background to Palaeohydrology*, edited by K. J. Gregory, pp. 69-100, John Wiley & Sons, Chichester.
Wang, H. F., and M. P. Anderson (1995), *Introduction to Groundwater Modeling - Finite Difference and Finite Element Methods*, Academic Press.
Ward, A. S. (2016), The evolution and state of interdisciplinary hyporheic research, *Wires-Water*, *3*(1), 83-103.
Ward, A. S., M. Fitzgerald, M. N. Gooseff, T. J. Voltz, A. M. Binley, and K. Singha (2012), Hydrologic and geomorphic controls on hyporheic exchange during base flow recession in a headwater mountain stream, *Water Resour Res*, *48*.
Ward, J. V., F. Malard, K. Tockner, and U. Uehlinger (1999), Influence of ground water on surface water conditions in a glacial flood plain of the Swiss Alps, *Hydrol Process*, *13*(3), 277-293.
Ward, J. V., K. Tockner, U. Uehlinger, and F. Malard (2001), Understanding natural patterns and processes in river corridors as the basis for effective river restoration, *Regul River*, *17*(6), 709-+.
Welcomme, R. L. (1989), Floodplain fisheries management, in *Alternatives in Regulared River Management*, edited by J. A. Gore and G. E. Petts, pp. 209-234, CRC Press, Boca ration, FL.
Westhoff, M. C., T. A. Bogaard, and H. H. G. Savenije (2010), Quantifying the effect of in-stream rock clasts on the retardation of heat along a stream, *Adv Water Resour*, *33*(11), 1417-1425.
Wiens, J. A. (1999), Landscape ecology: the science and the action, *Landscape Ecol*, *14*(2), 103-103.
Winter, T. C., J. W. Harwey, O. L. Franke, and W. M. Alley (1998), Ground water and surface water: A single resource, *U.S. Geol. Surv. Circ.*, *1139*, 79 pp.
Woessner, W. W. (2000), Stream and fluvial plain ground water interactions: Rescaling hydrogeologic thought, *Ground Water*, *38*(3), 423-429.
Wolman, M. G., and J. P. Miller (1960), Magnitude and Frequency of Forces in Geomorphic Processes, *J Geol*, *68*(1), 54-74.
Wondzell, S. M., J. LaNier, R. Haggerty, R. D. Woodsmith, and R. T. Edwards (2009), Changes in hyporheic exchange flow following experimental wood removal in a small, low-gradient stream, *Water Resour Res*, *45*.

Wu, G. D., L. C. Shu, C. P. Lu, X. H. Chen, X. Zhang, E. K. Appiah-Adjei, and J. S. Zhu (2015), Variations of streambed vertical hydraulic conductivity before and after a flood season, *Hydrogeol J*, *23*(7), 1603-1615.

Wu W. (2007), Introduction, in *Computational River Dynamics*, edited by Wu W., pp. 1-10, Taylor & Francis.

Chapter 2

2. Rapid identification of transience in streambed conductance by inversion of floodwave responses

Abstract

Streambed conductance controls the interaction between surface water and groundwater. However, the streambed conductance is often subject to transience. Directly measuring hydraulic properties in a river yields only point values, is time-consuming and therefore not suited to detect transience of physical properties. Here, we present a method to monitor continuously the transience in streambed conductance. Input data are time series of stream stage and near stream groundwater hydraulic head. The method is based on the inversion of floodwave responses. The analytical model consists of three parameters: x, the distance between the streambank and an observation well, α, the aquifer diffusivity, and a the retardation coefficient that is inversely proportional to the streambed conductance. Estimation of a is carried out over successive time windows in order to identify transience in streambed conductance. The method is tested using synthetic data and is applied to field data from the Rhône River and its alluvial aquifer (Switzerland). The synthetic analysis demonstrated the robustness of the proposed approach. Application of the method to the field data allowed identifying transience in streambed properties, following flood events in the Rhône River. This method requires transience in the surface water, and the river should not change its width significantly with a rising water level. If these conditions are fulfilled, this method allows for a rapid and effective identification of transience in streambed conductance.

This chapter has been published in Water Resources Research (Online since 5 February 2016): *Gianni, G., J. Richon, P. Perrochet, A. Vogel, and P. Brunner (2016), Rapid identification of transience in streambed conductance by inversion of floodwave responses, Water Resour. Res., 52, doi:10.1002/2015WR017154.*

2.1. Introduction

River-aquifer exchanges have been the focus of much research, due to its importance in water quality and quantity management, e.g. river bank filtration systems [*Hiscock and Grischek*, 2002], river restorations [*Kurth and Schirmer*, 2014] or contaminant transport across the interface between surface water and groundwater [*Smith and Lerner*, 2008]. One of the key factors that controls river-groundwater interactions is the streambed [*Sophocleous*, 2002; *Winter et al.*, 1998]. The streambed composition is continuously affected by sedimentation and erosion [*Coleman*, 1969; *Droppo and Stone*, 1994; *Frostick et al.*, 1984; *Fryirs and Gore*, 2013; *Levy et al.*, 2011; *Lisle*, 1989; *Schalchli*, 1992], chemical [*Du et al.*, 2013; *Smith and Lerner*, 2008] and biological processes [*Wang et al.*, 2014]. These processes affecting the streambed cause variations in its hydraulic properties, such as its hydraulic conductivity, thickness and heterogeneity [*Irvine et al.*, 2012; *Kalbus et al.*, 2009; *Levy et al.*, 2011; *Simpson and Meixner*, 2012].

Changes of up to two orders of magnitude of the streambed hydraulic conductivity after flood events have been documented in field studies [*Fette et al.*, 2005; *Genereux et al.*, 2008; *Hatch et al.*, 2010; *Wu et al.*, 2015]. Such changes significantly affect the exchange fluxes between the surface and the groundwater domains. If this transience is not taken into account, predictions on exchange fluxes will be unreliable. For example, numerical models simulating the interactions between surface water and groundwater typically assume streambed conductance to be constant. If streambed properties are transient, however, this assumption will cause a systematic bias to model predictions. It is therefore critical to understand if the system modeled is subject to such transience.

Several approaches to measure streambed hydraulic conductivity are commonly used, e.g. seepage meters [*Rosenberry*, 2008; *Woessner and Sullivan*, 1984], permeameters [*Landon et al.*, 2001; *Lee et al.*, 2015], laboratory measurements of streambed samples [*Rosenberry and Pitlick*, 2009b; *Schalchli*, 1992], thermal methods [*Hatch et al.*, 2010; *Mutiti and Levy*, 2010]. More recently, reach scale evaluation of the streambed hydraulic conductivity based on streamflow-front velocities has been proposed by *Shanafield et al.* [2014]. However, all of these methods are time-consuming. Also, the high degree of heterogeneity typically found in streambeds [*Calver*, 2001] makes extrapolation of the average hydraulic conductivity of the riverbed from point measurements questionable. Given the difficulty of directly measuring hydraulic properties of a streambed, detecting transience in these properties is even more challenging.

We present a method, requiring only stream stage and near stream water table time series, that, under given conditions, allows identifying transience in streambed hydraulic properties, specifically the streambed conductance. The method is based on a succession of inversion of an analytical model [*Ha et al.*, 2007; *M K Jha and Singh*, 2014; *M K Jha et al.*, 2008; *Reynolds*, 1987], *i.e.*, floodwave response model [*Hall and Moench*, 1972; *M K Jha et al.*, 2004], that calculate the aquifer response, in terms of hydraulic heads, to stream stage variations. The approach allows estimating the retardation coefficient of the streambed [*Hall and Moench, 1972; Hantush, 1965*], which is inversely proportional to the streambed conductance. We show that estimating this parameter for successive time steps allows detecting changes in the streambed conductance. The approach is tested using synthetic data and field data from the Rhône River (Switzerland).

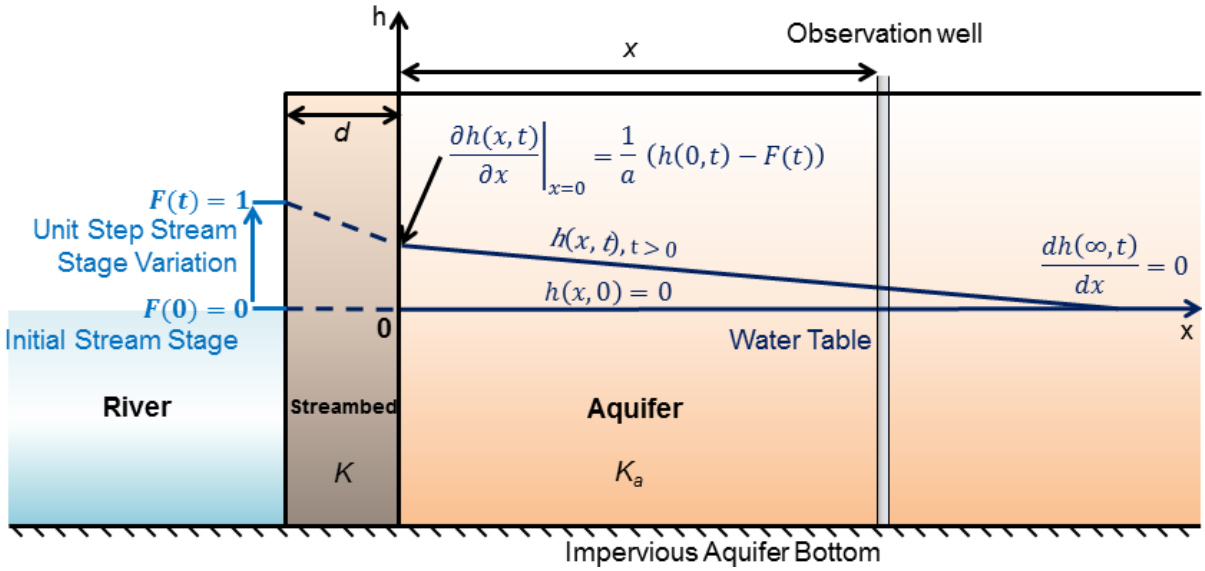

Figure 2.1: Sketch of the mathematical model describing the propagation of head $h(x,t)$ that represents the aquifer response to a unit step increase of the stream stage along with the initial and boundary conditions, **equations 2.2** to **2.4**. K_a is the aquifer hydraulic conductivity, K is the streambed hydraulic conductivity, d is the streambed thickness, and x is the distance between the streambed and the observation well. The stream is considered fully penetrating and is separated from the aquifer by a homogeneous vertical layer.

2.2. Methods

2.2.1. Overview

This approach is based on the response of an aquifer to transience in the river stage. The required input data and parameters are: continuous stream stage and riparian water table time series; the distance of the observation well to the streambank and the diffusivity of the aquifer. The method consists of three iterative steps: 1) the floodwave response is calculated using a convolution between an aquifer unit step response and stream stage variations; 2) the discrepancies between simulated aquifer responses and field observations are minimized through estimation of the streambed retardation coefficient; 3) the inversion is repeated for successive time windows in order to detect variations in the estimated retardation coefficient and thus in the streambed conductance.

2.2.2. Floodwave response model

The variation of hydraulic heads h [L] in one dimension along the distance x [L] and time t [T] can be expressed through:

$$\frac{\partial h(x,t)}{\partial t} = \alpha \frac{\partial^2 h(x,t)}{\partial x^2} \qquad \textbf{2.1}$$

where α [L^2 T^{-1}] is the hydraulic diffusivity, expressed by the ratio $K_a d_a/S$ where K_a [L T^{-1}] is the hydraulic conductivity of the aquifer, d_a [L] the thickness of the aquifer and S [-] the storativity. **Figure 2.1** illustrates the conceptual model used to develop and solve **equation 2.1** in order to calculate the aquifer response to variations of stream stage. This requires an initial condition (**equation 2.2**) and boundary conditions (**equations 2.3** and **2.4**). These equations represent the hydraulic head variations of an aquifer of infinite horizontal extent to a step variation of stream stage. It is assumed that the initial hydraulic head throughout the aquifer and stream stage is equal to 0, and that a streambed, with hydraulic properties different to the aquifer, is present:

$$h(x,0) = 0 \qquad \textbf{2.2}$$
$$dh/dx(\infty,t) = 0 \qquad \textbf{2.3}$$

$$\left.\frac{\partial h(x,t)}{\partial x}\right|_{x=0} = \frac{1}{a}\,(h(0,t) - F(t)) \qquad \textbf{2.4}$$

where $F(t)$ [L] represents the stream stage and is equal to 1 after a unit step variation. a [L] is the retardation coefficient and represents the effective thickness of aquifer required to cause the same head loss as the streambed layer [*Hantush*, 1965]. a is expressed by dK_a/K, where d [L] is the thickness of the streambed and K [L T^{-1}] the hydraulic conductivity of the streambed. The retardation coefficient is inversely proportional to the streambed conductance per square meter C [T^{-1}], defined as K/d [*Hantush*, 1965; *Kollet and Zlotnik*, 2007]. The distance x represents the distance from the streambank. The analytical solution of **equation 2.1** along with **equations 2.2** to **2.4** is given by [*Carslaw and Jaeger*, 1959; *Hall and Moench*, 1972]:

$$h(x,t) = \operatorname{erfc}\left(\frac{x}{2\sqrt{\alpha t}}\right) - \exp\left(\frac{x}{a} + \frac{\alpha t}{a^2}\right)\operatorname{erfc}\left(\frac{x}{2\sqrt{\alpha t}} + \frac{\sqrt{\alpha t}}{a}\right) \qquad \textbf{2.5}$$

where erfc and exp are the complementary error function and the exponential function. The variable x represents the distance from the outer edge of the streambank along the x-axis. In practice, x represents the distance to the streambank of a vertical observation well from which water table time series are recorded.

Only three parameters are used in **equation 2.5**: the distance between the observation well and the streambank x, the diffusivity of the aquifer α, and the retardation coefficient a. The first term on the right-hand side of **equation 2.5** represents the aquifer response without a clogging layer. The second term represents the effect of the streambed on the aquifer response. Increase in the value of a will increase the head loss generated by the streambed.

Using the analytical solution **equation 2.5**, referred from now on as $P(x,t)$, *Hall and Moench* [1972] presented a convolution method to solve aquifer response to any stream stage variations. Assuming $F(0) = 0$, the piezometric level $h(x,t)$ is calculated using the convolution product:

$$h(x,t) = \int_0^t F'(\tau)\,P(x,t-\tau)\,d\tau \qquad \textbf{2.6}$$

where $F'(t)$ is the stream stage change and τ is the variable of integration. The discrete form of **equation 2.6** is used from here on to numerically compute the aquifer response to stream stage variations. The influence of the numerous simplifying assumptions on the applicability and reliability of the proposed method to identify streambed transience will be discussed in the section *Discussion 2.5*.

2.2.3. Retardation coefficient estimation

The retardation coefficient a can be estimated using parameter estimation approaches which minimize the Sum of Squared Error between observed and calculated heads (SSE):

$$SSE = \sum_{i=1}^{m}(H_i - h_i)^2 \qquad \textbf{2.7}$$

where m is the number of hydraulic head observations H, while h represents the calculated head for a given time step i. We used a gradient descent algorithm based on the variation of **equation 2.7** with a termination criterion consisting of a minimum residual of estimated a between two iterations.

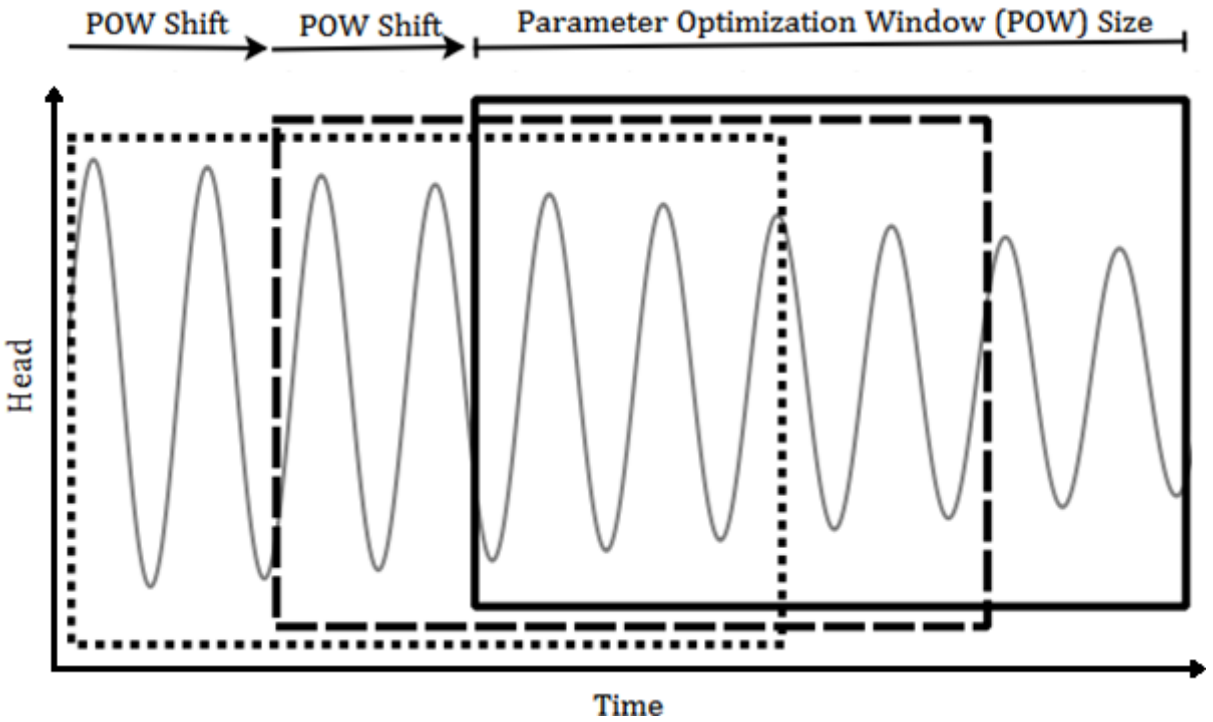

Figure 2.2: Schematic graphics (No unit scales) of the Parameter Optimization Window (POW) parameters: Size and Shift. The Size of the POW [T] is the length of time for which each estimation process is pursued (i.e. the length of the rectangles). The Shift of the POW [T] is the time separating the beginning of two successive POW (i.e. the distance, along the Time-axis, between the beginnings of two successive rectangles) . Within each POW the estimated retardation coefficient *a* is assumed constant and the inversion process estimates its value by minimizing the *SSE* between field and simulated hydraulic heads.

In order to detect transience in the retardation coefficient, the available time series of field data are subdivided into successive and partially overlapping time intervals (time windows), referred to as Parameter Optimization Window (POW), because an Optimization of the Parameter *a* is pursued within each Window. **Figure 2.2** illustrates the two parameters of the POW: the size [T] and the shift [T]. Within each POW, the retardation coefficient *a* is assumed to be constant and is estimated using stream stages and hydraulic heads time series contained in the POW. Therefore, the size of the POW determines the number of observations used during each inversion and the shift determines the total number of inversions and thus the number of estimations of the parameter *a* within the study period. The sensitivity of the estimation to the POW size has been explored and is presented in the next section. The entire approach including the convolution and parameter estimation was implemented in *MATLAB* [2014].

2.3. Synthetic data analysis and sensitivity to the POW

2.3.1. Model setup

Using numerical modeling we tested (1) if the method can detect transience in the streambed conductance and (2) the sensitivity of the results to the POW size. First, synthetic data have been generated using the numerical simulator *HydroGeoSphere* [2013]. During the simulation, the streambed conductance was varied by changing the hydraulic conductivity of the streambed in time, and the groundwater responses to stream stage variations are calculated. Then the retardation coefficient *a* is estimated using the simulated heads. Finally, the estimated and simulated streambed conductances are compared.

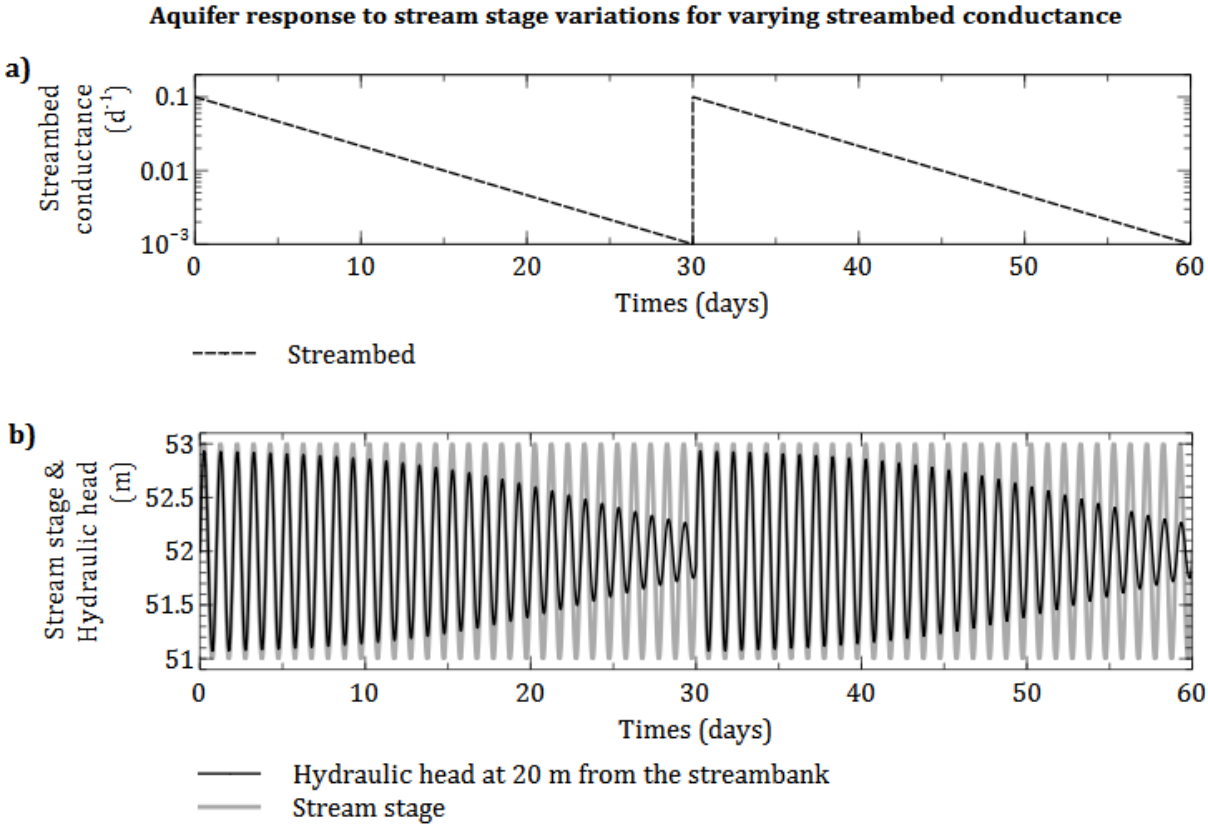

Figure 2.3: (a) Transience in streambed conductance. (b) The stream stage input function (sinusoid of period 1 day, magnitude 1 m and damping factor of 0) and the groundwater response at 20 m from the streambank. The relation between the magnitude of the aquifer response and the value of the streambed conductance is clearly observable.

The model geometry is similar to the mathematical model in **Figure 2.1**, but of limited horizontal extent (500 m wide). The depth of the cross-section is 50 m. The initial condition is a hydrostatic head of 52 m throughout the entire model domain. The head condition imposed on the left side (river side) starts with a value of 52 m (initial condition) and varies between 51 m and 53 m in order to represent stream stage dynamics. The variations are generated using a sinusoidal function of period 1 day and magnitude of 1 m (**Figure 2.3b**). On the opposite side, (right side at 500 m from the river side) a constant head boundary of 52 m is fixed throughout the entire simulation. The bottom and top sides of the model are no flow boundaries. The aquifer has a homogeneous hydraulic conductivity K_a, of 1 md^{-1} and a specific storage S_s of 10^{-4} m^{-1}, the porous media is fully saturated and confined. The horizontal streambed thickness, d, is 1 m, thus the streambed conductance C, is 1 d^{-1}. In order to represent clogging and unclogging processes, the streambed conductance C varies exponentially from 0.1 to 0.001 md^{-1} over 30 days. At the end of the 30th day, C is steeply raised from 0.001 to 0.1 md^{-1} within 0.01 day (around 15 min), simulating a fast unclogging of the streambed (e.g. erosion by flood event or excavation in the streambed). Then the same exponential decrease is repeated a second time over another period of 30 days. **Figure 2.3a** shows the imposed C over the 60 days. The time series of the stream stage and hydraulic head variations at 20 m from the streambank constitute the input data. The method is tested for different POW sizes: 1 day; 5 days; 10 days. The POW shift is 1 hour. A residual value between two successive estimations of a of 0.1 m is used as termination criterion.

2.3.2. Results of the synthetic data analysis

Figure 2.4 shows the imposed and estimated variations of the retardation coefficient. The retardation coefficient a is estimated and the corresponding C value is calculated according to

known K_a value. In the same way values of *a* in the forward simulation are calculated then compared to the estimated values of *a*. In **Figure 2.4b**, **2.4c** and **2.4d**, the ratio Estimated *C* to Imposed *C* is represented in order to monitor the accuracy of the estimation process.
Continuous variations of the streambed conductance are detected for the different POW (**Figure 2.4b**, **2.4c,** and **2.4d**). According to the size of the POW, the estimation of *a* was carried out between the 3rd and 57th day, and between the 5th and the 55th day for the POW sizes of 5 days and 10 days respectively.
For the three POW sizes, the value of *a* between the 1st and the 25th day are well estimated (*i.e.*, between 50% and 150% of the imposed values). The same applies to the timespan between the 35th and the 55th day. Between the 25th and 35th day the accuracy of the estimation of *a* differs for the different POW sizes. For an increasing POW size, larger mismatches between estimated and imposed conductances can be observed (*i.e.*, under 50% or over 150% of the imposed value). The bias in the estimation of *a* appears when the POW includes hydraulic heads from before or after the sharp change of the imposed *C* on the 30th day. The highest error is made when the POW is centered on the sharp decrease of *C* (500% of the imposed *C*). Moreover, the beginning of the decrease appears 5 days and 10 days too early for the POW sizes of 5 days and 10 days respectively. It appears that the estimation of the value of *a* and its transience is increasingly biased when *C* undergoes a sharp and sudden alteration, for an increasing size of the POW.
In **Figure 2.4b**, sinusoidal variations of *a* are observed. These oscillations show that the parameter *a* tends to be systematically under- or overestimated. The reason for that is the sinusoidal variation of the stream stage and the fact that the convolution assumes an initially relaxed state of the system. Transient hydraulic heads due to stream stage variations prior the current POW leads to an under- or overestimation of *a*. For larger POW sizes this effect is reduced by the increasing ratio of water table variations triggered by stream transience in the current POW to water table variations triggered by stream transience in the previous POW. This analysis shows that the choice of POW can influence the estimated conductance. However, transience in streambed conductance was clearly identified, independent of the choice of the POW. As this method is aiming to identify whether streambed properties are subject to transience, error in the absolute value is not of concern.

2.4. Field data investigation

2.4.1. Study site description

The study site is a floodplain of the Rhône River located in the southern part of Switzerland (**Figure 2.5**). The Rhône glacial valley is filled with approximately 600 m of quaternary deposits [*Besson et al.*, 1991]. The lower 450 m are composed of a succession of different glacial deposits. A layer of fine lacustrine deposits is found from a depth between 150 m to 50 m. This layer is considered as the lower limit of the alluvial aquifer. The 50 m thick alluvial aquifer is composed of post-lacustrine gravelly river deposits. The aquifer is heterogeneous and composed by alternation of gravel and sandy silty-loam layers. The Rhône River is characterized by a glacio-nival dynamics with a high water level in summer and a low water level in winter. Daily variations of approximately 1 m of the Rhône River are caused by hydropeaking resulting from upstream hydro-electricity generation [*Briody et al.*, 2016; *Francis et al.*, 2010; *Nilsson et al.*, 2005; *Sawyer et al.*, 2009] (**Figure 2.5**).

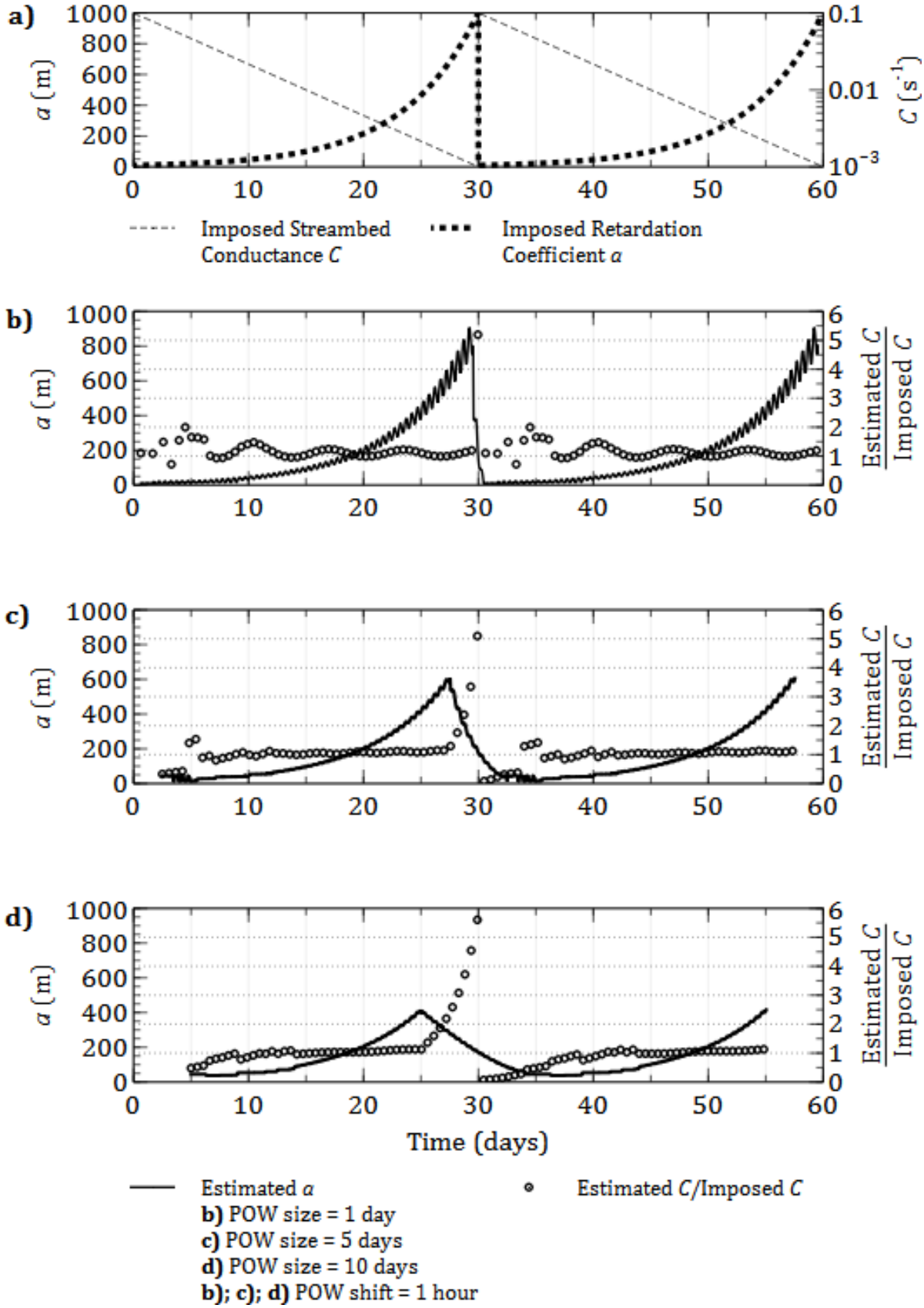

Figure 2.4: **a**) Streambed conductance *C* imposed in the simulation and the corresponding retardation coefficient *a*. **b**), **c**) and **d**) show the estimated retardation coefficients and the ratio Estimated *C* to Imposed *C* for different values of the size of the Parameter Optimization Window (POW) (1, 5 and 10 days). The shift of the POW is 1 day for the 3 POW sizes. From **b**) to **d**) a variation in the accuracy of the estimation of *a* with respect to the POW size can be observed.

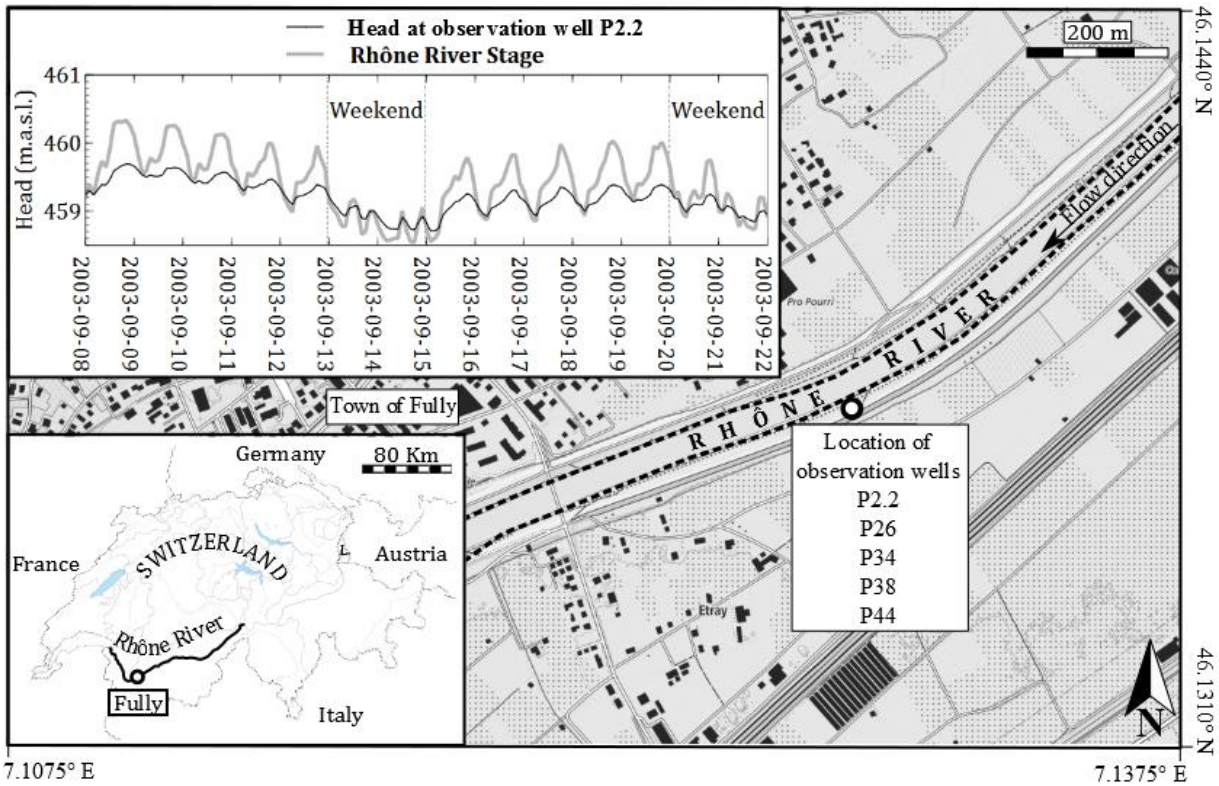

Figure 2.5: Map displaying the location of the study site, Town of Fully, and of the observation wells (WGS 84 coordinate system). The observation wells P2.2, P26, P34, P38, and P44 are located at 2.2, 26, 34, 38 and 44 m from the streambank. The graph (up left corner) shows the Rhône River variations and hydraulic heads at P2.2 during the month of September 2003. The daily variations of the Rhône River stage are due to the exploitation of hydro-electricity (lower stream stage during the weekend is due to lower electricity demand).

A river gauge and 5 observation wells are installed along a line perpendicular to the riverbank, P2.2, P26, P34, P38 and P44 with the respective distances from the river bank of 2.2 m, 26 m, 34 m, 38 m and 44 m. The depth of measurement of each observation is approximately 5 meters below the yearly average of the water table elevation at these points. The river is 52 m wide. The aquifer hydraulic conductivity and specific yield S_y was measured through an aquifer test ($K_a = 6\ 10^{-4}$ ms^{-1} and $S_y = 0.2$). The aquifer is unconfined, thus the storativity S, is approximated by the specific yield S_y,

The hydraulic head and stream stage data have been measured from 1 January 2000 to 31 December 2003 with a time step of 1 hour. This timespan includes a 100-year flood event that happened on the 15 October 2000 (**Figure 2.6**).

2.4.2. Results

The retardation coefficient *a* is optimized for every POW shift of 1 day to obtain the observed groundwater responses. The analysis is carried out for all boreholes individually. According to the daily periodic variations of the Rhône River in the study area due to hydropeaking (5 significant variations of the stream stage a week) a POW size of 7 days covering a week of daily stream stage hydraulic head transience was chosen. With this setting, we obtained a total number of POW of 1445 for each observation well. A residual value between two successive estimations of *a* of 0.1m is used as termination criterion for the parameter estimation. **Figure 2.6** shows the time series of the Rhône River stage (*dark blue dots*) and the observation well P2.2 (*light blue dots*). For the sake of clarity, the other boreholes are not plotted, but produced similar results.

The results for P2.2 are plotted in **Figure 2.7**. The retardation coefficient estimated during the inversion varies between 20 and 150 m over the study period (*red dots*) suggesting the transient

nature of the streambed conductance. **Figure 2.7** also shows the minimal value of the *SSE* reached during each estimation of *a* (*yellow triangles*). In order to quantify how well the simplified analytical solution can reproduce the observed hydraulic heads variations in the different boreholes the Nash-Sutcliffe Efficiency was calculated and provided a satisfying value of 0.99.

2.4.3. Interpretation of the field data analysis

The timeline of the study period has been subdivided into 5 periods. These sub-periods are characterized by different states and dynamics of the gradient between the Rhône River and the riparian water table.

- Periods (1) (see **Figure 2.6** and **Figure 2.7**): This annual low water season (approximatively between November and April) is characterized by a Rhône River stage lower than the riparian water table. Due to the hydroelectricity generation, the level of the Rhône River increases and decreases on a daily basis (especially during the week, period where energy demand is high) with an amplitude of about 1 m (see **Figure 2.5**). Within this period no significant variations of the retardation coefficient are observed (variations of *a* around 10 m). This stability could be explained by periodic gradient inversion between the river and the groundwater: When the aquifer is drained by the river, fine sediments are partly washed away due to the upward seepage of groundwater. When the gradient is reversed (hydropeaking), fine sediments are deposited in the streambed, lowering the hydraulic conductivity and thus the streambed conductance. The alternation of erosion and deposition processes results in only minimal changes of the streambed conductance. This hypothesis can be supported by the rapid decrease of the retardation coefficient observed during the last weeks of December 2002 (Period (5), see **Figure 2.6**) when the hydropeaking is reduced significantly (see **Figure 2.7**, "Hydropeaking Reduction") at around 20% of its typical values during the investigated periods.
- Periods (2) and period (3) (see **Figure 2.6** and **Figure 2.7**): During high water seasons (approximately between May and October), the parameter *a* increases. Within the entire study period, the value of *a* is approximatively 2 to 3 times higher during the high water periods than during the low water periods. In summer when the surface water level is constantly above the riparian water table, a unidirectional infiltration of the river tends to decrease the conductance of the streambed due to the deposit of a lot of fine particles originating from overland flow generated by snowmelt [*Gurnell et al.*, 1996]. During the Period 3, which corresponds also to high water season, a larger gradient (1 m to more than 2 m, **Figure 2.6**) and a stronger variation of *a*, compared to those in Period (2), is observed. The reason for the exceptionally high stream stage during this period is the massive glacier melt caused by the heatwave of summer 2003. Between May 2003 and September 2003 the parameter *a* presents an increase of more than 200% (from 40 m to 150 m over 4 months) with a slope of 1 md^{-1}. However, at the end of Period (3), *a* undergoes a 60% decrease and reach a value of 60 m. This drop of *a* is concomitant with a decrease of the stream stage. The reduced gradient between the stream and the groundwater and its inversion may have caused an unclogging of the streambed (low water period, Periods (1)).

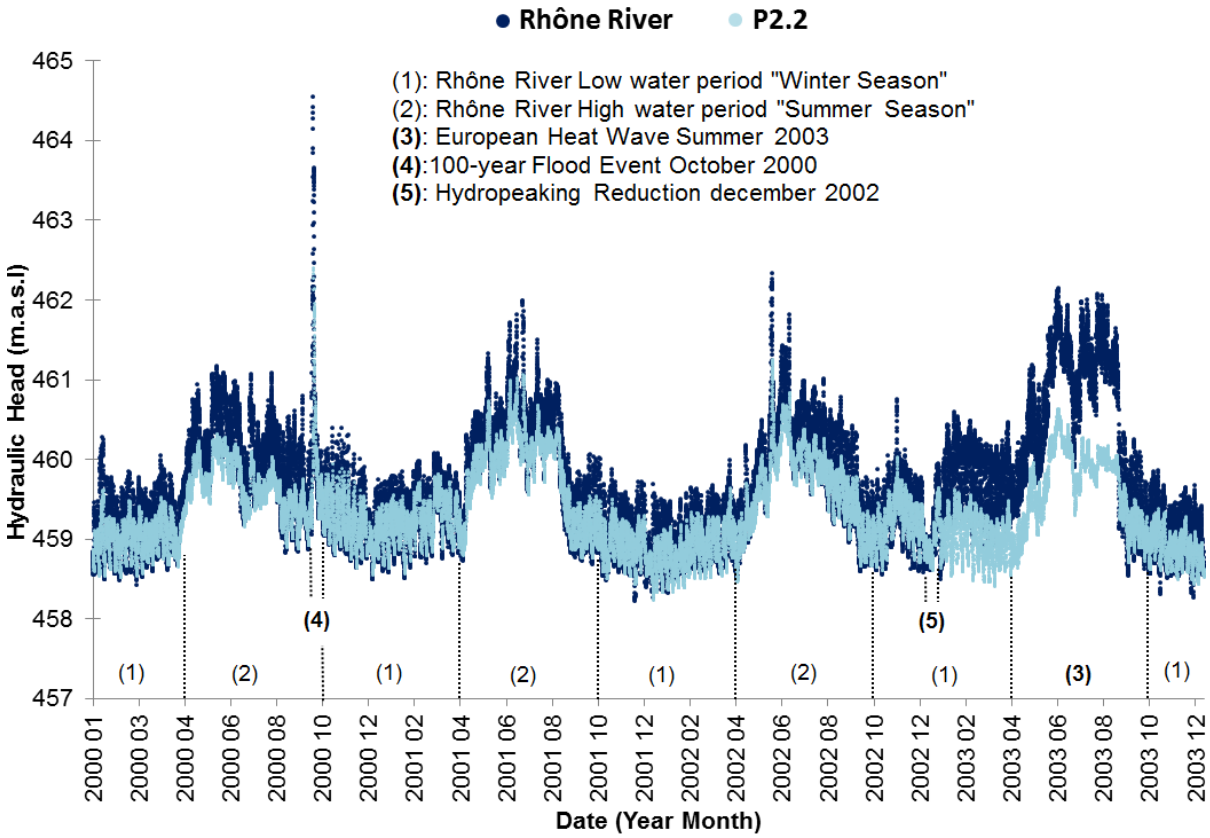

Figure 2.6: Rhône River (Fully, Switzerland) stage variations (dark blue dots) between 1 January 2000 and 31 December 2003, and the hydraulic head variations, during the same period, 2.2 m from the streambank (light blue dots). The estimation of the retardation coefficient *a* using this time series is shown in **Figure 2.7**. The time series is subdivided into 5 periods, with periods (1) and (2) that are repeated annually (low water period in winter and high water period in summer) and covers noteworthy events: a heat wave (3), a 100-year flood (4) and hydropeaking reduction (5).

- Period (4) (see **Figure 2.6** and **Figure 2.7**): This period is marked by a 100-year flood event (**Figure 2.6**) occurring between 13 and 17 October 2000, with a climax on the 15 October. We can observe a drop of *a* (80% drop, see **Figure 2.7**), indicating a significant rise of the streambed conductance. The *SSE* (**Figure 2.7**) increases significantly (250%) compared to its average value. As shown in the *Subsection 2.3.2*, the assumption of a constant value of *a* within a POW can reduce the fit of simulated data with observed data when important and rapid changes of the streambed conductance occur within the POW. It can be assumed that during the flood event high shear stress can mobilize the largest grains and stones (armor layer), protecting the finer grains trapped underneath, which are responsible for the low streambed hydraulic conductivity. The finer grains can be washed away and thus the streambed conductance increases [*Chin et al.*, 1994; *Schalchli*, 1992].

In order to assess to which extent the distance between a borehole and the river affects the results a correlation matrix of estimated *a* between the 5 observation wells was calculated. The correlation coefficients between the estimated *a* range from 0.88 to 0.98. Therefore, the transience in streambed properties at this field site can be identified from different distances. All the above-mentioned trends, obtained using observation well P2.2, were identified for the other observation wells.

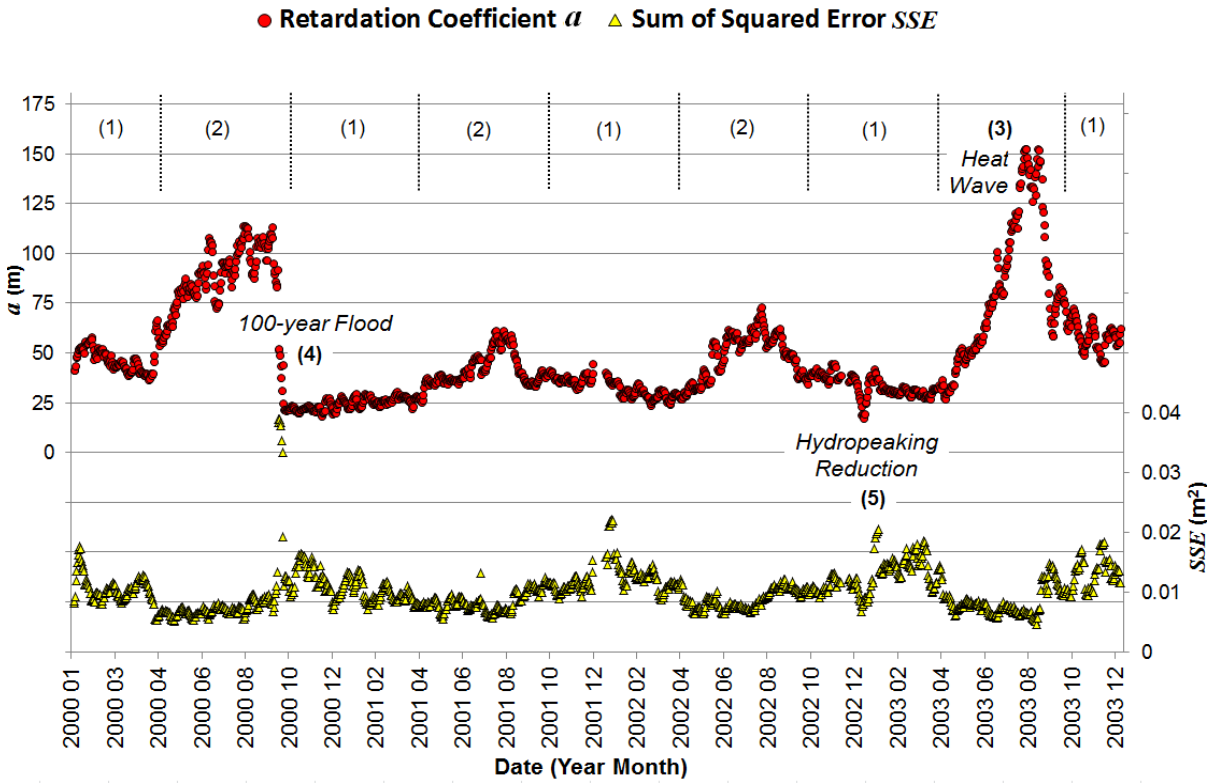

Figure 2.7: Plot of the estimated values of the retardation coefficient, *a*, for the observation well P2.2 (red dots) and of the values of the residual sum of squares *SSE* between field and simulated hydraulic heads for each POW (yellow triangles). The highest value of *SSE* occurred when the retardation coefficient varies strongly (100-year flood). (1), (2), (3), (4) and (5) refers to the periods described in **Figure 2.6**.

2.5. Discussion

Several simplifying assumptions were made in the proposed methodology. For example, it is assumed that the distance *x* of the piezometer to the river does not change with a rising water table, which implied a rectangular shape of the river. This is a critical assumption and limits the applicability of the method to rivers with such a rectangular shape, as the reduced distance between the river and the observation well will result in a decrease of *a*, even though there is no change in streambed conductance. For natural streams with an irregular bathymetry, caution is advised in the application of the proposed method.

Also, homogeneity is assumed for both the aquifer and streambed properties. This assumption is however not critical for the analysis. The estimated streambed conductance represents the average hydraulic properties of the river reach in the vicinity of the borehole. Changes to the streambed structure due to erosion or deposition processes will affect the average hydraulic properties of the streambed, even if the streambed is heterogeneous.

Furthermore, it is assumed that the river is fully penetrating which implies a one-dimensional water flux in a confined aquifer. However, the influence of partially penetrating streambed can be reasonably lumped in the estimation of the retardation coefficient by substitution of a horizontal additional stretch of the main aquifer [*Hantush*, 1965].

It is also assumed that changes of the water table elevations are exclusively related to the transience in the river. This may be problematic if additional hydraulic stresses are present, e.g. groundwater abstraction or recharge by rain. To limit such effects, the observation well should be close enough to the stream edge. In the field example, transience of the streambed was identified for all observation wells (with a distance up to 44 meters from the river).

As illustrated with the synthetic data, the choice of POW has a certain effect on the estimated values of *a*. On the one hand, the choice of a smaller POW size appears to be more suitable

when sharp and sudden changes of the streambed conductance occur. On the other hand, the POW size should be large enough to include a significant amount of observations of stream stage variations and its related aquifer responses. However, for all POWs tested we could clearly identify the transience imposed on the streambed conductance.
Finally, to employ the presented convolution approach, transience in the river is required. Therefore, the reliability of the estimation will be affected if the system is steady or lacking of transience in the stream. On the one hand, streambed conductance transience can occur and yet not be detected because of the lack of floodwave response to analyze. On the other hand, calibration may result in wrong values of the retardation coefficient by fitting noise or measurement errors. This will be the case if insufficient transience is present in the stream. Therefore, the goodness of fit between observed and modeled data will provide a first indication whether sufficient transience is present in the stream. Furthermore, the time series of data should have a sufficiently fine temporal resolution to capture these variations.
The interpretation of the results pointed out the relation between fluvial dynamics (climatic events) and streambed clogging and unclogging events. The results obtained with the presented method tend to confirm the influence of the magnitude of the gradient, its direction, and its dynamics (*i.e.* duration and intensity of the gradient variations) on the streambed conductance. The clogging processes have been observed in laboratory and field tests with streambed hydraulic conductivities ranging from values 2 to 20 times lower for downward seepage (infiltration of the surface water into the groundwater) than for upward seepage [*Rosenberry and Pitlick*, 2009; *Schalchli*, 1992]. Nevertheless, we observed from the results that flood events (Period (4)) can cause a decrease in the streambed conductance probably due to important alteration and erosion of the riverbed sedimentary structure.

2.6. Conclusions

The hydraulic properties of streambed control surface water-groundwater interactions. However, they are hard to measure, and detecting transience is even harder. Numerous field studies documented important changes of hydraulic properties related to erosion and sedimentation processes. The presented method aims at rapidly identifying transience in streambed conductance. To apply the method, time series of river stage and water table data are required as well as a certain transience in the river. The rivers need to have a rectangular shape. If these conditions are present, the approach has significant advantages compared to directly measuring hydraulic properties in the streambed. It is very simple in terms of field instrumentations and workload. Moreover, the estimation can be done on very large and/or fast flowing rivers where direct measurements of the streambed hydraulic properties are virtually impossible. However, given the simplifying assumptions, it is important to note that if no transience is detected, this is no conclusive proof that streambed properties are constant.
The method has been employed successfully in a field case, and a clear transience in the streambed conductance was identified. This has important implications on any quantitative approach aiming at understanding the dynamics between surface- and groundwater in these regions. Above all, this transience should be considered in future modeling approaches.

2.7. References

Besson, O., J. Rouiller, W. Frei, and H. Masson (1991), Campagne de sismique-reflexion dans la vallée du Rhône (entre Sion et Martigny, Suisse), *Bull. Murithienne*, *109*, 45-63.

Briody, A. C., M. B. Cardenas, P. Shuai, P. S. K. Knappett, and P. C. Bennett (2016), Groundwater flow, nutrient, and stable isotope dynamics in the parafluvial-hyporheic zone of the regulated Lower Colorado River (Texas, USA) over the course of a small flood, *Hydrogeol J*, *24*(4), 923-935.

Calver, A. (2001), Riverbed permeabilities: Information from pooled data, *Ground Water*, *39*(4), 546-553.

Carslaw, H. S., and J. C. Jaeger (1959), *Conduction of Heat in Solids*, 2nd ed., Oxford at the Clarendon Press, London.

Chin, C. O., B. W. Melville, and A. J. Raudkivi (1994), Streambed Armoring, *J Hydraul Eng-Asce*, *120*(8), 899-918.

Coleman, J. M. (1969), Brahmaputra River - Channel Processes and Sedimentation, *Sediment Geol*, *3*(2-3), 129-239.

Droppo, I. G., and M. Stone (1994), In-Channel Surficial Fine-Grained Sediment Laminae .1. Physical Characteristics and Formational Processes, *Hydrol Process*, *8*(2), 101-111.

Du, X. Q., Z. J. Wang, and X. Y. Ye (2013), Potential Clogging and Dissolution Effects During Artificial Recharge of Groundwater Using Potable Water, *Water Resour Manag*, *27*(10), 3573-3583.

Fette, M., R. Kipfer, C. J. Schubert, E. Hoehn, and B. Wehrli (2005), Assessing river-groundwater exchange in the regulated Rhone River (Switzerland) using stable isotopes and geochemical tracers, *Appl Geochem*, *20*(4), 701-712.

Francis, B. A., L. K. Francis, and M. B. Cardenas (2010), Water table dynamics and groundwater-surface water interaction during filling and draining of a large fluvial island due to dam-induced river stage fluctuations, *Water Resour Res*, *46*.

Frostick, L. E., P. M. Lucas, and I. Reid (1984), The Infiltration of Fine Matrices into Coarse-Grained Alluvial Sediments and Its Implications for Stratigraphical Interpretation, *J Geol Soc London*, *141*(Nov), 955-965.

Fryirs, K., and D. Gore (2013), Sediment tracing in the upper Hunter catchment using elemental and mineralogical compositions: Implications for catchment-scale suspended sediment (dis)connectivity and management, *Geomorphology*, *193*, 112-121.

Genereux, D. P., S. Leahy, H. Mitasova, C. D. Kennedy, and D. R. Corbett (2008), Spatial and temporal variability of streambed hydraulic conductivity in West Bear Creek, North Carolina, USA, *J Hydrol*, *358*(3-4), 332-353.

Gurnell, A., D. Hannah, and D. Lawler (1996), Suspended sediment yield from glacier basins, *Erosion and Sediment Yield: Global and Regional Perspective*.

Ha, K., D. C. Koh, B. W. Yum, and K. K. Lee (2007), Estimation of layered aquifer diffusivity and river resistance using flood wave response model, *J Hydrol*, *337*(3-4), 284-293.

Hall, F. R., and A. F. Moench (1972), Application of Convolution Equation to Stream-Aquifer Relationships, *Water Resour Res*, *8*(2), 487-&.

Hantush, M. S. (1965), Wells near Streams with Semipervious Beds, *J Geophys Res*, *70*(12), 2829-2838.

Hatch, C. E., A. T. Fisher, C. R. Ruehl, and G. Stemler (2010), Spatial and temporal variations in streambed hydraulic conductivity quantified with time-series thermal methods, *J Hydrol*, *389*(3-4), 276-288.

Hiscock, K. M., and T. Grischek (2002), Attenuation of groundwater pollution by bank filtration, *J Hydrol*, *266*(3-4), 139-144.

HydroGeoSphere (2013), *User Manual*, Anquanty Inc., Waterloo, Ontario, Canada.

Irvine, D. J., P. Brunner, H. J. H. Franssen, and C. T. Simmons (2012), Heterogeneous or homogeneous? Implications of simplifying heterogeneous streambeds in models of losing streams, *J Hydrol*, *424*, 16-23.

Jha, M. K., and A. Singh (2014), Application of genetic algorithm technique to inverse modeling of tide-aquifer interaction, *Environ Earth Sci*, *71*(8), 3655-3672.

Jha, M. K., D. Namgial, Y. Kamii, and S. Peiffer (2008), Hydraulic Parameters of Coastal Aquifer Systems by Direct Methods and an Extended Tide - Aquifer Interaction Technique, *Water Resour Manag*, *22*(12), 1899-1923.

Jha, M. K., K. Jayalekshmi, D. Machiwal, Y. Kamii, and K. Chikamori (2004), Determination of hydraulic parameters of an unconfined alluvial aquifer by the floodwave-response technique, *Hydrogeol J*, *12*(6), 628-642.

Kalbus, E., C. Schmidt, J. W. Molson, F. Reinstorf, and M. Schirmer (2009), Influence of aquifer and streambed heterogeneity on the distribution of groundwater discharge, *Hydrol Earth Syst Sc*, *13*(1), 69-77.

Kollet, S. J., and V. A. Zlotnik (2007), Evaluation of the streambed leakage concept in analytical models using data from three pumping tests, *Hydrogeol J*, *15*(6), 1051-1062.

Kurth, A. M., and M. Schirmer (2014), Thirty years of river restoration in Switzerland: implemented measures and lessons learned, *Environ Earth Sci*, *72*(6), 2065-2079.

Landon, M. K., D. L. Rus, and F. E. Harvey (2001), Comparison of instream methods for measuring hydraulic conductivity in sandy streambeds, *Ground Water*, *39*(6), 870-885.

Lee, B. J., J. H. Lee, H. Yoon, and E. Lee (2015), Hydraulic Experiments for Determination of In-situ Hydraulic Conductivity of Submerged Sediments, *Sci Rep-Uk*, *5*.

Levy, J., M. D. Birck, S. Mutiti, K. C. Kilroy, B. Windeler, O. Idris, and L. N. Allen (2011), The impact of storm events on a riverbed system and its hydraulic conductivity at a site of induced infiltration, *J Environ Manage*, *92*(8), 1960-1971.

Lisle, T. E. (1989), Sediment Transport and Resulting Deposition in Spawning Gravels, North Coastal California, *Water Resour Res*, *25*(6), 1303-1319.

MATLAB (2014), *8.3.0.532 (R2014a)*, The MathWorks Inc., Natick, Massachusetts.

Mutiti, S., and J. Levy (2010), Using temperature modeling to investigate the temporal variability of riverbed hydraulic conductivity during storm events, *J Hydrol*, *388*(3-4), 321-334.

Nilsson, C., C. A. Reidy, M. Dynesius, and C. Revenga (2005), Fragmentation and flow regulation of the world's large river systems, *Science*, *308*(5720), 405-408.

Reynolds, R. J. (1987), Diffusivity of a Glacial-Outwash Aquifer by the Floodwave-Response Technique, *Ground Water*, *25*(3), 290-299.

Rosenberry, D. O. (2008), A seepage meter designed for use in flowing water, *J Hydrol*, *359*(1-2), 118-130.

Rosenberry, D. O., and J. Pitlick (2009), Effects of sediment transport and seepage direction on hydraulic properties at the sediment-water interface of hyporheic settings, *J Hydrol*, *373*(3-4), 377-391.

Sawyer, A. H., M. B. Cardenas, A. Bomar, and M. Mackey (2009), Impact of dam operations on hyporheic exchange in the riparian zone of a regulated river, *Hydrol Process*, *23*(15), 2129-2137.

Schalchli, U. (1992), The Clogging of Coarse Gravel River Beds by Fine Sediment, *Hydrobiologia*, *235*, 189-197.

Shanafield, M., R. G. Niswonger, D. E. Prudic, G. Pohll, R. Susfalk, and S. Panday (2014), A method for estimating spatially variable seepage and hydraulic conductivity in channels with very mild slopes, *Hydrol Process*, *28*(1), 51-61.

Simpson, S. C., and T. Meixner (2012), Modeling effects of floods on streambed hydraulic conductivity and groundwater-surface water interactions, *Water Resour Res*, *48*, W02515.

Smith, J. W. N., and D. N. Lerner (2008), Geomorphologic control on pollutant retardation at the groundwater-surface water interface, *Hydrol Process*, *22*(24), 4679-4694.
Sophocleous, M. (2002), Interactions between groundwater and surface water: the state of the science (vol 10, pg 52, 2002), *Hydrogeol J*, *10*(2), 348-348.
Wang, T. Z., Y. K. Li, M. C. Liang, P. L. Yang, and Z. H. Bai (2014), Biofilms on the surface of gravels and aquatic plants in rivers and lakes with reusing reclaimed water, *Environ Earth Sci*, *72*(3), 743-755.
Winter, T. C., J. W. Harvey, O. L. Franke, and W. M. Alley (1998), *Ground water and surface water : a single resource*, vii, 79 p. pp., U.S. Geological Survey, Denver, Colo.
Woessner, W. W., and K. E. Sullivan (1984), Results of Seepage Meter and Mini-Piezometer Study, Lake Mead, Nevada, *Ground Water*, *22*(5), 561-568.
Wu, G. D., L. C. Shu, C. P. Lu, X. H. Chen, X. Zhang, E. K. Appiah-Adjei, and J. S. Zhu (2015), Variations of streambed vertical hydraulic conductivity before and after a flood season, *Hydrogeol J*, *23*(7), 1603-1615.

Chapter 3

3. Conceptualization and calibration of anisotropic alluvial systems: Pitfalls and biases

Abstract

Physical properties of alluvial environments typically feature a high degree of anisotropy and are characterized by dynamic interactions between the surface and the subsurface. Hydrogeological models are often calibrated under the assumption of isotropic hydraulic conductivity field and steady-state condition. We aim at understanding how these simplifications affect the prediction of water table elevation using physically based models and advanced calibration and uncertainty analysis approaches based on singular value decomposition and Bayesian analysis. Specifically, we present an analysis of the information content provided by steady-state hydraulic data compared to transient data with respect to the estimation of aquifer and riverbed hydraulic properties. It is showed that assuming isotropy or fixed anisotropy may generate biases both in the estimation of aquifer and riverbed hydraulic parameters and in the predictive uncertainty of water table elevations, which can be underestimated. Furthermore, when the anisotropy of the aquifer is indeed estimated jointly with the aquifer and riverbed hydraulic conductivities, in order to prevent estimation bias, it is demonstrated that the information content in steady-state hydraulic heads may be insufficient to uniquely estimate their values. We further explored the information content of transient data as a mean to achieve a better estimation of hydraulic parameters and to reduce the predictive uncertainty of water table elevation. The outcomes of the synthetic analysis are applied to the calibration of a dynamic and anisotropic alluvial aquifer system in Switzerland (The Rhône River). The transient calibration, instead of, or following a steady-state calibration, allows a reduction of the predictive uncertainty of the water table elevation. The results of the synthetic and real-world modeling and calibration exercises documented herein provide insight on future data acquisition as well as modeling and calibration strategies for these environments. They also provide an incentive for evaluation and estimation of commonly made simplifying assumptions, such as the aquifer anisotropy, in order to prevent underestimation of the predictive uncertainty.

3.1. Introduction

In the context of simulating river-aquifer interactions, the estimation of both aquifer and riverbed properties is often required [*Lavigne et al.*, 2010; *Maheswaran et al.*, 2016; *Yihdego et al.*, 2017]. Subsequently, the calibrated model may support predictions concerning aquifer response to changes in the river dynamics caused by river restorations [*Lehr et al.*, 2015; *Schneider et al.*, 2011] or climate changes [*Mas-Pla et al.*, 2012; *Mastrocicco et al.*, 2014]. In current modeling practice, models are often calibrated under the assumption (often made for no other reason than convenience) of horizontally isotropic hydraulic conductivity fields. However, alluvial aquifers are formed by successive vertical and horizontal overlays of channel-bar and channel-fill deposits [*Bridge and Demicco*, 2008]. At a broad scale, the continuity of these geological formations which present different hydraulic properties can lead to a high degree of anisotropy [*Jha et al.*, 2016; *Kenoyer*, 1988; *Zlotnik et al.*, 2011], reaching values as high as 20 [*Kruseman and de Ridder*, 1994]. The impact of horizontal anisotropy on flow through aquifers has been studied for the recovery of hydrocarbons, CO_2 sequestration, and in geothermics. *Willems et al.* [2017] shows that an incorrect assumption of isotropic condition can lead to significant underestimation of geological risks associated with geothermal doublets. For shallow alluvial aquifers, the horizontal anisotropy plays an important role in controlling the water table elevation throughout the aquifer [*Cihan et al.*, 2014; *Quiñones-Aponte*, 1989].

Numerous methods based on aquifer tests have been developed to estimate the horizontal aquifer anisotropy [*Kucuk and Brigham*, 1981; *Mathias and Butler*, 2007; *Mutch*, 2005; *Neuman et al.*, 1984]. Recently, innovative methodologies based on geophysical measurements (electrical anisotropy, values of microgravity) have been tested with success [*Al-Hazaimay et al.*, 2016; *Fernandez-Alvarez et al.*, 2016], but are still not widely used. Therefore, information on the degree of horizontal anisotropy of an aquifer may not be available. Furthermore, estimation of its value may be omitted from the model calibration process, with isotropy assumed for convenience. In some cases, the need for estimation of anisotropy may arise through an inability to achieve a satisfactory fit with observed heads, thereby obviating a structural component of misfit born of an erroneous assumption of isotropy. However, in other circumstances, an assumption of isotropy may not compromise the attainment of a satisfying fit with the calibration dataset, despite the fact that anisotropic condition may indeed prevail. Under these circumstances, estimate of hydraulic conductivities may incur bias as these parameters may adopt a surrogate role to compromise for the erroneous isotropy assumption. This, in turn, may engender bias in model predictions, which are sensitive to the horizontal anisotropy of the aquifer hydraulic conductivity. Additionally, the influence of the river on local groundwater dynamics may be significant. This influence is often dominated by riverbed hydraulic properties [*Fleckenstein et al.*, 2010; *Gianni et al.*, 2016; *Partington et al.*, 2017; *Winter et al.*, 1998]. It follows that estimation of the riverbed hydraulic conductivity should be included into the calibration process, and that uncertainty of its estimation (often considerable) should feature in model-based predictive uncertainty analysis.

The above discussion suggests the following set of questions:

(1) Can a false assumption of horizontal anisotropy of an alluvial aquifer influence the estimation of the water table elevation between measurement points, as well as the uncertainty associated with this estimation?

(2) What is the worth of steady-state head data in reducing uncertainties associated with estimation of riverbed and aquifer hydraulic properties, including the horizontal anisotropy of the aquifer?

(3) Does calibration against a transient dataset support a better estimation of these parameters and result in a reduced predictive uncertainty of heads at non-calibration points within an alluvial aquifer?

In summary, the aim of this work is to evaluate errors incurred by failure to take account of horizontal anisotropy within alluvial aquifers when predicting water table elevations at non-calibration points. It also explores ways in which non-uniqueness of parameter estimation, following the introduction of horizontal anisotropy as a calibration-adjustable parameter, may be reduced when a calibration dataset is only comprised of measurements of hydraulic head. The non-uniqueness, also referred to herein as "post-calibration parameter correlation" or simply "parameter correlation", results from an insufficiency of information provided by the calibration dataset with respect to that required for unique resolution of these correlated parameters. As it will be shown herein, many model outputs are sensitive only to the ratios between two parameters, rather than the individual parameters themselves. This is the source of their non-uniqueness.

First, an interpretative generic model of a river and the alluvial aquifer which surrounds it is defined. The results of forward modeling with respect to relations between parameter values and calculated water tables are presented. Then, the calibration and uncertainty analysis methodology is briefly described. The ramifications, in terms of predictive uncertainty, of assuming an isotropic aquifer are explored through post-calibration predictive uncertainty analysis. The worth, in terms of parameter uncertainty reduction, of head targets for steady-state and transient calibration is then analyzed for the case where the joint estimation of the aquifer and riverbed hydraulic conductivities as well as the horizontal anisotropy of the aquifer hydraulic conductivity is attempted. The outcomes of the synthetic model analysis are then used to support the calibration of a real-world model of an alluvial aquifer associated with the Rhône River in the area of Sion (Switzerland).

3.2. Generic modeling of a river and associated alluvial aquifer

In this section, an overview of the outcomes of forward modeling of a river and an alluvial aquifer system are presented. Heads in the alluvial aquifer along the *Central cross-section* (**Figure 3.1B**) of the aquifer are recorded for each chosen set of parameters. The potential for non-uniqueness in the estimation of the latter is thereby demonstrated and will be quantified in the following section using uncertainty analysis.

3.2.1. Conceptual model and design

A synthetic model is used to develop a conceptual understanding of model calibration and uncertainty analysis within the framework of river and associated alluvial aquifer. The conceptual model includes a losing river reach flowing in a shallow alluvial aquifer surrounded by impermeable geological formations (**Figure 3.1A**). It is assumed that the sedimentary constitution of the alluvial aquifer leads to a spatial heterogeneity oriented parallel to the river channel. This heterogeneity is considered to be pervasive, and therefore, to allow a representation as a general horizontal anisotropy of the hydraulic conductivity whose principal axes are oriented parallel (maximum value) and perpendicular (minimum value) to the river. The groundwater water table has a regional gradient, equal to the river slope, of 0.5%.

The numerical code that is used to simulate this system solves the general equation for two-dimensional horizontal flow in an unconfined anisotropic aquifer:

$$\frac{\partial}{\partial x}\left(K_x h \frac{\partial h}{\partial x}\right) + \frac{\partial}{\partial y}\left(K_y h \frac{\partial h}{\partial y}\right) = S_y \frac{\partial h}{\partial t} \qquad \textbf{3.1}$$

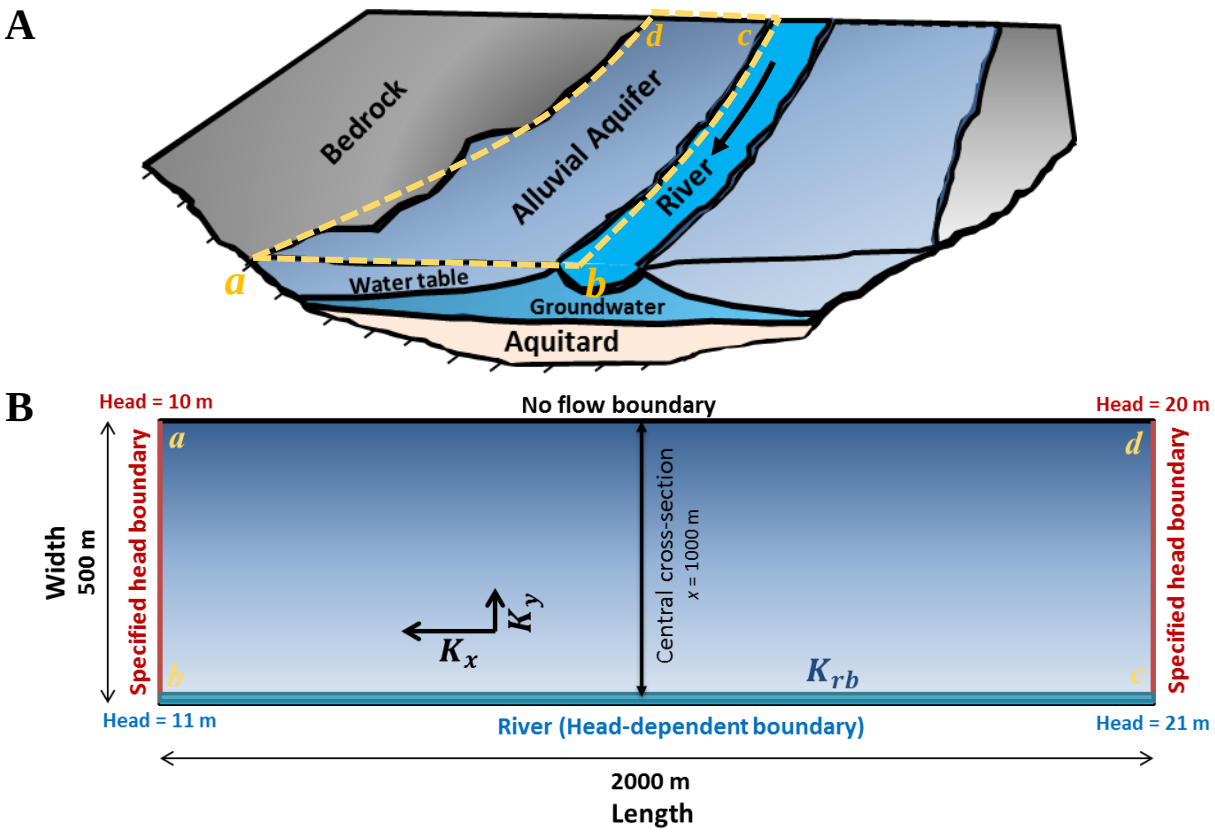

Figure 3.1: A) Conceptual model of an alluvial aquifer traversed by a losing river (flowing from c to b) and surrounded by an impermeable bedrock and an aquitard. B) Model design and boundary conditions defined from the conceptual model.

where h is the hydraulic head at a specific location at time t, K_x is the hydraulic conductivity along the x-axis, K_y is the hydraulic conductivity along the y-axis and S_y is the specific yield. The model has a no-flow boundary along its upper edge, a specified head boundary at its left and right edges, and a head-dependent boundary along its lower edge, representing the river. Flow into the model domain at any point along the latter boundary is calculated using Darcy's law from the head difference between the user-specified river stage and that pertaining to the aquifer immediately beneath the river at the same location. The heads over the model domain are obtained using the finite element numerical modeling code FEFLOW 7.0 [*Diersch*, 2014]. The dimensions of the model domain are 2 km in the longitudinal direction and 500 m in the transversal direction. The longitudinal length of the model domain is sufficiently large to limit the influence of fixed head boundary conditions on heads calculated along the *Central cross-section* (**Figure 3.1B**). These heads are the focus of the present study.

Specified heads along the right edge (line *cd*) and left edge (line *ab*) of the model domain are 20 m and 10 m respectively. The aquifer bottom elevation increases linearly from 0 to 10 m from the left boundary *ab* to the right boundary *cd*. The spatial model discretization consists of a 2x2 m structured squared mesh.

Along the lower edge of the model domain (line *bc*), a head-dependent boundary representing the river is imposed. The head values decrease linearly from 21 m to 11 m from *c* to *b*, for steady-state simulations. For transient simulations, the entire head-dependent boundary (river stage) varies according to a sinusoidal variation with an amplitude of 1 m and a period 2 days. Aquifer parameters are the hydraulic conductivity parallel to the river K_x (direction of maximum hydraulic conductivity) and the hydraulic conductivity perpendicular to the river K_y (direction of minimum hydraulic conductivity). The horizontal anisotropy of the aquifer A_h is

defined as the ratio K_y/K_x . The riverbed hydraulic properties is defined by the riverbed conductance K_{rb}.
The specific yield of the aquifer S_y is set to a value of 0.2, a typical value for silty-gravely material [*Morris and Johnson*, 1967]. Apart from groundwater recharge by river infiltration, no other recharge is applied to the aquifer under either steady-state or transient conditions.
Head values calculated along the *Central cross-section* (**Figure 3.1B**) will be firstly used to characterize the water table response to variations in the parameters K_x, A_h and K_{rb} and then as calibration targets and predictions in the following sections.

3.2.2. Water table sensitivity to model parametrization

In order to illustrate the potential non-uniqueness in values of K_x, A_h and K_{rb} estimated through calibration of a river-alluvial aquifer model, an analysis of the water table elevation dependence on these parameters is presented in this section. The synthetic model is run for different values of the parameters K_x, A_h and K_{rb} and the water table elevations, computed along the *Central cross-section*, are plotted.
Figure 3.2 shows water table elevations along the *Central cross-section*, computed for different values of the ratio K_x/K_{rb}, and horizontal anisotropy of the aquifer A_h. It appears that different combinations of K_x, A_h and K_{rb} can generate a same value of the water table elevation at certain distances from the river (*circles*). Therefore, suggesting potential non-uniqueness when these parameters are to be estimated against water table elevations. For example, an anisotropic aquifer with a A_h value of 0.5 and K_x/K_{rb} equal to 1 (*green dotted line*) may be confused with an isotropic aquifer with a A_h value of 1 and a K_x/K_{rb} ratio of 10, 50 or 100 (*circles*). Same observation can be made for different parameter combinations. Hence, only one head calibration target is insufficient to allow unique estimation of the three parameters (Unique estimation of three parameters based on a single observation is a mathematical impossibility, in any case.).
Moreover, **Figure 3.3** shows that calibration non-uniqueness can arise from post-calibration correlation between the parameters K_x and K_{rb} for a specified horizontal anisotropy, even where two or more head observation targets are included in the calibration dataset. It can be observed that, for a same value of the ratio K_x/K_{rb}, but different values of the respective parameters, water table profiles along the *Central cross-section* are identical for a same value of A_h. Hence, K_x and K_{rb} are therefore indivually irresolveable.
Finally, we consider only the estimation of horizontal anisotropy, **Figure 3.4** depicts heads calculated close to the river (*circle*), as well as heads calculated at increasing distances from the river edge for different values of A_h (*oval*). It can be observed that the estimation of horizontal anisotropy of the aquifer will be hindered by the flattening of the head profile with distance from the river. For instance, if the head measurement error is 1 cm, then an anisotropy of 0.01 cannot be distinguished from an anisotropy of 0.02 using head observations beyond a distance of about 400 m from the river.
The observations made in this section point out that the estimation of hydraulic parameters based on steady-state head data is likely to be non-unique. Furthermore, the degree of non-uniqueness will depend on the number and locations of head calibration targets. Where an important model prediction is sensitive to individual parameters whose values cannot be resolved through the inversion process, then parameter non-uniqueness will promulgate a high level of predictive non-uniqueness, i.e. uncertainty.

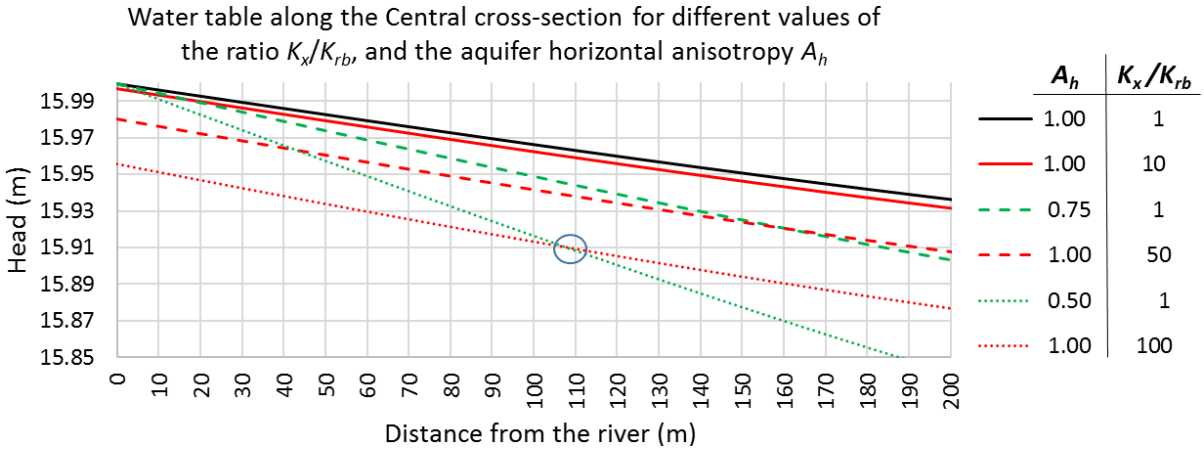

Figure 3.2: Water table elevations along the *Central cross-section* of the model domain. As a reference, the black solid line represents the water table elevation simulated using an isotropic aquifer A_h = 1 and K_x/K_{rb} = 1. The green lines depict the results for an anisotropic aquifer and K_x/K_{rb} = 1 while the red lines pertain to an isotropic aquifer and $K_x/K_{rb} > 1$. For all simulations, the value of K_x is equal to 10^{-3} m/s.

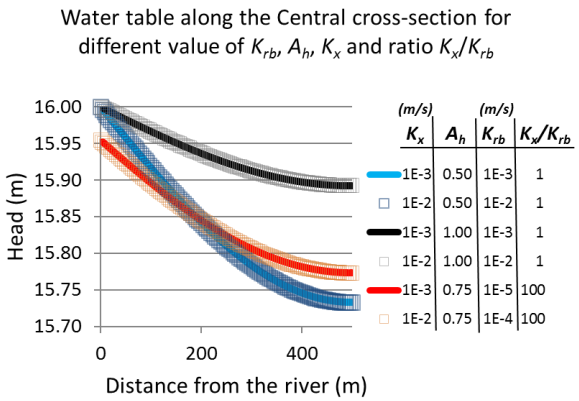

Figure 3.3: The graph shows that for same values of the ratio K_x/K_{rb} and A_h, even though the values of K_x and K_{rb} are different, the hydraulic heads along the *Central cross-section* of the model domain are identical (solid lines and square symbols represent groundwater heads). For instance, the hydraulic heads for the first and second row of the legend are the same, even though the values of K_x and K_{rb} are different (The same applies for the rows 3 and 4, and for the rows 5 and 6).

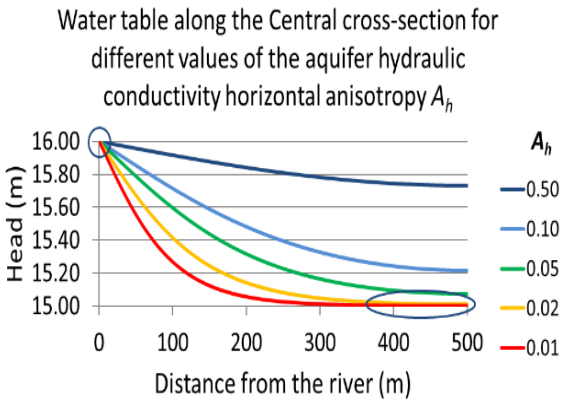

Figure 3.4: The graph shows the water table elevation along the *Central cross-section* for different values of A_h. It can be seen that the hydraulic gradient diminishes with distance from the river and that with increasing values of anisotropy, the values of heads convergence to a minimum. This minimum value represents the elevation of the water table without the influence of the river infiltration.

What may be worse, however, is that parameter uncertainty may be underestimated and predictions that are sensitive to either of these parameters may also be underestimated. So too can risks associated with a course of management action that relies on this prediction. This is explored in the following sections where we will attempt to demonstrate the necessity of including all of A_h, K_x and K_{rb} in the calibration process, despite the lack of uniqueness of the estimated value of the parameters, if predictive uncertainty is to be properly quantified.

Of course, ill-posedness of the inverse problem could also be relieved through supplementation of the calibration dataset with observed values of water fluxes through the riverbed. Unfortunately, however, the potential information gain achieved through the use of these measurements is often outweighed by the large amount of noise associated with measurements

of this type [*Brunner et al., 2012*; *Schilling et al.*, 2014], especially for large rivers with heterogeneous streambed hydraulic properties. [*Harmel et al.*, 2006; *Herschy*, 1995].

3.3. Methods: Parameter identifiability and predictive uncertainty

In this section, we present formal methods through which the well- or ill-posedness of an inverse problem can be evaluated, and through which the consequences for predictive uncertainty can be quantified [*Doherty*, 2015]. We apply these methods for the analysis of the calibration process of the river-aquifer model that was discussed in the preceding section.

3.3.1. Truncated singular value decomposition

A matrix Z has a null space if there exists a non-zero vector x for which:

$$0 = Zx \qquad \textbf{3.2}$$

The matrix Z represents the action of a model on its parameters x to produce a set of outputs employed for model calibration. If **equation 3.2** holds, then a null space exist. Consequently, if a parameter set can be found that fits the calibration dataset, it is possible to find another set of parameters that also fits the calibration dataset, simply through addition of x to the parameter set. Non-uniqueness, and the existence of a null space, are thus two descriptions of the same phenomenon.

The sensitivity matrix J of model outputs to estimated parameters (often referred to as the Jacobian matrix) is used to represent the linearized action of the model on its parameters under calibration condition. It can be used in place of Z in the above **equation 3.2** and thus singular value decomposition can be employed to regularize ill-posed inverse problems. It achieves this through subdividing parameter space into two orthogonal subspaces. One of these is the null space of J, as defined in **equation 3.2** (J replacing Z). Its orthogonal complement is defined as the solution space. Provided that certain conditions are met (see *Doherty* [2015]), a minimum error variance solution to an ill-posed inverse problem can be achieved through restricting solution of that problem to the solution space only. Meanwhile, exploration of the null space allows the identification of combinations of parameters that are inestimable, i.e. parameters that are either insensitive, or which exhibit a high degree of post-calibration correlation. Furthermore, it allows to explore the uncertainties that are associated with model predictions which are sensitive to individual members of correlated parameter pairs [*Doherty*, 2015; *Hunt et al.*, 2007]. Singular value decomposition of the sensitivity matrix J gives:

$$J = USV^t \qquad \textbf{3.3}$$

In **equation 3.3**, U is an orthonormal matrix whose columns span model output space, V^t is the transpose of V, another orthonormal matrix. The columns of V span the parameter space. S is a diagonal matrix whose diagonal elements contain singular values. These values are arranged from highest to lowest starting from the top and ranging to zero. The number of singular values, which are significantly different from zero, defines the number of dimensions of the solution space. The number of parameters minus the number of dimensions of the solution space is the dimensionality of the null space. According to where singular values approach zero, the V matrix can then be partitioned as [*Doherty*, 2015; *Moore and Doherty*, 2005]:

$$V = [V_1 V_2] \qquad \textbf{3.4}$$

This outcome is also referred as "truncated singular value decomposition". When partitioned in this way, the columns of V_1 span the solution space while those of V_2 span the null space. The columns of V_1 define combinations of parameters which are uniquely estimable on the basis of the calibration dataset, while the columns of V_2 identify combinations of parameters which belong to the null space, and are hence inestimable.

3.3.2. Parameter identifiability and predictive uncertainty

The identifiability of a parameter quantifies the ability of the calibration process to uniquely resolve its value. *Doherty and Hunt* [2009] show that this statistic can be viewed in two ways. Firstly, it is the square of the cosine between a parameter and the projection of that parameter into the calibration solution space. It is also the diagonal element of the resolution matrix as it pertains to that parameter. The resolution matrix R expresses the relationship between the value of a parameter as estimated through an ill-posed inverse problem and the true, but unknown, value of that parameter. Therefore, the resolution matrix is an orthogonal projection operator onto the calibration solution space expressed as:

$$R = V_1 V_1^t \quad \textbf{3.5}$$

If an inverse problem is well-posed, the resolution matrix is the identity matrix. Where it is ill-posed, the resolution matrix is rank-deficient. Each row of the resolution matrix defines a set of weights through which real-world parameters are averaged to form the value of an estimated parameter. Under these circumstances, the diagonal elements pertaining to at least some parameters will be less than 1, they may be as low as zero.

The identifiability of a parameter is thus a number that can range between 0 and 1. If it is 0, the calibration dataset carries no information with respect to that parameter. If it is 1, the parameter can be estimated uniquely, but not without error because of the presence of measurement noise in the calibration dataset. Where the identifiability of a parameter is between 0 and 1, the calibration dataset carries information with respect to a parameter, but insufficient information to support its unique estimation.

If a parameter is informed by the calibration dataset, but this information is insufficient for its unique estimation, this is an outcome of the sharing of calibration information with other parameters. The parameter thus suffers post-calibration correlation with one or more of the other parameters. The identities of these other parameters, and the extent of their correlations, may be ascertained through inspection of the columns of the V_2 matrix, which span the calibration null space. However, an alternative means of specifying this correlation is to examine the posterior parameter covariance matrix calculated using the linearized form of Bayes equation as [Doherty, 2015]:

$$C_{post(k)} = C_{pre(k)} - C_{pre(k)} J^t \left[J C_{pre(k)} J^t + C_{(\varepsilon)} \right]^{-1} J C_{pre(k)} \quad \textbf{3.6}$$

In **equation 3.6**, $C_{pre(k)}$ is the prior covariance matrix of parameters that are estimated through the calibration process while $C_{(\varepsilon)}$ is the covariance matrix of measurement noise.

Let s be a prediction made by a calibrated model. Let the elements of the vector y_s contain sensitivities of this prediction with respect to model parameters. The post-calibration variance of the uncertainty of this prediction, σ_s^2, is easily calculated from the posterior covariance matrix of parameters using the standard relationship for propagation of variance:

$$\sigma_s^2 = {y_s}^t C_{post(k)} y_s \quad \textbf{3.7}$$

That gives:

$$\sigma_s^2 = {y_s}^t C_{pre(k)} y_s - {y_s}^t C_{pre(k)} J^t \left[J C_{pre(k)} J^t + C_{(\varepsilon)} \right]^{-1} J C_{pre(k)} y_s \quad \textbf{3.8}$$

The first term on the right of **equation 3.8** is the prior (i.e. pre-calibration) uncertainty variance of the prediction while the second term quantifies the reduction in predictive uncertainty variance achieved through conditioning by the calibration dataset.

In the following section, we employ **equation 3.8** under the assumption that anisotropy is completely known (and assumed to be 1.0), and under the assumption that it is not. The assumption of known anisotropy is simulated in **equation 3.8** through the allocation of zero

prior variance to this parameter. It will be shown that the cost of this convenience is a significant underestimation of the posterior uncertainties of model predictions.

3.4. Parameters estimation and predictive uncertainty biases

3.4.1. Bias in parameters estimation

During the model calibration, an objective function, representing the average discrepancies between simulated and observed heads, is calculated. If an inverse problem is well-posed, model calibration is achieved through minimizing this objective function. If it is ill-posed, the objective function is reduced under regularization constraints to a value that is commensurate with that expected from measurement noise. In real-world model calibration, so-called "structural noise" born of model inadequacies also contributes to model-to-measurement misfit. In the present synthetic model, structural noise exists only to the extent that horizontal anisotropy is given an incorrect value.

Water table elevations along the *Central cross-section* of the synthetic model were calculated using parameter values of $K_x = 10^{-3}$ m/s, $K_{rb} = 10^{-4}$ m/s and $A_h = 0.1$. They were calculated at a spacing of 25 m over the 500 m length of this section. They were then used as head targets for model calibration wherein isotropic conditions were assumed, $A_h = 1$. The parameters K_x and K_{rb} were estimated.

For each calibration instance, a pair of 2 water table elevations, extracted along the *Central cross-section*, was selected to comprise the calibration dataset. A total of 10 sequences of well pairs were defined in this manner. Each sequence was characterized by a different distance of the closest observation to the river. These 10 sequences were thus named after the closest well to the river (along the *y-axis* in **Figure 3.5A**) which are *y = 0, 50, 100, 150, 200, 250, 300, 350, 400* and *450* m (see *symbols* in the legend of **Figure 3.5A** and **B**). Each member of each sequence was comprised of a pair of wells; the distance between these 2 wells increases by steps of 25 m. The first separation distance between head observations is 0 m, which allow to encompass the limiting case considering only one well. The number of head observations in each sequence depends on the distance of the closest well to the river, which defines the sequence. For example, the sequence defined by a distance of 0 m of the closest well to the river ($y = 0$ in **Figure 3.5A** and **B**) contains 21 pairs of wells, i.e. the initial distance of separation distance between head observations of 0 plus the 20 steps of 25 m until a final distance of 500 m. By comparison, the sequence that begins with the closest well to the river at 150 m contains only 15 pairs of wells.

For each calibration exercise, the model-to-measurement misfit was minimized. No synthetic noise was added to the head measurements. Hence, failure to achieve an objective function of zero was an outcome of structural noise incurred by the assumption of horizontal isotropy that was employed when calibrating the model. Recall that observations comprising the calibration dataset were computed using a A_h value of 0.1 and that during the calibration the model was wrongfully assumed isotropic. By calibrating the model against each pair of heads that comprise each sequence, the pattern of structural error that emerged from a false assumption of horizontal isotropy has been monitored.

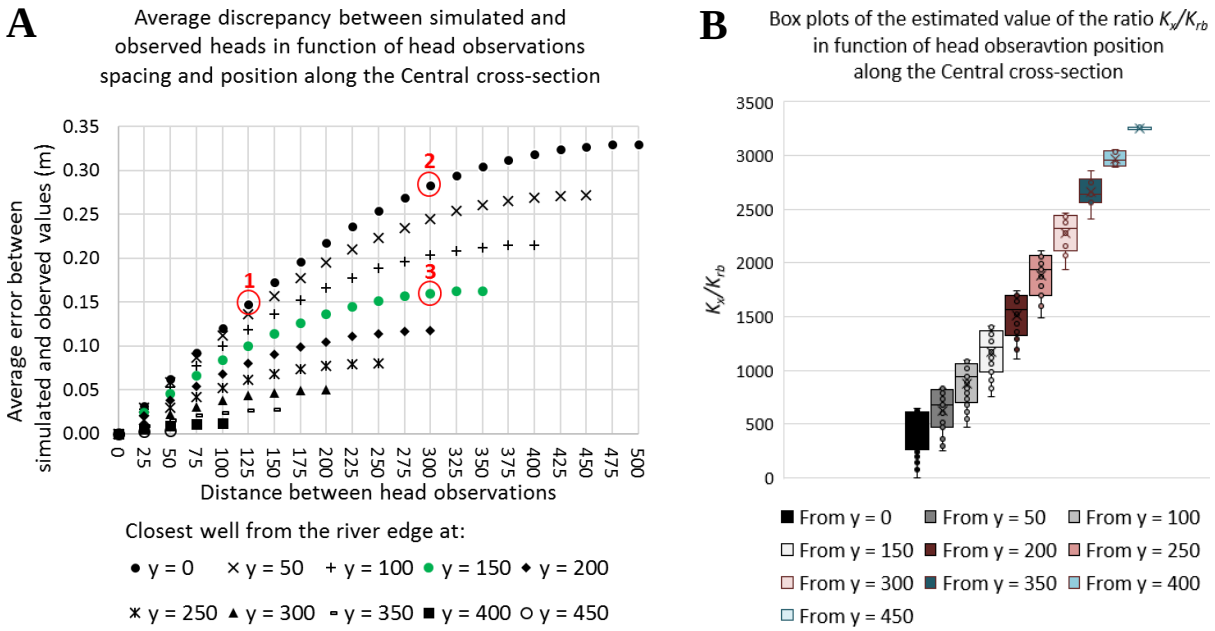

Figure 3.5: A) Post-calibration average error between simulated ($A_h = 1$) and observed ($A_h = 0.1$) heads plotted against inter-observation-wells distances (*x-axis*) for different values of the distance of the closest well to the river (*symbols in the legend*). **B**) Box plots of estimated values of the ratio K_x/K_{rb} including all well pairs for each sequence.

Figure 3.5A depicts the final average error between observed head values and their computed counterparts plotted against the distance between the wells of each pair (*x-axis*) for each sequences (*symbols*). On the one hand, it can be observed that, for all sequences, the value of the average discrepancy between simulated and observed heads increases with increasing distance between the wells of each pair (*x-axis*). On the other hand, the average error decreases with increasing distance from the river edge of the closest well to the river within each pair (*symbols*). For instance, in **Figure 3.5A**, the *red circle 1* shows the post-calibration average error with a closest well to the river located at the river edge (y = 0) and a second well at a distance of 125 m from the first one (along the *Central cross-section*). The *red circle 2* represents the average error with the same first well (y = 0) and a more distant well at 300 m from it. In both cases, the closest well to the river is the same; only the distance separating this well from the second one changes. It can be observed that, because of the increased distance separating the two wells, the average misfit is higher for the *red circle 2* than for the *red circle 1*. For the *red circle 2* and *red circle 3*, the distance separating the two wells in these cases is the same (same value on the *x-axis*). However, the average misfit is higher for the *red circle 2* than for the *red circle 3*. This is an outcome of the fact that the closest well to the river for *red circle 3* is greater than that for the *red circle 2*. Moreover, considering that for *red circles 1* and *3* the average errors are the same, we reach the conclusion that not only the distance between the wells influences the value of the post-calibration misfit, but also the distance between the river and the closest well to the river.

Furthermore, it can be observed in **Figure 3.5A** that for many pairs of wells, the final average error between observed and simulated heads achieved through calibration of the model under a false assumption of isotropy can approach zero (It is zero for *x = 0*). Therefore, considering real-world datasets, certain values of the post-calibration average error between simulated and observed heads may be commensurate (or less) with the one expected according to measurement error that would prevail in the datasets. Consequently, many of the fits depicted in **Figure 3.5A** could thus be construed as "good" or "satisfying" fits".

The error in the estimation of the ratio K_x/K_{rb} achieved through these calibration exercises is shown in **Figure 3.5B**. Each box plot represents the range of values estimated for K_x/K_{rb} for a

sequence of wells pairs. A systematic overestimation of this ratio can be observed, this being an outcome of estimating it under the false assumption of isotropy. Overestimations by more than two orders of magnitude occur for most of the sequences (*y = 150* to *y = 450*).
In sum, the results of this calibration exercise demonstrated that not only may an erroneous assumption of horizontal isotropy of the hydraulic conductivity go unnoticed (Misfit commensurate with expected measurement noise), they also demonstrated that wrong assumption of horizontal isotropy of the aquifer might lead to significant error in the estimation of key parameters, such as K_x to K_{rb}. These parameters adopt a surrogacy role to compensate the structural error and achieve the better fit possible. Consequently, their estimations are systematically biased by the structural error. The next section demonstrates a further outcome of mistakenly assuming horizontal isotropy, this being considerable underestimation of predictive uncertainty.

3.4.2. Bias in predictive uncertainty

In this section, the pre-calibration and post-calibration uncertainties of the predictions of water table elevations at distances of 10, 20, 40, 100, 200 and 400 m from the river along the *Central cross-section* have been calculated. In each case, a head observation at one of the distances aforementioned is used as calibration target and the uncertainty in the predictions at the remaining distances from the river are calculated.
The predictive uncertainty is calculated using **equation 3.8**. In each case, post-calibration predictive uncertainties are calculated for two different calibration setup. In the first place, the model is assumed to be horizontally isotropic; in this case only K_x and K_{rb} are estimated. Secondly, all the three parameters K_x, K_{rb} and A_h are estimated. The post-calibration predictive uncertainty is then assessed for both calibration parametrizations. $C_{(\varepsilon)}$ was assumed to be diagonal with elements equal to 0.01 m^2 (corresponding to a standard deviation of measurement noise equal to 0.1 m). $C_{pre(k)}$ was also assumed to be diagonal, with all diagonal elements equal to 1.0 for K_x and K_{rb}, and 0.5 for A_h (the values pertain to the logs base 10 of the estimated parameters).
Figure 3.6 shows the results of the pre- and post-calibration uncertainties estimation. The *squares* represent the pre-calibration (*red*) and post-calibration (*green*) standard deviations of predictive uncertainty calculated using models that estimate only K_x and K_{rb} (A_h was assumed to be 1). The *triangles* represent the pre-calibration (*red*) and post-calibration (*green*) standard deviations of predictive uncertainty for models that estimate K_x, K_{rb} and the aquifer anisotropy A_h. It can be observed that for all cases that admit no prior uncertainty on A_h by excluding it from the calibration process, predictive uncertainties associated with water table elevations calculated along the *Central cross-section* of the model domain are in systematically underestimated. This underestimation follows from the false assumption of perfect knowledge of A_h. Furthermore, if prior uncertainty in A_h is admitted (*triangles*) it can be seen that the position of the calibration target, exerts a significant influence on the uncertainty of predicted water table elevations. A high uncertainty remains when the calibration targets are close to the river and when water table elevations are predicted far from it.
The above analysis illustrates the importance of including aquifer horizontal anisotropy as an adjustable parameter in the uncertainty analysis process. Failure to include it as an adjustable parameter in the calibration process may result in an unquantifiable parameter and predictive bias. Inclusion of A_h in the calibration process does not result in unique estimation of its value. However, it does remove bias in the predictive uncertainty.

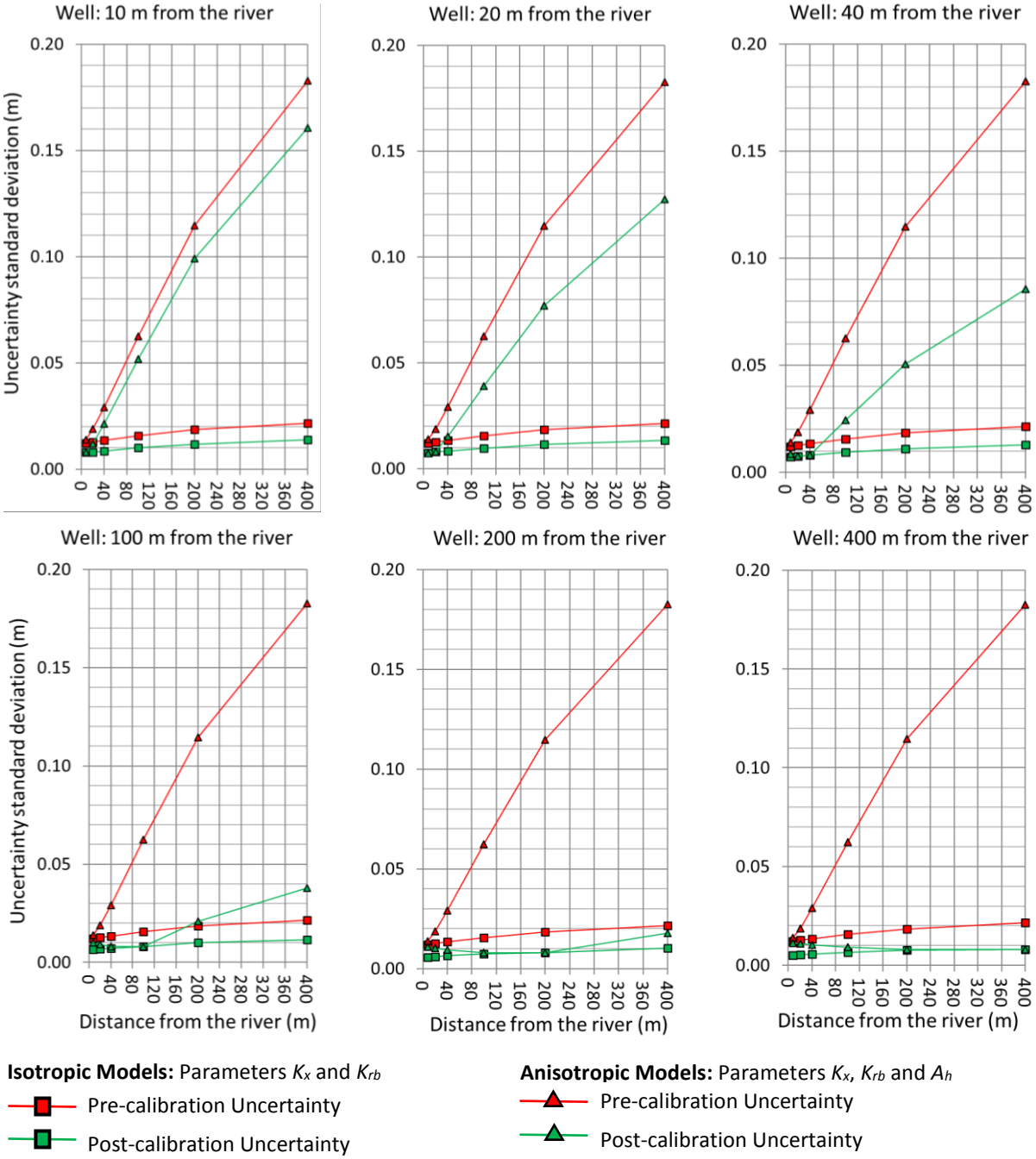

Figure 3.6: Estimation of the pre- and post-calibration standard deviations of predictive uncertainties of heads for calibration processes including solely K_x and K_{rb} (assuming knowledge of A_h) and calibration processes including all parameters K_x, K_{rb} and A_h at different distances from the river edge (10, 20, 40, 100, 200 and 400 m). The title of each graph designates the wells (distance from the river edge) used as calibration targets for the estimation of the post-calibration predictive uncertainty standard deviation for the two abovementioned calibration strategies.

It is worth noting here, that modern calibration codes that include numerical regularization are not troubled when asked to solve an ill-posed inverse problem. In fact, recognition of the ill-posedness of the problem is essential to obtain a solution to that problem which is of minimized error variance; see *Doherty* [2015].

In the next section, the identifiability of K_x, K_{rb} and A_h parameters, and thus the potential reduction of their uncertainties and those of the sensitive predictions, is analyzed and quantified

by calculating the resolution matrix R obtained when truncated singular value decomposition is employed as a numerical regularization device.

3.5. Calibration approaches and parameters identifiability

The previous section showed that omitting the horizontal anisotropy from the calibration and predictive uncertainty analysis process could cause an artificial reduction in the perceived uncertainty of water table elevation predictions. Moreover, whereas in some cases of model calibration an incorrect assumption of isotropic condition can be revealed by a compromised fit with the calibration dataset, in other cases an acceptable fit with that dataset can be achieved (i.e. a fit that is commensurate with that expected from measurement noise). Therefore, unbiased estimation of parameters and avoidance of underestimation of predictive uncertainty appears to only be achieved where horizontal anisotropy is therefore explicitly included in the calibration and predictive uncertainty analysis process. Nevertheless, the question of how to reduce to a minimum the parameters uncertainty, and thus the predictive uncertainty, when considering all parameters, which prevents bias but causes even more non-uniqueness, remains. In this section, the capacity of calibration datasets, consisting of observed steady-state and transient heads, to constrain the values of K_x, K_{rb} and A_h, is analyzed.

3.5.1. Steady-state calibrations

First, the calibration dataset is comprised of a head observation in only one well located along the *Central cross-section* at 100 m from the river. The modeled aquifer is anisotropic with $A_h = 0.5$, K_x/K_{rb} is equal to 100 and K_x is equal to 10^{-3} m/s. The information content of the calibration dataset with respect to these parameters, i.e. the identifiability of these parameters, is equal to the respective diagonal elements of the resolution matrix R calculated using **equation 3.5**. These are listed in **Table 3.1**. The dimensionality of the solution space is one (only one observation). **Table 3.1** shows that the identifiability of A_h is close to zero while those of K_x and K_{rb} are around 0.5. Similar results to those depicted in **Table 3.1** are obtained at other observation well locations along the *Central cross-section*. The post-calibration correlation between the K_x and K_{rb} parameters can be revealed through principal component analysis of $C_{post(k)}$ calculated using **equation 3.6**. The eigenvectors forthcoming from this analysis are also shown in **Table 3.1**. The large values of the components corresponding to K_x and K_{rb} in the eigenvector, corresponding to the highest eigenvalue, evince the high post-calibration correlation between these two parameters and explain why their individual identifiability are less than 1.0. In sum, where the calibration dataset is comprised of a single well, the one-dimensional solution space does not permit to estimate unique values for K_x, K_{rb} and A_h. Furthermore, the correlation between the parameters K_x and K_{rb} is pointed out by the analysis of the parameter solution space**.**

Where more wells are added to the steady-state calibration dataset (wells along the *Central cross-section*), the results are as shown in **Table 3.2**. The S matrix has two non-zero singular values, indicating a solution space dimensionality of 2. Therefore, the null space has only one dimension. The values of K_x and K_{rb} remained highly correlated and solely their ratio can be estimated with a higher certainty. However, A_h is uniquely identifiable. Nevertheless, the lower value of the second singular value associated with its estimation results in a high degree of potential contamination of this estimate by noise associated with the calibration dataset.

Table 3.1: Results of the inversion process using one well. S is the matrix of singular values, V_1 defines combinations of parameters which are uniquely estimable on the basis of the calibration dataset, R is the resolution matrix (the values along its diagonal represent the identifiability of each parameter). *Eigenvectors* is the matrix resulting from the decomposition of $C_{post(k)}$, the post calibration parameter error covariance matrix. The parameter names are displayed next to associated row, values are rounded to the second decimal, symmetric values of the resolution matrix are replaced by the symbol * and null values are replaced by the symbol - for better readability).

S		
0.50	-	-

	R		
K_x	**0.04**	0.04	0.12
K_{rb}	*	**0.04**	0.12
A_h	*	*	**0.37**

V_1
0.20
0.19
0.61

	Eigenvectors		
K_x	-0.71	0.11	-0.70
K_{rb}	-0.70	-0.11	0.70
A_h	0.00	0.99	0.15

Table 3.2: Results of the inversion using two wells or more. The overall description is similar to **Table 3.1**.

S		
0.57	-	-
-	0.10	-
-	-	-

	R		
K_x	**0.50**	0.50	0.00
K_{rb}	*	**0.49**	0.00
A_h	*	*	**1.00**

V_1	
0.00	0.71
0.00	0.70
1.00	0.00

	Eigenvectors		
K_x	-0.70	-0.71	-0.03
K_{rb}	-0.71	-0.70	-0.03
A_h	0.00	0.04	0.99

Consequently, the calibration of the parameters using steady-state head data is characterized by non-uniqueness (and hence post-calibration correlation). However, inclusion of all three parameters in the calibration and uncertainty analysis processes constitutes a better calibration strategy than omitting one of them as it allows estimation of the ratio between K_x and K_{rb} without bias and, for certain dispositions of head measurements, may allow estimation of A_h, albeit with uncertainty inherited from noise in the head measurements. The avoidance of bias that follows from the inclusion of A_h in the calibration process results from the fact that not fixing this parameter value prevent K_x and K_{rb} to adopt surrogate roles to compensate for this parameterization defect (i.e. Structural error). Nevertheless, through steady-state calibrations, the uncertainty on the parameters cannot be minimized to the uncertainty related to measurement error due to the lack of identifiability. Therefore, the next section explores the potential gain in parameters identifiability that can be achieved by calibration against transient data.

3.5.2. Transient calibrations

The same parameter set is calibrated using a transient head dataset. Transience in aquifer heads is instigated by varying the river stage. This is implemented in the numerical model by varying the head in the head-dependent (i.e. Cauchy boundary) that represents the river. The head ascribed to this boundary is sinusoidal with an amplitude 1 m and period 2 days. The response of the water table within the aquifer is recorded at intervals of 0.1 days along the *Central cross-section* at 10 m from the river edge. This provides 10 head observations, equally distributed over a single day, for use as calibration targets. The value of the specific yield S_y is fixed to 0.2. First, temporal head differences are used as calibration targets rather than absolute values of heads.

Table 3.3: Results of the inversion process using transient well observations (10 head observations at 10 m from the river). The model is calibrated against head difference targets. The overall description is similar to **Table 3.1**.

S		
2.00	-	-
-	0.10	-
-	-	0.00

R			
K_x	**0.19**	-0.00	0.49
K_{rb}	*	**1.00**	-0.00
A_h	*	*	**0.49**

V_1	
-0.31	-0.63
0.90	-0.44
-0.31	-0.63

	$Eigenvectors$		
K_x	-0.76	0.41	0.50
K_{rb}	-0.05	0.73	-0.69
A_h	0.65	0.55	0.53

Table 3.4: Results of the inversion process using two transient wells (10 head observations) close, at 10 m, and far, at 400 m, from the river. The model is calibrated against head value targets (not the differences). The overall description is similar to **Table 3.1**.

S		
0.60	-	-
-	0.07	-
-	-	0.01

R			
K_x	**1.00**	0.00	0.00
K_{rb}	*	**1.00**	0.00
A_h	*	*	**1.00**

V_1		
0.02	-0.23	-0.97
-1.02	0.97	-0.23
1.00	0.01	0.01

	$Eigenvectors$		
K_x	-0.97	0.22	0.00
K_{rb}	-0.22	-0.97	-0.00
A_h	0.00	-0.00	1.00

The use of differences rather than absolutes in real-world calibration is recommended by *White et al.* [2014] as it provides some defense against wrong initial conditions in the aquifer. Outcomes of the calibration process are shown in **Table 3.3**. In contrast to calibration against a steady-state dataset, the transient dataset provides enough information to identify K_{rb}. However, inspection of $C_{post(k)}$ reveals that the level of post-calibration correlation between K_x and A_h is high. Only the value of K_{rb} and the product of K_x with A_h (i.e. K_y) can be estimate with a high degree of certainty.

From these results, it can be inferred that the information content provided by the two calibration approaches, steady-state and transient, are relevant for certain parameters, different for each, but that complement one another. The steady-state calibration dataset allows to constrain the value of A_h and the ratio K_x/K_{rb}, provided that at least two head observations at sufficiently different distances from the river are included in the calibration dataset. The transient component of the calibration dataset (which can include only one well which, ideally, should be situated close to the river) supports the estimation of K_{rb}, and thus K_x. Therefore, by successively performing a steady-state and a transient calibration, or conversely, and retaining the reduced parameters uncertainties of the first chosen calibration, it can be shown that the estimation of the 3 parameters can be achieved with a high degree of certainty (identifiability close to 1).

The combined effect of these two approaches can be tested by calibrating the model using near and far river transient data. A calibration process is pursued using head values as calibration targets (not the differences). Two wells, one close to the river edge (10 m) and another sufficiently distant (400 m) are employed as calibration targets to jointly estimate the 3 parameters. In order to prevent initial condition in the aquifer to influence the estimation process, a spin-up period of 30 days is imposed prior the beginning of the river transience. Outcomes of this transient calibration are presented in **Table 3.4**. It can be observed that the estimation of the 3 parameters using transient values near and far from the river achieves a

dimensionality of the solution space of 3, the number of parameters requiring estimation. Therefore, the resolution matrix *R* becomes equal to the identity matrix, this indicating that the values of all parameters are individually estimable. Additionally, principal component analysis of the post-calibration parameter error covariance matrix (*Eigenvectors*) shows that each eigenvector is dominated by one parameter and hence that post-calibration parameter correlation has been reduced to a lower level.
According to the outcomes of this synthetic analysis, the next section discusses calibration approaches and predictive uncertainty analysis of a real-world river-aquifer system located in the glacial valley of the Rhône River (Canton of Valais in Switzerland).

3.6. Case study

The purpose of the case study is the estimation of the values K_x, K_{rb} and A_h and the analysis of the uncertainty of the prediction of the water table elevation at the airport of Sion (Capital of the canton of Valais in Switzerland, see **Figure 3.7**).

3.6.1. Site description

The site is located in the valley of the Rhône River near the city of Sion (**Figure 3.7**). The aquifer consists of alluvial deposits from the Rhône River, which are composed of sandy gravels and silts (**Figure 3.8**, stratigraphic unit E). *Glenz* [2013] estimated that, overall, the Rhône valley alluvial aquifer is predominantly composed of gravel (64 %), silt (16 %) and sand (13 %) [*Canton du Valais*, 2010]. The aquifer is unconfined. Specific yield S_y is relatively uniform and average value of 0.2 is assumed based on *Morris and Johnson* [1967] for gravel (coarse) and silt material. Hydraulic conductivity values between 10^{-2} and 10^{-4} m/s have been estimated by in-situ aquifer tests, analysis of granulometric curves, and by calibration of previous models [*Glenz*, 2013; *Richon et al.*, 2010; *Rovina + Partner AG*, 2009; *Vogel*, 2003]. The nature of alluvial sediments suggests that the alluvial aquifer is likely to be characterized by a certain degree of horizontal anisotropy, with a higher conductivity in the direction of the river corridor, i.e. 27° from the East and counterclockwise. The depth of the alluvial aquifer is approximately 40 m [*Glenz*, 2013; *Sartori et al.*, 2011]. It is underlined by lacustrine deposits of clay and silt that can be considered as an aquitard [*Sartori et al.*, 2011] (**Figure 3.8**, stratigraphic unit D).
Horizontal limits of the model domain are of 2 types: physical and hydraulic. Along the aquifer, the model area is limited by equipotential lines, upstream and downstream, which are extracted from the head values of nearby observation wells. The lateral physical limit is constituted of geological units of low hydraulic conductivity (**Figure 3.9**, geological units A, B, C and D). **Figure 3.9** shows the geometry of these formations (*Colored areas*) and the hydrostratigraphic units (*White zone*) that corresponds to the modeled aquifer.

3.6.2. Model calibration and predictions

The numerical model mesh is discretized into 38’700 elements (simulation employs the finite element method), with an average area of 101 m^2 and a standard deviation of 23.5 m^2. **Figure 3.10A** shows the model domain and the perimeter boundaries: Specified head (equipotential lines upstream and downstream); head-dependent (river along the south boundary) and no flow boundaries (impermeable limit along the north boundary). The locations of the steady-state head observations (Wells *w1* to *w8*, see *red dots*), of the transient head observations (*w1*, see *red dot*) and of the prediction (*Prediction*, see *green dot*) are also shown in this figure. **Figure 3.10B** shows the pre- and post-calibrating mismatch between field measurement and simulated head values. **Figure 3.10C** shows the post-calibration match between transient observed and simulated heads. The Nash-Sutcliffe Efficiency of the match between model outputs and field measurements is 0.7

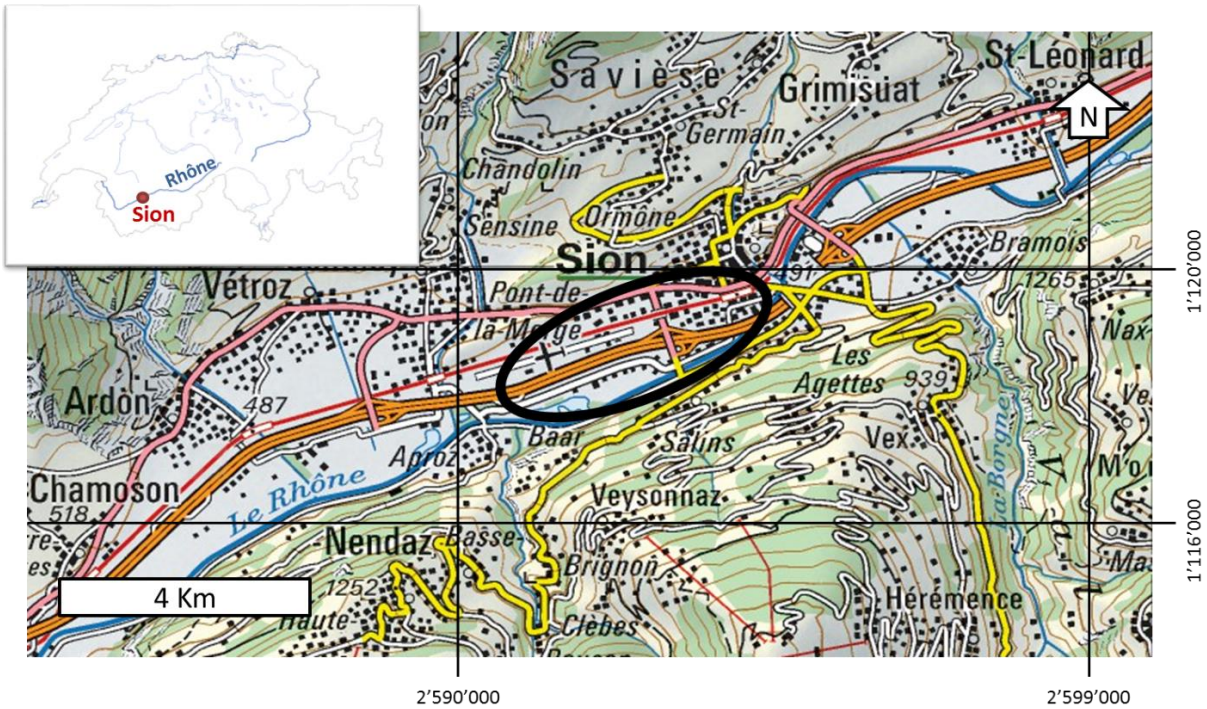

Figure 3.7: Situation map of the modeled site. The city of Sion (capital of the canton of Valais), its airport (schematized plane and landing strip) and its communication channels (Pink lines: national road; orange: Highway and yellow lines: cantonal road) crisscrossing the alluvial valley (Swiss National Map 1:200'000 – CN200, Reference system CH 1903+ /LV95).

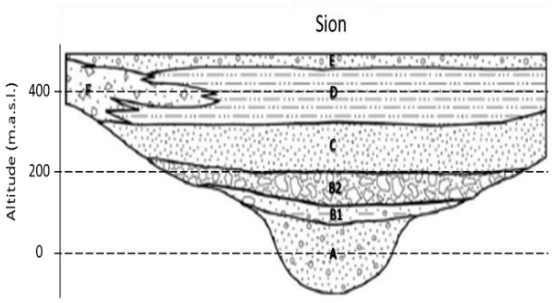

Figure 3.8: Geological cross-section of the Rhône valley [*Besson et al.*, 1993] established from geophysical measurement (reflection-seismic) representing the different stratigraphic units in the study zone. (**A**) Infraglacial channel deposits; (**B1**) and (**B2**) Morain deposits, respectively, lodgement till and meltout till; (**C**) Glacial lake deposits; (**D**) Lacustrine deposits; (**E**) Post-lacustrine deposits; (**F**) Dejection cones of tributaries.

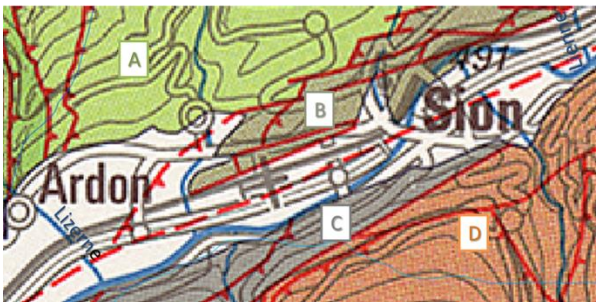

Figure 3.9: Tectonic map, area of Sion, from the Lienne River to the Lizerne River. The white area represents the Rhône alluvial aquifer and the material produced by the dejection cones. The green area (**A**) represents the Wildhorn thrust sheet, the brown area (**B**) represents the zone of Sion-Courmayeur, the gray area (**C**) represents the Houillère zone and the red area (**D**) represents the Pontis thrust sheet. The red lines represent observed and supposed faults.

Figure 3.11 displays the comparison between pre- and post-calibration predictive uncertainty standard deviations obtained through the different calibration approaches described in *section 3.5* and summarized hereafter (***a)*** to ***d)***). The predictive uncertainty standard deviations were calculated using **equation 3.8** (The properties and values of $C_{pre(k)}$ and $C_{(\varepsilon)}$ are the same as those provided in *Section 3.5*).

***a) Steady-state calibration (fixed value of the anisotropy)*:** Calibration of the 2 parameters K_x and K_{rb}. The parameters $A_h$is assumed to be known and is given a value of 1 defining an isotropic aquifer with respect to its hydraulic conductivity.

b) Steady-state calibration (estimation of the anisotropy)*:** Calibration of the 3 parameters K_x, K_{rb} and A_h. As demonstrated in the synthetic analysis, the pre- and post-calibration predictive uncertainty are higher than for the calibration approach ***a), due to the added uncertainty on A_h that propagates to the uncertainty of the prediction.

c) Transient calibration constrained by the results of b) (Head differences targets)*:** The 3 parameters K_x, K_{rb} and A_h are first estimated using steady-state data (Calibration approach ***b)). As shown in the synthetic model calibrations, the uncertainty of A_h is reduced, however, the uncertainties in values of K_x and K_{rb} remain significant after the calibration process, despite the fact that their ratio can be estimated. Their calibrated values and post-calibration uncertainties are then used as initial values and prior uncertainties in the transient calibration respectively. Then, using only head difference targets, the information content of the near stream aquifer response to river transience (*w1* in **Figure 3.10A**) supports unique estimation of the value of K_{rb} and the already constrained ratio of K_x/K_{rb} allows to provide a unique estimate of K_x. Therefore, the uncertainty of the head prediction resulting from successive steady-state and transient calibrations is significantly lowered.

d) Transient calibration (Head values targets)*:** The 3 parameters K_x, K_{rb} and A_h are estimated using a transient calibration by fitting the head value targets (not head differences) of near river and far river heads. The execution time of this calibration is significantly higher than the previous one due the addition of a spin-up period of 30 days to prevent wrong initial condition of the water table elevation to affect the estimation. The post-calibration predictive uncertainty achieved with this calibration approach is of the same order as that attained through the calibration approach ***c).

The estimated values of the parameters K_x, K_{rb} and A_h are, for the approach achieving minimum prediction uncertainty standard deviation (i.e. *Steady-state constrained Transient Anisotropic*), 6.6 10^{-4} m/s, 2.3 10^{-7} s^{-1} and 0.27 respectively. Therefore, the hydraulic conductivity parallel to the Rhône River is approximately 3.7 times higher than that perpendicular to the river.

The outcomes of the predictive uncertainty analysis based on the calibration approaches used in the present section are in accordance with the results of the synthetic analysis. In summary, we can observe the underestimation of the predictive uncertainty when the parameter representing the anisotropy of the hydraulic conductivity of the aquifer is omitted from the steady-state calibration process compared to the one for which it is included (See ***a)*** and ***b)*** from **Figure 3.11**). Subsequently, the uncertainty of the prediction, computed by the steady-state calibration, without bias, is further reduced by the information content provided by the transient dataset (See ***b)*** and ***c)*** from **Figure 3.11**). The results of ***c)*** are confirmed by the results of the approach ***d)***.

3.7. Discussion

The presented analysis assumes a homogeneous anisotropic aquifer. While this approximation can be true at a broad-scale, the origin of the broad-scale anisotropy is the lateral heterogeneity of the aquifer material deposited by fluvial dynamics. However, for predictions of water table elevations (these being less sensitive to small-scale heterogeneity), the assumption of hydraulic property homogeneity is reasonable. In the same tokens, the homogeneity assumed for the conductance of the streambed is not critical for the analysis. The estimated streambed conductance represents average hydraulic properties of the river reach in the vicinity of the observation wells. It is worth noting, however, that the estimation of values of streambed conductance when these are either very high or very low can be difficult. In the former case the aquifer is extremely well connected to the river; in the latter case, it is not connected at all.

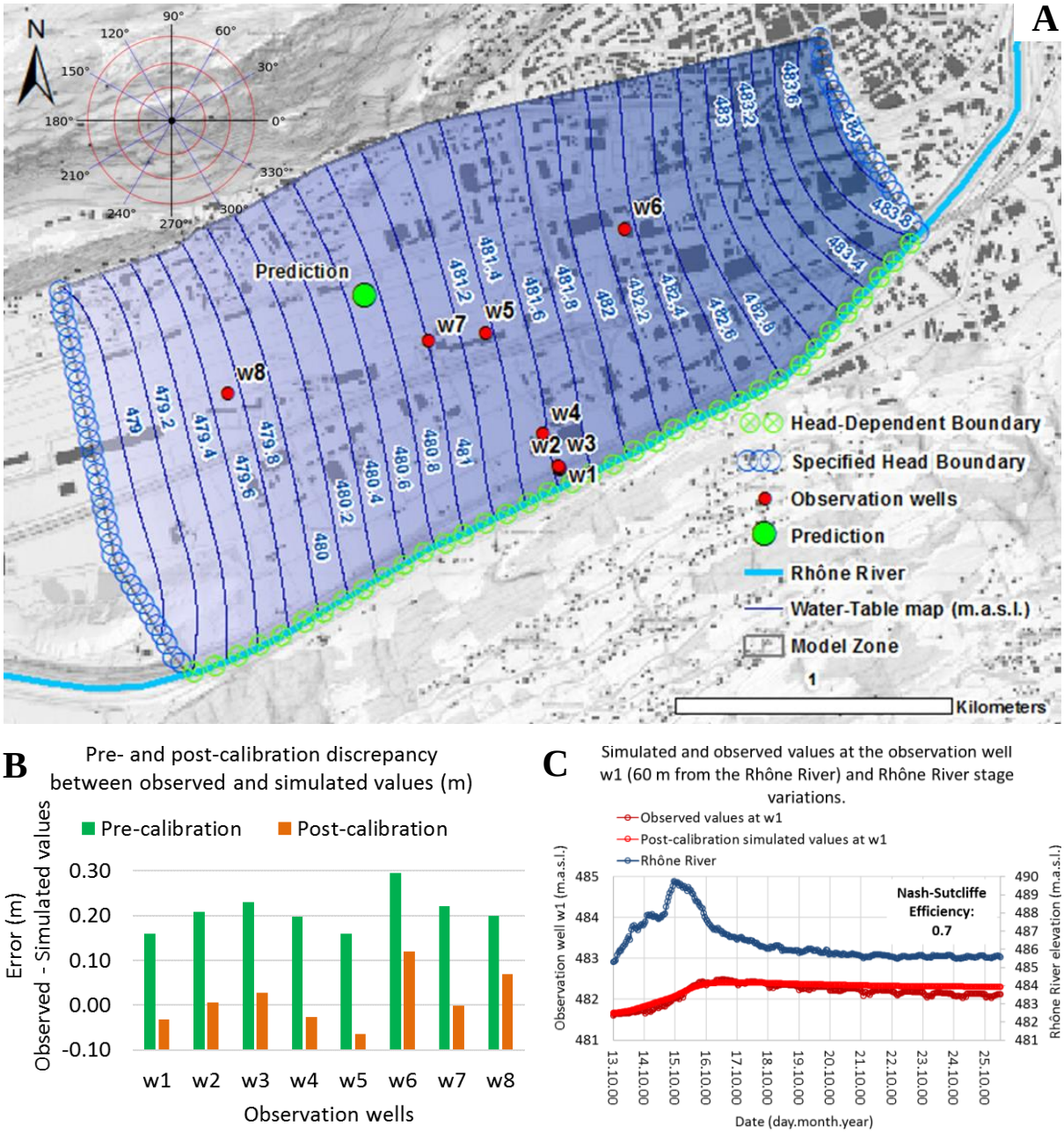

Figure 3.10: A) Model domain (*Translucent blue area*), perimeter boundaries (*Blue and green circles*), observation wells (*Red dots*) and prediction (*Green dot*). The water table map represents the post-calibration head distribution. **B)** The pre- and post-calibrating error between field measurements and simulated values. **C)** The post-calibration fit between transient observed and simulated heads, which is quantified by the value of the Nash-Sutcliffe Efficiency.

The synthetic and real-world cases discussed herein also assumed that changes in the water table elevation are exclusively related to changes in river stage. This assumption can be questionable if additional hydraulic stresses, affecting the domain (for example groundwater abstraction or recharge from irrigation or rain), are not taken into account in the model design, which may consequently introduced further structural noise. Nevertheless, the effect of other stresses on the estimation can be lessen by providing the calibration with observation wells close to the stream edge and by calibrating against head differences.

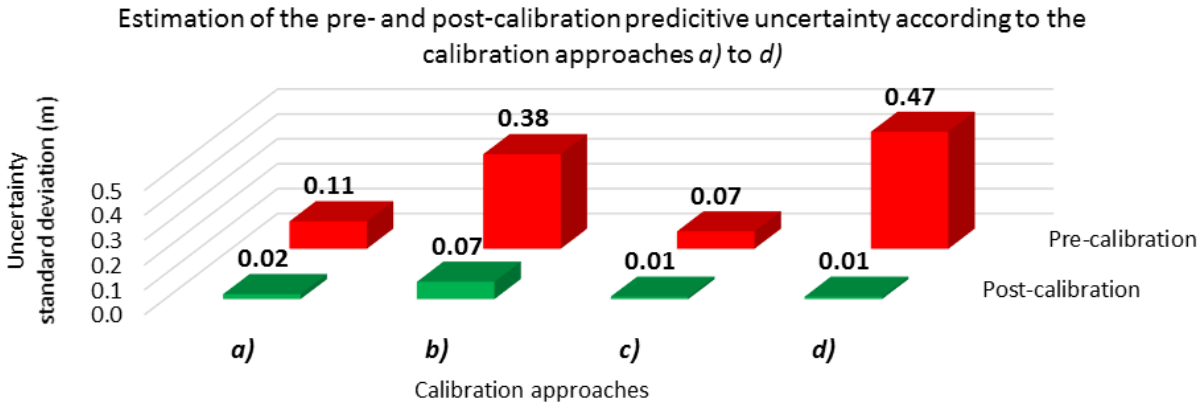

Figure 3.11: Graph of the pre- (*Red histograms*) and post-calibration (*Green histograms*) predictive uncertainties calculated for different calibration approaches: steady-state calibrations; steady-state constrained transient calibration (head differences) and transient calibration (head values). See the text for a detailed description of the calibration approaches *a)* to *b)*.

The results of the case study show that transient calibration using near and far river head observations can be sufficient to uniquely estimate K_x, K_{rb} and A_h and to reduce the predictive uncertainty to the same extent as a calibration process that involves an initial steady-state calibration followed by a transient calibration. However, in real-world calibration scenarios, the calibration process for transient models using absolute target values often requires a spin-up period in order to achieve a pseudo-steady-state initial condition in accordance with the estimated values. In this case, an estimation of the duration of the spin-up period can be calculated by the aquifer response time [*Haitjema*, 2006]. Nevertheless, according to the values of the hydraulic properties, the length of the spin-up period can significantly increase the execution time of the simulation. Calibration often required a large number of runs of the model, even for a small number of parameters, therefore the total calibration time could be significant. Therefore, the information on certain parameters, such as the anisotropy of the aquifer hydraulic conductivity, provided by steady-state calibration and the reduction of its uncertainty can allow a reduction of the number of parameters estimated through transient simulation and thus reducing the calibration execution time when computation resources are limited. It remains that the specific yield S_y of the aquifer should be relatively well known, i.e. a low prior uncertainty, given that estimation of its value may be correlated with other parameters.

Steady-state head data alone only constrain the ratio of recharge and hydraulic conductivity [*Haitjema*, 2006]. Using only head targets leads to correlated parameters, i.e. the effects of changes generated by one parameter can be offset by changes of others such that model outputs are not appreciably changed. Therefore, the inclusion of flux targets, e.g. river infiltration, in addition to heads, can increase the estimability of the parameters. However, similar to head targets, flux targets have associated measurement error, and in practice, their measurement error is commonly larger than those for heads because of the difficulty to measure fluxes accurately in the field. Here the analysis has been pursued at the limit situation where flux information is not available or uninformative due to high measurement errors. This limitation allowed to focus on the information content of head targets with respect to aquifer and river hydraulic parameters using modern predictive uncertainty and parameter identifiability analysis as well as rapid and efficient calibration approaches to circumvent parameter correlations.

3.8. Conclusions

Alluvial aquifers typically feature a high degree of anisotropy due to sediment deposition/erosion processes related to fluvial dynamics. Also, the anisotropy of the aquifer

hydraulic conductivity controls the groundwater flow and the distribution of the water table elevations throughout the aquifer. An increasing number of studies are aiming at anticipating variations in the water table elevation within such environment in the framework of river restorations and adaptation to climate changes. Most of the information that is available on the behavior of the system, and on its hydraulic properties, is available through head measurements.

This study presented an application of modern estimation and uncertainty analysis in calibration and prediction of environmental models in the context of river-aquifer interactions. Data worth and reduction of predictive uncertainty variance has been explored through synthetic modeling and calibration of steady-state and transient models. The calibration approaches have been applied to the Rhône River-aquifer model in the area of Sion (Switzerland). It was shown that the uncertainty of the prediction may be significantly reduced using transient calibration datasets comprised only of heads.

The present study showed that:

- Different values of the aquifer and riverbed hydraulic conductivity and aquifer anisotropy can generate similar values for hydraulic heads throughout the alluvial aquifer.
- History matching based on head targets may lead to a satisfying fit, even if a wrong value for aquifer anisotropy is assumed. The value of the post-calibration model-to-measurement misfit will depend on the distance between the head targets and the distance from the closest well to the river.
- Assuming a value of aquifer anisotropy rather than allowing its adjustment through the calibration process can lead to significant error in the estimation of key parameters, such as K_x to K_{rb}. These parameters adopt a surrogacy role to compensate the structural error and achieve the better fit possible. Consequently, their estimations are systematically biased by the structural error.
- Assuming a value of aquifer anisotropy rather than allowing its adjustment through the calibration process can lead to an underestimation of the uncertainties associated with head predictions in wells that do not comprise the calibration dataset.
- The joint estimation of the 3 parameters K_x, K_{rb} and A_h is limited by the correlation between these parameters when the calibration dataset is comprised of only steady-state heads. However, this limitation can be overcome by supplementing the calibration dataset with transient heads. This allow unique estimation of these parameters and then a reduction of the uncertainties of predictions of water table elevations.

From this, it follows that the common practice of conveniently assuming isotropic conditions may not be desirable. Not only does it have the disadvantage to induce unquantifiable bias in important model predictions. It also inhibits the ability of the calibration targets to inform the parameter during the calibration.

In consequence, the present work supports a broader principle that should be applied to environmental model calibration in general. Where one or more parameters cannot be estimated uniquely, the problem of their non-unique inference should not be addressed by fixing some and estimating others. This can lead to the adoption of surrogate roles by the estimated parameters, and an inference of the uncertainties of critical predictions, which may be too low. Risks may therefore be underestimated.

3.9. References

Al-Hazaimay, S., J. A. Huisman, E. Zimmermann, and H. Vereecken (2016), Using electrical anisotropy for structural characterization of sediments: an experimental validation study, *Near Surf Geophys*, *14*(4), 357-369.

Besson, O., R. Marchant, A. Pugin, and J.-D. Rouiller (1993), Campagne de sismique-réflexion dans la vallée du Rhône entre Sion et St-Maurice: Perspectives d'exploitation géothermique des dépôts torrentiels sous-glaciaires, *Bulletin du Centre d'Hydrogéologie, Université de Neuchâtel*, *12*, 39-58.

Bridge, J. S., and R. V. Demicco (2008), Rivers, alluvial plains, and fans, in *Earth Surface Processes, Landforms and Sediment Deposits*, edited by J. S. Bridge and R. V. Demicco, pp. 365-462, Cambridge University Press.

Brunner, P., J. Doherty, and C. T. Simmons (2012). Uncertainty assessment and implications for data acquisition in support of integrated hydrologic models, *Water Resour Res*, *48*(7).

Canton du Valais (2010), BD-for, Borehole database.

Cihan, A., Q. L. Zhou, J. T. Birkholzer, and S. R. Kraemer (2014), Flow in horizontally anisotropic multilayered aquifer systems with leaky wells and aquitards, *Water Resour Res*, *50*(1), 741-747.

Diersch, H.-J. G. (2014), *FEFLOW Finite Element Modeling of Flow, Mass and Heat Transport in Porous and Fractured Media*, Springer.

Doherty, J. (2015), *Calibration and Uncertainty Analysis for Complex Environmental Models*, first ed., 227 pp., Watermark Numerical Computing.

Doherty, J., and R. J. Hunt (2009), Two statistics for evaluating parameter identifiability and error reduction, *J Hydrol*, *366*(1-4), 119-127.

Fernandez-Alvarez, J. P., A. Gonzalez-Quiros, and D. Rubio-Melendi (2016), Assessment of the value of microgravity to estimate the principal directions of the anisotropic transmissivity of aquifers from pumping tests: A study using a Hough transform based automatic algorithm, *J Appl Geophys*, *134*, 172-182.

Fleckenstein, J. H., S. Krause, D. M. Hannah, and F. Boano (2010), Groundwater-surface water interactions: New methods and models to improve understanding of processes and dynamics, *Adv Water Resour*, *33*(11), 1291-1295.

Gianni, G., J. Richon, P. Perrochet, A. Vogel, and P. Brunner (2016), Rapid identification of transience in streambed conductance by inversion of floodwave responses, *Water Resour Res*, *52*(4), 2647-2658.

Glenz, D. (2013), Inverse Modeling of Groundwater Flow in Rhone Alluvial Aquifer, Impact of the Third Rhone Correction, 172 p.

Haitjema, H. (2006), The role of hand calculations in ground water flow modeling, *Ground Water*, *44*(6), 786-791.

Harmel, R. D., K. W. King, B. E. Haggard, D. G. Wren, and J. M. Sheridan (2006), Practical guidance for discharge and water quality data collection on small watersheds, *T Asabe*, *49*(4), 937-948.

Herschy, R. (1995), General purpose flow measurement equations for flumes and thin plate weirs, *Flow Meas Instrum*, *6*(4), 283-293.

Hunt, R. J., J. Doherty, and M. J. Tonkin (2007), Are models too simple? Arguments for increased parameterization, *Ground Water*, *45*(3), 254-262.

Jha, S. K., G. Mariethoz, G. Mathews, J. Vial, and B. F. J. Kelly (2016), Influence of Alluvial Morphology on Upscaled Hydraulic Conductivity, *Groundwater*, *54*(3), 384-393.

Kenoyer, G. J. (1988), Tracer Test Analysis of Anisotropy in Hydraulic Conductivity of Granular Aquifers, *Ground Water Monit R*, *8*(3), 67-70.

Kruseman, G. P., and N. A. de Ridder (1994), Analysis and Evaluation of Pumping Test Data, Publication 47,, *International Institute for Land Reclamation and Improvement*.

Kucuk, F., and W. E. Brigham (1981), Unsteady-State Water Influx in Elliptic and Anisotropic Reservoir-Aquifer Systems, *Soc Petrol Eng J*, *21*(3), 309-314.

Lavigne, M. A., M. Nastev, and R. Lefebvre (2010), Numerical Simulation of Groundwater Flow in the Chateauguay River Aquifers, *Can Water Resour J*, *35*(4), 469-485.

Lehr, C., F. Poschke, J. Lewandowski, and G. Lischeid (2015), A novel method to evaluate the effect of a stream restoration on the spatial pattern of hydraulic connection of stream and groundwater, *J Hydrol*, *527*, 394-401.

Maheswaran, R., R. Khosa, A. K. Gosain, S. Lahari, S. K. Sinha, B. R. Chahar, and C. T. Dhanya (2016), Regional scale groundwater modelling study for Ganga River basin, *J Hydrol*, *541*, 727-741.

Mas-Pla, J., E. Font, O. Astui, A. Mencio, A. Rodriguez-Florit, A. Folch, D. Brusi, and A. Perez-Paricio (2012), Development of a stream-aquifer numerical flow model to assess river water management under water scarcity in a Mediterranean basin, *Sci Total Environ*, *440*, 204-218.

Mastrocicco, M., N. Colombani, and A. Gargini (2014), Modelling present and future Po river interactions with alluvial aquifers (Low Po River Plain, Italy), *J Water Clim Change*, *5*(3), 457-471.

Mathias, S. A., and A. P. Butler (2007), Flow to a finite diameter well in a horizontally anisotropic aquifer with wellbore storage, *Water Resour Res*, *43*(7).

Moore, C., and J. Doherty (2005), Role of the calibration process in reducing model predictive error, *Water Resour Res*, *41*(5).

Morris, D. A., and A. I. Johnson (1967), Summary of Hydrologic and Physical Properties of Rock and Soil Materials as Analyzed by the Hydrologic Laboratory of the U.S, *Geological Survey 1948e1960. U.S. Geological Survey Water Supply Paper 1839-D*, 42.

Mutch, R. D. (2005), A distance-drawdown aquifer test method for aquifers with areal anisotropy, *Ground Water*, *43*(6), 935-938.

Neuman, S. P., G. R. Walter, H. W. Bentley, J. J. Ward, and D. D. Gonzalez (1984), Determination of Horizontal Aquifer Anisotropy with 3 Wells, *Ground Water*, *22*(1), 66-72.

Partington, D., R. Therrien, C. T. Simmons, and P. Brunner (2017), Blueprint for a coupled model of sedimentology, hydrology, and hydrogeology in streambeds, *Rev Geophys*.

Quiñones-Aponte, V. (1989), Horizontal Anisotropy of the Principal Groundwater-Flow Zone in the Salinas Alluvial-Fan, Puerto-Rico, *Ground Water*, *27*(4), 491-500.

Richon, J., A. Vogel, C. Badertscher, and A. Parriaux (2010), Modélisation hydrogéologique d'un renforcement de digue : cas du Rhône à Sion, *Master en Sciences et Ingénierie de l'Environnement, EPFL*.

Rovina + Partner AG (2009), Beurteilung der GW-Beeinträchtigungen auf Stufe Generelles Projekt, 48 p.

Sartori, M., M. Burri, J.-L. Epard, H. Masson, and J.-B. Pasquier (2011), Geological Map 1:25'000 - Sion (LK 1306), *Swiss Geological Atlas, GeoCover*.

Schilling, O. S., J. Doherty, W. Kinzelbach, H. Wang, P. N. Yang, and P. Brunner (2014), Using tree ring data as a proxy for transpiration to reduce predictive uncertainty of a model simulating groundwater-surface water-vegetation interactions, *J Hydrol*, *519*, 2258-2271.

Schneider, P., T. Vogt, M. Schirmer, J. Doetsch, N. Linde, N. Pasquale, P. Perona, and O. A. Cirpka (2011), Towards improved instrumentation for assessing river-groundwater interactions in a restored river corridor, *Hydrol Earth Syst Sc*, *15*(8), 2531-2549.

Vogel, A. (2003), Relation entre le lac de la gravière des Épines et la nappe phréatique de la plaine alluviale du Rhône (Valais, Suisse), *Centre d'hydrogéologie de Neuchâtel*.

White, J. T., J. E. Doherty, and J. D. Hughes (2014), Quantifying the predictive consequences of model error with linear subspace analysis, *Water Resour Res*, *50*(2), 1152-1173.
Willems, C. J. L., H. M. Nick, M. E. Donselaar, G. J. Weltje, and D. F. Bruhn (2017), On the connectivity anisotropy in fluvial Hot Sedimentary Aquifers and its influence on geothermal doublet performance, *Geothermics*, *65*, 222-233.
Winter, T. C., J. W. Harvey, O. L. Franke, and W. M. Alley (1998), *Ground water and surface water : a single resource*, vii, 79 p. pp., U.S. Geological Survey, Denver, Colo.
Yihdego, Y., G. Reta, and R. Becht (2017), Human impact assessment through a transient numerical modeling on the UNESCO World Heritage Site, Lake Naivasha, Kenya, *Environ Earth Sci*, *76*(1).
Zlotnik, V. A., M. B. Cardenas, and D. Toundykov (2011), Effects of Multiscale Anisotropy on Basin and Hyporheic Groundwater Flow, *Ground Water*, *49*(4), 576-583.

Chapter 4

4. Model development, predictions and uncertainty analysis of water table elevation. 3rd Rhône River Correction – Zone of Sion-Vétroz

Abstract

The 3rd Rhône River Correction project will modify the Rhône riverbed and increase its discharge capacity in order to protect the population from inundation of the alluvial plain. This report provides forecasting and related uncertainty of the water table elevation in the area of Sion (Capital of Valais, Switzerland) in the framework of the modifications projected by the 3rd Rhône River Correction. First, a conceptual model of the study site was developed using historical research data and results, geological maps, climatic data, as well as analysis of the flow system based on head observations. From the conceptual model, hard and soft knowledge were synthesized in a finite element numerical model and flow was simulated using the governing equation for unconfined saturated flow. A base model was parameterized with values for the aquifer, the Rhône riverbed, the tributaries beds, and the drainage network. Then, this model served as an initial condition for the calibration of two-dimensional zonal steady-state and three-dimensional heterogeneous transient models. The latter, achieving the lowest value for the post-calibration objective function, was subsequently used to assess the uncertainty in the future elevation of the water table throughout the aquifer domain. The predictive uncertainty related to the calibration of the model has been estimated using linear uncertainty analysis. Additionally, scenario modeling based on the uncertainty in the future hydraulic and geomorphologic properties of the Rhône riverbed was carried out. In conclusion, the uncertainties in the variations of the water table are dominated by the uncertainty in the future properties of the Rhône riverbed with variations ranging from 0.2 to 2 m, including both positive and negative variations, while the uncertainty related to the calibration of the model presents a standard deviation ranging from 0.05 to 0.3 m. Therefore, although the overall Rhône River stage will be lowered following the work undertaken by the 3rd Rhône River Correction, the surrounding water table elevation may increase (in the absence of drainage control measures) or decrease, according to the evolution of the hydraulic properties of the Rhône riverbed.

4.1. Introduction

The 3rd Rhône River Correction is modifying the Rhône River cross-section between Brigue and Lake Geneva in order to protect the Rhône alluvial valley from flood events. In view of its urbanization and economic importance, the area of Sion (Capital of the canton of Valais) has received a specific attention regarding the consequences of the project on the groundwater table dynamics (**Figure 4.1**). Previous investigations demonstrated that lowering and widening of the Rhône River cross-section, which will cause a decrease of the Rhône River stage, will also lead to a decrease of the surrounding water table [*Glenz*, 2013; *Rovina + Partner AG*, 2009]. Additionally, the Rhône River modifications may also affect the sedimentation/erosion processes which may lead to variations in both the hydraulic and geomorphologic properties of the Rhône riverbed. As riverbed properties control the interaction between river and groundwater, the impact of changes in the Rhône riverbed properties on the uncertainty in the future water table elevation should be investigated and estimated.

The purpose of this report is the prediction and the related uncertainty of the future elevation of the water table in the area of Sion-Vétroz. This purpose will guide the establishment of a conceptual model and then the design of the numerical model. The consequences of the potential increase or decrease of the water table elevation following the modification of the Rhône riverbed are summarized in **Table 4.1.** In the previous chapters, investigation of river-aquifer interaction demonstrated the importance of the riverbed and aquifer hydraulic conductivities parameters on the calibration and prediction of hydrogeological models.

The schematization of the hydrologic cycle considered in the study zone is presented in **Figure 4.2**. The background represents the global water cycle [*Fetter*, 2001] from which elements characterizing the study zone are synthesized in the foreground inset. It can be observed that the relevant processes considered in the model development are the interaction between the surface water and the saturated zone of the groundwater as well as the recharge of the groundwater related to the effective precipitation over the study area. The surface water features are essentially composed of the Rhône River and its tributaries as well as the lakes (gravel pits) and the drainage network present in the study zone.

The workflow defined in order to meet the modeling purpose is schematized in the flowchart presented in **Figure 4.3** and is summarized step-by-step below in accordance with the next four sections:

(1) The first step of the forecasting process is the definition of a conceptual model of the study zone. *Haitjema* [1995] defined a groundwater conceptual model as "*a simplification of a real-world groundwater problem such that (1) it captures the essential features of the real-world problem and (2) it can be described mathematically*". In other words, the conceptual model will tend to establish a description of the important characteristics and dynamics of the river-alluvial aquifer interaction system in the area of Sion that will be subjected to numerical simulation.

(2) Following the definition of the conceptual model, numerical models with different space and time dimensions (two-dimensional, three-dimensional, steady-state and transient), and different parameterization schemes (zonation and interpolation from pilot points) are developed.

(3) Then, the calibration processes are carry out through the estimation of relevant hydrogeological parameters. The efficiency of each calibration process is evaluated regarding the extent of the discrepancies between simulated and observed heads.

(4) Finally, the forecasting, as well as the related uncertainties, are computed. The estimation of the uncertainties is pursued through three approaches:

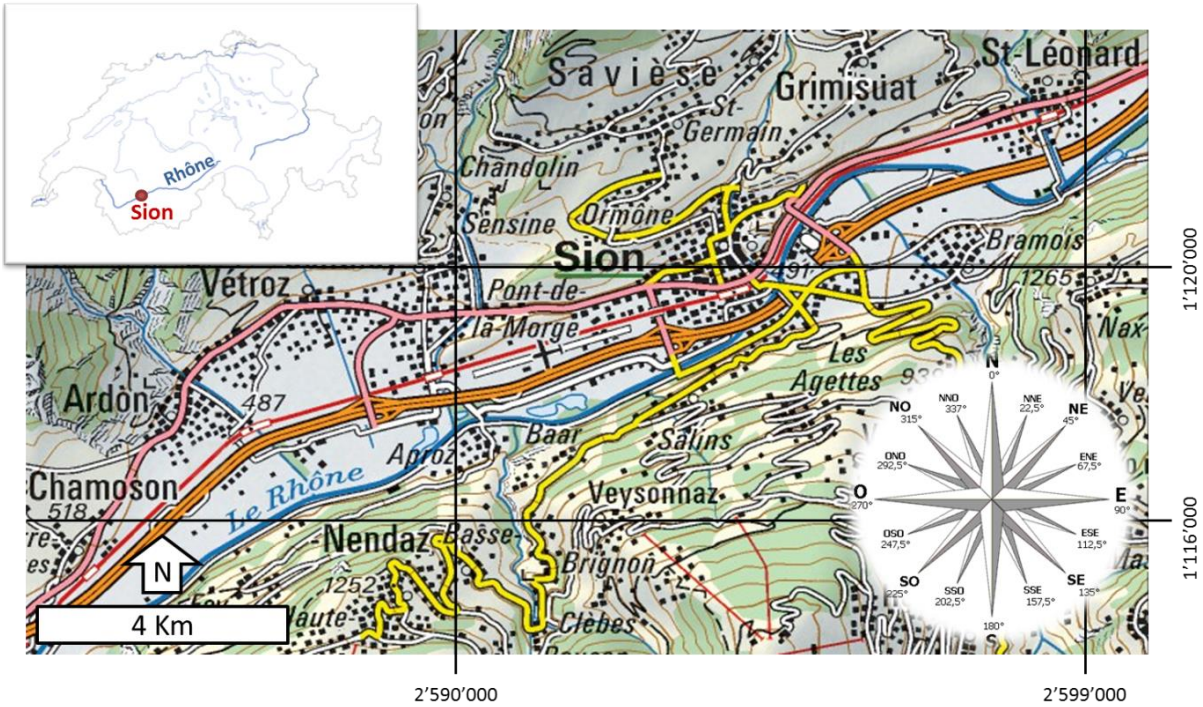

Figure 4.1: Situation map of the study site. The city of Sion (capital of the canton of Valais) and communication channels (*Pink lines*: national road; *orange lines*: Highway and *yellow lines*: cantonal road) crisscrossing the alluvial valley. The Rhône River and its main tributaries are represented by the *blue lines* (Swiss National Map 1:200'000 – CN200, Reference system CH 1903+ /LV95).

Table 4.1: List of potential negative consequences of variations in the water table elevation.

Increase of water table	Decrease of water table
- Water infiltration in underground infrastructures. - Asphyxia of plants roots. - Leaching of contaminated sites causing pollution of groundwater and surface water. - Flooding of ground surfaces causing damages, instabilities of surface structures and break-up of communication channels.	- Land subsidence. - Decreasing efficiency or drying up of wells. - Reduction of water in streams, irrigation channels, and lakes. - Decreasing humidity of the shallow subsurface, that can have negative consequences for wetlands and crops productions.

- First, the uncertainty related to the calibration of the model is estimated. The uncertainty related to imperfect knowledge of the current model parameters and stresses is, prior to the calibration process, delimited by expert knowledge (i.e. ranges of values commonly accepted for the study site) and, posterior to the calibration process, minimized by the information content provided by the calibration targets. The reduction of the uncertainty of the prediction of management interest will depend on the sensitivity of the prediction to the estimated parameters and the post-calibration uncertainty of the parameters.
- Then the uncertainties related to scenario modeling regarding the potential evolution of the hydraulic and geomorphologic properties of the Rhône riverbed are estimated:
  - Scenario modeling uncertainty related to the influence on the water table elevation of the development of alternate bars within the Rhône riverbed, which is likely to happen following widening of the Rhône River cross-section.
  - Scenario modeling uncertainty related to the influence on the water table elevation of the potential evolution of the Rhône riverbed hydraulic conductivity, especially in the case of an unclogging of the riverbed.

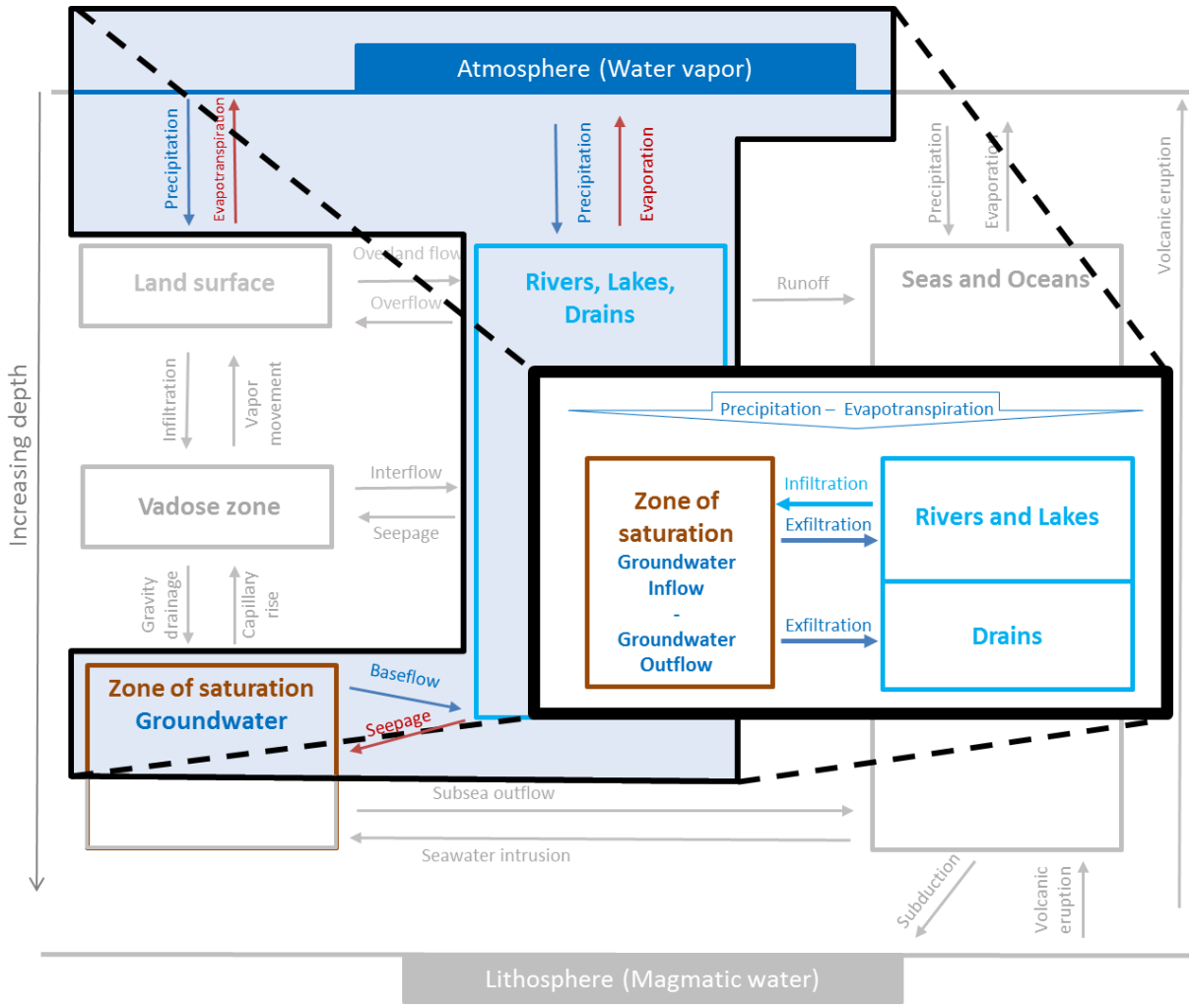

Figure 4.2: Foreground: Simplified hydrologic cycle considered in the study zone. Background: General hydrologic cycle (modified from *Fetter* [2001]).

4.2. Conceptual model

The conceptual model is established by summarizing and analyzing the qualitative and quantitative information on the study site in order to define the relevant components to include into the numerical model that will be used for parameter estimation, forecasting and uncertainty analysis. First, historical research, data compilation, and results are synthesized and discussed. Then, the flow system is assessed using the available spatially distributed average head measurements.

The presented conceptual model of the Rhône Valley is characterized by:

1) The definition of the hydrological conditions along the boundaries of the study site and the hydrostratigraphic units, which are a refinement of geological formations classification according to their hydrogeological properties, such as the transmission and storage properties.
2) The hydraulic features and stresses, sources and sinks of water, present in the study zone and their relative importance to the overall groundwater budget.
3) The groundwater flow system defined by statistics computed from the available head measurements and through a block diagram summarizing the relevant components of the study site. Finally, a simplified and partial groundwater budget is established.

These three points, which support the development of the conceptual model, are developed in the next three subsections.

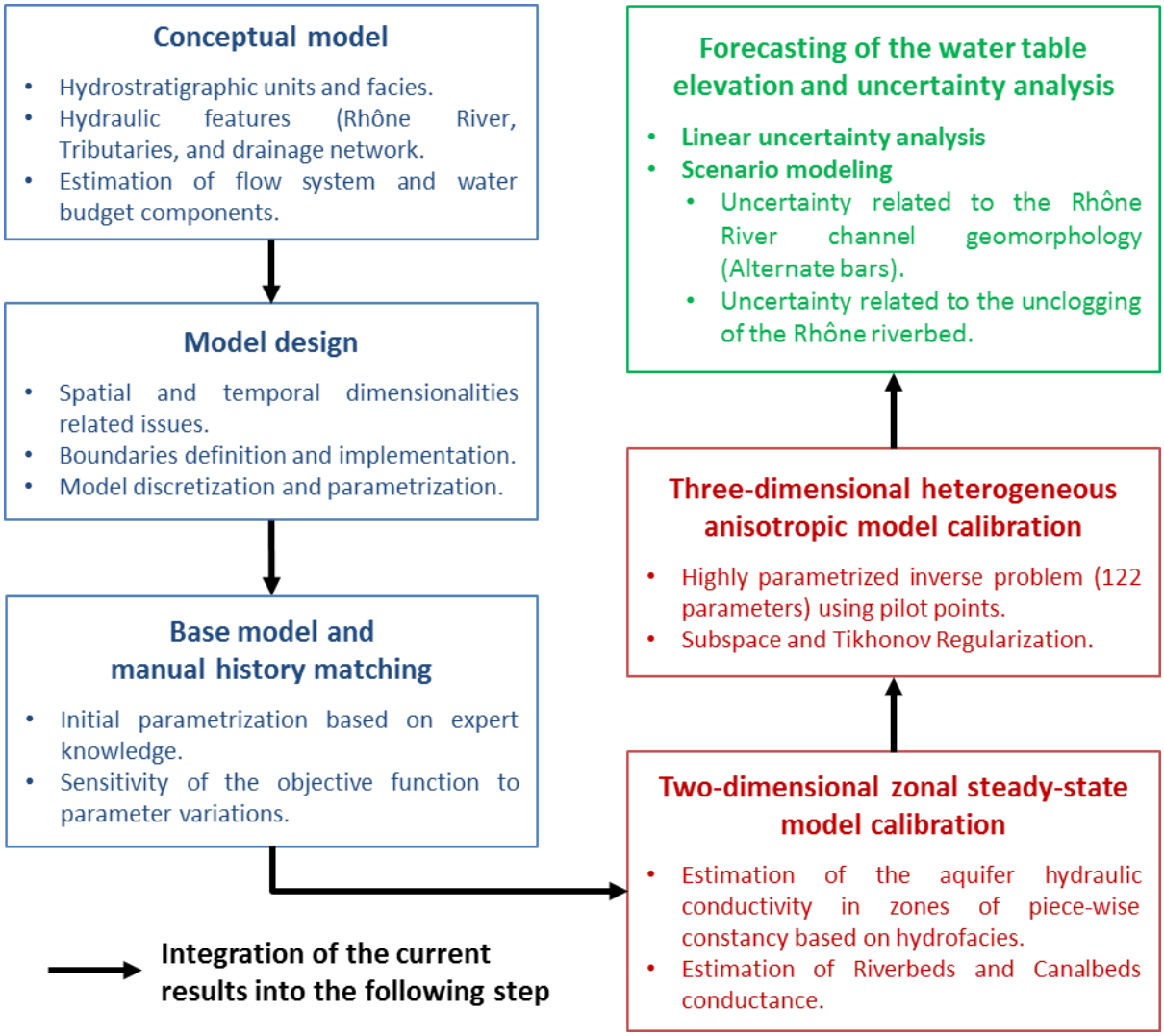

Figure 4.3: Schematic flowchart of the workflow for the numerical model conception, the parameter estimation and the forecasting/uncertainty analysis.

4.2.1. Hydrostratigraphy and boundaries

The aquifer consists of alluvial deposits from the Rhône River and the dejection cones composed of sandy gravel and silt. *Glenz* [2013] estimated that, overall, the Rhône Valley alluvial aquifer is predominantly composed of gravel, 64 %, then silt, 16 % and sand, 13 %. [*Canton du Valais*, 2010]. The aquifer is unconfined and a generic value for the specific yield S_y of 0.2 can be approximated using *Morris and Johnson* [1967] for gravel (coarse) and silt material. Aquifer hydraulic conductivities ranging between 10^{-2} and 10^{-4} m/s have been estimated from a compilation of in-situ aquifer tests, analysis of granulometric curves and modeling results [*Glenz*, 2013; *Richon et al.*, 2010; *Rovina + Partner AG*, 2009; *Vogel*, 2003]. Due to the intrinsic heterogeneity of alluvial formations, broad-scale hydraulic conductivity can vary with the direction of the river course geometry. Therefore, vertical and horizontal anisotropy of the hydraulic conductivity can both affect groundwater flow. *Richon et al.* [2010] considered a vertical anisotropy of 10 (ratio between horizontal and vertical hydraulic conductivity). The thickness of the aquifer is approximately 40 m [*Glenz*, 2013; *Sartori et al.*, 2011]. Due to an insufficient number of full penetrating boreholes in the area, no isopach map of the hydrostratigraphic units is available or can be interpolated.

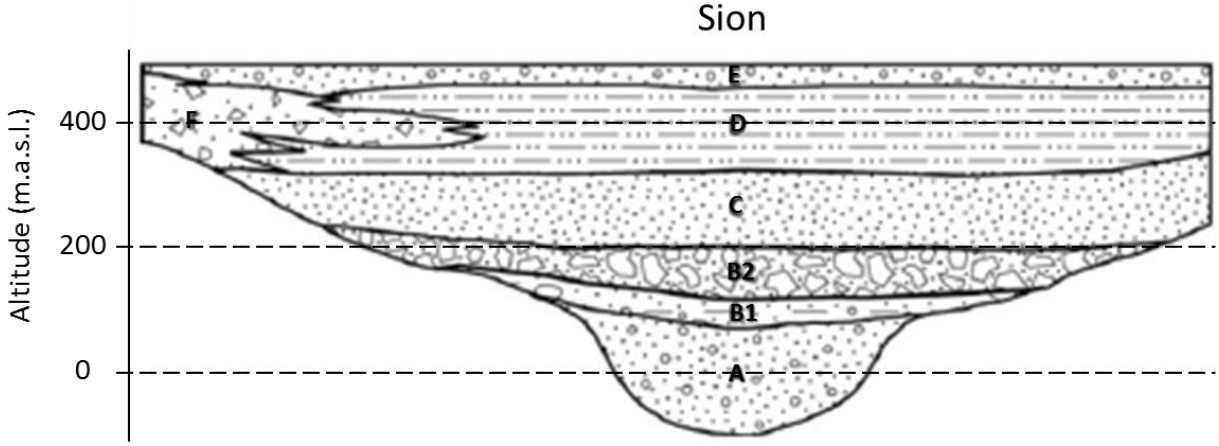

Figure 4.4: Cross-section of the Rhône Valley sedimentary basin **[***Besson et al.*, 1993] established from geophysical measurement (reflexion-seismic) representing the different stratigraphic units from which hydrostratigraphic units and hydrofacies present in the study zone are defined. **(A)** Infraglacial channel deposits; **(B1)** and **(B2)** Moraine deposits, respectively, lodgement till and meltout till; **(C)** Glacial lake deposits; **(D)** Lacustrine deposits; **(E)** Post-lacustrine deposits; **(F)** Dejection cones of tributaries.

Figure 4.4 shows a geological cross-section established from geophysical measurements [*Besson et al.*, 1993] in the sedimentary deposits of the Rhône Valley. The total thickness of the sedimentary basin, resulting from the last glacial retreat (15'000 BP), is more than 10 times the overlying alluvial aquifer. Furthermore, the study aquifer is vertically limited at the top by the soil surface (unconfined aquifer, lithology E in **Figure 4.4**) and at the bottom by the underlying thick, more than 100 m, and relatively impervious, formation of lacustrine deposits (Lithology D in **Figure 4.4**) [*Sartori et al.*, 2011]. In summary, the quaternary geological deposits can be decomposed into three hydrostratigraphic units [*Landry*, 1986]: A deep confined aquifer for which the hydraulic characteristics remain little known; a layer of lacustrine deposit of low hydraulic conductivity and a superficial alluvial aquifer of relatively high hydraulic conductivity. According to the modeling purpose and because of the lack of constraining data, the potential recharge by leakage from the deep aquifer into the superficial alluvial aquifer through the confining layer (lacustrine deposit) will not be taken into account. Lateral limits of the domain are of two types: Physical and hydraulic. The model area is geographically limited by the Lienne River, upstream (East), and the Lizerne River, downstream (West). These rivers represent the limits of the study zone. However, in view of the canalization of these rivers, they do not constitute physical limits for the model. Therefore, the simulation area will be extended further upstream and downstream. Then, water table elevations extracted from the head observations dataset will be imposed to the model along these upstream and downstream limits. Geological units of low hydraulic conductivities delineate the lateral physical limits (North and South). **Figure 4.5** shows the geometries of these formations (*Colored area*) and of the hydrostratigraphic unit (*White zone*), which corresponds to the modeled aquifer. **Figure 4.6** represents a zonal discretization of the alluvial plain hydrostratigraphic unit (*White zone* in **Figure 4.5**) according to the geological map (1:25000). This zonation will be used for the definition of hydrofacies zonation and parameter assignment during the calibration process of the two-dimensional steady-state model.

4.2.2. Hydraulic features and stresses

The surface hydraulic features presented in this section are the main sources and sinks considered in the conceptual model. In the study area, the Rhône River flowing from the Nord-East to the South-West and its tributaries are predominantly sources with respect to the groundwater.

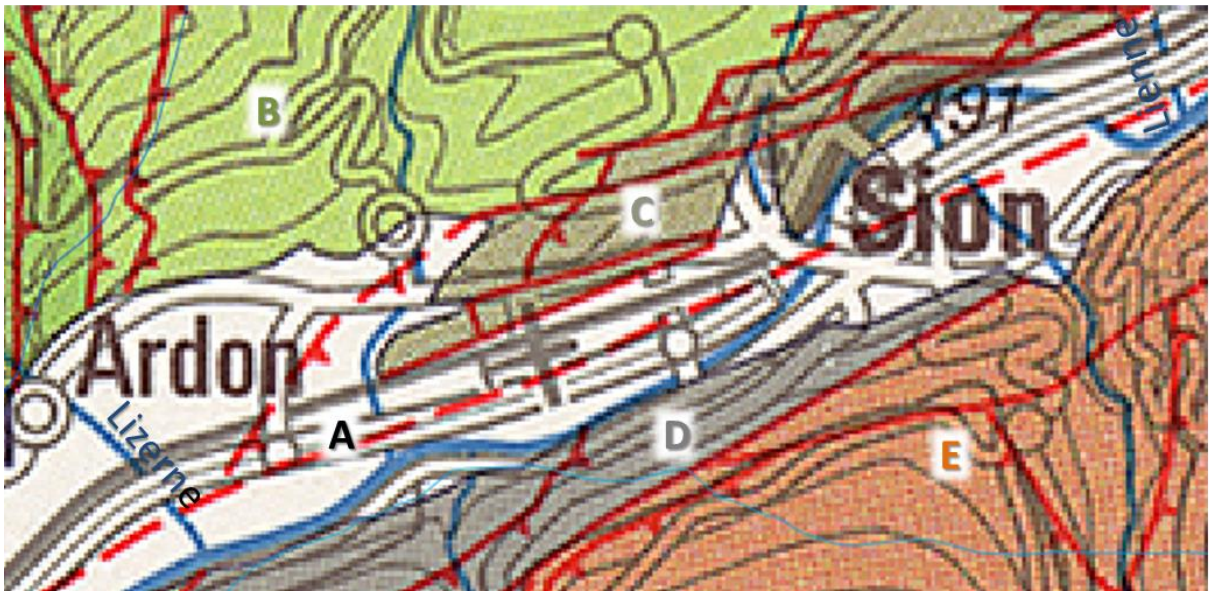

Figure 4.5: Tectonic map of the area of Sion from the Lienne River to the Lizerne River. The *White area* (A) represents the Rhône alluvial deposits and the material produced by the dejection cones. The *Green area* (B) represents the Wildhorn thrust sheet, the *Brown area* (C) represents the zone of Sion-Courmayer, the *Grey area* (D) represents the coal zone and the *Red area* (E) represents the Pontis thrust sheet. The *red lines* represent faults observed in the field and the *dashed red lines* supposed faults.

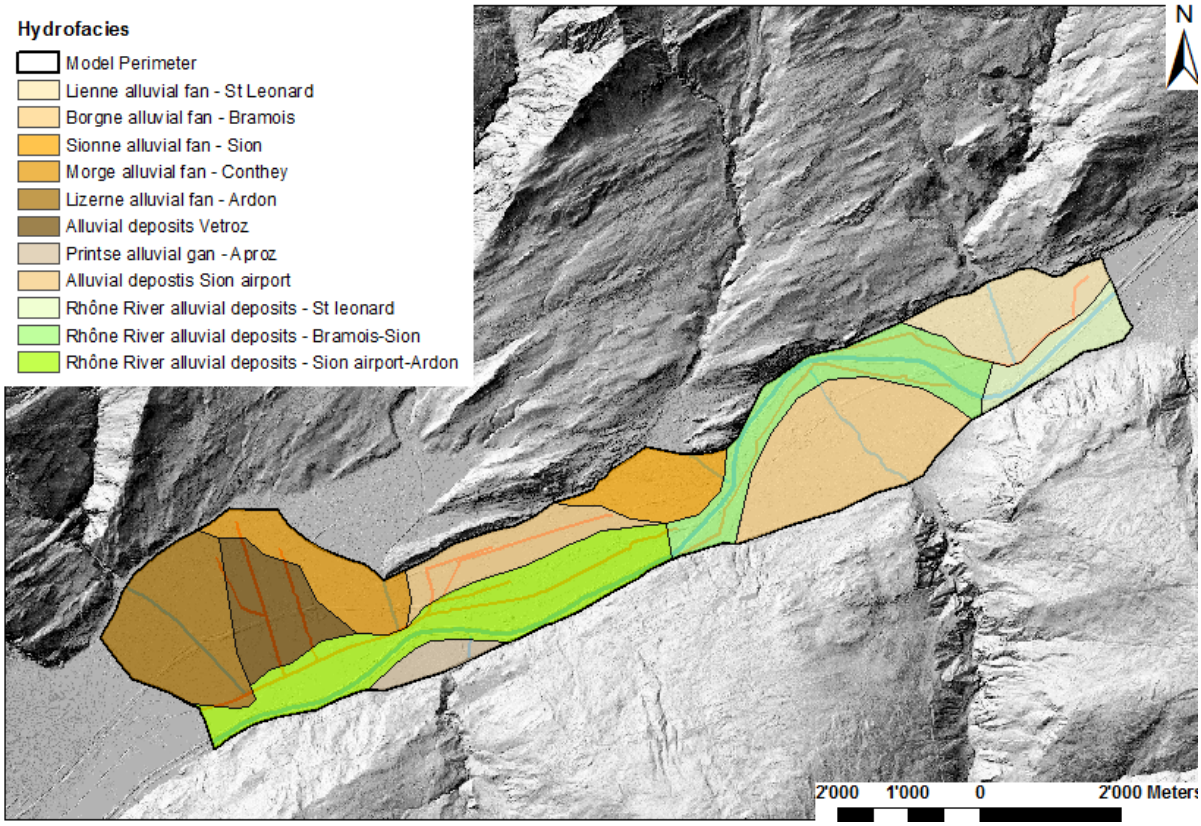

Figure 4.6: Mapping of the hydrofacies in the study zone. Each zone is defined according to the GeoCover (1:25000), Swisstopo established from the Swiss Geological Atlas. The background map is a hillshade of the digital elevation map (2x2) Alti3D Swiss. The line features that can be seen in the zones are the Rhône River and its tributaries (*blue lines*), and the drainage network (*red lines*), see **Figure 4.7**.

Nevertheless, the high degree of channelization and impermeable lining of large reaches of the Rhône tributaries limits their infiltration into the ground and therefore their contribution to the groundwater recharge. Conversely, open channels that crisscross the alluvial plain act as drains, and consequently, constrain the elevation of the water table. The importance of the drainage ditches was pointed out at the regional scale by *Glenz* [2013] and at local scale by *Grindat et al.* [2014]. Other sinks are represented by groundwater pumping, comprising eleven wells, essentially for domestic and irrigation purposes. Furthermore, gravel pit excavated in the aquifer and reaching far below the water table (until 40 m) influence the system flow [*Grindat et al.*, 2014]. **Figure 4.7** displays the hydraulic features described in this section, expect from the gravel pits that will be detailed in a following subsection.

4.2.2.1. Rhône River and its tributaries

In the study zone, the Rhône River drains a surface of 3350 km^2 (Federal gaging station at the kilometer 64.34 from the mouth of the Rhône River with the Lake Geneva) and is around 50 m wide. Apart from seasonal variations, low water during winter and high water during the summer, the hydrological regime of the Rhône River is significantly influenced by hydropeaking (hydroelectric station of Bramois km 67.66 and Chandoline km 65.36), with a daily variation of the river stage of 0.6 m. The Rhône River stage for the current and forecast low water season has been calculated [*Niederer et Pozzi*, 2010] using the one-dimensional hydraulic simulation code HEC-RAS [*US Army Corps of Engineers*, 2010]. The values of the Rhône River stage calculated with the HEC-RAS models are used in the hydrogeological models as internal boundaries during the calibration and prediction processes. The average Rhône River water temperature over the year is 7.0 °C. Average highest and lowest temperatures are respectively 3.8 and 8.9 °C. The average temperatures range of the Rhône River can cause a variation of the hydraulic conductivity of the media, due to variations in the viscosity and density of the water, of around 15%. As it has been shown in *Chapter 2*, the variations of the hydraulic conductivity, due to the alteration of the riverbed permeability, can be several orders of magnitude higher than the variations caused by changes in the water properties alone.

In the area of Sion, six main tributaries of the Rhône River are present. These tributaries are enumerated from upstream to downstream (**Figure 4.7**). Upstream, the Lienne River joins the Rhône River at an elevation of 495 m. It represents the upper limit of the study zone and is likely to have a small to negligible influence on the groundwater system due to its channelization. Then the Borgne River, which is at the origin of the dejection cone of Bramois that constrains the Rhône River to the northern border of the Rhône Valley, joins the Rhône River at an elevation of 493 m. Across the city of Sion, flows the Sionne River that joins the Rhône River at an elevation of 490 m. Five kilometers downstream, the Printse River flows across the village of Aproz and is related to the hydraulic dam of Cleuson. On the opposite side of the valley, the Morge River, which represents the limit between the commune of Sion and Conthey, joins the Rhône River at an elevation of 477 m and is at the origin of the dejection cone of Conthey from which a groundwater inflow in the modeled zone is considered [*Glenz*, 2013]. Finally, the Lizerne River, flowing between the commune of Vétroz and Ardon, represents the downstream limit of the study zone. Overall, the tributaries are channelized by artificial low permeable beds along a major part of their course (**Figure 4.8**) and therefore, their influence on the groundwater system, in terms of water infiltration, is assumed to be limited, if not negligible.

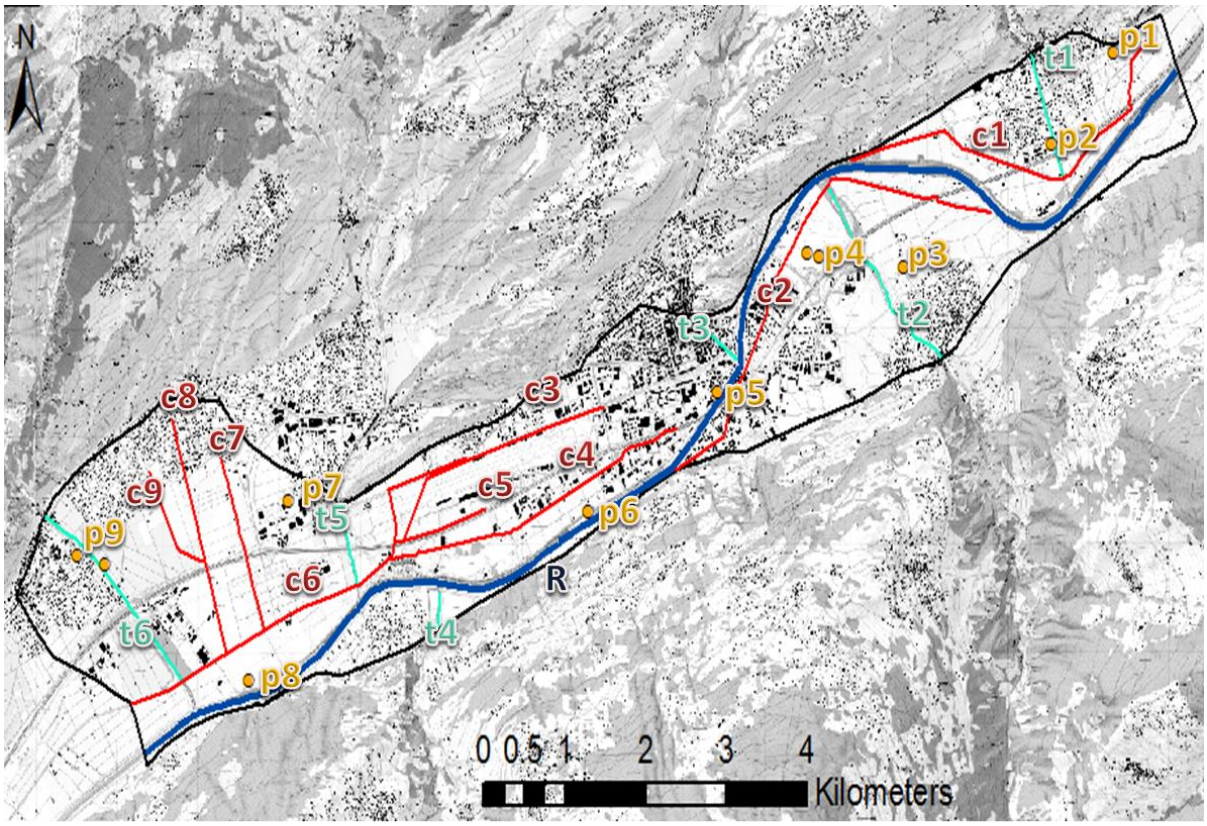

Model Perimeter

R: Rhône River

Tributaries

t1: Lienne River
t2: Borgne River
t3: Sionne River
t4: Printse River
t5: Morge River
t6: Lizerne River

Canals

c1: Uvrier Canal
c2: Vissigen Canal
c3: Blancherie Canal
c4: Iles Canal
c5: Polonais Canal
c6: Sion-Riddes Canal
c7: Vetroz Upstream Canal
c8: Vetroz Downstream A Canal
c9: Vetroz Downstream B Canal

Pumping Wells

p1: Leonard
p2: Uvrier
p3: Préjeux/Bramois
p4: Champsec 1 & 2
p5: St. Marguerite
p6: Ronquoz
p7: Poujes
p8: Seba Aproz
p9: Nayas & Botza

Figure 4.7: Map representing the model perimeter (*Black line*), the Rhône River (*Dark blue line*), the tributaries (*Light blue line*), drainage network (*Red lines*) and the pumping wells (*Orange dots*).

4.2.2.2. Canals and lakes

Nine canals, acting mainly as drains, are present in the modeling area. Their representation is important as they drain the groundwater and therefore limit the elevation of the water table. The water inflow into the canals is discharged further downstream directly into the Rhône River. Previous studies acknowledged their impact on the water table elevation in both low and high water conditions [*Glenz*, 2013; *Grindat et al.*, 2014]. The canals considered in the conceptual model are enumerated from upstream to downstream and their characteristics will be discussed in the model design section: Uvrier; Vissigen; Blancherie; Iles; Polonais; Sion-Riddes; Vetroz Upstream; Vetroz Downstream A and B (**Figure 4.7**).

Figure 4.8: Artificial bed of the Lizerne River (Position coordinates: 587950 116490 (CH1903 /LV95) close to its mouth at the Rhône River, pointing upstream the Lizerne River).

Figure 4.9: Bathymetry measurement in the Epines gravel pit lake (July 2014, picture from Simone Grindat).

Apart from these canals open to the surface, an undefined quantity of underground drains is present in the study area. These underground drains were constructed during the Second World War and their positions and depths have not been mapped. These omitted drains can introduce structural errors in the model, and parameters, such as hydraulic conductivity, can have a surrogate effect to compensate the absence of simulated drains, in particular in highly parameterize calibrations using, for example, Pilot Points. The surrogate role of hydraulic conductivity estimated at pilot points throughout the domain has been briefly analyzed and the results are presented in **Figure 4.10**. The left images in **Figure 4.10**, represents the forward models for which a drain is defined (*purple lines* in figure **1a**, **2a** and **3a**) and from which the observation heads (*flags*) are used as calibration targets during the calibration processes. The calibration processes estimate the hydraulic conductivity of the domain, using 50 pilot points uniformly distributed over the domain. However, the drains are not implemented in the models that are calibrated, thereby introducing a structural error, caused by the absence of the head-dependent boundaries representing the drains (*purple lines* in figure **1a**, **2a**, and **3a**). It can be observed that although the forward models are constituted of homogeneous aquifers with a hydraulic conductivity of 86.4 m/d, the estimation of the hydraulic conductivity within the model domain at the pilot points tend to be whether overestimated (up to 170 m/d) or underestimated (down to 30 m/d) in order to accommodate the absence of the drains (**Figure 4.10 1b**, **2b**, and **3b**). Moreover, **Figure 4.10 1b** and **3b** show that, using solely 2 head targets close to each other, lead to the estimation of a similar heterogeneous hydraulic conductivity field although the orientations of the drains, in the forward models, are different, horizontal and vertical respectively. However, **Figure 4.10 2b** shows that by increasing the information provided by more head targets distributed along the drain this issue can be circumvented and a better identification of the drain geometry can be achieved. Nevertheless, it remains that the surrogate role taken by the hydraulic conductivity to accommodate the failure to implement the drainage network in the model can lead to wrong estimations of the hydraulic conductivity field. The consequences on prediction of water table elevation can be envisioned, as the constraining effect of the drain will cease when the surrounding water table decreases below the bottom elevation of the drain, while the effect of a low hydraulic conductivity will by pervasive whatever the elevation of the water table is.

In conclusion, the simulation of the drainage network, regarding is location and depth, is essential for a better estimation of the prediction related to variations of the water table elevation.

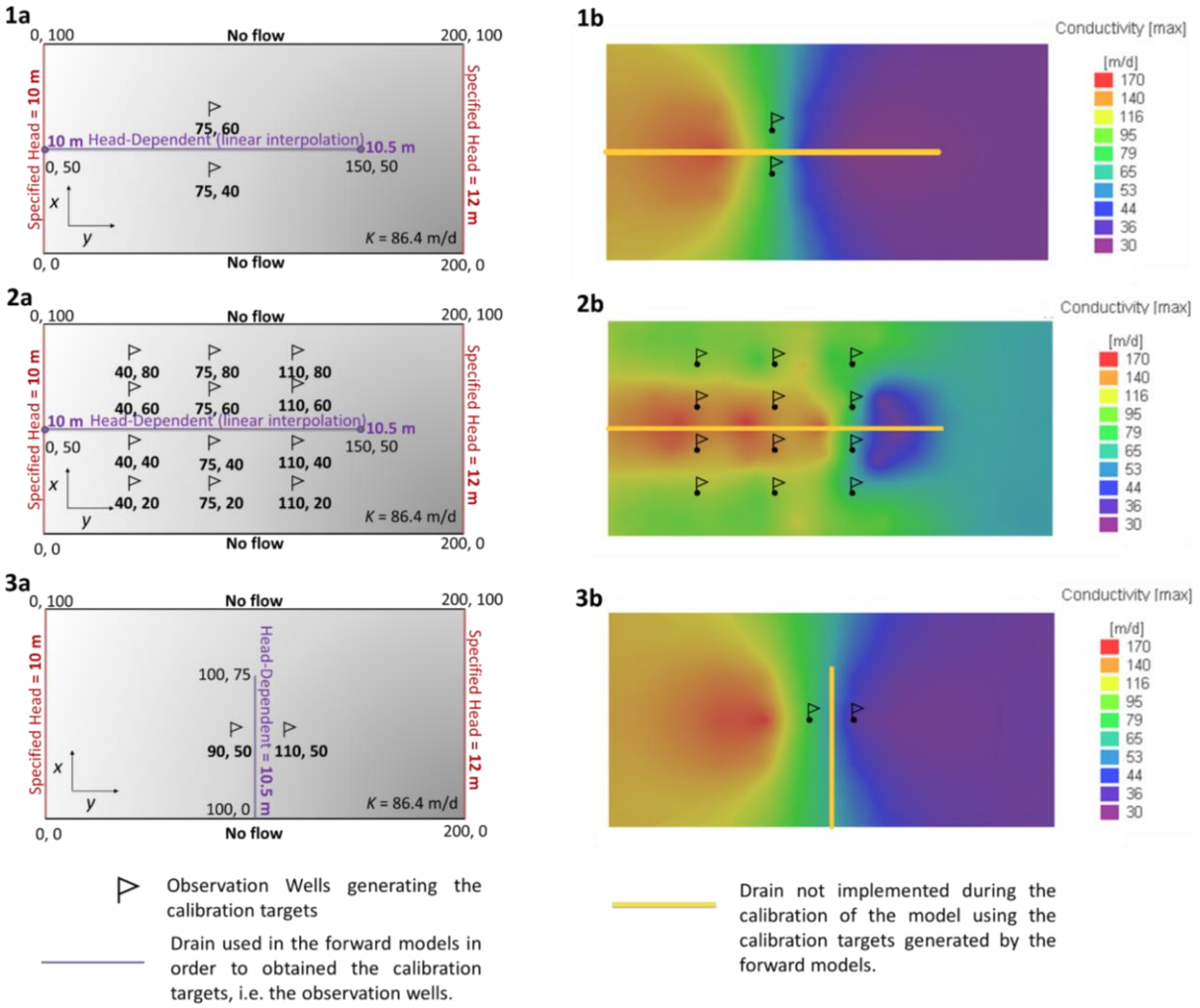

Figure 4.10: The figures on the left side, **1a**, **2a**, and **3a**, represent the model design of 3 two-dimensional areal models with different drain setup. The perimeter (No flow and Specified head) boundaries as well as internal (Head-dependent) boundaries are specified to simulate a general groundwater flow and the influence of a longitudinal or perpendicular drain. The hydraulic conductivity of the model zone is homogeneous and isotropic with a value of 86.4 m/d and the drain conductance is equal to 10^3 d^{-1}. Each model is run and the values of heads at the different observation wells are recorded and are subsequently used during the calibration process. The figures on the right side, **1b**, **2b**, and **3b**, show the resulting calibration of the hydraulic conductivity field using Pilot Points approach based on 50 pilot points uniformly distributed over the model domain. In the calibrated models the drains are not simulated and the surrogate role taken by the estimation of the hydraulic conductivity of the domain at the different pilot points is clearly visible. Basically, for **1b** and **3b** the hydraulic conductivity is underestimated before the drain and overestimated after the drain in order to match the calibration targets. For **2b**, where more observation wells border the zone where the drain is supposed to be, a zone of high hydraulic conductivity is estimated.

Lakes (Former gravel pits) are present in the study zone (**Figure 4.9** and **Figure 4.11**) due to the excavation of the aquifer material for economic purposes. These gravel pits constitute lakes in the landscape (outcrop of the groundwater). No surface water inflow or outflow influence the gravel pits. Their recharge comes essentially from groundwater inflow and direct precipitations. They can be defined as flow-through lakes focusing part of the groundwater flow, i.e. the groundwater flow is modified close to the gravel pits, the water table declines at inflow sides of the lake and rises at outflow sides [*Kuchovsky et al.*, 2008]. Consequently, their implementation in the model can be required in order to limit the structural errors and the possible consequences in the estimation of the hydraulic conductivity field of the aquifer, as previously discussed.

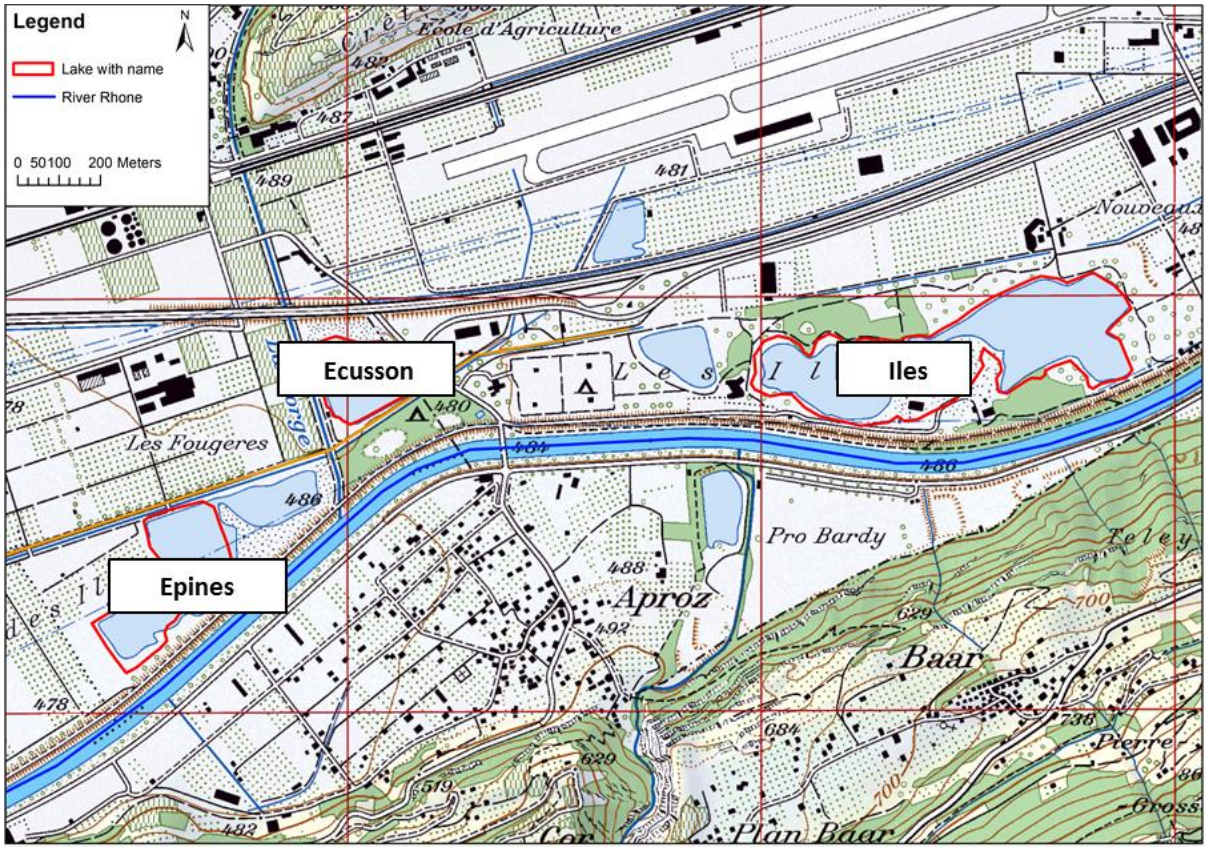

Figure 4.11: Situation map of the gravel pits lakes Iles, Ecusson, and Epines. Their locations with respect to the model domain can be visualized in **Figure 4.1** next to the village of Aproz.

More specifically, three gravel pits are considered in the study area. They are located west of the city of Sion along the right edge of the Rhône River: Iles, Ecusson and Epines [*Vogel*, 2003] (**Figure 4.11**).

The bathymetry of the lake has been established using Acoustic Doppler Profiler during summer 2014 (**Figure 4.12** and **Figure 4.13**). The Lake of Ecussons (**Figure 4.14**) and the Lake of Epines have a maximum depth of 29 and 37 m respectively. Concerning the Lake of Iles, the bathymetry used is based on the measurement carried out by *Geometres Center SA* [2013] and present a maximum depth of 40 m. Their penetration in the aquifer is significant, given that the maximum depth tends to reach the assumed depth of the aquifer bottom. Therefore, their influence on the groundwater flow should be represented in the model.

4.2.2.3. Recharge and pumping wells

The Rhône Valley is protected against precipitation both from the south and from the north (Alps Mountains). Therefore, a contrasted precipitation distribution let the alluvial plain relatively dry compared to the high volume of precipitation in the mountains. However, recharge by precipitation directly over the aquifer is considered significant [*GéoVal Ingénieurs-Géologues SA*, 1986; *Glenz*, 2013]. Nevertheless, regarding the relative importance of the recharge by the Rhône River compared to rain recharge, the effect of precipitation close to the Rhône River is found to be masked by variations in the Rhône River stage. The mean annual precipitation amounts in the area of Sion is 600 mm [*Glenz*, 2013]. Monthly averages (From the year 2000 to 2013) are shown in **Figure 4.15**.

Figure 4.12: Acoustic Doppler Profiler mounted on a float geolocalised by GPS and moved with an electric boat.

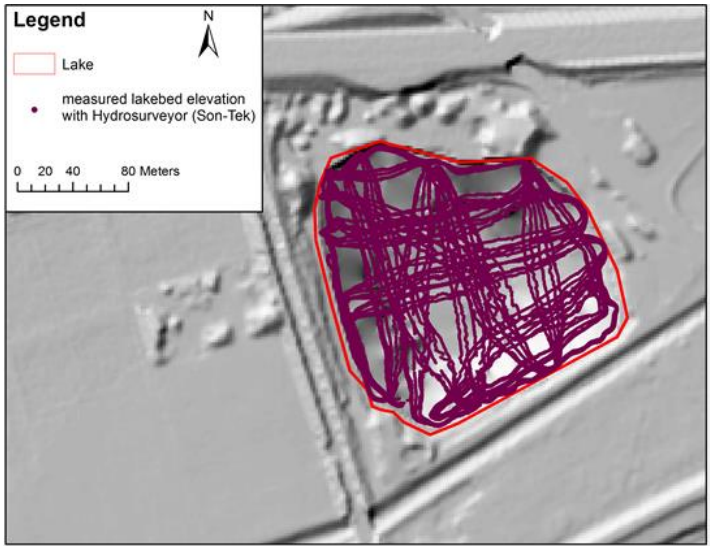

Figure 4.13: Measurement tracks and points of the bathymetry using the Acoustic Doppler Profiler on the Lake of Ecusson.

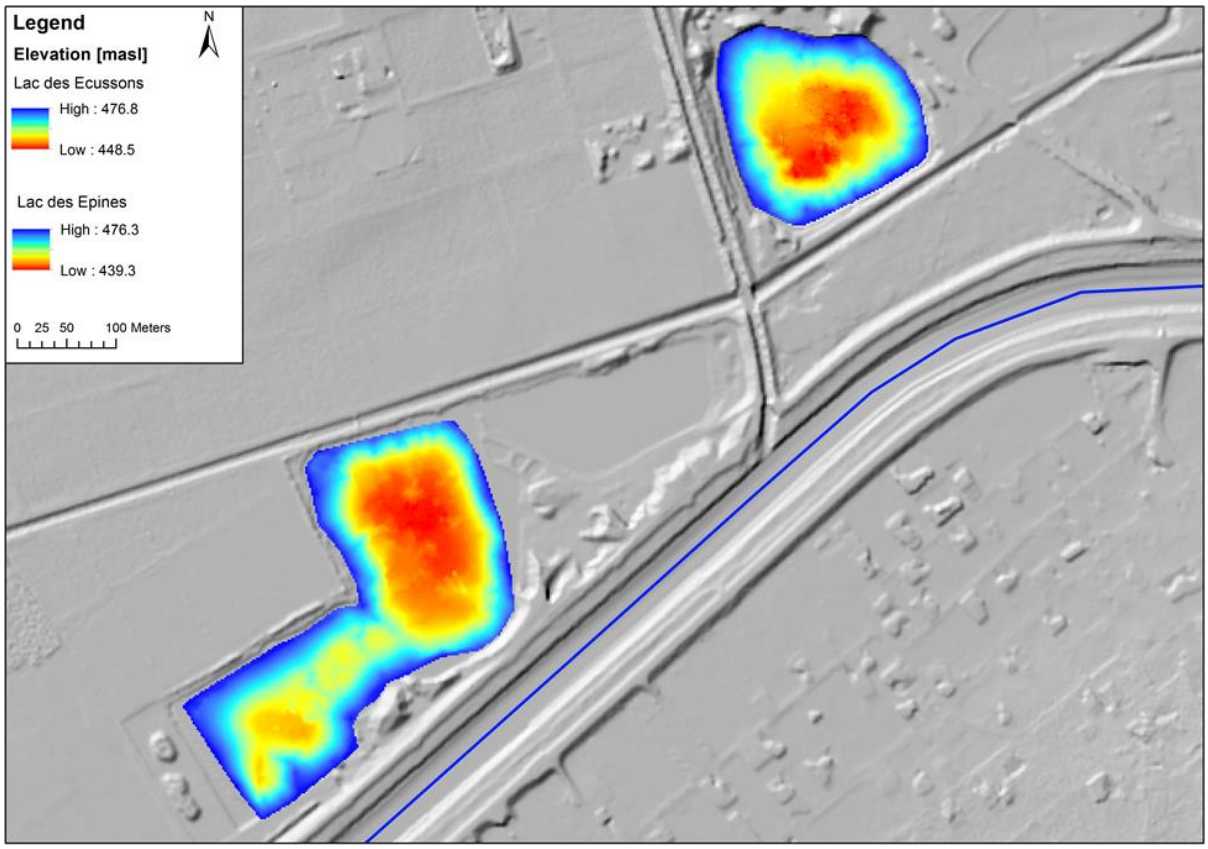

Figure 4.14: Bathymetric map of the lake of Ecusson (*Top*) and the lake of Epines (*Bottom*). The background map is a hillshade of the digital elevation map (2x2) Alti3D Swiss.

The yearly average recharge was calculated as the difference between the mean annual precipitation amounts and the mean actual evaporation and gives a value of 150 mm/y, i.e. less than half a millimeter a day (0.41 mm/d). According to the value of the specific yield of 0.2 defined previously.

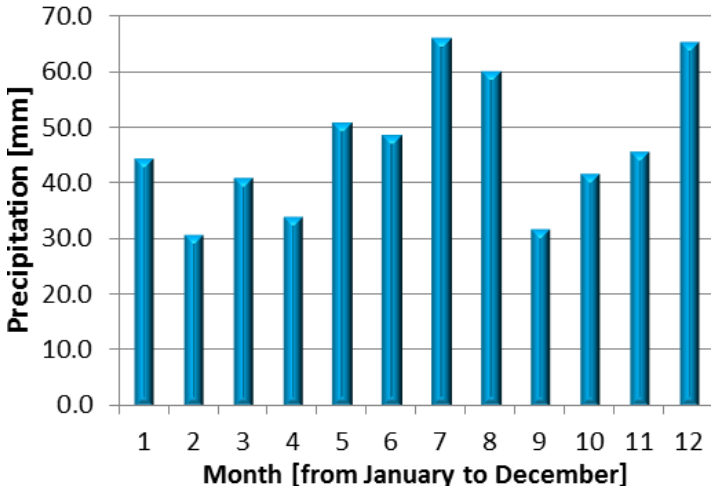

Figure 4.15: Monthly averaged precipitation in the area of Sion between 2000 and 2013 (According to SwissMeteo).

Table 4.2: Localization (Reference system CH 1903+ /LV95) of the 11 pumping wells and their daily average discharges [*Glenz*, 2013]. A same ID Map is assigned for pumping wells relatively close one from the other, e.g. Champsec1 and Champsec 2 have the same ID Map p4.

Name	**ID Map**	**X-coordinate**	**Y-Coordinate**	**Discharge** (m^3/d)
Leonard	p1	599310	122575	810
Uvrier	p2	598530	121720	150
Préjeux/Bramois	p3	596710	120580	150
Champsec 1	p4	595513	120710	540
Champsec 2	p4	595654	120665	540
St. Marguerite	p5	594400	119420	600
Ronquoz	p6	592810	118310	1200
Poujes	p7	589100	118400	270
Seba Aproz	p8	588615	116740	190
Botza	p9	586830	117820	520
Nayas	p9	586480	117820	130

An important source of recharge in the study area has been defined as a groundwater inflow coming from the dejection cone of Conthey (Morge River) [*Glenz*, 2013]. This flux has been estimated at a value of 0.04 m/d over a distance of 2500 m. No other groundwater influx or outflux is considered, except the upstream alluvial aquifer limit groundwater influx and downstream alluvial aquifer limit groundwater outflux.
The groundwater of the alluvial aquifer is tapped by eleven pumping wells. Their daily average pumping rates are shown in **Table 4.2**. The total daily average sink in the study area caused by the discharges of the eleven pumping wells is 5100 m^3/d (**Figure 4.7** displays the location of each pumping wells referred by its ID Map).

4.2.3. Flow system and groundwater budget

The flow system is characterized by the groundwater and surface water flow lines. Using the available dataset of head measurements in the model domain (i.e. 179 observation wells), statistics related to the hydraulic gradient and its direction are computed using all triplets of wells (**Figure 4.16** and **Figure 4.17**) presenting acceptable angles ratio and a sufficient difference between the highest and the lowest values [*Devlin and Schillig*, 2017]. **Figure 4.18** shows the distribution of the calculated hydraulic gradients for all acceptable observation wells triplets. The minimum and maximum hydraulic gradient are respectively $2.7\ 10^{-4}$ and $2.9\ 10^{-3}$, the averaged value, including its standard deviation, being $1.2 \pm 0.7\ 10^{-3}$.

The values of the hydraulic gradient allow to estimate the discharge velocity and to express a ratio between the inertial and viscous forces by calculating the Reynolds number:

$$R = \frac{q\rho d}{\mu} \qquad \textbf{4.1}$$

where q is the discharge velocity, ρ is the water density, d is the average grain diameter and μ is the water viscosity. A value of 10^3 kg/m^3 and 1.4 10^{-3} kg.m^{-1}.s^{-1} are used for the water density and viscosity respectively. Considering the average composition of the aquifer estimated in the *Subsection 4.2.1 Hydrostratigraphy and boundaries*, a value of 8.5 mm is calculated for d. The maximum value of the hydraulic gradient is used to calculate q and thus a maximum value of the Reynolds number R of 0.17 is calculated. R being inferior to 1, the resistive forces of viscosity are predominant and thus Darcy's law is applicable for the mathematic simulations.
In the same way, **Figure 4.19** shows the distribution of the flow directions toward which the groundwater is flowing. The direction is calculated as the angle from the east and counterclockwise. The minimum and maximum hydraulic gradient directions are respectively E55 and E327.7, the averaged value, including its standard deviation, is E229$\pm$31. Estimation of the system flow characteristics closed to the dejection cone of Conthey shows a hydraulic gradient of 1.4 10^{-3} and a flow direction E246. The direction of the gradient confirms the influx originating from the dejection cone of Conthey (Morge River) into the alluvial groundwater. Along the Rhône River, the hydraulic gradient shows a higher value than the average one and the flow directions confirm infiltration of the Rhône River along certain reaches, e.g. along Sion airport (**Figure 4.20**).
Figure 4.21 summarized the conceptual model, presented as a block diagram, established from the analysis of the data and shows the different components of the system flow that have been implemented in the numerical model developed in the next section.
Finally, a groundwater budget is established according to the defined conceptual model. It gathered the important components and processes into a quantitative framework according to the hydrologic equation (law of mass conservation):

$$Inflow = Outflow \pm \Delta\, Error \qquad \textbf{4.2}$$

$Inflow$ corresponds to all amounts of water that are added into the domain. Conversely, $Outflow$ represents all the amounts of water that are removed from the domain. $\Delta\, Error$ represents the error in estimating the $Inflow$ and $Outflow$ components for steady-state condition.
The modeled area has been extended upstream the Lienne River (1700 m) and downstream the Lizerne River (700 to 1000 m) according to estimated equipotential lines for low water over the period 1993-2003. The total modeled area is 27'222'870 m^2. The length of the Rhône River in this area is 15'750 m. Groundwater flow and infiltrating water are calculated according to Darcy's law [*Darcy*, 1856] which multiplies the hydraulic gradient with the hydraulic conductivity of the media in order to obtain the specific discharge. The specific discharge [L.T^{-1}] is then multiplied by the area that it crosses to obtain the discharge [L^3.T^{-1}]. The values of the parameters used in the estimation of the water budget are synthesized in **Table 4.3**. The gradient is estimated using observation wells triples at the upstream limit, downstream limit, Conthey dejection cone and along the Rhône River.
For the hydraulic conductivity of the aquifer (thickness of 40 m) and the Rhône riverbed (thickness of 1 m), values of 10^{-3} m/s and 10^{-5} m/s are retained respectively [*Glenz*, 2013; *Rovina + Partner AG*, 2009] and an average gradient between Rhône River stage and nearby water table of 3.1 % is estimated.

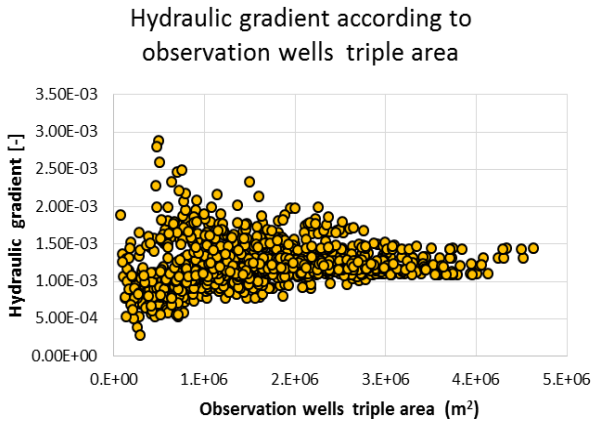

Figure 4.16: Plot of the calculated hydraulic gradient of the water table according to the area defined by the 3 observation wells used for the estimation.

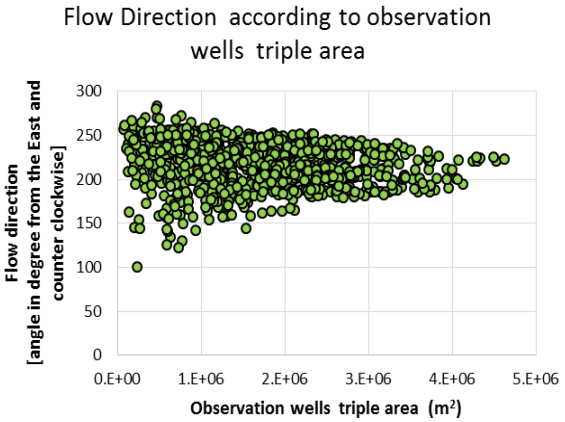

Figure 4.17: Plot of the calculated flow direction of the groundwater of the water table according to the area defined by the 3 observation wells used for the estimation.

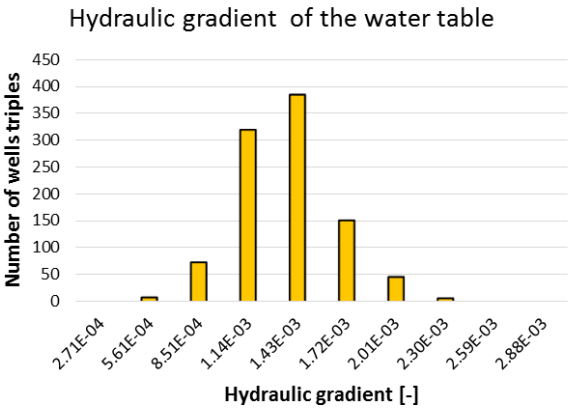

Figure 4.18: Histogram of the distribution of water table hydraulic gradient over the model domain.

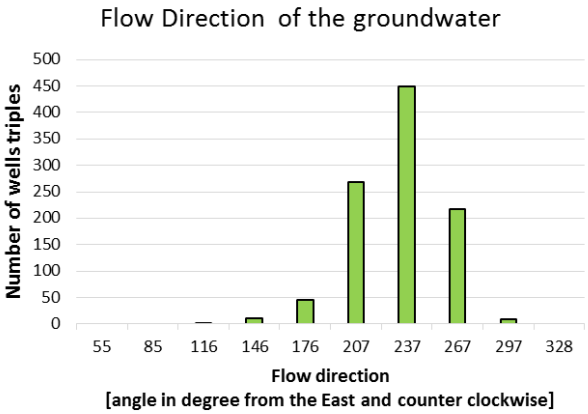

Figure 4.19: Histogram of the distribution of groundwater flow direction over the model domain.

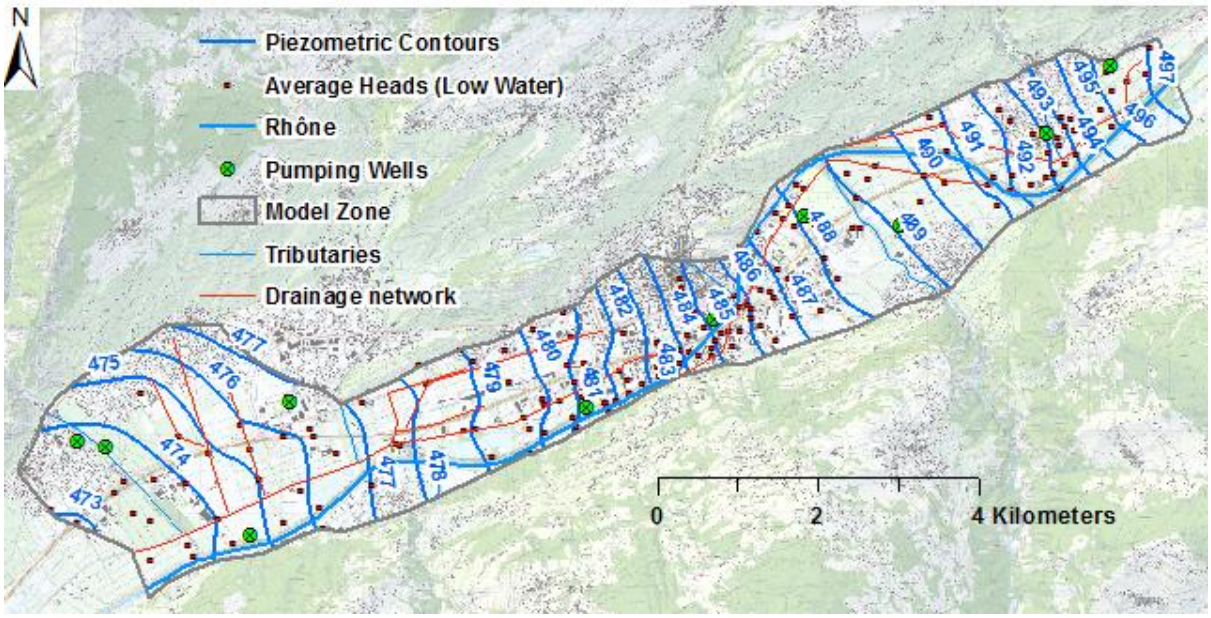

Figure 4.20: Piezometric contours map [m] for the low water season based on the head dataset (period 1993-2003).

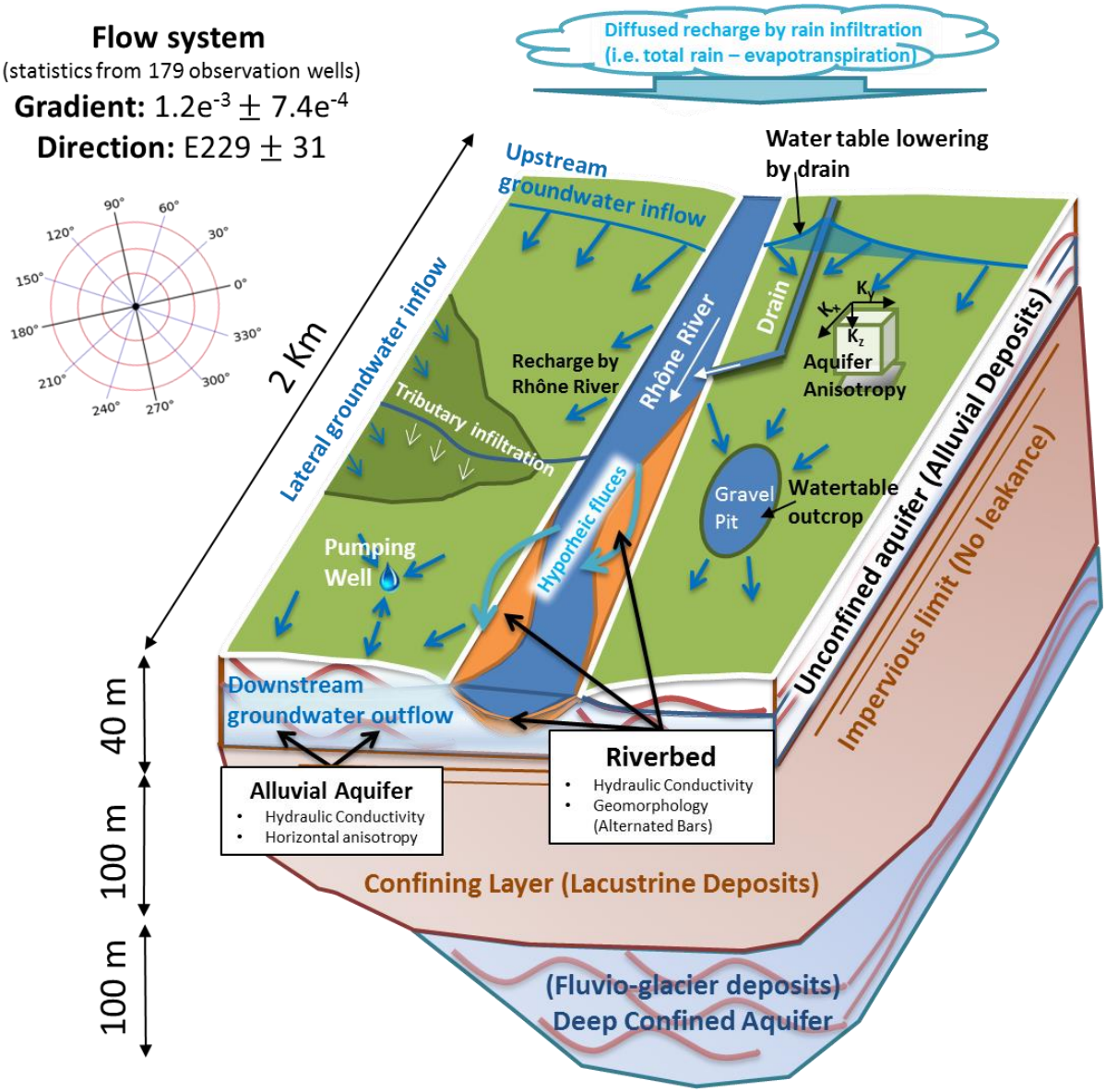

Figure 4.21: Block diagram displaying the conceptual model describing the groundwater system, including associated surface water bodies, hydrostratigraphic units, hydraulic and morphologic characteristics of surface and groundwater media and the flow system statistics.

The length of the cross-section of the upstream and downstream aquifer limits are 1085 and 2401 m respectively. The flux coming from the alluvial cone of Conthey has a magnitude of 0.04 m/d along a horizontal distance of 2500 m. The water budget is purposefully deprived of the drains that represent $Outflow$ because of their complexity and the density of the network. The consequence of this omission is evaluated based on the results of the water budget.

Table 4.4 shows the conceptual model water budget. It appears that the inflow is not compensated by the extraction of water by pumping wells or by the downstream limit groundwater outflow, which is insufficient although the downstream aquifer cross-section is greater than the upstream aquifer limit.

The main recharge seems to be related to the Rhône River infiltration (51.8%) and the rain recharge (27%). The value of the groundwater inflow from the alluvial cone of Conthey is the smallest term and is similar to the value of the Upstream limit groundwater inflow.

Table 4.3: Parameters values used in the estimation of the water budget.

Water Budget Parameters	Values	Units
Recharge by rain		
Rain infiltration	$4.1e^{-4}$	m/d
Model area	$27.2e^{6}$	m^2
Recharge by the Rhône River		
Rhône riverbed hydraulic conductivity	0.864	m/d
Rhône River stage – groundwater gradient	$3.1e^{-2}$	-
Rhône River length	15'750	m
Rhône River width	50	m
Groundwater flow		
Aquifer hydraulic conductivity	86.4	m/d
Groundwater gradient	$1.2e^{-3}$	-
Aquifer depth	40	m
Upstream aquifer width	1085	m
Downstream aquifer width	2401	m

Table 4.4: Conceptual model water budget (The removal of water by the drainage network is not taken into account, same for the potential influx from tributaries). NE means Not Estimated.

$\boldsymbol{Inflow}$	**Unit** (m^3/d)	$\boldsymbol{Outflow}$	**Unit** (m^3/d)
Rain recharge	11'164	Pumping wells	5100
Upstream limit groundwater inflow	4500	Downstream limit groundwater outflow	9957
Conthey dejection cone groundwater inflow	4000	Drains	NE
Rhône River infiltration	21'092		
Tributaries infiltration	NE		
Total $Inflow$	40'756	Total $Outflow$	15'057
	$\Delta\ Error$	+25'699	

Although water budget based on the simplification of the conceptual model and the field data can have important uncertainty, the strong imbalance of this water budget tends to point out the necessity of including other sink terms. The omitted subtractions of water by the drainage network appear to be of the same order, even greater, than the aquifer recharge by the Rhône River infiltration. Nevertheless, imbalance could also be partly due to the overestimation of the rain recharge or the Rhône River infiltration.

In the next section, the numerical model is designed according to the defined conceptual model. The description and discussion of the numerical model design will support the calibration approaches, two-dimensional steady-state and three-dimensional transient, which will be the purpose of the section following the next one.

4.3. Model design

4.3.1. Model dimensionality

4.3.1.1. Spatial dimension

Regional scale groundwater numerical model from Sierre to Evionnaz (60 Km) has been constructed in two-dimension by *Glenz* [2013] and local (a few kilometers) model in the study area have been developed in three-dimension by *Richon et al.* [2010] and *Grindat et al.* [2014]. It is arguable that because only one hydrostratigraphic unit is considered for the modeling of the Rhône alluvial aquifer, a two-dimensional model using the Dupuit-Forchheimer approximation for unconfined aquifer can be used [*Dupuit*, 1863; *Forchheimer*, 1886; 1898]:

$$\frac{\partial}{\partial x}\left(K_x h \frac{\partial h}{\partial x}\right) + \frac{\partial}{\partial y}\left(K_y h \frac{\partial h}{\partial y}\right) = S_y \frac{\partial h}{\partial t} - R \qquad \textbf{4.3}$$

Where K_x and K_y are the hydraulic conductivities of the aquifer along the direction x and y respectively [L.T^{-1}] (see conceptual model **Figure 4.21**), S_y, previously defined in *Subsection 5.2.1 Hydrostratigraphy and boundaries*, is the specific yield [-] and R is a recharge term [L.T^{-1}]. The term $\partial h/\partial t$ represents the variation of head with the time t and is equal to 0 for steady-state simulations. Dupuit-Forchheimer **equation 4.3** assumed horizontal flow with no vertical components, therefore the third dimension represented by the z axis (see conceptual model **Figure 4.21**) is absent from the equation. The transmissivity is therefore calculated by multiplying the hydraulic conductivity along the direction considered by the hydraulic head, assuming that the reference hydraulic head equal to 0 is set at the bottom of the aquifer for the xy location. In other words, h should represent the saturated thickness b of the unconfined aquifer. The two-dimensional approximation is appropriate when the thickness of the aquifer is small relative to the horizontal dimension of the model and is therefore often employed for regional model. However according to the relatively small width of the valley relative to the Rhône River and the presence of stacks near the river edges (City of Sion, Airport, Vissigen neighborhood, etc.) it is necessary to determine whether the two-dimensional simplification is acceptable. Comparisons between three-dimensional and two-dimensional models representing hydraulic features, such as partially penetrating hydraulic features, as it is the case for the Rhône River and the drains crisscrossing the study area, show that heads calculated by the Dupuit-Forchheimer approximation are almost identical from those calculated using a three-dimensional model when the distance d is greater than [*Haitjema*, 2006]:

$$2.5b\sqrt{\frac{K_x}{K_z}} \qquad \textbf{4.4}$$

Where K_x is equal to K_y, i.e. the aquifer conductivity is horizontally isotropic. The computation of **equation 4.4** for the study area gives a value of 316 m. **Figure 4.22** shows that the area around the Rhône River (*red strip*) characterized by the calculated value is significant and includes important stakes such as inhabited zones of the domain, in particular the east part of the city of Sion. Three-dimensional modeling may therefore be important for the defined modeling purposed in the study area. For three-dimensional groundwater modeling, the flow through the unconfined aquifer is not vertically integrated and the governing equation is:

$$\frac{\partial}{\partial x}\left(K_x \frac{\partial h}{\partial x}\right) + \frac{\partial}{\partial y}\left(K_y \frac{\partial h}{\partial y}\right) + \frac{\partial}{\partial z}\left(K_z \frac{\partial h}{\partial z}\right) = S_y \frac{\partial h}{\partial t} - W \qquad \textbf{4.5}$$

where the flow along the vertical direction z is computed according to Darcy's law and potential volumetric inflow or outflow rate are represented by the variable W.

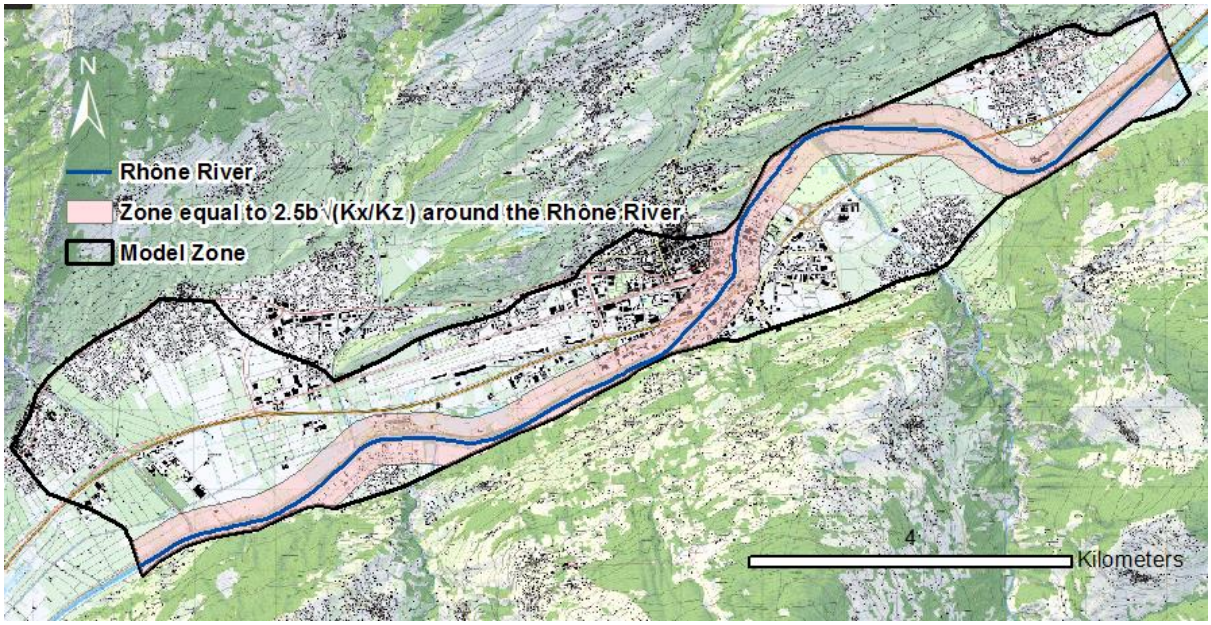

Figure 4-22: Area (*reddish surface*) surrounding the Rhône River where an error in the estimation of the water table can potentially be incurred following the use of the Dupuit-Forchheimer assumptions (two-dimensional model).

4.3.1.2. Temporal dimension

Local and regional models of the study area have been calibrated and used for forecast in steady-state conditions [*Glenz*, 2013; *Grindat et al.*, 2014; *Richon et al.*, 2010] and in transient [*Richon et al.*, 2010] conditions for a strengthening of the Rhône River embankments along the Vissigen Neighborhood, city of Sion (anticipated measure II in Sion).

The success of the calibration is related, on the one hand, to the appropriate conceptualization of the model and its numerical implementation and, on the other hand, to the calibration dataset available. In the Rhône Valley, a large set of point in time measurements of the water table have been recorded. Within the model domain, point in time values in 179 observation wells are available for steady-state calibration. For each well, a pseudo steady-state value has been computed by averaging the measurements at each observation well over a period of 10 years (1993-2003). These average head targets can thus be used for the calibration of a steady-state model. Moreover, the data gathered during the low water season are ideal for the calibration of a steady-state model because during this period, the water table is at a seasonal quasi-steady-state (**Figure 4.23**).

Nevertheless, although head measurement can be made with high accuracy (error of 0.5 cm) their uncertainty can still be significant and much higher than the instrumental error because of relative representability of the system steady-state condition. For the calibration of the transient model, time series of water table records are required. The total number of transient observations is important (according to the measurement time step). However, the locations where these measurements are made are fewer. In the model area, five probes installed along the Rhône River for continuous water table measurement: *16_SHGN6543*; *47_B3*; *68_tr-55*; *90_04K04* and *107_04E01* are used for the transient calibrations. **Figure 4.24** shows both steady-state and transient measurements locations.

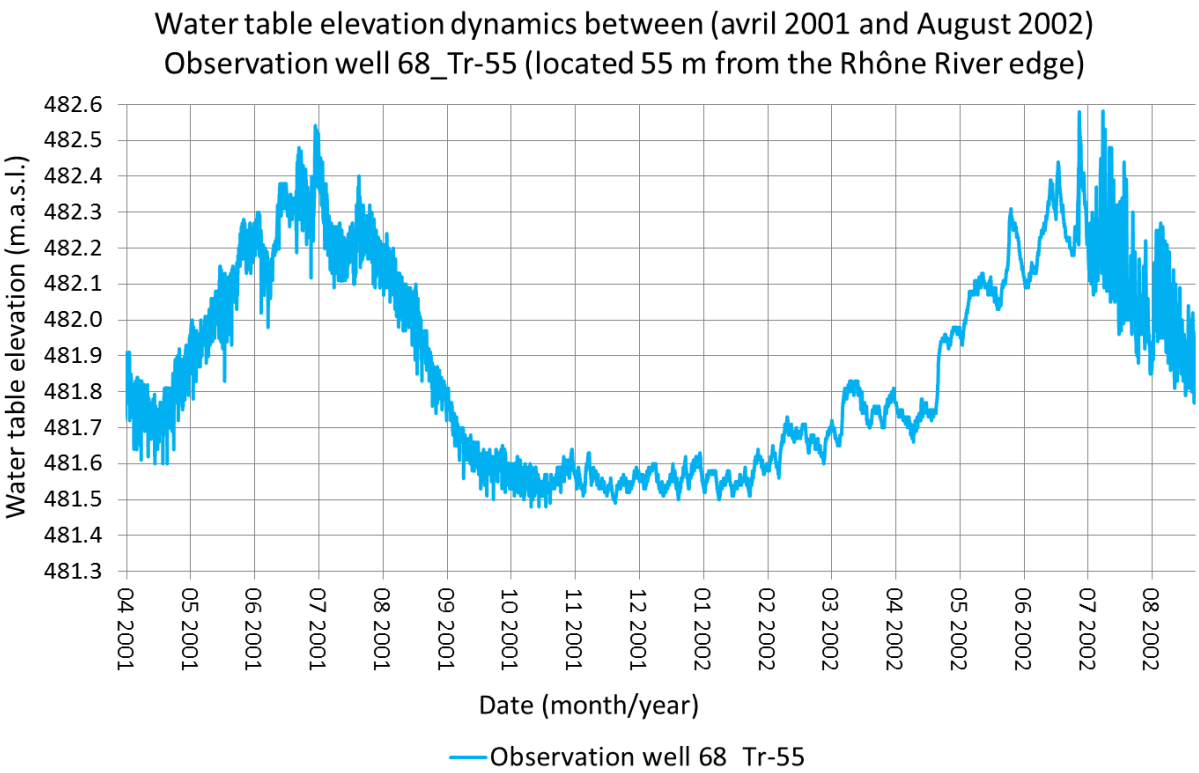

Figure 4.23: Near Rhône River water table variations throughout the years 2001-2002. It can be observed that during the winter season (from September to March) the water table can be considered at a seasonal quasi-steady-state. In this situation, point in time field measurements can be considered to be representative of the average elevation.

According to the parameters already defined (the hydraulic isotropic conductivity K ranging between 10^{-2} and 10^{-4} m/s) and for a period of 1 year (period of the seasonal variations), the aquifer response time (dimensionless) can be estimated using:

$$\frac{1}{4P}\frac{S_y L^2}{Kb} \qquad \textbf{4.6}$$

Where P is the 1 year period expressed in days and L is the average distance between the Rhône River and the lateral model boundaries estimated at a value of 1 Km. **Equation 4.6** gives values between 0.004 and 0.4. According to *Haitjema* [2006] this range of values characterizes a groundwater system that can be simulated using successive steady-state model of time-average conditions. Nevertheless, the highest value calculated with K enters in the range of required transient models (Values superior to 0.1). For the most part, this result agrees with preceding steady-state approaches used at a regional scale [*Glenz*, 2013]. Nevertheless, in order to calibrate the hydraulic conductance of the riverbed, *Gianni et al.* [2016] (see *Chapter 2*) showed that the riverbed conductance could be estimated using transient data from river stage and nearby observation wells. Therefore, transient calibration can increase the identifiability of riverbed hydraulic conductance. Transient calibrations require two additional parameters than steady-state simulations: a storage term, already defined as the specific yield S_y for unconfined aquifer and the initial values of hydraulic heads throughout the model. The pre-transience hydraulic head distribution being influence by new values assigned to the parameters during the calibration process, a spin-up period is established before the transience of the model is actually simulated. During the spin-up period, the elevation of the water table progressively varies according to the set of parameters used in the iteration and is assumed to have reached steady-state condition prior the inception of the transience.

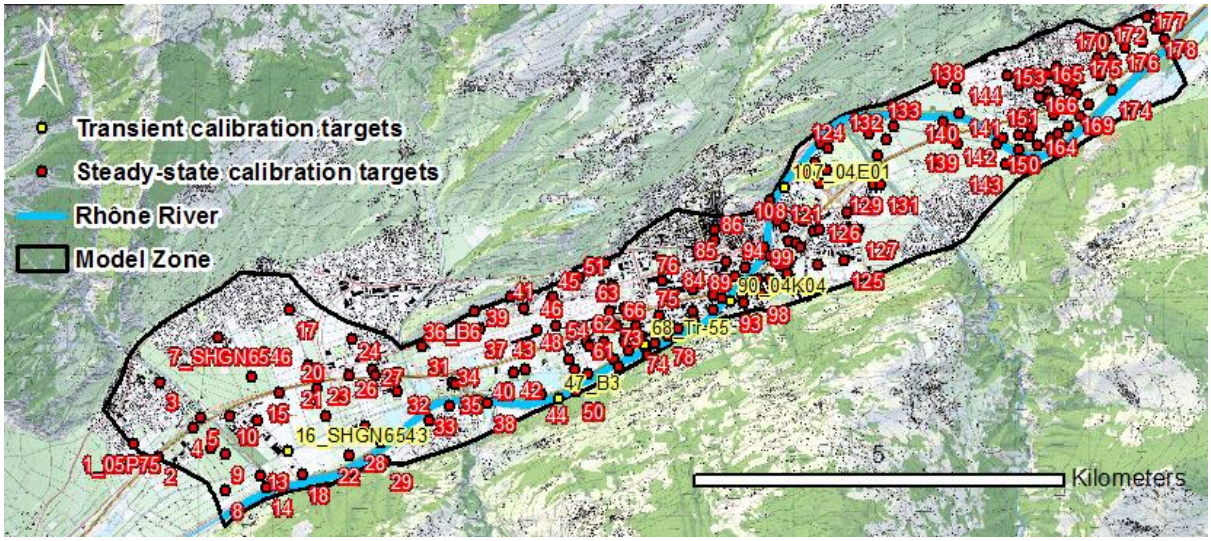

Figure 4.24: Model calibration targets steady-state and transient. The total measurement data set comprises 179 observation wells (included transient probes). For readability, not all the labels (observation well names) are displayed.

Therefore, the spin-up period should be long enough for heads to be stabilized, according to the parameters set used by the iteration, before the transience occurs. In the case of the present model, the duration of the spin-up period is estimated using the groundwater system time constant:

$$\frac{S_y L^2}{Kb} \qquad \textbf{4.7}$$

Equation 4.7 gives a theoretical range of values between 5.8 and 578 days for the spin-up period. In the same way, as for the aquifer response time, the highest value corresponds to the lower limit of the hydraulic conductivity and is unlikely to represent the real average value of the natural system.

This section discussed the spatial and temporal dimensions acceptable for the modeling of the groundwater system in the area of Sion. In view of these elements, a three-dimensional model may be appropriate for the modeling purpose and a transient simulation can provide further information on the estimated parameters. The next section presents the mathematical boundaries used in the model design.

4.3.2. Boundaries implementation

Three types of mathematical model boundaries are used, both along the domain perimeter and internally. According to the defined conceptual model, these boundaries are characterized by physical features and equipotential lines (constant heads). **Figure 4.25** shows the setting of the model boundaries.

4.3.2.1. Perimeter Boundaries

The perimeter of the model domain delimits the alluvial aquifer (including alluvial cones) and is defined as no flow boundary except for the following limits. Upstream, the water table boundary is represented by a specified head interpolated from the piezometers *177* (497.02 m), *178* (497.38 m), *179_03D51* (497.77 m) and a piezometer located outside of the model domain at several meters from the lower corner of the upstream section (498.15 m).

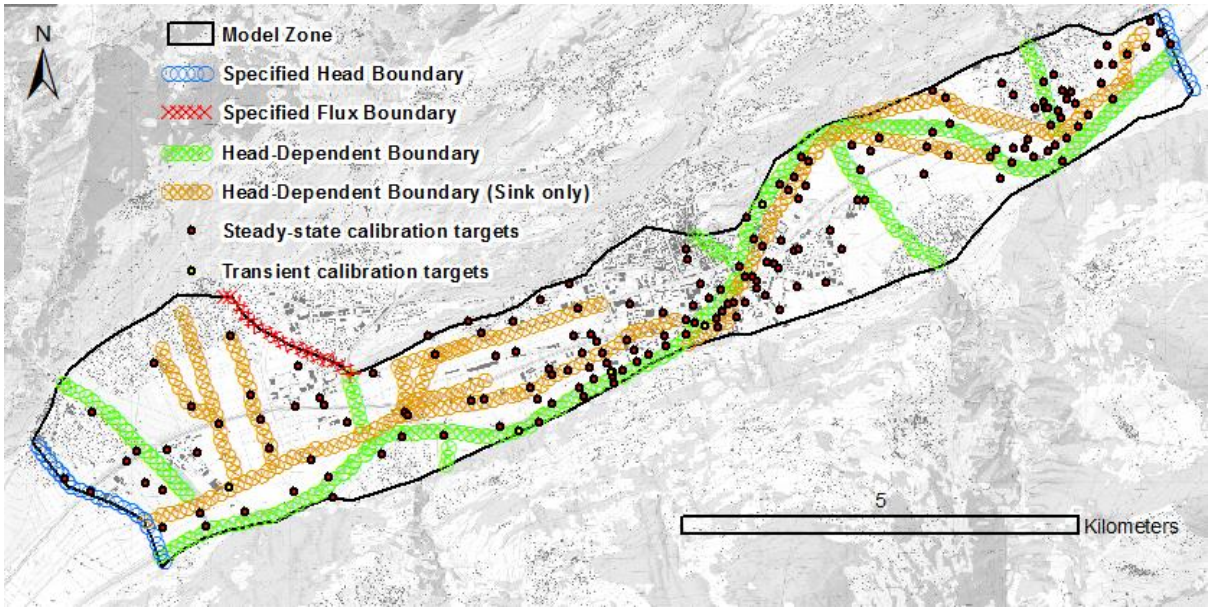

Figure 4.25: Top view of the three-dimensional numerical model that shows the implementation of mathematical boundary conditions. Specified head conditions are, for upstream and downstream equipotential lines, interpolated from observation wells (Values are applied to the whole thickness of the aquifer). Specified flux condition is used for the groundwater inflow coming from the dejection cone of Conthey (Values are applied to the whole thickness of the aquifer). The head-dependent condition is used to simulate the hydraulic potential of the Rhône River and its Tributaries (Values are applied to the top slice nodes only). Head-dependent condition with flux constraint (The hydraulic feature allows removal of water only and therefore prevents inflow when the specified head is higher than the surrounding groundwater head) is used to simulate the bottom elevation of the drains present in the model domain (Values are applied to the top slice nodes only).

Downstream, the water table boundary is represented by a specified head interpolated from the piezometers *1_05P75* (473.06 m), *2* (472.90 m) and *8* (473.28 m). Along the upstream limit of the alluvial cone of the Morge River, previous studies recognized and quantified a groundwater influx of 0.04 m/d [*Glenz*, 2013]. This value will be used as specified influx along the model boundary corresponding to the alluvial cone of the Morge River.

4.3.2.2. Internal boundaries

Head-dependent boundaries are used to simulate partially penetrating surface water bodies, such as the Rhône River and its tributaries. The setting of head-dependent boundaries involves the definition of a conductance parameter C [T^{-1}]. This parameter controls the vertical exchange flux q_{HDB} and represents the hydraulic properties of the riverbed.

$$q_{HDB} = -C_{rb}(h - h_{HDB}) \quad \textbf{4.8}$$

$$C_{rb} = \frac{K_{rb}}{b_{rb}} \quad \textbf{4.9}$$

where h [L] is the hydraulic head in the aquifer below the river, h_{HDB} [L] is the head specified to the node that represent the river, and K_{rb} [LT^{-1}] and b_{rb} [L] are respectively the hydraulic conductivity and the thickness of the riverbed. The values of C will be estimated during the calibration process.

Similarly, the drainage network present in the model domain, which removes water from the groundwater system, is simulated using head-dependent boundaries. Nevertheless, a supplementary condition is imposed, $q_{HDB} \leq 0$, to prevent infiltration of water into the aquifer. Using this inequality, the boundary condition is deactivated when the drain elevation is higher than the surrounding water table. Hence, drains represent only sink (removal of groundwater) and never source of water.

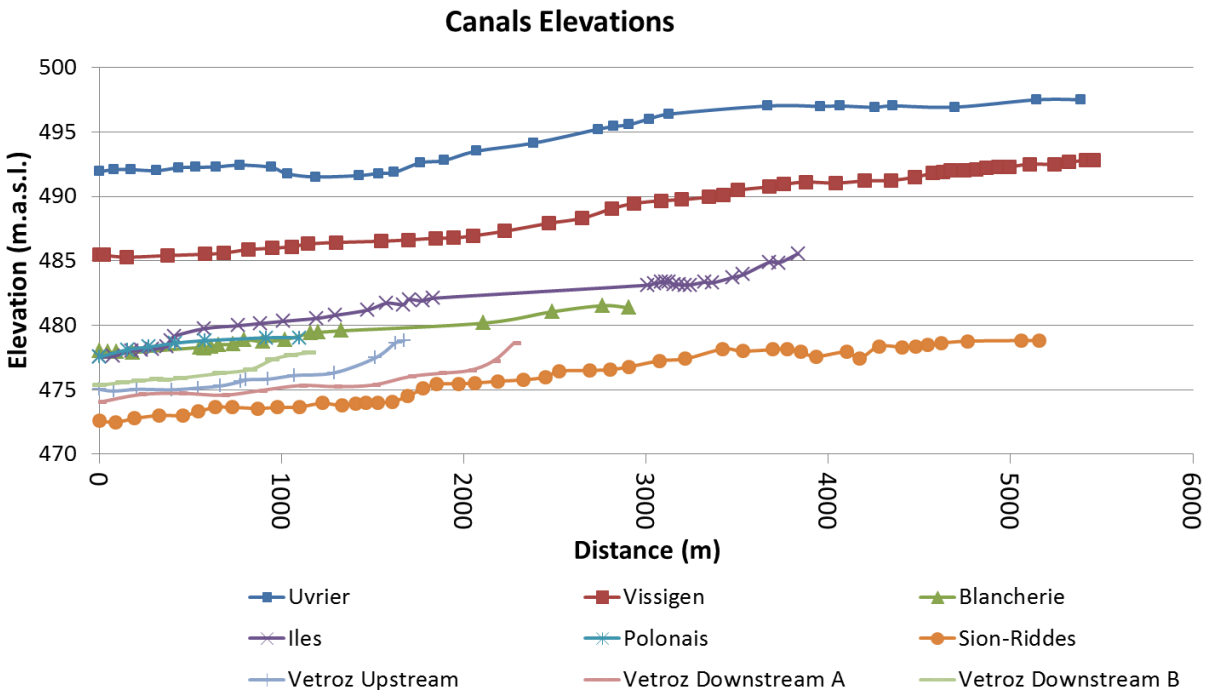

Figure 4.26: Plot of the bottom elevation of the 9 drainage canals. The x-axis represents the distance starting at the downstream part of the drain and following its talweg.

Figure 4.26 shows the specified hydraulic head imposed as a head-dependent boundary for the nine drainage channels distributed in the model. These elevations have been obtained by extraction of the values of surface elevations from the Swiss Digital Elevation Model (2 m by 2 m) [*Swisstopo*, 2012]. The sensitivity of the water table to the conductance of the canalbeds (drains) will be investigated during the calibration process. However, because these canals essentially exfiltrate groundwater, initial assumptions will be made that their beds is relatively unclogged and therefore an arbitrary high value of the conductance will be initially set so that surrounding aquifer hydraulic properties control the flow into the drains.
The point in space sinks represented by the eleven pumping wells are implemented using specified flow boundary and the areally distributed source represented by the recharge by precipitation is implemented using a specified flux boundary (On the top layer for three-dimensional models) over the all domain.
The next section describes the model discretization as well as the pre-calibration material properties parametrization and the set of parameters that will be estimated during the calibration process.

4.3.3. Model discretization and parametrization

In this section, the spatial and temporal discretization of the model is described, as well as the model parametrization and the parameters that will be estimated during the calibration process.

4.3.3.1. Spatial and temporal discretization

The spatial discretization of the model was guided by the modeling purposed and thus relatively smaller nodal spacing, close to the surface hydraulic features, is imposed (**Figure 4.27**). In order to avoid interpolation errors, each observation well is located on a node in the mesh.
The domain and the governing equation are discretized with triangular prisms and using a finite element method respectively. Each layer is constituted of a total number of 83'206 elements, which respect the Delaunay criterion. The aspect ratio (ratio between the largest triangle side to the smallest triangle side) is maintained inferior to 3, the average maximum interior angle is 85.8° with a standard deviation of 14.1°. The vertical discretization split the hydrostratigraphic unit into 4 layers for a total number of elements of 332'824.

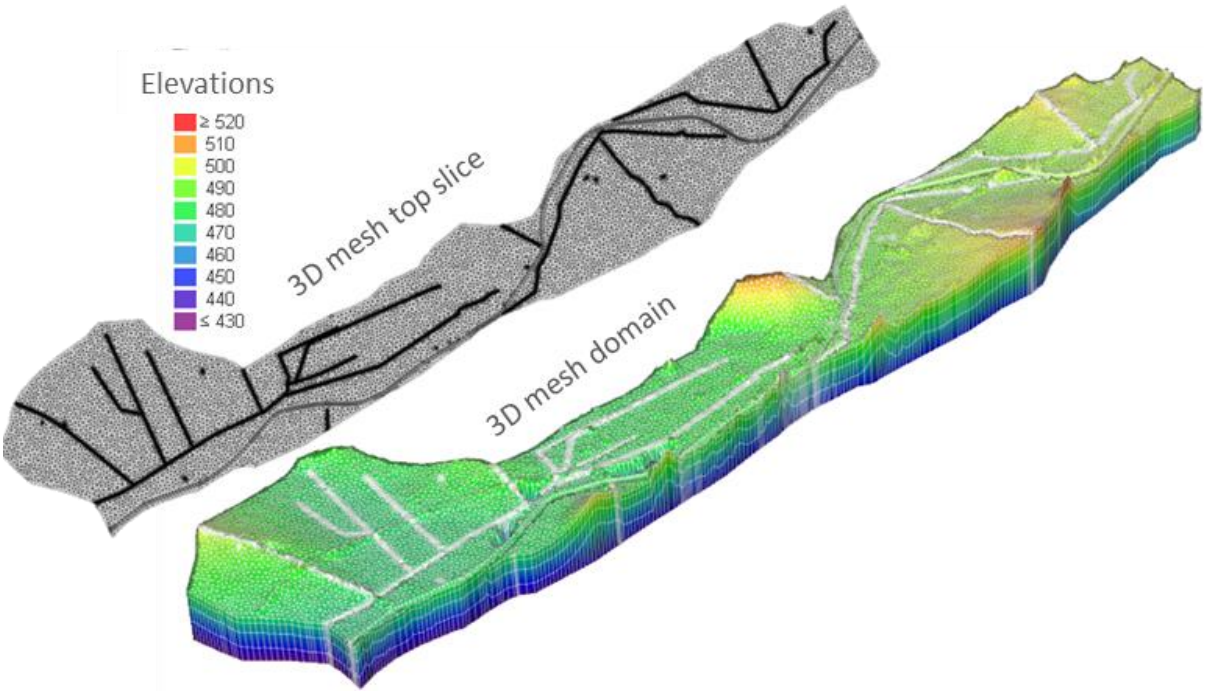

Figure 4.27: Three-dimensional mesh domain in a perspective view (bottom) and in a top view (top).

The average elemental diameter is 25.1 m with a standard deviation of 24.5 m. This discretization is assumed to be sufficient to allow the calibration of a heterogeneous hydraulic conductivity field. A non-uniform anisotropy angle simulating the variations of the direction of the Rhône River will be enforced during the calibration process by varying the angle of anisotropy at each element during the interpolation (Kriging) from the estimated value at the pilot points locations. Therefore, a heterogeneous hydraulic conductivity field is generated that follows the shape of the Rhône River and tend to mimic the potential geological structures resulting from the sedimentation processes.

The average layer thickness is 10.5 m with a standard deviation of 4.4 m (4 layers with an expanding nodal spacing inferior to 1.5). The vertical discretization is necessary to accommodate the vertical variation in heads generated by vertical flux caused by partially penetrating hydraulic features such as the Rhône River and its tributaries as well as the superficial drainage network. This number of layers ensures that heads in the middle layer of the alluvial aquifer are computed using values of vertical leakance based entirely on its own vertical hydraulic conductivity K_z [*Anderson et al.*, 2015].

Internal boundaries and observation wells are placed on a predefined node located at the exact boundary position.

Fluid flow boundary conditions comprise 435 nodes with specified head condition (Upstream and downstream equipotential lines), 210 nodes with specified flux condition (Conthey dejection cone) and a total of 23'276 nodes with head-dependent condition (Rivers and drains) from which 18'242 have a maximum flow constraint of 0 (Drains).

Concerning the temporal discretization employed during transient simulations, an adaptive time stepping explained in *Diersch* [2014] is used:

$$\Delta t_{n+1} = \Delta t_n \left(\frac{\varepsilon}{d_{n+1}} \right)^B \qquad \textbf{4.10}$$

Where Δt_n and Δt_{n+1} are the current and next time step respectively, ε is the closure criterion or error tolerance, d_{n+1} is the absolute value of the local truncation error and B a constant equal to 1/3.

4.3.3.2. Parameters assignment

As shown in **equation 4.3** and **4.5**, the distribution of the hydraulic heads is a function of the hydraulic parameters and especially of the aquifer hydraulic conductivity K. The uncertainty on its value in each element of the model mesh is essentially due to its heterogeneity given that variations of several orders of magnitude can happen over relatively short distance [*Fetter*, 2001; *Heath*, 1983]. Moreover, acquaintance of potential heterogeneity is all the more important considering the study hydrogeological system is an alluvial plain crossed by several alluvial fan originating from rivers flowing through different lithologies.

In the same way, riverbed conductance is difficult to measure in the field, especially for large river such as the Rhône River. Moreover, the high degree of heterogeneity typically found in riverbed [*Calver*, 2001; *Rosenberry et al.*, 2008] makes upscaling of point measurements of hydraulic properties particularly problematic. Therefore, the conductance of the Rhône riverbed will be estimated during the calibration process as well as these from the tributaries and the drains.

Hydrologic stresses such as recharge by rain and pumping wells have been estimated from metrological data (SwissMeteo) for the former and determined by request to the persons in charge for the latter [*Glenz*, 2013]. Therefore, their values will not be calibrated in the model. For the recharge, a piecewise constant recharge rate is assigned to the whole domain. In the same way, surface water constraints obtained from corrected digital elevation model (Tributaries and drains) and hydraulic simulations (Rhône River) for head-depend boundaries will also not be estimated.

Two methods of mesh population will be used: zonation and interpolation. Zonal parametrization will be achieved using the geologically based hydrofacies composition of the study zone displayed in the *Conceptual Model* section (**Figure 4.6**). This method imposes homogeneity of the estimated values within each zone and no interpolation methods are required to populate the mesh elements. When this approach as the advantage of limiting the number of parameters to be estimated it cannot accommodate potential heterogeneity within the predefined zones. Conversely, the interpolation scheme will use parameter values estimated at specified locations to compute by interpolation values at every elements in the mesh. This process is known as the Pilot Point method [*Doherty*, 2003; *Gomez-Hernandez et al.*, 1997; *Ramarao et al.*, 1995]. Within the alluvial aquifer hydrostratigraphic unit, the interpolation from pilot points allows for a gradation in the hydrogeological properties. This approach has the advantage to allow more flexibility in the representation of the heterogeneity than the zonation approach. However, use of Pilot Points method leads generally to a highly parameterized model, i.e. large number of parameters and possibly more parameters than observations because a large number of pilot points must be spread over the model and the value of the parameter at each pilot point has to be estimated. Highly parameterized models lead often to non-unique solutions in the estimation of the parameters and render often the problem intractable. Nevertheless, regularization method by problem expansion (Tikhonov) or reduction (Singular Value Decomposition, see *section 3.3 Parameter estimability and predictive uncertainties* in *Chapter 3*) can make the inversion process tractable [*Doherty*, 2015; *Doherty and Hunt*, 2010]. Interpolation between the pilot points is done using geostatistical method via kriging. The kriging is based on parameter correlation according to the distance of separation and is characterized by a variogram. For the study, the spatial interpolation parametrization is complemented by a spatial variation of the anisotropy angle in order to simulate the horizontal anisotropy of the aquifer hydraulic conductivity caused by the fluvial sedimentation/erosion processes related to variation in the Rhône River flowing direction. Therefore, a mapping of the anisotropy angle for each element of the mesh is done according to the flowing direction of the Rhône River.

Table 4.5: Pre-calibration parametrization of the base model.

Feature	Property	ID	Value	Unit
Rhone Alluvial Plain				
Rhone Aquifer	Hydraulic Conductivity	Aq	10^{-3}	m/s
Rhone River				
Rhone Riverbed	Infiltration Conductance	Rh_I	10^{-6}	s^{-1}
Rhone Riverbed	Exfiltration Conductance	Rh_O	10^{-4}	s^{-1}
Tributaries				
Lienne Riverbed	Infiltration Conductance	Le_I	10^{-9}	s^{-1}
Borgne Riverbed	Infiltration Conductance	Bo_I	10^{-9}	s^{-1}
Sionne Riverbed	Infiltration Conductance	Si_I	10^{-9}	s^{-1}
Printse Riverbed	Infiltration Conductance	Pr_I	10^{-9}	s^{-1}
Morge Riverbed	Infiltration Conductance	Mo_I	10^{-9}	s^{-1}
Lizerne Riverbed	Infiltration Conductance	Le_I	10^{-9}	s^{-1}
Canals				
Uvrier Canal	Exfiltration Conductance	Uv_O	1	s^{-1}
Vissigen Canal	Exfiltration Conductance	Vi_O	1	s^{-1}
Iles Canal	Exfiltration Conductance	Il_O	1	s^{-1}
Blancherie Canal	Exfiltration Conductance	Bl_O	1	s^{-1}
Polonais Canal	Exfiltration Conductance	Po_O	1	s^{-1}
Sion-Riddes Canal	Exfiltration Conductance	SR_O	1	s^{-1}
Vetroz Upstream Canal	Exfiltration Conductance	V__O	1	s^{-1}
Vetroz Downstream A Canal	Exfiltration Conductance	VA_O	1	s^{-1}
Vetroz Downstream B Canal	Exfiltration Conductance	VB_O	1	s^{-1}

Table 4.5 shows the parametrization of the base model that will serve as an initial state regarding the hydraulic properties of the model for subsequent calibration processes. This parameterization will be increased in the following models by adding spatially varying values for the hydraulic conductivity of the aquifer and the Rhone riverbed (Pilot Points). In the base model, the hydraulic conductivity of the aquifer is considered homogeneous and isotropic over the whole area.

The Rhone riverbed is considered to be a resisting layer with a conductance of 10^{-4} s^{-1} and 10^{-6} s^{-1} in infiltrating and exfiltrating conditions respectively. Subsequently, this parameter will be estimated. The tributary beds are considered impervious (very low conductance), thus no infiltration from these streams into the groundwater is initially enforced. As their positions are higher than the surrounding water table, no exfiltration of the groundwater into these streams is expected. The canals are considered as drains and their surface unclogged. Therefore, the conductance is set to a high value so that aquifer properties around the drain control the flow.

Based on the conceptual model established in the precedent section, this section has developed the setup of the numerical model of the Rhône River and its alluvial aquifer. The following section (*4.4*) is introduced with a brief presentation of the numerical modeling and inversion code as well as the metric chosen to evaluate the parameter estimation processes. Then, in the first subsection, (*4.4.1*) the discrepancies between simulated and observed heads are calculated for the base model and a manual trial-and-error history matching is carried out in order to assess the sensitivity of the model output to parameter value variations. Subsequently, the following subsections present the results of the calibration processes of the two-dimensional zonal steady-state (*4.4.2*) and three-dimensional heterogeneous transient simulations (*4.4.3*). The purpose of the calibration process is to support the credibility of the forecast of future water table elevation, and to reduce the predictive uncertainty, by achieving a satisfying fit, relatively to the assumed measurement error, between observed (179 observation wells) and simulated heads.

4.4. Models calibration

The groundwater modeling code selected is FEFLOW [*Diersch*, 2014], a verified, with long track record finite element code adapted for calibration and uncertainty analysis using the automated parameter estimation code PEST [*Doherty*, 2015].

The groundwater flow code FEFLOW has been chosen because of the flexibility of the Finite Elements method in designing complex perimeter and internal features, the accuracy of the water balance, the capacity of increasing execution speed by using different equation-system solvers and parallel computing, and its acceptance amongst the groundwater modeling community and the 3rd Rhône River Correction project stakeholders. The equation-system solvers are selected according to their performance in terms of execution time and solution accuracy on the numerical model related in particular to the model node number and whether the simulation is steady-state or transient.

- For the two-dimensional steady-state model with a discretization comprising less than 200'000 mesh elements, the algebraic multigrid solver (SAMG) with a flow solution residual inferior to 5 10^{-5} m^3/d.
- For the three-dimensional transient model, the default iterative solver pre-conditioned conjugate-gradient (PCG) with a termination criterion of 10^{-5} has been chosen.

In the following simulations and calibrations of the model variants, summary statistics will be given by:

- The Mean Error, ME:

$$ME = \frac{\sum_{i=1}^{n}\left(h_{m_i} - h_{s_i}\right)}{n} \quad \textbf{4.11}$$

- The Mean Absolute Error, MAE:

$$MAE = \frac{\sum_{i=1}^{n}\left|h_{m_i} - h_{s_i}\right|}{n} \quad \textbf{4.12}$$

- The Root Mean Squared Error, $RMSE$:

$$RMSE = \sqrt{\frac{\sum_{i=1}^{n}\left(h_{m_i} - h_{s_i}\right)^2}{n}} \quad \textbf{4.13}$$

where n is the number of observations used during the calibration process, i is an index that refer to an observed value h_m and its counterpart simulated value h_s.

4.4.1. Base model

The base model retains the parametrization defined in the previous *Subsection 4.3.3.2 Parameters assignment* (See **Table 4.5**). Based on the homogeneous and isotropic value of the aquifer hydraulic conductivity a forward simulation of the two-dimensional variant of the numerical model design is executed. The results of the simulation in terms of errors between simulated and measured heads are presented in the **Figure 4.28**.

Figure 4.28A maps the errors between observed and simulated values as well as both the piezometric map of observed and simulated values. The errors are significant, in particular in the upstream part of the model and in the alluvial cone of Conthey, with values ranging from -2.83 to 1.36 m. **Figure 4.28B** and **C**, and **Table 4.6** display and quantify the positive bias of the simulated values, i.e. the mean error is significantly inferior to 0 with a value of -0.59 (See *ME* in **Table 4.6**). Although the maximum error is equal to 1.36 m, the 91th percentiles equal to 0.02 m (a value close to 0) confirms that the bias is essentially positive, i.e. simulated values are higher than observed values.

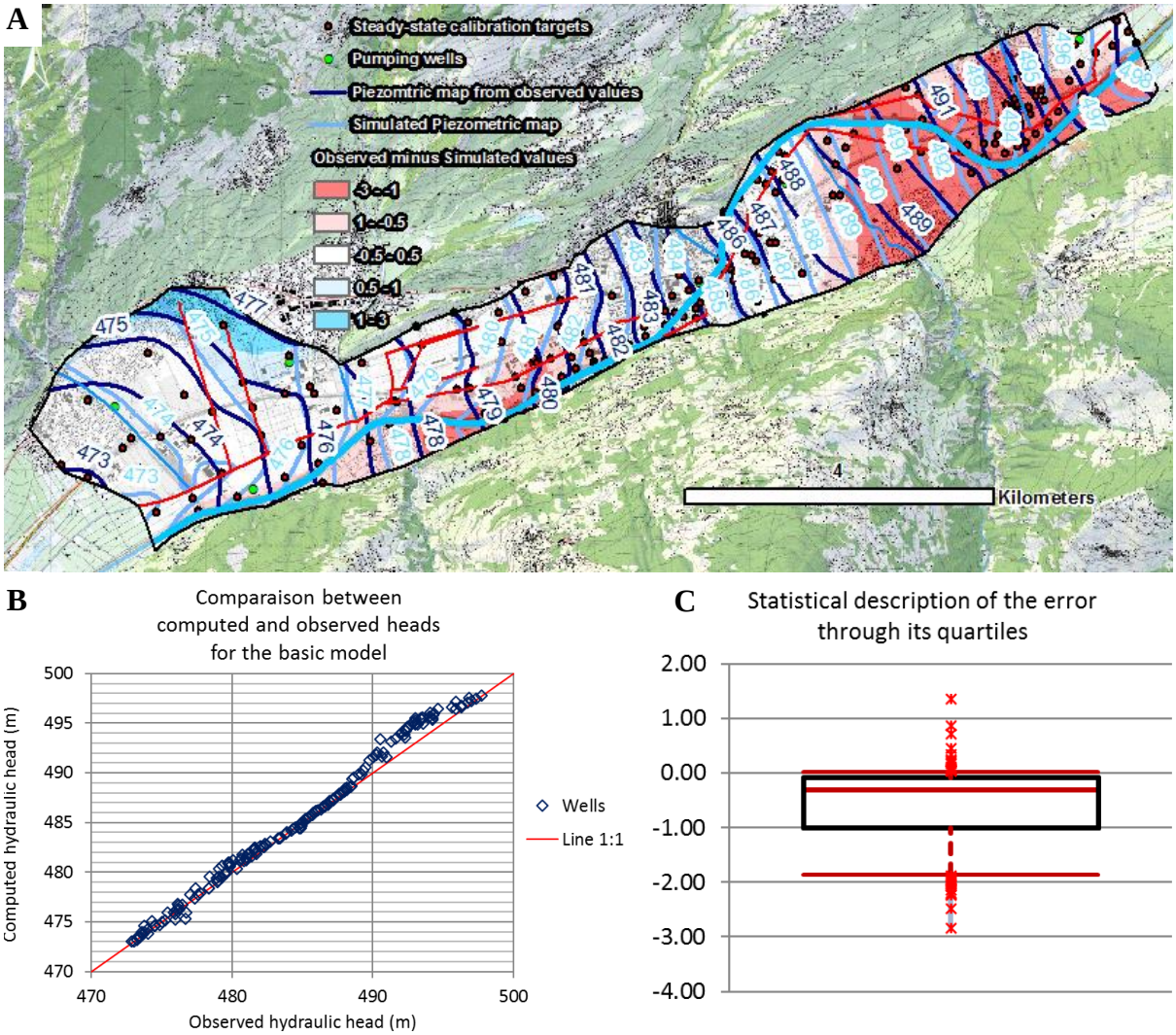

Figure 4.28: Visual and statistical descriptions of the base model run. **A)** Piezometric map from observed heads (calibration targets) and simulated heads. The colored area represents the spatial distribution of residual errors (differences between observed and simulated values). **B)** Scatter plot of observed heads versus simulated heads. **C)** Statistical description of the error between observed and simulated heads (Boxplot).

Table 4.6: Summary statistics of the calibration results for the forward simulation of the base model. The unit is the meter.

ME		***MAE***	***RMSE***	***Target range***	$\frac{RMSE}{Target\ range}$	**Standard deviation**	
-0.59		0.65	0.93	25	3.7%	0.67	
Percentiles	**Min**	**9th**	**25th**	**Median**	**75th**	**91th**	**Max**
	-2.83	-1.86	-1.00	-0.31	-0.08	0.02	1.36

The water budget presented in **Table 4.7** shows the balance between the inflows and outflows that gives a negligible error of 9 m^3/d, inferior to 0.03% of the hydrologic cycle. The amount of water that goes through the model domain is around 35'590 m^3/d. This value is of the same order of magnitude as the value calculated during the establishment of the conceptual model (See *4.2.3 Flow system and groundwater budget*). The inflow is dominated by the Specified flux comprising the alluvial fan of Conthey and the recharge by rain, and by the Head-dependent boundaries, essentially represented by the Rhône River infiltration. The tributaries in view of the low conductance of their bed infiltrate a negligible amount of water, i.e. less than 1%. Concerning the upstream groundwater inflow, its value represents 22% of the total inflow which represents less than 62% of the downstream groundwater outflow.

In order to assess the sensitivity of the mean absolute error, which is equal to 0.65 (See **Table 4.6**), to the variation of the parameters values, the results of a manual trial-and-error history matching is presented in **Figure 4.29**. The results show that increasing the values of the tributary beds conductance leads to an increase in the value of the MAE. A similar, although smaller, trend can be observed for decreasing values of the canal beds. Conversely, decrease of the Rhône riverbed conductance clearly leads to a decrease of the MAE with a minimum for values ranging between 10^{-6} and 10^{-8} m/s. However, further decrease of the conductance of the Rhône riverbeds causes the MAE to rise. This observation is consistent with the computed errors between observed and simulated values that show that the simulated values tend to be higher than the observed ones, especially in the upstream part of the model domain. Therefore, decrease of the Rhône River infiltration caused by decrease in the riverbed conductance will lower the surrounding water table elevation and thus reduce the discrepancies between simulated and observed heads. Nevertheless, further reduction of the Rhône riverbed conductance, preventing a sufficient infiltration of the Rhône River can lead to important decreases of the surrounding water table and thus caused the MAE to increase. In summary, this analysis suggests that the conductance of the Rhône riverbed should be calibrated and that spatial variation of its values may reduce the post-calibration value of the MAE. Concerning the hydraulic conductivity of the aquifer, an increase of its value causes a reduction the MAE. However, value of 0.1 m/s are not consistent with expert knowledge based on aquifer tests. The reduction of the MAE is related to the increase in the value of the ratio between aquifer horizontal hydraulic conductivity and the Rhône River infiltration flux that tend to flatten the simulated head profile and thus, for the base model, reducing the discrepancies between simulated and observed heads.

In summary, the results of the forward simulation of the base model show that the errors between simulated and observed heads are significant, with a $RMSE$ of 0.91 and a ratio $RMSE/(Target\ range)$ of 3.7%. Moreover, a bias toward too high elevations of the water table (ME = -0.59) is present. Also, a manual trial-and-error history matching has been pursued and demonstrated the possibility of reducing the MAE by varying the values of the model parameters. Consequently, further calibrations, using more flexible and efficient parameter estimation approaches through automated trial-and-error history matching appear to be necessary and is the objective of the next sections. As mentioned previously, the main point in achieving a better fit, relatively to the assumed measurement error, between observed and simulated heads, is to increase the confidence in the forecast of future water table elevation and to reduce its uncertainty.

4.4.2. Calibration of the two-dimensional zonal steady-state model

4.4.2.1. Calibration approach and model parametrization

The automated trial-and-error calibration process aims at estimating a set of model parameters using algorithms such as the gradient method (Gauss-Levenberg-Marquardt) described in *Section 1.5 Hydrogeological modeling* at *Chapter 1*. The efficiency of the calibration process is assessed by quantifying the simulated to observed values misfit. Therefore, the positions and the values of the head observations constrain the estimation of the parameters and the information provided is referred as "hard knowledge". Furthermore, the validity of the values estimated for each parameter is assessed using so-called "soft knowledge" or "expert knowledge", i.e. range in which the values of estimated parameters are deemed to be consistent with the conceptual model (values reported for the site from field and laboratory measurements or from literature). Generally, the "soft knowledge" is enforced within the calibration process by imposing limits to the values that a parameter can adopt.

Table 4.7: Water budget for the forward simulation of the base model. The flow components of the water budget are decomposed according to the *Boundary types*, the *Hydraulic features* and the *Elements of the water cycle*.

Inflows								Outflows							
Boundary types	**m³/d**	**%**	**Hydraulic features**	**m³/d**	**%**	**Elements of the water cycle**	**m³/d**	**%**	**%**	**m³/d**	**Elements of the water cycle**	**%**	**m³/d**	**Hydraulic features**	**%**	**m³/d**	**Boundary types**
Specified head boundaries	7261	**22.3**	Upstream aquifer limit	7261	**22.3**	Upstream groundwater inflow	7261	**22.3**	**36.1**	11773	Downstream groundwater outflow	**36.1**	11773	Downstream aquifer limit	**36.1**	11773	**Specified head boundaries**
Specified flux boundaries	14119	**43.3**	Lateral aquifer recharge	2955	**9.1**	Alluvial fan of Conthey	2955	**9.1**	**15.7**	5100	Pumping wells	**15.7**	5100	Focused discharge	**15.7**	5100	**Specified flux boundaries**
			Diffuse	11164	**34.3**	Effective rain	11164	**34.3**	**17.0**	5527	Rhône River	**17.0**	5527	Rhône River			
			Rhône River	10891	**33.4**	Rhône River infiltration	10891	**33.4**	**7.7**	2514	Uvrier Canal	**31.3**	10185	Drainage network			
			Tributaries	323	**1.0**	Lienne River	40	**0.1**	**2.3**	764	Vissigen Canal						
						Borgne River	95	**0.3**	**1.4**	454	Iles Canal						
						Sionne River	26	**0.1**	**3.9**	1281	Blancherie Canal						
Head-dependent boundaries	11214	**34.4**				Printse River	12	**0.0**	**2.2**	711	Polonais Canal						
						Morge River	28	**0.1**	**13.6**	4428	Sion-Riddes Canal						
						Lizerne River	122	**0.4**	**0.1**	33	Vetroz Upstream Canal				**48.2**	15712	**Head-dependent boundaries**
									0.0	0	Vetroz Downstream A Canal						
									0.0	0	Vetroz Downstream B Canal						
								TOTAL									
	32594	**100**		32594	**100**		32594	**100**	**100**	32585		**100**	32585		**100**	32585	
								Δ Error									
								9 m³/d									

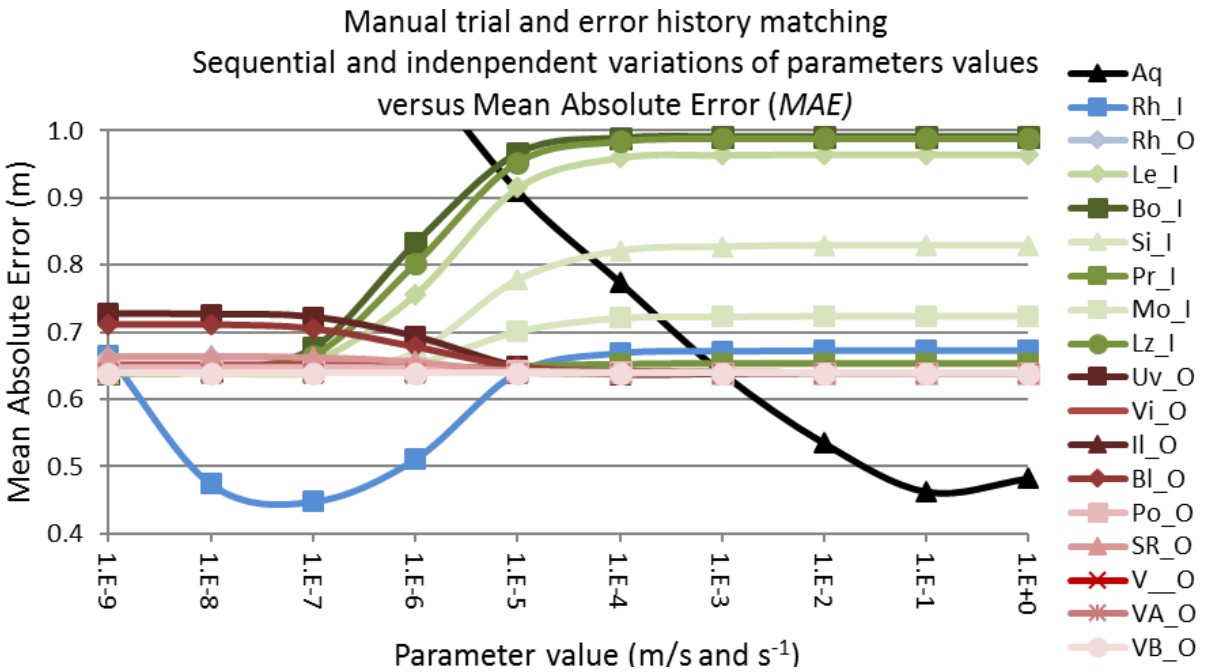

Figure 4.29: Evolution of the Mean Absolute Error (The MEA is equal to 0.65 for the Base model) for different value of the parameters. Each parameter takes values from 1e-9 to 1 and the other parameters remain at their original values (See **Table 4.5**).

The underlying assumption of the calibration process is that by achieving a satisfying fit, relatively to the assumed measurement error, between observed and simulated heads the confidence in the forecast of future water table elevation and the reduction of its uncertainty can be improved. As demonstrated in the previous *Chapter 3*, the credibility of the prediction uncertainty is supported by the assumption that the model defects are minimized regarding the prediction of interest. In order to reduce the large structural error induced by considering only one value of hydraulic conductivity for the all aquifer domain, hydrogeological zones based on the geological model of Sion [*Sartori et al.*, 2011], are defined. The zonal discretization of the hydraulic conductivity of the aquifer allows to formulate an overdetermined (well-posed) inverse problem by maintaining the number of calibration parameters (56 parameters, see **Table 4.8**) at a lower value than the number of observations (179 observations) [*Hill and Tiedeman*, 2007]. Zonal discretization involves that within a specified zone all elements will be assigned a same estimated value of hydraulic conductivity.
The model domain is divided into eleven zones (**Figure 4.30**). The firsts three zones represent a segmentation of the Rhone alluvial plain nearby the Rhône River and excluding the alluvial cones from the tributaries as well as the area of Sion airport. This segmentation allows potential variations of the hydraulic conductivity of the river alluviums before, within and after the alluvial cone of the Borgne River. The other sections of the model represent essentially variations in the geology due to the nature of the alluvial cones of the different tributaries of the Rhône River.

4.4.2.2. Calibration results and estimated parameters

The results of the automated calibration in terms of history matching are summarized in **Table 4.9**. The calibration achieved a value of the mean average error, *MAE*, of 0.11 m, which represents a significant reduction of the residual error compared to the base model for which it was 0.65 m. Moreover, the mean error, *ME*, is very close to 0 (-0.01 m), i.e. no significant model bias is present after the parameter estimation process. In the same way, the reduction of the post-calibration root means squared error, *RMSE*, (from 0.93 to 0.15 m) and standard deviation (from 0.67 to 0.11 m) support the efficiency this calibration.

Table 4.8: List and number of the parameters estimated during the automated calibration process. The In-transfer rate and Out-transfer rate [T^{-1}] represent the conductance of the different hydraulic features when the surface water infiltrates the groundwater and exfiltrates the groundwater respectively.

Parameters	Type	Number
Alluvial plain	Zonation	11
Rhône River In-transfer rate	Pilot Points	15
Rhône River Out-transfer rate	Pilot Points	15
Tributaries In-transfer rate	Zonation	6
Canals Out-transfer rate	Zonation	9
		56

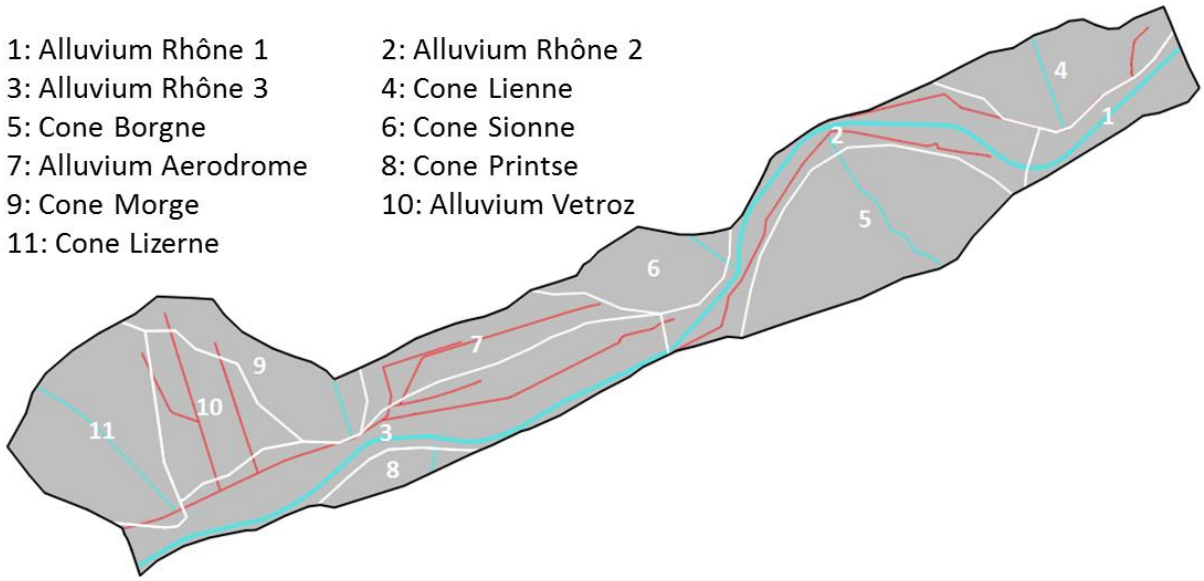

Figure 4.30: Definition of the 11 hydrofacies based on the geological model of Sion [*Sartori et al.*, 2011].

Table 4.9: Summary statistics and quantification of the calibration results of the two-dimensional zonal steady-state model. The unit is the meter.

ME	MAE	$RMSE$	$Target\ range$	$\frac{RMSE}{Target\ range}$	Standard deviation	
-0.01	0.11	0.15	25	0.6%	0.11	
Percentiles	**Min**	**9th**	**25th**	**Median**	**75th**	**91th**	**Max**
	-0.68	-0.18	-0.09	-0.00	0.06	0.16	0.45

Figure 4.31A shows the distribution of the residual errors that range from -0.68 to 0.45 within the study area (values inferior to -0.68 are present outside of the study zone close to the upstream model boundaries). The scatter plot and box plot of the **Figure 4.31B** and **C** synthesize the calibration results and allow to visualize its efficiency in particular in the upstream part of the model domain. A summary of the estimated parameters is presented in **Table 4.10**. It can be observed that the area of the alluvial fan of the Borgne River presents the highest value of hydraulic conductivity (1.2 10^{-3} m/s), which is consistent with previous studies [*GéoVal Ingénieurs-Géologues SA*, 1986]. Also, the value estimated for the near Rhône River alluviums range from 3.2 to 7.9 10^{-4} m/s, which are values in accordance with expert knowledge. The lowest value is found at the Printse alluvial cone (2.3 10^{-6} m/s), which can result from the lower identifiability of the parameters in this area given that no observation is present within it (**Figure 4.24** and **Figure 4.25**), except at its border along the Rhône River. This assumption is confirmed by the computation of the parameter identifiability (the method is presented in *Chapter 3*) that is close to 0 (See **Table 4.11**).

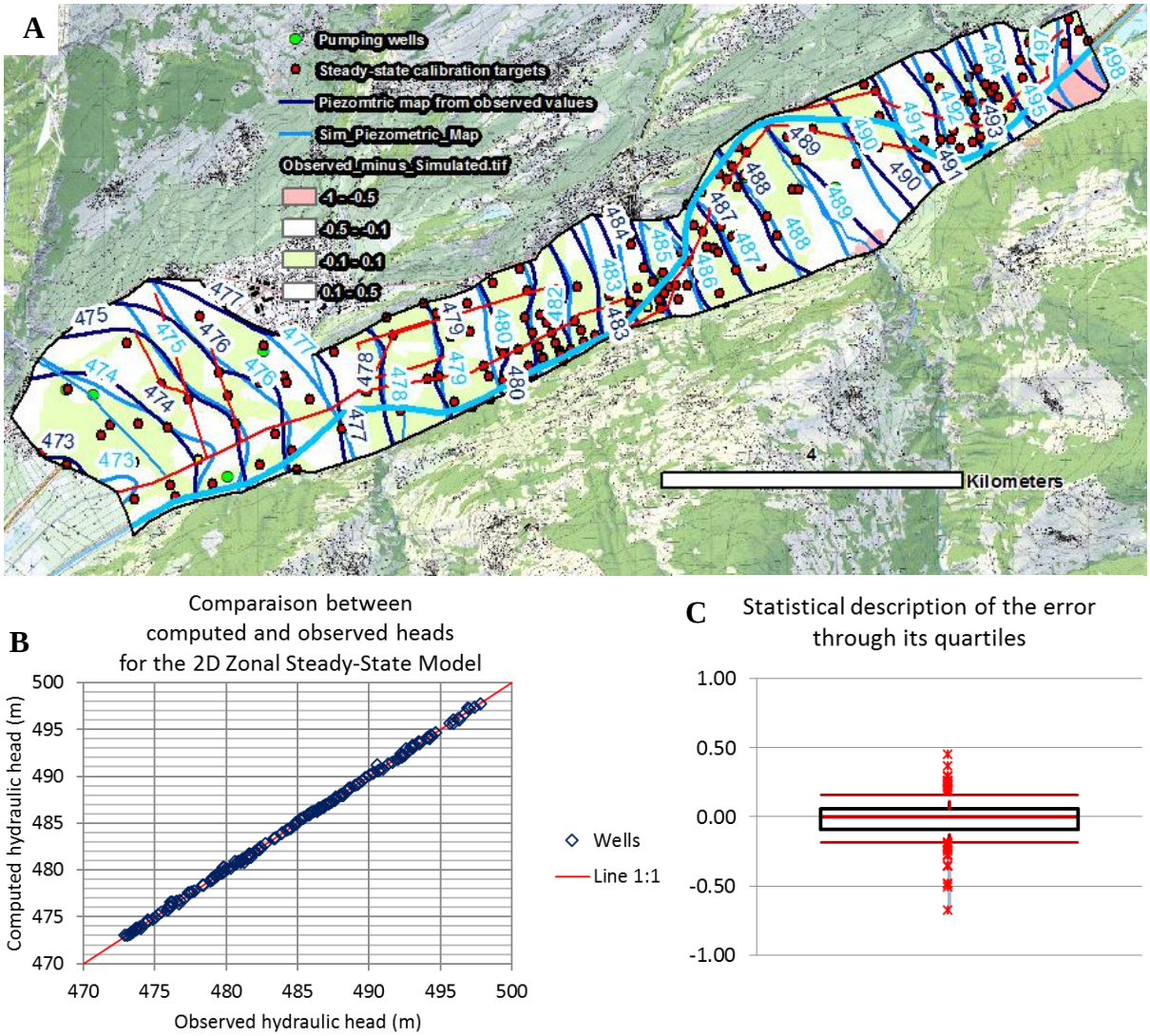

Figure 4.31: Visual and statistical descriptions of the two-dimensional zonal steady-state model calibration. **A)** Piezometric maps from observed data (calibration targets) and simulated heads. The colored area represents the spatial distribution of residual errors (the difference between observed and simulated values). **B)** Scatter plot that shows observed head targets versus simulated heads. **C)** Statistical description of the error between observed and simulated heads (Boxplot).

Concerning the tributaries and canals, it can be observed that the values of the conductance of their beds remain close to their initial values. This implies that variations of these parameters are not necessary to improve the matching between the simulated and observed values. Also, their values are maintained to their initial one due to the regularization constraint imposed to each parameter, which penalized the calibration process when a variation of the initial value of a parameter does not lead to a reduced residual error. The computation of the parameters identifiability and post-calibration uncertainty reduction shown in **Table 4.11** point out the inefficiency of the calibration process in estimating values for these parameters.

The minimum, maximum, average and standard deviation values of the In-transfer and Out-transfer rate of the Rhône riverbed, which represent the values of the riverbed conductance for the case of gaining and losing river respectively are shown in **Table 4.10**. The average values are 7.4 10^{-6} and 7.0 10^{-4} m/s respectively. Although the value of the standard deviation (4.3 10^{-5} and 3.3 10^{-3} m/s) shows that the absolute values vary along the course of the Rhône River, **Figure 4.32A** and **B** inform us that the identifiability of the In- and Out-transfer rates of the Rhone riverbed is limited to a few points in both cases.

Table 4.10: Estimated values for each parameter and summary statistics.

Hydraulic Conductivity (m/s)

	Estimated value
Alluvium Rhône 1	$3.2\ 10^{-4}$
Alluvium Rhône 2	$7.9\ 10^{-4}$
Alluvium Rhône 3	$4.6\ 10^{-4}$
Cone Lienne	$4.1\ 10^{-4}$
Cone Borgne	$1.2\ 10^{-3}$
Cone Sionne	$5.8\ 10^{-4}$
Alluvium Aerodrome	$1.2\ 10^{-3}$
Cone Printse	$2.3\ 10^{-6}$
Cone Morge	$2.2\ 10^{-5}$
Alluvium Vetroz	$1.5\ 10^{-5}$
Cone Lizerne	$5.0\ 10^{-5}$
Hydrostratigraphic unit average	$4.5\ 10^{-4}$

In-transfer Rate (d^{-1})

	Estimated value	Minimum	Maximum	Average value	Standard deviation
Rhone Riverbed		$1.3\ 10^{-9}$	$7.5\ 10^{-4}$	$7.4\ 10^{-6}$	$4.3\ 10^{-5}$
Lienne Riverbed	$9.8\ 10^{-10}$				
Borgne Riverbed	$1.0\ 10^{-9}$				
Sionne Riverbed	$8.7\ 10^{-10}$				
Printse Riverbed	$9.9\ 10^{-10}$				
Morge Riverbed	$6.5\ 10^{-9}$				
Lizerne Riverbed	$7.2\ 10^{-9}$				

Out-transfer Rate (d^{-1})

	Estimated Value	Minimum	Maximum	Average Value	Standard Deviation
Rhone Riverbed		$2.4\ 10^{-5}$	$5.2\ 10^{-2}$	$7.0\ 10^{-4}$	$3.3\ 10^{-3}$
Uvrier Canalbed	1.1				
Vissigen Canalbed	1.0				
Blancherie Canalbed	1.0				
Iles Canalbed	0.9				
Polonais Canalbed	1.0				
Sion-Riddes Canalbed	1.0				
Vetroz Up. Canalbed	1.0				
Vetroz Do. A Canalbed	1.0				
Vetroz Do. B Canalbed	1.0				

The Out-transfer rate value is well identifiable in the exfiltrating part of the groundwater, i.e. along the city of Sion and in the downstream part of the Borgne alluvial cone. Along the rest of the Rhone River, the Out-transfer rate can solely be constrained by expert knowledge, either by constraints on the initial value (as it is the case in this calibration process) or by a constraint of homogeneity. Here the first condition has been chosen to highlight the none-identifiability of the parameters.

4.4.2.3. Discussion on the two-dimensional steady-state calibration

The steady-state calibration using average hydraulic heads allowed to estimate the value of the aquifer hydraulic conductivities and therefore to significantly reduce the discrepancies between simulated and observed heads. However, numerous parameters, in particular, the hydraulic properties of the Rhône riverbed, present a low identifiability. In *Chapter 2*, it was shown that transience, especially aquifer response to river stage transience, provides information to the calibration of the hydrogeological properties of the riverbed. Furthermore, transience in the Rhone River due to Hydropeaking generates inversion in the river-groundwater gradient that would be favorable to the estimation of both In- and Out-transfer rates.

The zones of piecewise constant parameters based on geological formations neglect and constrain potential heterogeneity and anisotropy of the aquifer (*Chapter 3*).

Table 4.11: Identifiability and relative uncertainty variance reduction of the estimated parameters according to the calibration dataset.

Parameter	Identifiability	Relative Uncertainty Variance Reduction
Hydraulic Conductivity		
Alluvium Rhône 1	0.9	0.7
Alluvium Rhône 2	1	1
Alluvium Rhône 3	0.9	0.8
Alluvium Aerodrome	0.7	0.6
Cone Printse	0.0	0.0
Cone Borgne	0.3	0.3
Cone Morge	0.5	0.5
Cone Sionne	0.2	0.3
Cone Lienne	0.9	0.7
Alluvium Vetroz	0.9	0.5
Cone Lizerne	1.0	1.0
Out-transfer Rate		
Uvrier Canalbed	0.0	0.0
Vissigen Canalbed	0.0	0.0
Blancherie Canalbed	0.0	0.0
Iles Canalbed	0.0	0.0
Polonais Canalbed	0.0	0.0
Sion-Riddes Canalbed	0.0	0.0
Vetroz Up. Canalbed	0.0	0.0
Vetroz Down. A Canalbed	0.0	0.0
Vetroz Down. B Canalbed	0.0	0.0
Out-transfer Rate		
Sionne Riverbed	0.0	0.0
Printse Riverbed	0.0	0.0
Lizerne Riverbed	0.0	0.0
Lienne Riverbed	0.0	0.0
Borgne Riverbed	0.0	0.0
Morge Riverbed	0.0	0.0

Moreover, the abrupt changes of value across the boundaries are often not geologically realistic. Manual regularization by zones in which expression of heterogeneity is limited can lead to bias in the estimation of predictive uncertainty. However, it was shown that the hydraulic properties of the domain might not be uniquely estimable all over the domain due to a lack of data in certain zones. Nevertheless, because predictions of water table elevation concern the whole domain it seems necessary to assess the uncertainty of the hydraulic conductivity over the whole domain. This involves that parameters, which cannot be uniquely estimated, should be present in the model in order to better quantify the predictive uncertainty. Although the errors between simulated and observed heads has been significantly decreased by the calibration of the two-dimensional zonal steady-state model, a calibration using pilot points would probably reach a better fit. A highly parameterized approach using pilot points distributed throughout the model would allow to extract further information from the calibration dataset when it is possible and at the same time, it may increase the level of non-uniqueness when the calibration does not provide sufficient information, which may lead to a better assessment of the uncertainty associated with the predictions. Nevertheless, addition of soft knowledge and collapse of the problem dimensionality through singular value decomposition may be required in order to ensure the stability of the inverse problem and to prevent potential over-fitting, which can arise in a highly parametrized model.
In summary, highly parametrized models can be tractable and have the advantage, compared to zonal models, to not simplify the conceptual hydraulic conductivity field beforehand.

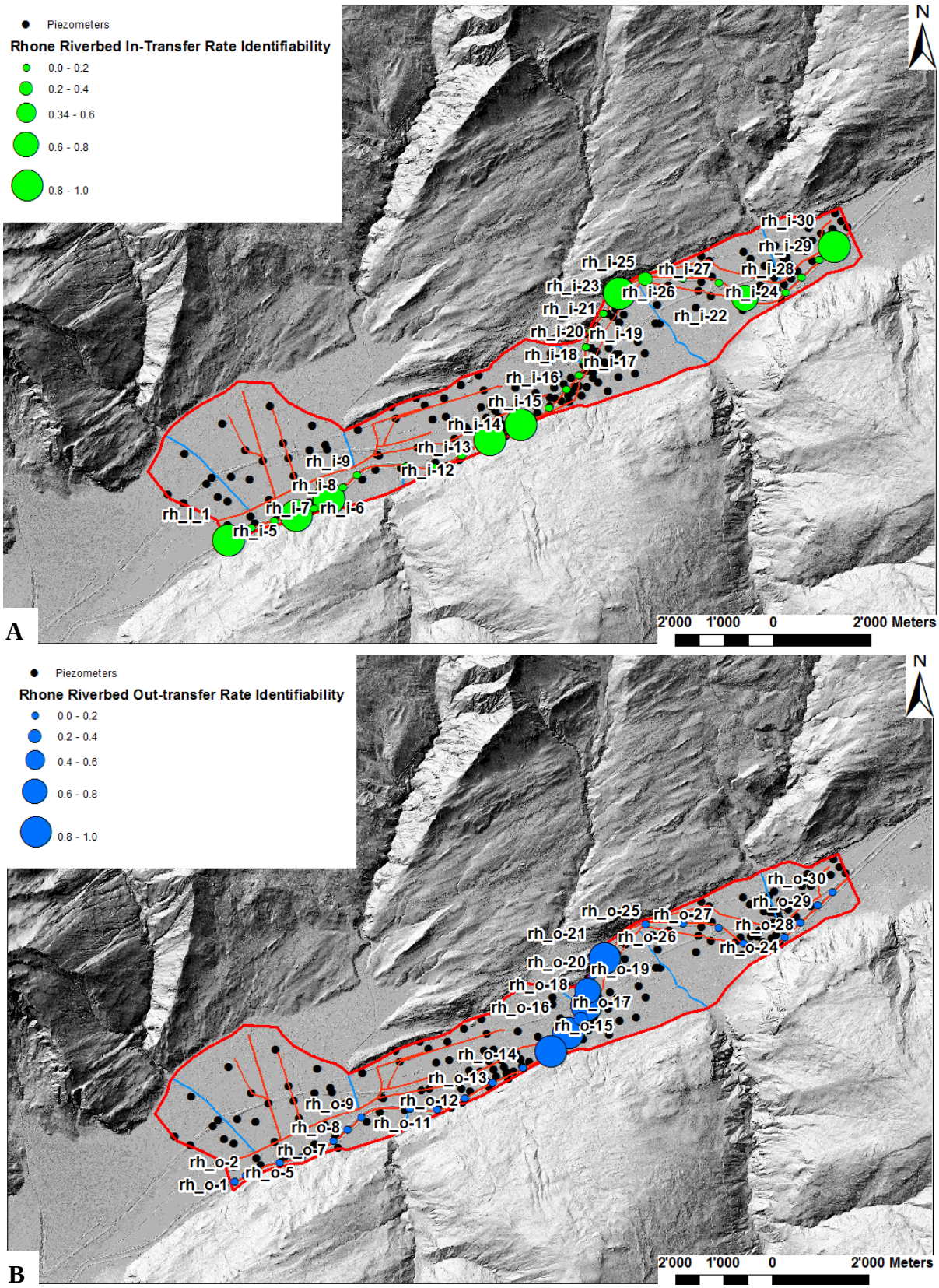

Figure 4.32: Values of the parameter identifiability of the In- and Out-transfer rates of the Rhone riverbed. The values range between 0 and 1. A value close to one means that the value of the parameter is estimable according to the defined calibration dataset and conversely for a value of 0.

Concerning the two-dimensionality of the domain, it was shown in the previous section *4.3.1 Model dimensionality* that errors may arise around partially penetrating hydraulic features. This is the consequences of not taking into account vertical fluxes. Moreover, in areally two-dimensional simulations the In- and Out-transfer rates have a limited physical sense, regarding the estimation of the real riverbed conductance, as the flux exchanges are assumed to occur along the whole depth of the domain. Another consequence that follows from this assumption is that the domain is hydraulically partitioned by the surficial hydraulic features. As the forecast is tightly related to the consequences of the modification of the Rhone River stage, which is a partially penetrating hydraulic feature, the accuracy of its simulation and thus its interaction with the surrounding groundwater should be pursued.
From this discussion, it follows that in order to meet the modeling purpose, the definition of a more complex model that take into account the following features should be pursued:

- The vertical fluxes: Design of a three-dimensional model.
- The potential heterogeneity and anisotropy of the hydraulic conductivity field: Design of a highly parameterized model including distributed pilot points over the aquifer domain during the calibration. Moreover, the value of the horizontal anisotropy of the hydraulic conductivity estimated in *Chapter 3* will be taken into account when defining the interpolation scheme between the pilot points.
- Transient calibration: Addition of information provided by transient aquifer responses to the Rhône River stage variations, due to daily hydropeaking, in order to increase the identifiability of the hydraulic parameters.

4.4.3. Calibration of the three-dimensional transient model

4.4.3.1. Model parametrization and initial conditions

According to the discussion in the previous subsection and following the model design described in the *Subsection 4.3.3 Model discretization and parametrization*, a three-dimensional variant of the numerical model was established (**Figure 4.33**) with a homogeneous thickness of the aquifer of 40 m. Also, the simulation of the gravel pit lakes described in the *Subsection 4.2.2.2 Canals and lakes*, are included in the mesh domain and a high value of hydraulic conductivity is given to the elements constituting the lakes (10^9 m/s) in order to simulate their influence on the surrounding groundwater.
Concerning the estimation of the potential heterogeneity, a set of 51 pilot points are placed in a uniform pattern to ensure coverage over the entire model domain (**Figure 4.34**). The pilot points are positioned on the plan view of the model domain and the estimated horizontal hydraulic conductivities are assumed to be homogeneous, same values, along the vertical axis. The estimations of the aquifer hydraulic conductivities over the domain are not constrained by geological data. Each pilot point defining the hydraulic conductivity of the aquifer is identified by the term k_x followed by a number (see **Figure 4.34**), i.e. k_x*-1* to k_x*-51*. Furthermore, for each element, a horizontal anisotropy angle is associated, according to the flow direction of the Rhône River and the interpolation by kriging of the hydraulic conductivity, over the domain from the pilot points, is endowed with an anisotropy factor of 4, i.e. in the direction of the anisotropy angle associated with the mesh element. The value of 4 is chosen according to the result obtained in *Chapter 3*. Therefore, the heterogeneous hydraulic conductivity follows the direction of the Rhône River and tend to mimic the potential geological structures resulting from the fluvial sedimentation processes.
The parametrization of the Rhône riverbed regarding the estimation of its conductance is defined by a set of 28 pilot points for each In- and Out-transfer rates.
The same setup as in the previous section is used for the calibration of the tributarybeds and canalbeds.

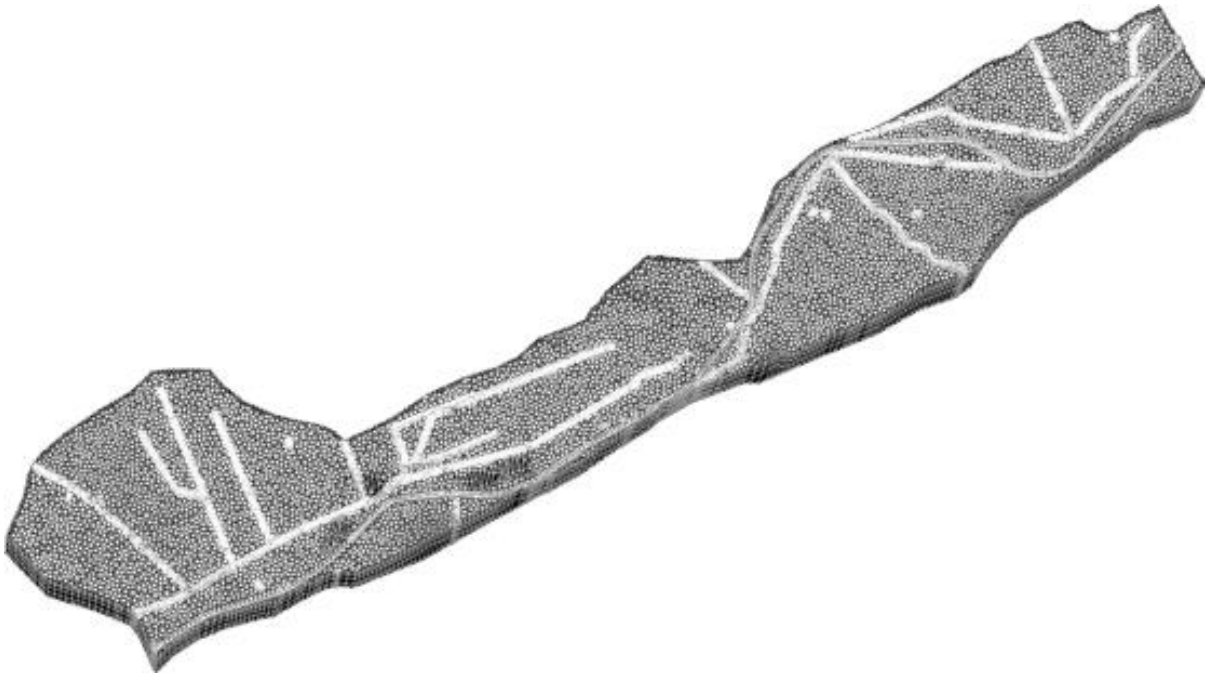

Figure 4.33: Three-dimensional variant of the model mesh of the study site.

The total amount of parameters estimated during the calibration process is 122. As mentioned previously the tractability of the inverse problem is ensure by a regularization scheme, named the hybrid SVDA/Tikhonov approach [*Doherty*, 2015; *Doherty and Hunt*, 2010], which presents the advantage of both reducing the execution time of the calibration process and increasing the likelihood of obtaining geologically realistic parameter fields.
Based on the estimation made in section *4.3.1 Model dimensionality* a spin-up period of 50 days is introduced prior the simulation of the transience. Therefore, the consistency between the model hydrogeological parameters and the initial heads is ensured and prevent the inappropriate adjustment of the heads in the early time of the transience that would not reflect the aquifer response to the Rhône River stage variations [*Franke et al.*, 1987].
Head difference targets are preferred over absolute values in order to increase the signal-to-noise ratio. Moreover, calibration against variations tend to protect the calibration process from bias incurred by wrong initial conditions [*Anderson et al.*, 2015]. The duration of the transient simulation is of 5 days and 5 observation wells positioned along the Rhône River constitute the transient head targets: *16_SHGN6543*; *47_B3*; *68_Tr-55*; *90_04K04*; *107_04E01* (See **Figure 4.24** for their locations and **Figure 4.38** for the results). The total number of transient observations amounts to 172, with a number of 23, 37, 49, 26 and 37 for each well respectively. An average of 6.9 time steps for each day is calculated.

4.4.3.2. Calibration results and estimated parameters

The results of the calibration are synthesized in the **Figure 4.35** and in the **Table 4.12**. Compared to the previous model, the mean average error and the standard deviation are further reduced to 0.07 m. The maximum and minimum error are also reduced from 0.45 to 0.36 and -0.68 to -0.28 respectively. **Figure 4.36A** shows the parameter identifiability for all pilot points used in the calibration of the aquifer hydraulic conductivity (K_x*-1* to K_x*-51*) and for the In- and Out-transfer rates of the Rhône riverbed. The information provided by the transient data allows a better identifiability of the Rhône riverbed hydraulic properties, especially for the In-transfer rate. However, estimability of the Out-transfer rate remains limited.

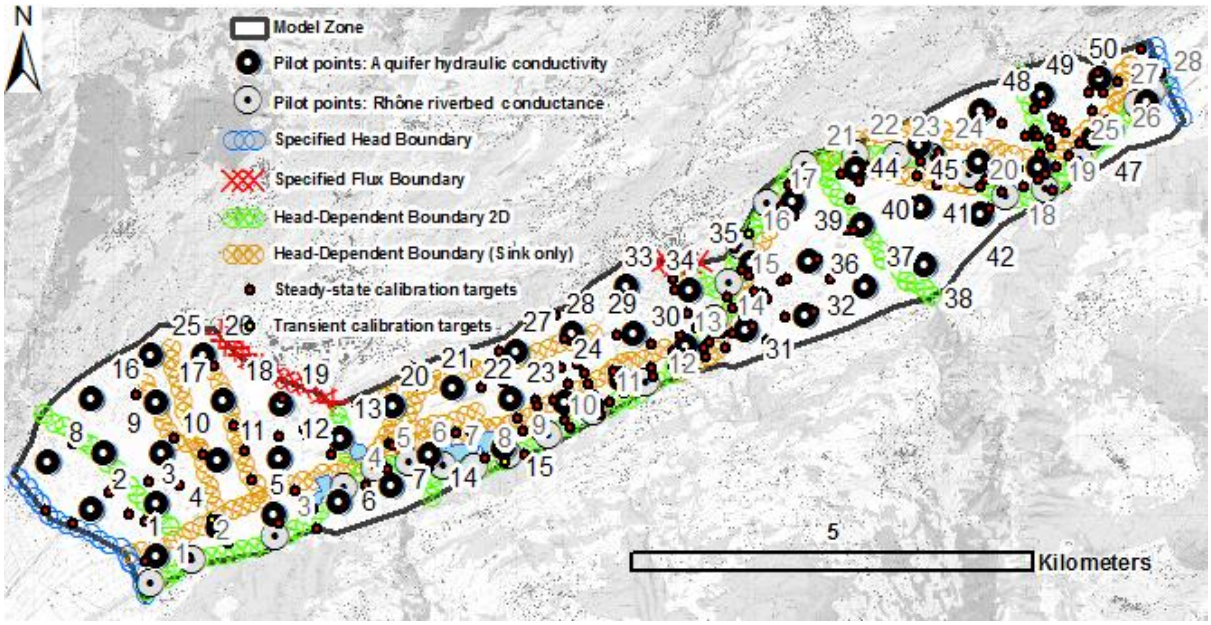

Figure 4.34: Model setup of the three-dimensional transient model including the Pilot Points method setup used during the parameter estimation process for the alluvial aquifer domain and the Rhône riverbed.

Overall, the identifiability is support by the proximity of the transient observations with respect to the estimated pilot points defining the hydraulic properties of the Rhône riverbed. The quality of the identifiability is pointed out by the value of the singular values that influence the parameter identifiability. Each value (*x-axis* in **Figure 4.36B**) of the 88 singular values (*y-axis* in **Figure 4.36B**) is related to an eigenvector, named *eig1* to *eig88*. The highest the value of the singular value is, the highest is the strength of the related eigenvector in identifying the parameter value. In **Figure 4.36A**, this is visualized by a gradation of red, for which a darker shade corresponds to higher singular value related eigenvector and thus a higher parameter identifiability. Consequently, the estimated values of the aquifer hydraulic conductivity appear to be well constrained by the calibration dataset and are consistent with expert knowledge (**Figure 4.37**).

Figure 4.38 shows the graphs of the transient observed and simulated values, as well as the resulting piezometric map. It can be observed that due to the simulation of the lakes, the isoline map of the water table are influenced by them (due to the imposed high value of the hydraulic conductivity of the mesh elements composing the lakes, i.e. 10^9 m/s). Moreover, gaining and losing part of the Rhône River can be visualized through the observation of water table contours that form a V, pointing upstream and downstream respectively.

Concerning the post-calibration fit of the transient observations. The observation wells *47_ B3*, *68_Tr-55*, *90_04K04*, and *107_04E01* present a relatively good fit, quantify by a Nash-Sutcliffe Efficiency coefficient (NSE) superior to 0, which values are 0.27, 0.23, 0.74 and 0.60 respectively. A value of the NSE close to 1 and superior to 0 meaning that the simulated heads are more accurate than the mean of the observed heads. Concerning the observation well *16_SHGN6543*, the NSE is significantly inferior to 0 (-4.5). The influence of the canal Sion-Riddes (**c6**, see **Figure 4.6**) seems to constrain the simulated data, i.e. given that no transience in the canal stage is included in the model (No information available), the fixe heads along the canal constrain the values at the observation well *16_SHGN6543* that do not show significant variation during the simulation.

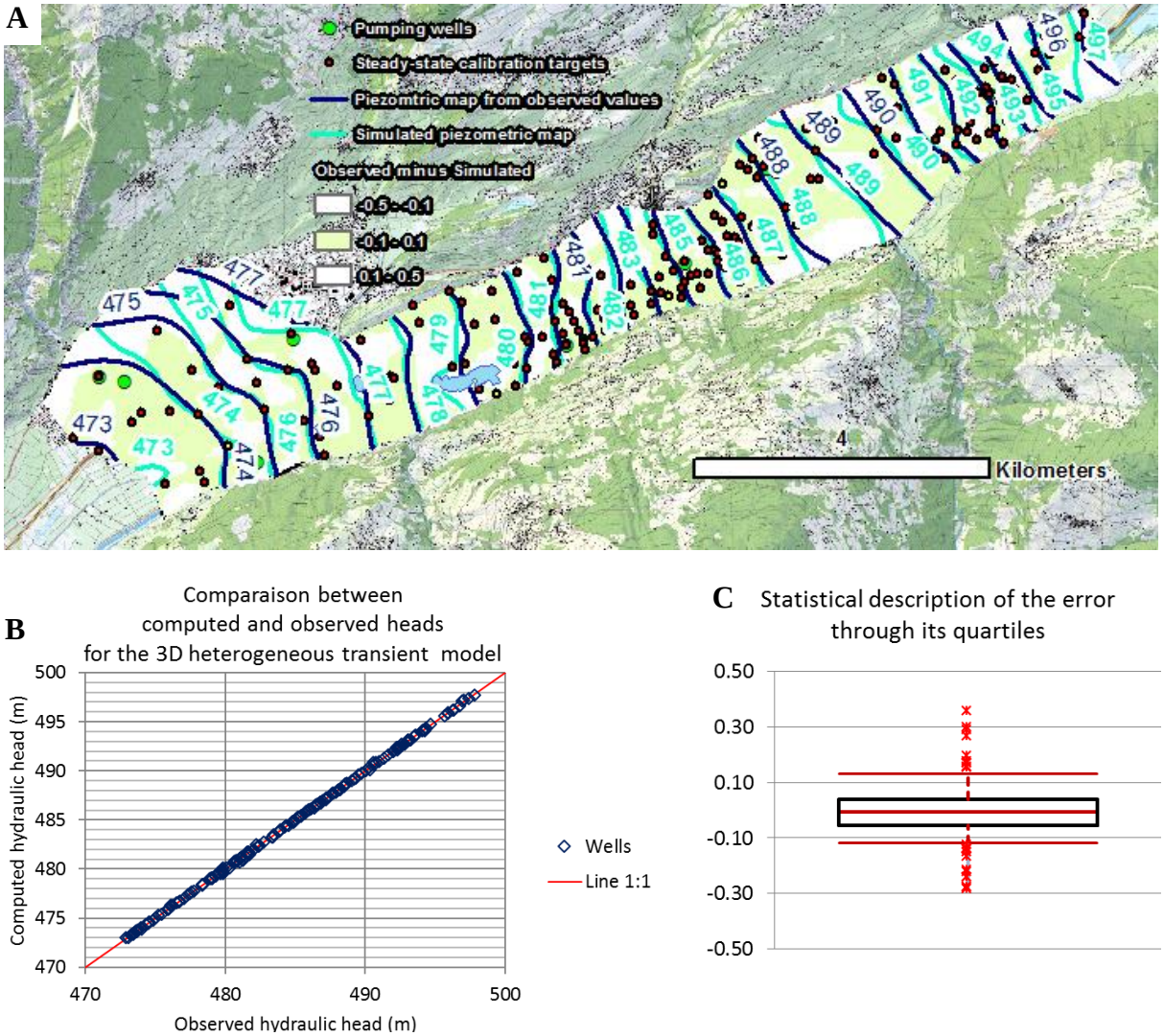

Figure 4.35: Visual and statistical descriptions of the three-dimensional heterogeneous transient model calibration. **A)** Piezometric maps from observed data (calibration targets) and simulated heads. The colored area represents the spatial distribution of residual errors (the difference between observed and simulated values). **B)** Scatter plot that shows observed head targets versus simulated heads. **C)** Statistical description of the error between observed and simulated heads (Boxplot).

Table 4.12: Summary statistics of the results of the three-dimensional transient model. The unit is the meter.

ME		***MAE***	***RMSE***	***Target range***	$\frac{RMSE}{Target\ range}$	**Standard deviation**
-0.01		0.07	0.10	25	0.4%	0.07
Percentiles	**Min**	**9th**	**25th**	**Median**	**75th**	**91th**	**Max**
	-0.28	-0.12	-0.05	-0.01	0.04	0.13	0.36

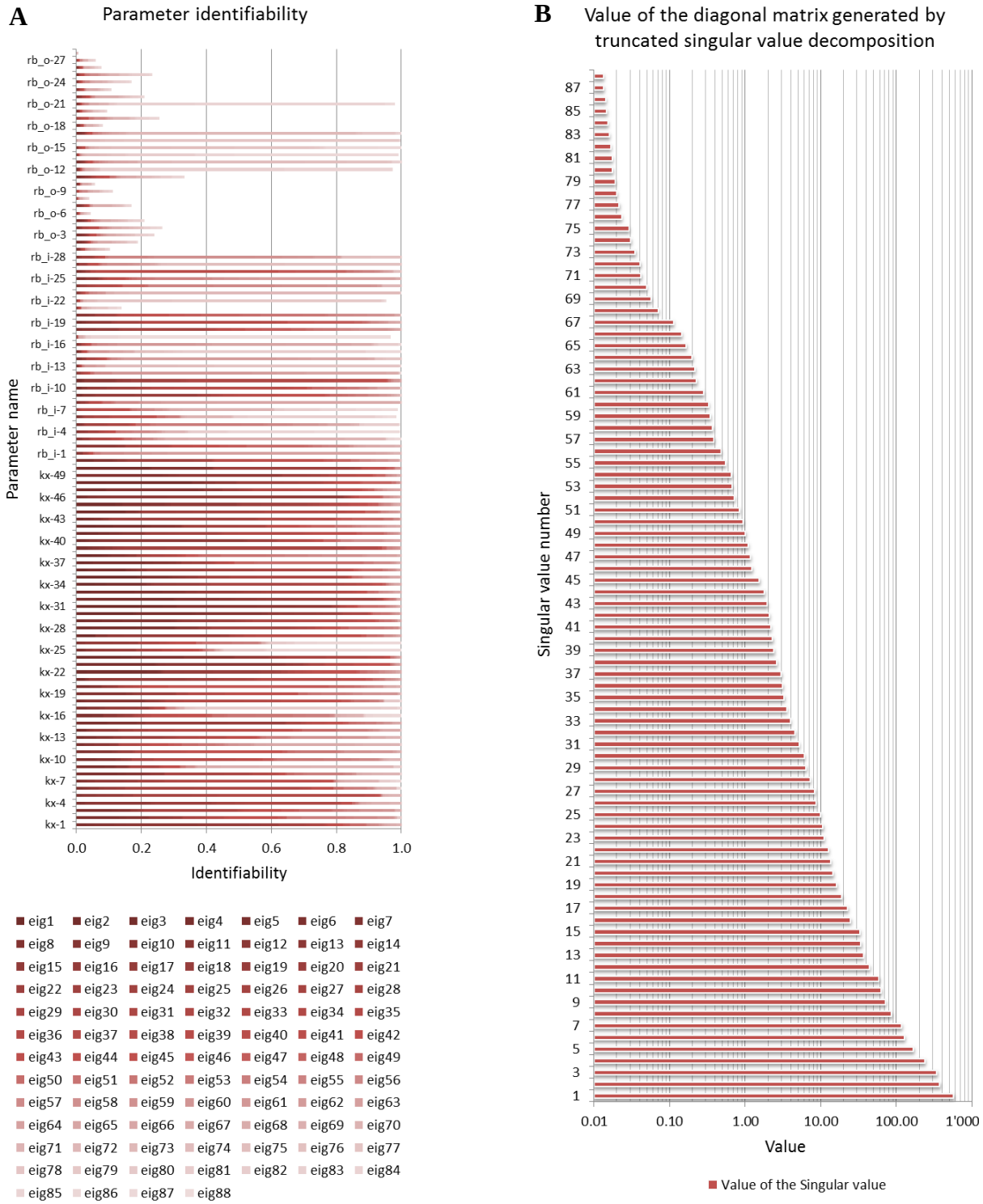

Figure 4.36: Parameter identifiability. K_x is the hydraulic conductivity of the aquifer for the pilot points 1 to 51; rb_i and rb_o are the Rhone Riverbed In- and Out-transfer rates respectively.

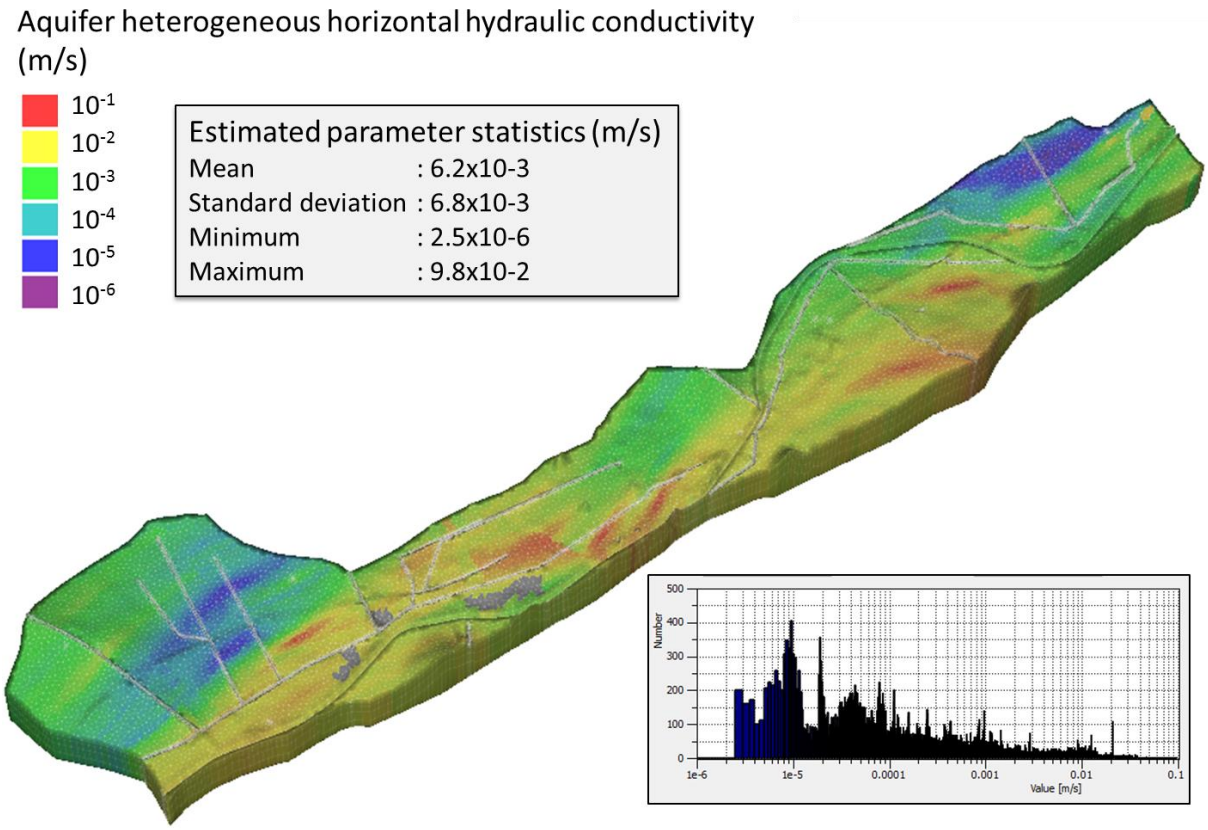

Figure 4.37: Values of the estimated aquifer hydraulic conductivity for each element. The histogram presents the distribution of the hydraulic conductivity throughout the model domain.

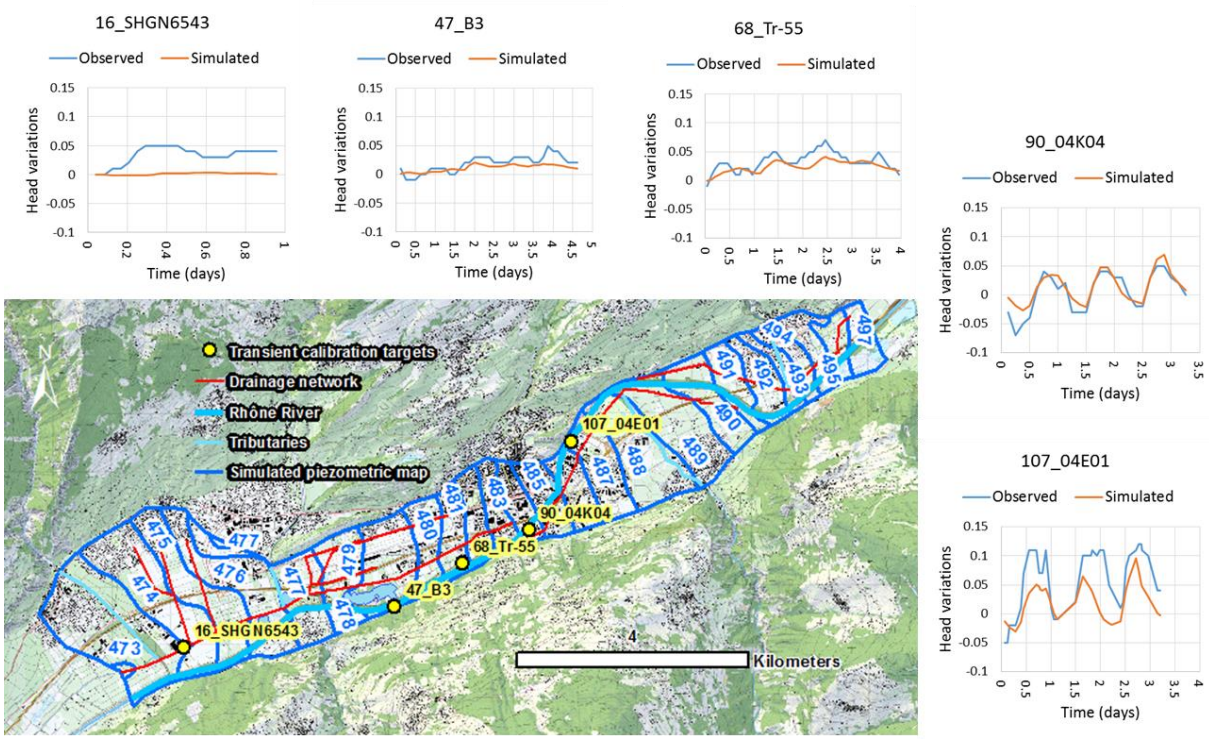

Figure 4.38: Map showing the location of the wells used for the transient calibration and their observed and post-calibration simulated hydrographs.

Figure 4.39: Geographical map of the study zone from 1802 established under the influence of Napoleon Bonaparte. The map represents the Rhône River prior the 1st Rhône River correction. The natural braided shape of the Rhône River can be observed as well as the riparian vegetation of the alluvial plain (wetlands). The high hydraulic conductivity zone estimated during the calibration process (**Figure 4.37**) can be related to the natural form of the Rhône River, the geometry of the geographic components of the alluvial plain and the alluvial cones, which are characterized by different sediment deposits and therefore different hydraulic properties (*M. Lechevalier, CHAN-F/14/10191* and *10192*).

4.4.3.3. Discussion of the three-dimensional heterogeneous anisotropic transient model

First, the flexibility in the estimation of the heterogeneity of the aquifer hydraulic conductivity provided by the use of pilot points allowed to improve the fit between observed and simulated data without violating the expert knowledge.
Secondly, the information content provided by the aquifer response to the Rhône River stage variations (transient simulations) improved the estimation of the Rhône riverbed hydraulic properties represented by the In- and Out-transfer rates.
Finally, concerning the resulting heterogeneous hydraulic conductivity field, the local variation of the hydraulic conductivity can be interpreting according to the natural hydrodynamics and geometry of the geographic components of the alluvial plain, prior and posterior to the regulation measures that started in 1863. **Figure 4.39** shows a geographical map of the study zone established in 1802 that support the geological realism of the estimated anisotropic heterogeneous hydraulic conductivity field.

4.5. Scenario modeling and uncertainty analysis

The purpose of the present hydrogeological modeling is to provide forecasting and related uncertainty of the water table elevation in the area of Sion (Capital of Valais, Switzerland) in the framework of the modifications projected by the 3rd Rhône River Correction. Based on the calibrated three-dimensional heterogeneous model and the future Rhône River stage, the estimation of the future water table elevation and its uncertainty is carried out. **Figure 4.40** shows the Rhône River profiles prior, at an intermediate stage, and after the 3rd Rhône River Correction for the low water condition.
Figure 4.40A shows that the enlargement of the Rhône River cross-section at the upstream part of the model, between the Lienne River and the Borgne River, will lead to a decrease in the Rhône Rive stage. From the mouth of the Borgne River until the end of the city of Sion the Rhône riverbed will be essentially lowered due to the urban constraint. The riverbed will progressively be lowered with a maximum of 2.4 m between the bridges Vissigen and St-Marguerite (km 65,917). Downstream of the urban crossing of Sion widening of the riverbed will be realized by displacing one of the lateral levees. Both modifications, lowering and widening of the riverbed, will result in a lowering of the Rhône River stage, although the variations are mitigated along the downstream part of the study zone (Between the Sionne River and the Lizerne River). Due to the connection between the Rhône River and its alluvial aquifer, it is expected that the surrounding water table elevation will decrease (See *Chapter 1).*

Concerning the intermediate stage, the results of hydraulic simulations, presented in **Figure 4.40B**, show that the Rhône River stage will remain relatively stable in the upper part of the study zone. However, at this intermediate stage, the Rhône River stage will decrease beyond the expected long-term elevation from the downstream of the city of Sion to the Lizerne River.

The model calibrated in the previous section is used to estimate the potential water table variations and uncertainties. Three major components of the predictive uncertainty have been identified and are quantified in this section, i.e. uncertainties related to the model calibration and to scenario modeling regarding the hydraulic and geomorphologic properties of the future Rhône riverbed:

1. The uncertainty related to the calibration of the model, i.e. the propagation of the uncertainty of the estimated parameters onto the values of the water table elevation predictions. This uncertainty analysis is pursued by using linear uncertainty analysis.
2. The morphology of the Rhône riverbed, especially along the enlarged reaches for which hydrogeomorphogical studies assumed that a geomorphology dominated by a succession of riffles and pools may develop, i.e. alternate bars.
3. The hydraulic properties of the Rhône riverbed, i.e. its conductance (In- and Out-transfer rates).

4.5.1. Predictive uncertainty related to the parameter estimation

The pre- and post-calibration predictive uncertainties are calculated using a linear uncertainty analysis based on the sensitivity of the prediction to the uncertainty of the pre- and post-calibration values of the model parameters. The method employed is based on the linearization of the model through the calculation of the sensitivity matrix J, and on Bayesian theory, expressing the capacity of the calibration dataset to reduce the parameters uncertainty. The approach is described in the precedent *Chapter 3* in the *Section 3.3 Methods: Parameter identifiability and predictive uncertainty*. The distribution of the parameters and measurement uncertainties is assumed to be normally distributed and is expressed by the pre-calibration covariance matrix of parameters, $C_{pre(k)}$, and measurement errors $C_{(\varepsilon)}$ that are diagonal matrices containing the parameters and measurement error variances, which have values of 1 (logarithm of the parameter variances) and 0.1 m respectively. The benefit of the calibration process, related to the information content of the calibration dataset regarding the estimation of the parameters and its influence on the reduction of the predictive uncertainty standard deviation is computed using **equation 3.8** from *Chapter 3*. The **Figure 4.41** shows the pre- and post-calibration uncertainties of the prediction of the water table elevation. The results demonstrate the benefit of the calibration process in reducing the uncertainty of the predictions, which reache a maximum value of 2 m before the calibration process and is decreased to a maximum value of 0.25 m under the constraint of the calibration dataset. Regarding the modeling purpose, which is to estimate the future elevation of the water table after the modification of the Rhône River cross-section, the predictions can be made with greater certainty, in particular in the zone of major issues, such as the crossing of the city of Sion, for which the uncertainty is reduced by a factor 2 to 5.

In the next section, the impact on the regional and local (hyporheic flow) water table elevation of potential evolutions of the geomorphology of the Rhône riverbed (Alternate bars), which concerns especially river reaches that will be widened, is analyzed.

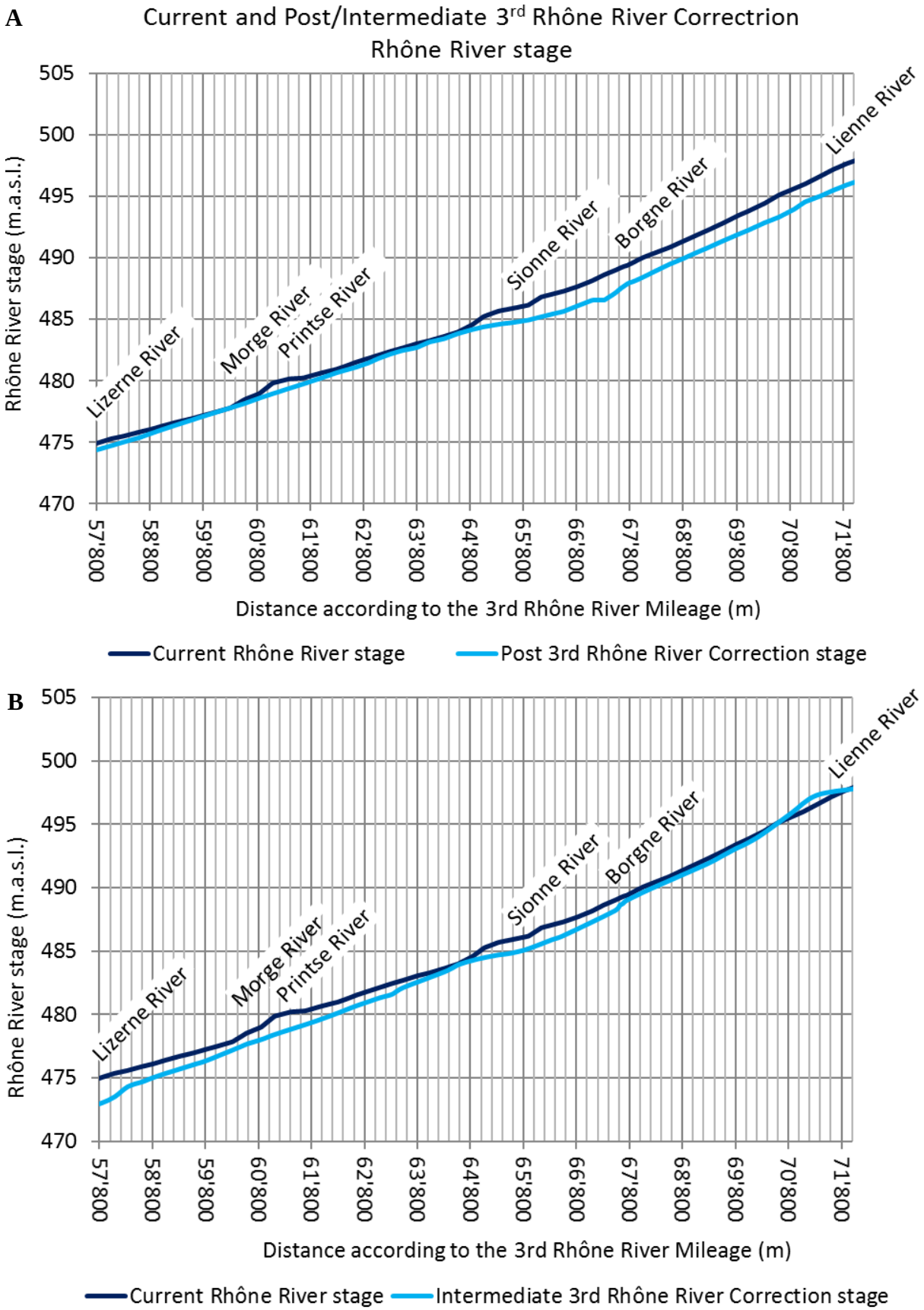

Figure 4.40: Longitudinal profiles of the current and future Rhône River stages, i.e. post and intermediate 3rd Rhône River Correction, **A** and **B** respectively. The names of the 6 tributaries of the Rhône River are provided for a better localization of the profile. The mileage along the *x-axis* corresponds to the distance along the Rhône River starting from its mouth with the Lake Geneva (Niederer + Pozzi Umwelt AG, 2015, HEC-RAS simulations).

4.5.2. Uncertainty related to the future geomorphology of the Rhône riverbed

The purpose of this section is to estimate the variations incurred by the water table due to the variations of the Rhône River stage related to riverbed geomorphology, especially in the case of alternate bars, which is the hydrogeomorphology likely to develop within the widened reaches of the Rhône River (Niederer + Pozzi Umwelt AG, 2016).

Current practices in river management that aim at improving habitat and ecological functions, or at protecting riverside inhabitants from flood events, opt for an increase of the width of the river cross-section. In many circumstances, this enlargement leads to the formation of alternate bars within the channel. When the river is connected to its floodplain and groundwater system, the consequences of riverbed alterations on the regional and riparian water table and hyporheic flow required to be assessed through preliminary analysis. In order to pursue such analysis, modern fully coupled physically based numerical models can be used to forecast future river-aquifer interactions [*Brunner and Simmons*, 2012]. A compared analysis of synthetic simulations of trapezoidal and alternate bars riverbeds can provide an estimation of the error incurred by riverbed simplification (trapezoidal cross-section) on the water table elevation. Previous studies supported this approach and showed that riffle-pool sequences are likely to enhance the dynamics between the river and the subsurface [*Kasahara and Hill*, 2008].

The conceptual model used to design the numerical model is based on the future widened reach of the Rhône River in the study zone, downstream of the city of Sion (*Yellow range* in **Figure 1.4** in *Chapter 1*). The model domain is defined by a parallelepiped rectangle for which the length is 5640 m, the width is 2000 m and the depth 40 m.

Along the central longitudinal part of the model (y = 0), the future widened Rhône River is simulated with a width of 90 m and an average slope of its riverbed of 0.13% (**Figure 4.42**). At the upstream edge of the river, the riverbed bottom is at an elevation of 108.3 m (x = 5640 m) and at an elevation of 100.7 m (x = 0 m) at the downstream edge of the river. No flow boundaries surround the model domain in order to generate infiltrating conditions, i.e. losing river, upstream and exfiltrating conditions, i.e. gaining river, downstream.

The Rhône River stage is simulated using the two-dimensional (depth-averaged) flow equation, based on the diffusion wave approximation on the Saint-Venant equations, for the low water condition according to a discharge of 49 m/s (**Figure 4.43**). Then, the results under real flow conditions (i.e. riffles and pools morphologies) are taken into account and the Rhône River stage for the flat bottom simulation is corrected accordingly. Six different types of riverbed morphologies are implemented in the model and the hydraulic simulations (computation of the Rhône River stage) followed by hydrogeological simulations have been carried out. The **Table 4.13** names the 6 morphologies and their characteristics. The *Flat* morphology corresponds to a river with a flat bottom inclined with a constant gradient of 0.13% from the upstream limit to the downstream limit of the model. It represents also the average elevation of the alternate bars riverbed morphologies. Five variants of alternate bars morphologies are considered. The *Medium* variant is the reference morphology. Its characteristics are calculated from the values of the riverbed width, the river flow and the sediment discharge capacity [*Zarn*, 1997]. Therefore, the *Medium* variant has a wavelength of 850 m. i.e. the distance between the beginning of a bar and the beginning of the next one. The bars and pools amplitudes are 1.2 and -2.7 above and below the average elevation equal to 0 represented by the *Flat* morphology at each cross-section. The *Short* and *Long* variants present a wavelength smaller (600 m) and higher (1100 m) than the *Medium* variant but retain the bars and pools amplitudes of the *Medium* variant. Conversely, the *Deep* and *Shallow* variants retain the wavelength of the *Medium* variant but the amplitudes of the bars and pools are increased and decreased respectively compared to the *Medium* variant.

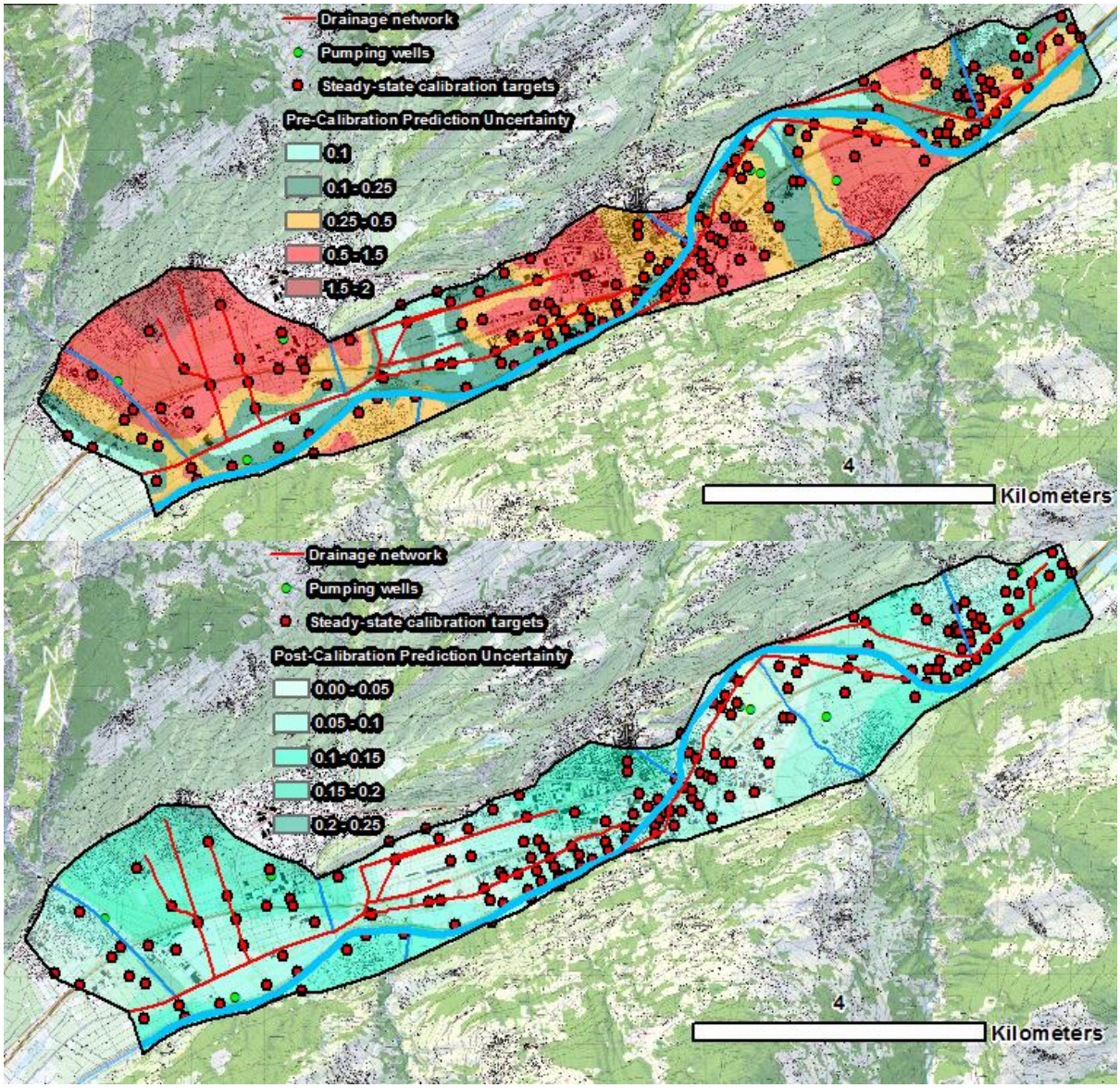

Figure 4.41: Pre- and Post-calibration standard deviations of the prediction uncertainties of the water table elevation.

The three-dimensional surfaces of the alternate bars have been defined using slope discontinuity curves based on observations of physical models made in laboratory and on aerial photographs (Roger Kolb 2015, Niederer + Ponzi). Each alternate bars model comprised several bars (13 bars), and bars shortcuts, i.e. diminution of the bars elevation along the riverbank, are simulated for a few of them (3 shortcuts) for more realism and to assess their influence on the river-groundwater interactions. **Figure 4.44** shows the hydraulic heads for the hydrogeological simulations of the *Flat* and *Medium* geomorphologies. It can be observed that compared to the symmetry of the head distribution in the *Flat* riverbed, the *Medium* alternate bars show an asymmetry of the heads, which can be higher and lower than the river stage on each side of the river. Therefore, the variations of the gradient around the river entail more complex interactions between the river and the surrounding groundwater. **Figure 4.45** shows the movement of water (particles tracking) for the two riverbed morphologies and confirms the dynamics infiltrating and exfiltrating flows in the case of alternate bars riverbed. Furthermore, the **Figure 4.46** shows that the riparian dynamic water flow is limited to a certain extent around the river that could be defined as the hyporheic flow zone. The magnitude of the exchanges within alternate bars morphologies is quantified in **Figure 4.47**, where the flux rate is computed

at each node of the mesh. The negative flux rates identify exfiltration of the groundwater into the river, and conversely, the positive flux rates identify infiltration of the river water into the groundwater. It can be observed that a significant exfiltration of the groundwater into the river occurs following the riffles, at the beginning of the pools, and that infiltration essentially occurs at the downstream part of the pools and with a higher magnitude along the side channels (bars shortcuts) between the riverbanks and the bars.

Figure 4.48 displays the difference between the river stage and the riparian water table at 10 m from the riverbank for flat bottom and alternate bars riverbed. It can be observed that compared to the *Flat* bottom model, where the river is whether losing (upstream part) or gaining (downstream part), the alternate bars morphology shows that infiltration and exfiltration occur all along the simulated river. As previously observed, the infiltration are essentially along the riffles, and conversely, at the locations of the pools (the *black dotted line* represents the alternate bars riverbed talweg.

In order to show the influence of the development of alternate bars and the consequences of the evolution from one riverbed morphology to another riverbed morphology, the regional water table elevation variation is calculated for each model variant and the results are synthesized in **Table 4.14** under real flow conditions**.**

In summary, the results of the simulations showed that the riverbed morphology may influence the local and regional surface of the water table. On the regional scale, the variations of the water table elevation for the different amplitude and wavelength of the simulated alternate bars geomorphology are close to 0 cm for the expected *Medium* alternated bars morphology when considering river flow under real conditions (i.e. riffles and pools morphologies). Departure from the *Medium* alternate bars morphology will lead to small positive or negative variations of the water table of a few centimeters. On the local scale (hyporheic flow), the flow patterns are significantly different between flat bottom and alternate bars rivers:

- For flat bottom rivers: Unidirectional fluxes, infiltrating or exfiltrating, depending on the state of the river, i.e. losing or gaining, respectively.
- For alternate bars rivers: The interactions supported by gradient variations along the river reach lead to a dynamic hyporheic flow, i.e. relatively important exfiltration and infiltration along the same reach in both dominant gaining and losing conditions of the river.
    - Exfiltration of the groundwater in the pools.
    - Infiltration into the groundwater along the riffles.
    - Relatively stronger infiltration along the bars shortcuts and against bars heads.

In the next section, the analysis of the consequences of the uncertainty in the future conductance of the Rhône riverbed in the study zone is estimated through different scenarios assuming an increase in the values of the Rhône riverbed conductance.

4.5.3. Uncertainty related to the future conductance of the Rhône riverbed

The scenario modeling approach of this section is supported by the uncertainty related to the future conductance of the Rhône riverbed. The impact on the predictions of the future water table of variations of the riverbed conductance compared to the one estimated for the three-dimensional heterogeneous model is analyzed.

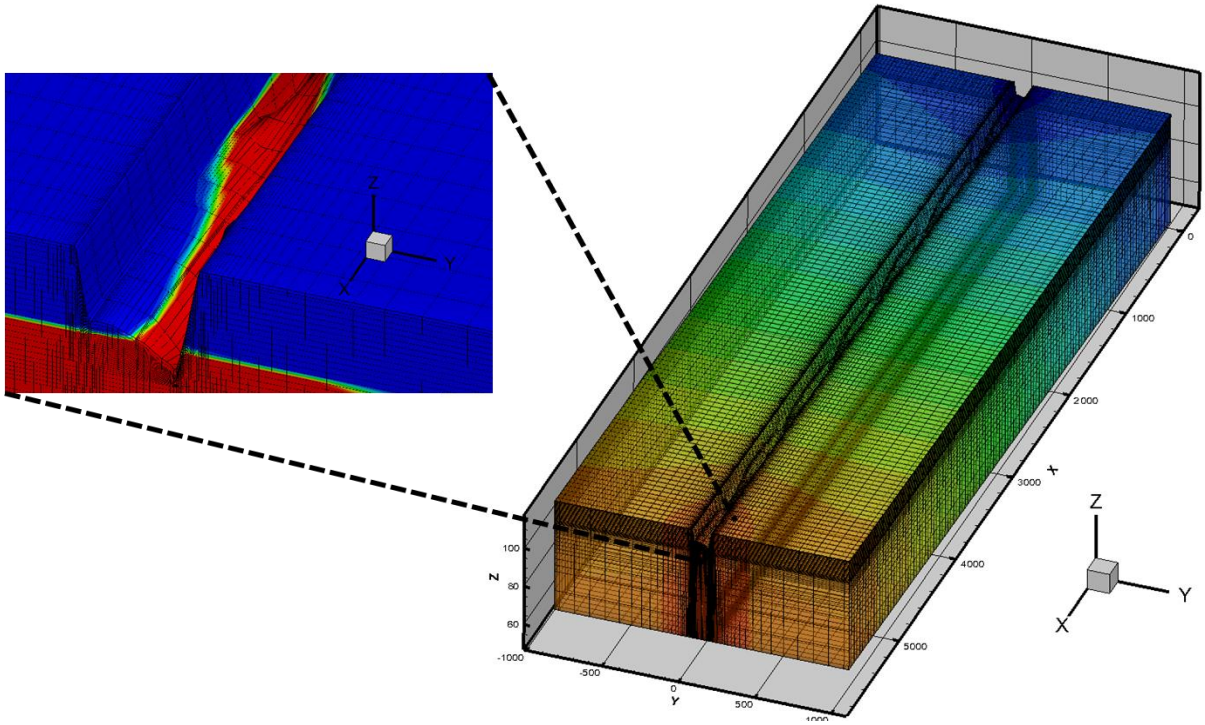

Figure 4.42: Numerical model design. On the right is represented the three-dimensional model domain (length of 5800 m and width of 2000 m). The orange color represents higher head values and the blue represents lower head values. On the left, the inset shows in red the saturated zone for the surface water and the groundwater. The blue volume is the unsaturated zone.

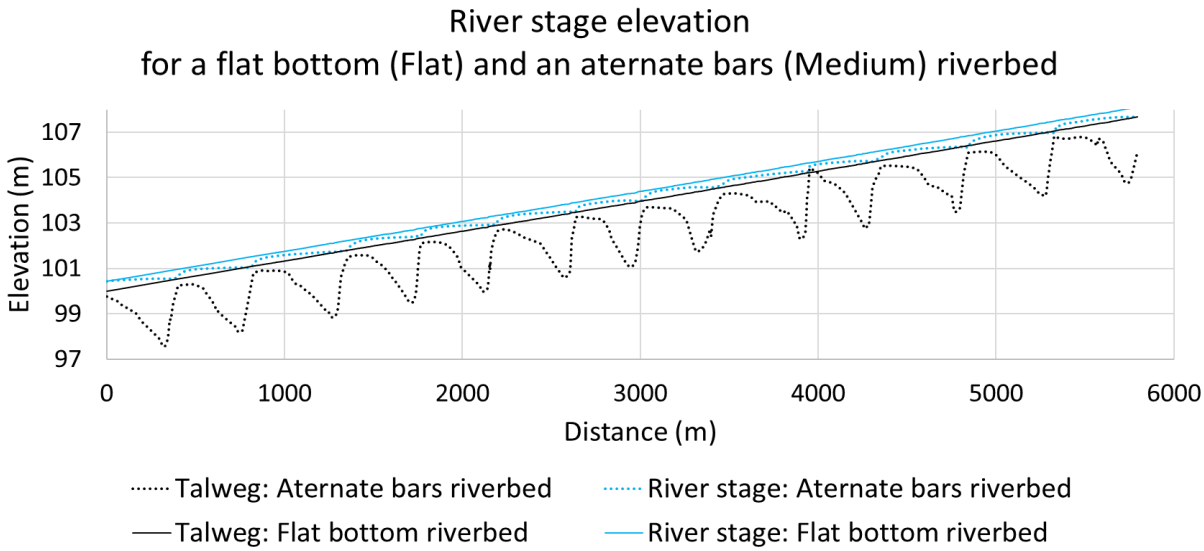

Figure 4.43: River stage and riverbed talweg elevations for flat bottom and alternate bars riverbed morphologies.

Table 4.13: Parametrization of the riverbed morphologies based on the wavelength and the amplitude of the bars and pools compared to a flat riverbed that represents the average elevation of the riverbed bottom (value of 0 for the bars and pools amplitude).

Name	**Wavelength** (m)	**Amplitude bars** (m)	**Amplitude pools** (m)
Flat	0	0	0
Short	600	1.2	-2.7
Medium	850	1.2	-2.7
Long	1100	1.2	-2.7
Deep	850	1.3	-3.0
Shallow	850	0.9	-2.1

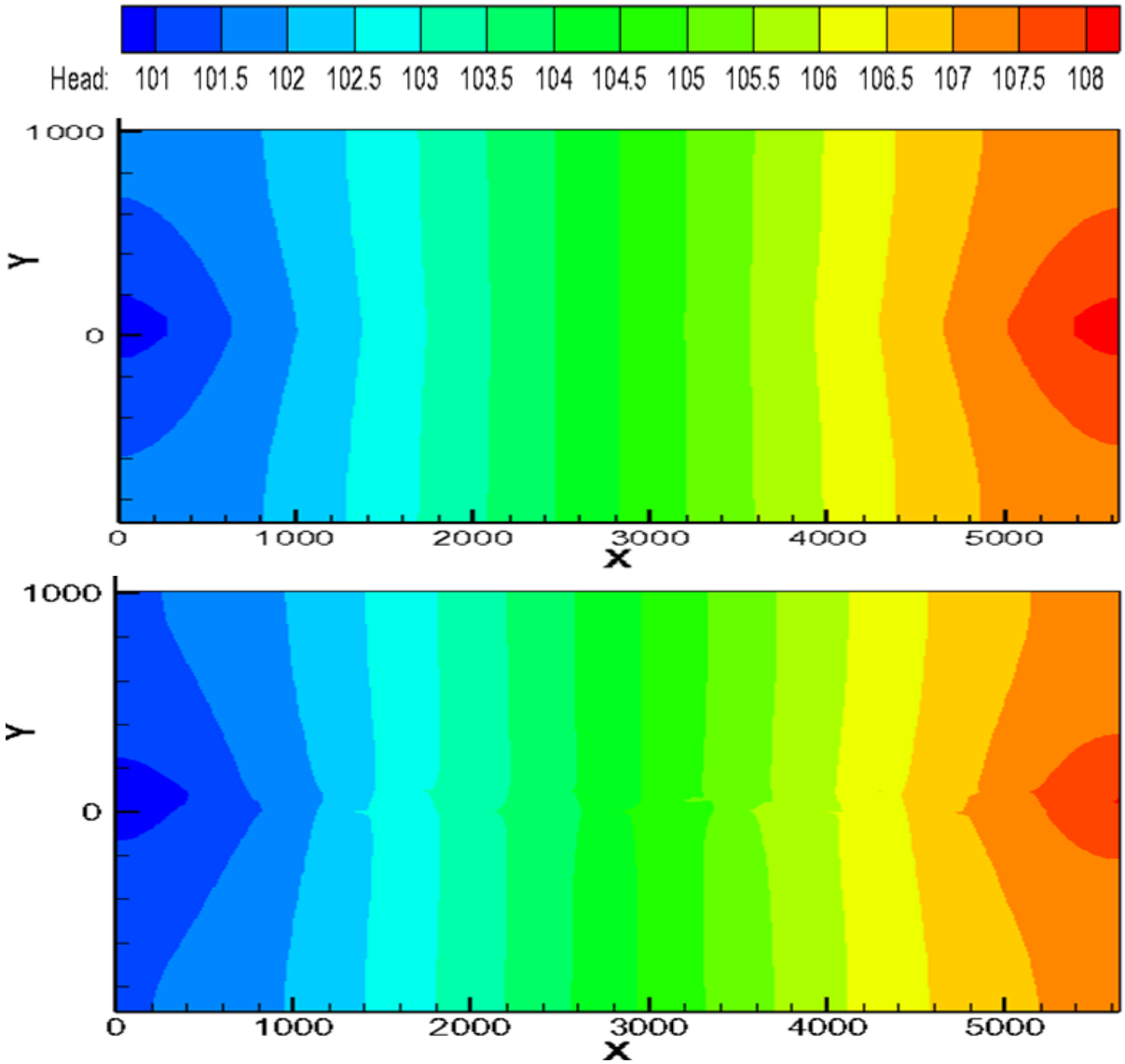

Figure 4.44: Map of the hydraulic head values. On the top is represented the top view of the flat bottom riverbed model and on the bottom, the alternate bars riverbed.

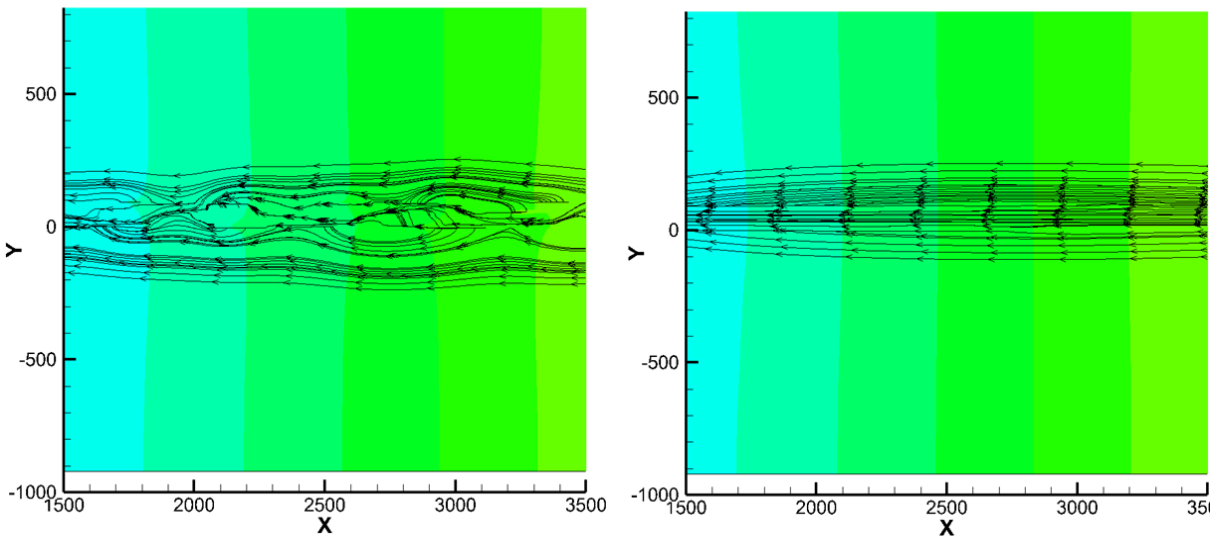

Figure 4.45: Particle tracking near the river. On the left is represented the particle motion for alternate bars riverbed and on the right, for flat bottom riverbed.

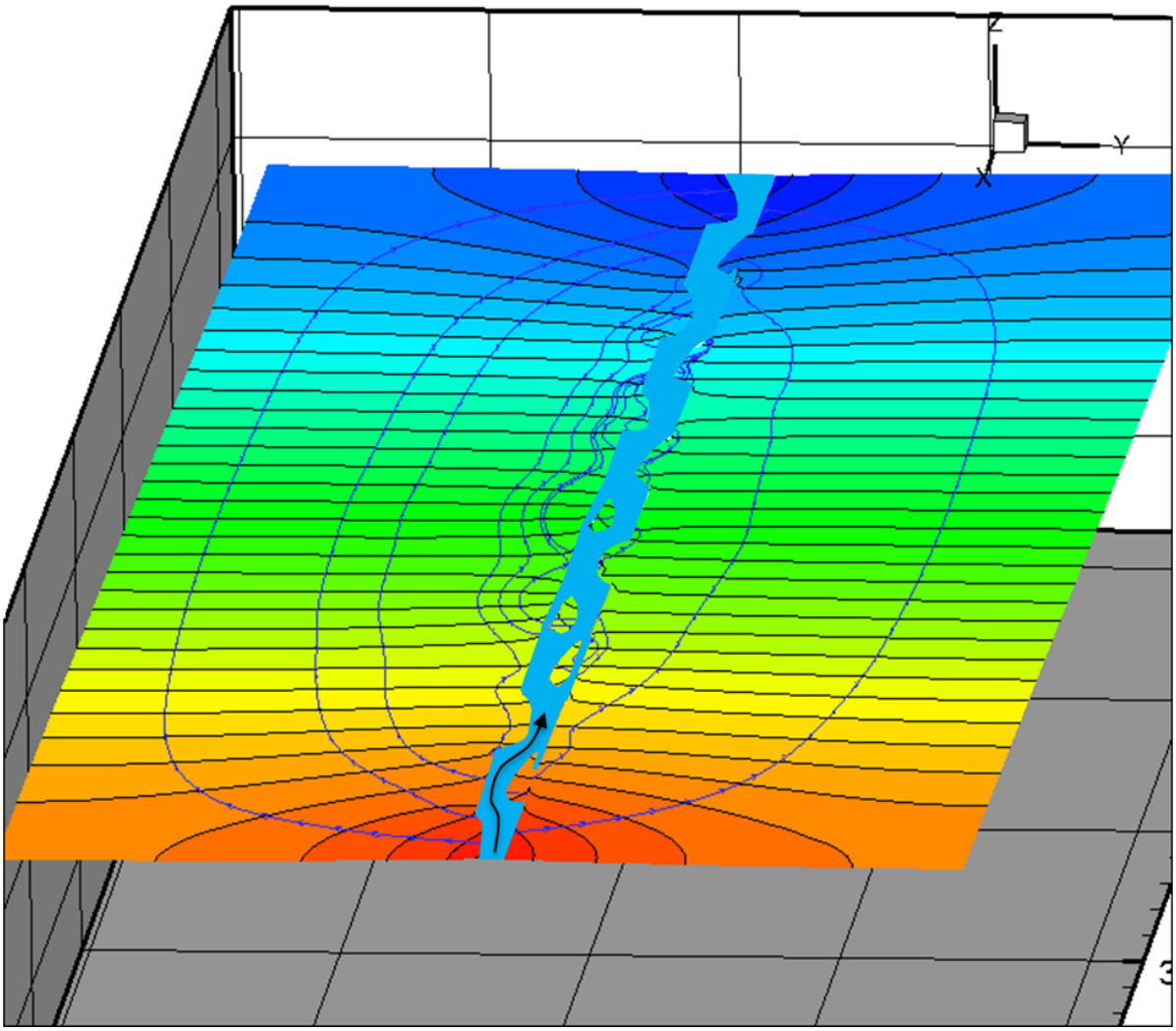

Figure 4.46: A three-dimensional representation of the water table (the *orange color* represents higher head values and the *blue color* represents lower head values). The particle tracking paths show the motion of the water at local and regional scales around an alternate bars riverbed. Along the central part, the *blue area* represents the surface of the flowing river and the *black arrow* indicates the direction of the flow.

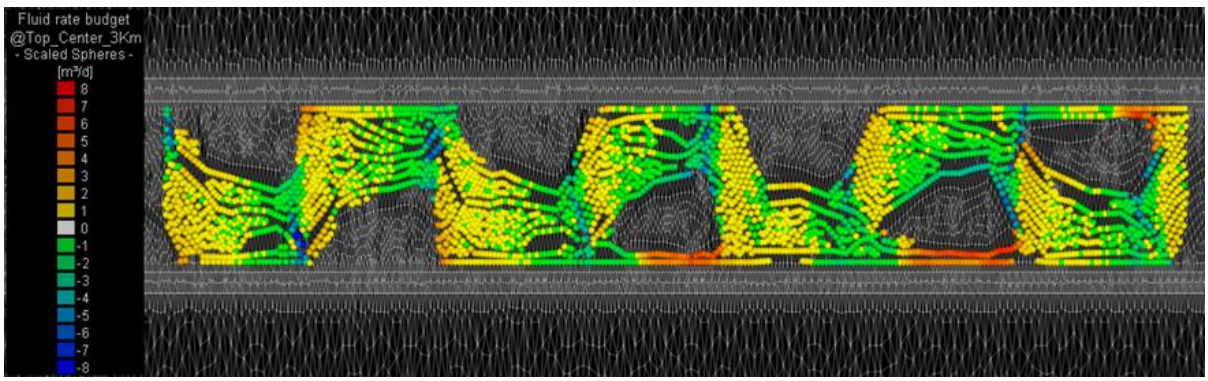

Figure 4.47: Flux rates at the surface of the riverbed for an alternate bars riverbed. The *orange color* represents infiltration of the surface water into the aquifer and the *blue color* represents exfiltration of the groundwater. A significant exfiltration occurs after the riffles (beginning of the pools) and infiltration occurs at the downstream part of the pools and along the side channels between the riverbanks and the bars.

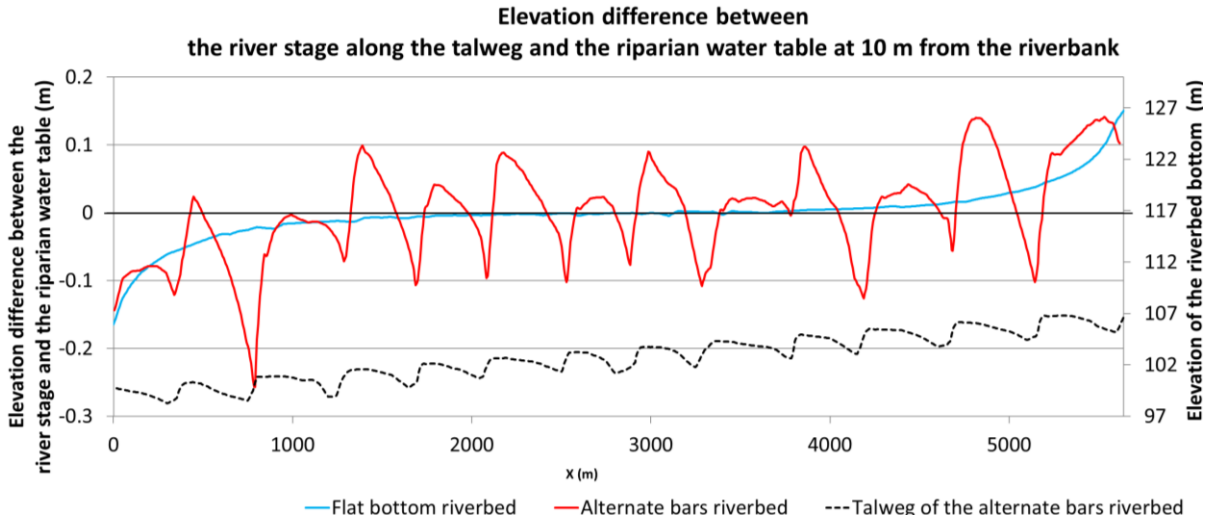

Figure 4.48: Elevation differences between the river stage and the riparian water table (10 m from the riverbank) along the river for flat bottom and alternate bars rivers.

Table 4.14: Variations of the water table elevation at a regional scale caused by the variations of the geomorphology of the Rhône riverbed and under real flow conditions. The variations are calculated for changes from the geomorphology designated in the row to the one designated in the column of the table. For example for a *Flat* bottom riverbed (row 1) evolving to a *Short* alternate bars riverbed (column 1), the regional water table decrease of 0.01 m.

		Alternate bars				
	Unit (m)	Short	Medium	Long	Deep	Shallow
Flat bottom	Flat	0.01	0.00	-0.05	-0.01	0.02
Alternate bars	Short	0	-0.01	-0.06	-0.02	0.01
	Medium	*	0	-0.05	-0.01	0.02
	Long	*	*	0	0.04	0.07
	Deep	*	*	*	0	0.03
	Shallow	*	*	*	*	0

First, **Figure 4.49A** shows the results for the post 3rd Rhône River stage (**Figure 4.40A**) and for different values of the riverbed conductance (**Figure 4.49 B** to **E**). From the top map to the bottom map, the estimated conductance is increased by a factor of 10 between each map. Then, the results are synthesized in **Figure 4.50A** and **B**, which display the highest and lowest water table following the variations of its elevation compared to the current elevation. In other words, **Figure 4.50A** displays the minimal decrease (positive values) of the water table after the Rhône River Correction, where the negative values involve an increase of the water table elevation. Conversely, the **Figure 4.50B** display the maximal decrease (positive values) of the water table after the Rhône River Correction, where the negative values still involve an increase of the water table elevation.

The **Figure 4.50C** displays the uncertainty in the variations related to the future values of the riverbed conductance, which is an outcome of the difference between the potential variations of the water table elevation presented in the **Figure 4.50A** and **B**. Finally, **Figure 4.50D** combines the uncertainty related to the model calibration, expressed as a standard deviation, to the scenario modeling uncertainty related to the Rhône riverbed conductance presented in **Figure 4.50C**.

The results show that the highest uncertainties are in the upper part of the study zone (between 1 and 2 m). The predictions in the area of the city of Sion are relatively well constrained (around 0.3 m). The predictions in the lower part of the commune of Sion (airport of Sion) until the Lienne River have a moderate uncertainty, relatively to the other parts of the model, with variations ranging from 0.1 to 0.8 m.

The results for the intermediate 3rd Rhône River Correction stage (**Figure 4.40B**) are synthesized in the **Figure 4.51A** to **D** following the same order and description as in the **Figure 4.50**.

In summary, it can be observed that the potential variations of the water table throughout the model depend on the location. Four main locations can be distinguished, based on the local response of the water table to increase of the Rhône riverbed conductance:

- In the area comprising the city of Sion, the variations of the elevation of the water table are relatively well constrained even for an increase of the conductance of the Rhône riverbed (**Figure 4.50A** to **E**).
- In the area extending from the middle of the domain (downstream part of the commune of Sion) until the downstream part of the model (Lienne River, downstream limit of the commune of Vétroz) that comprise the airport of Sion, the elevation of the water table remains relatively stable compared to the current water table elevation (**Figure 4.50A**). However, the increase of the conductance leads to a rise in the water table elevation with a maximum value of 0.88 m (**Figure 4.50E**). Nevertheless, the increase is limited at the location of the airport of Sion due to the presence of the Blancherie Canal (**Figure 4.6**, **c3**) and along the commune of Conthey and Vétroz due to the presence of the Sion-Riddes Canal (**Figure 4.6**, **c6**).
- In the upper part of the commune of Conthey and Vétroz as well as in the upper part of the airport of Sion the elevation of the water table remains relatively stable compared to the current elevation for the lowest estimation of the conductance of the Rhône riverbed as well as for higher values (**Figure 4.50A** to **E**). The reason for this stability is essentially due to drainage network mentioned at the previous bullet point.
- In the upper part of the commune of Sion, until the Lizerne River, the variations of the water elevation are the most important and strongly dependent on the evolution of the Rhône riverbed conductance. Increase or decrease of the water table elevations can be the consequence of alterations of the Rhône riverbed cross-section within an uncertainty range of 2 to 3 m (**Figure 4.50D** and **Figure 4.51D**).

In summary, the strongest variations of the water table during and after the Rhône River Correction are expected to occur in the upper part of the study zone, within a range of more than 2 m, in the absence of drainage control measures. This uncertainty is strongly related to the variations of the conductance of the Rhône riverbed and can lead to whether an increase in absolute value of the water table or a decrease of the water table elevation (up to 1.4 m). In the middle part of the study zone comprising the city of the Sion, the range is much lower, with a value of 30 cm. The absolute elevation of the water table will tend to decrease with a value up to 1.7 m according to the estimation presented in this document. Finally, the downstream part of the domain presents a moderate uncertainty, relatively to the other areas of the domain, with a value reaching 90 cm and an absolute variation that tends to a decrease of the water table elevation up to a value of 80 cm.

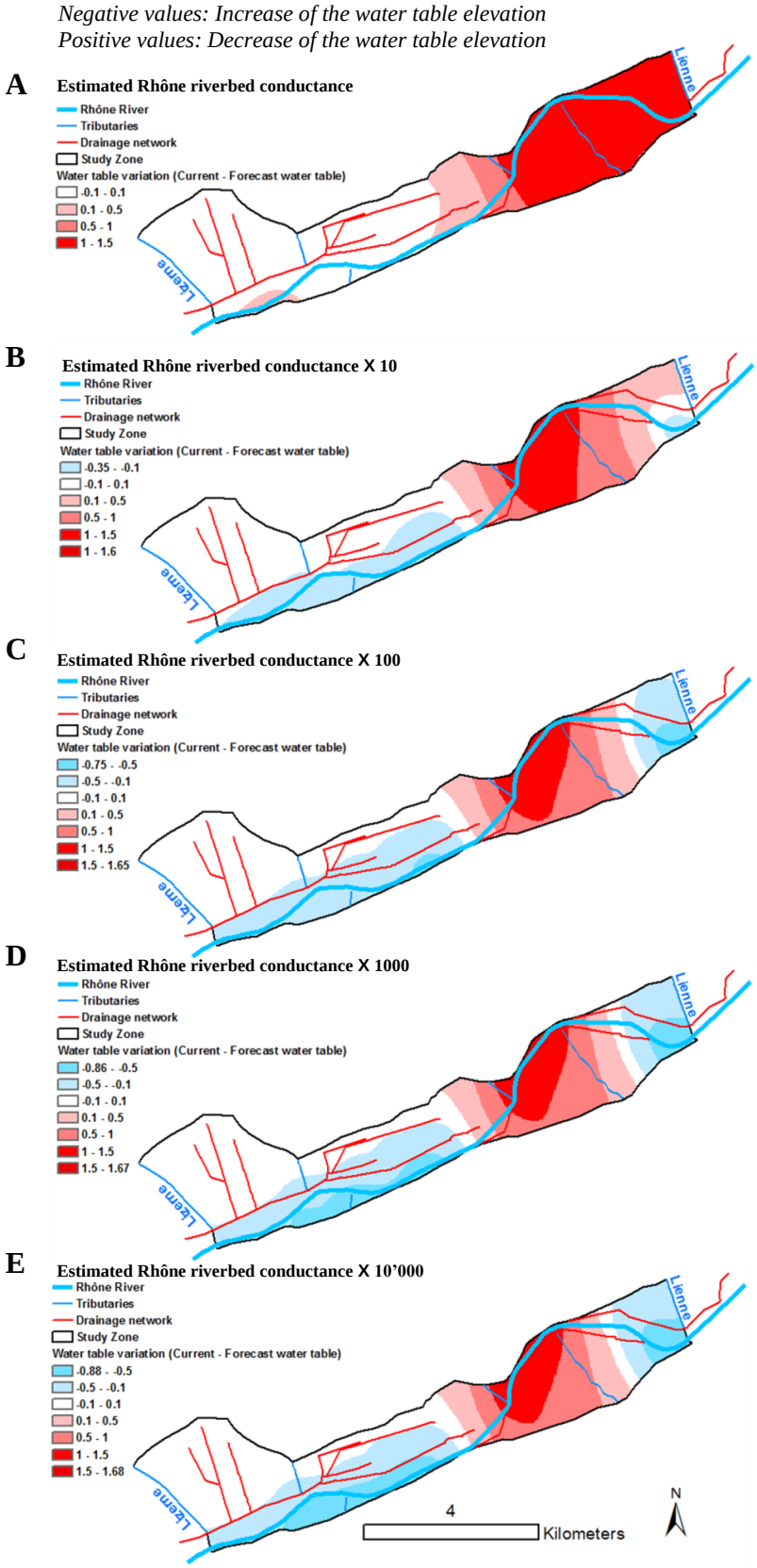

Figure 4.49: Water table variations for different values of the Rhône riverbed conductance. The top image **A** represents the variation of the water table according to the estimated values of the riverbed conductance. Then from this image to the next ones, **B** to **E**, the conductance is increased sequentially by a factor of 10, until reaching a factor of 10^4, **E**.

Post Rhône River Correction

Negative values: Increase of the water table elevation
Positive values: Decrease of the water table elevation

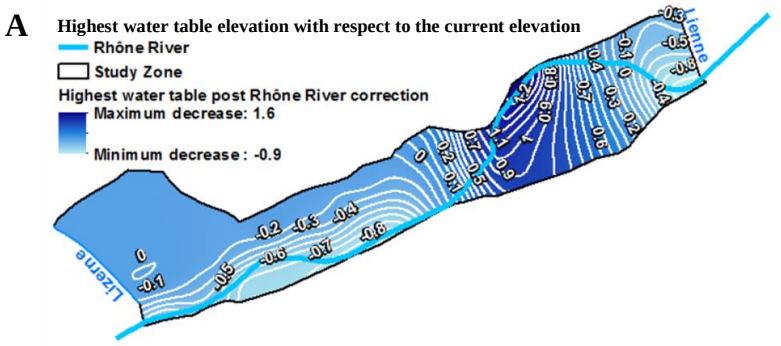

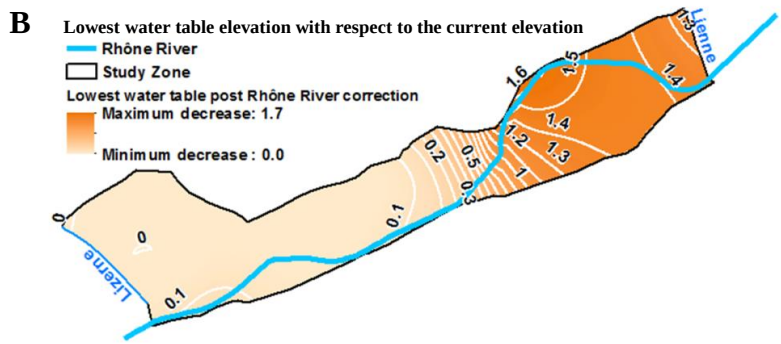

Post Rhône River Correction

Spread of the potential water table elevation variations

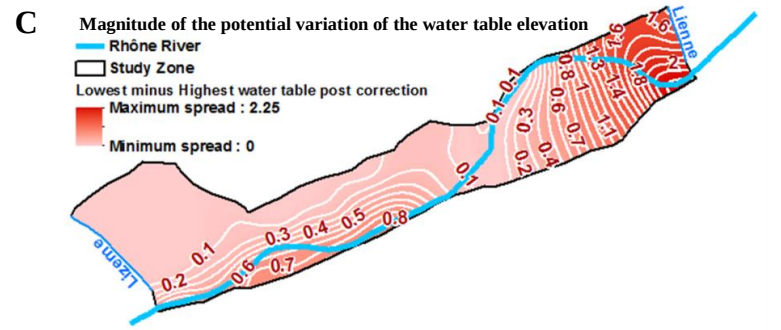

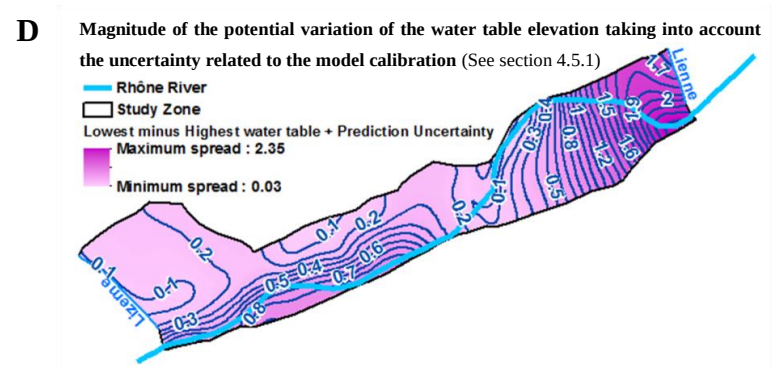

Figure 4.50: A and **B** show the maximum and minimum water table elevation variations compared to the current elevation for an increase in the future conductance of the Rhône riverbed (within the limit of the simulated values (See **Figure 4.49**). **C** shows the difference between the maximum and minimum elevation variations, i.e. **B − A**. **D** shows the addition to **C** of the uncertainty related to the calibration of the model previously estimated using linear uncertainty analysis.

Negative values: Increase of the water table elevation
Positive values: Decrease of the water table elevation

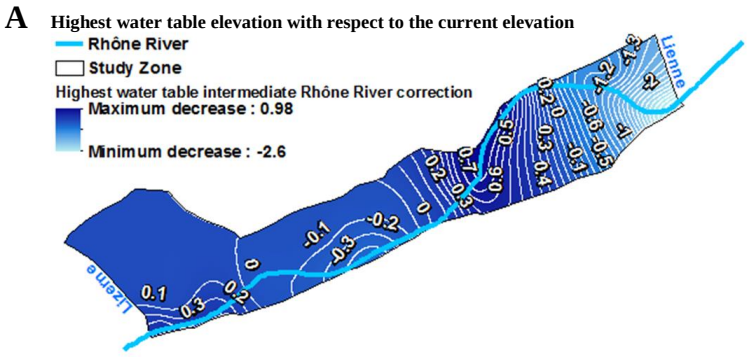

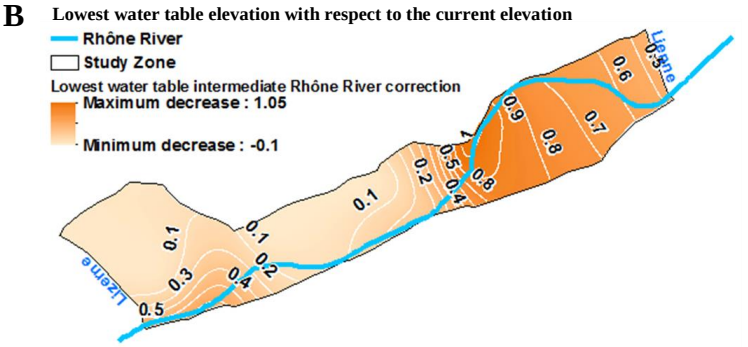

Spread of the potential water table elevation variations

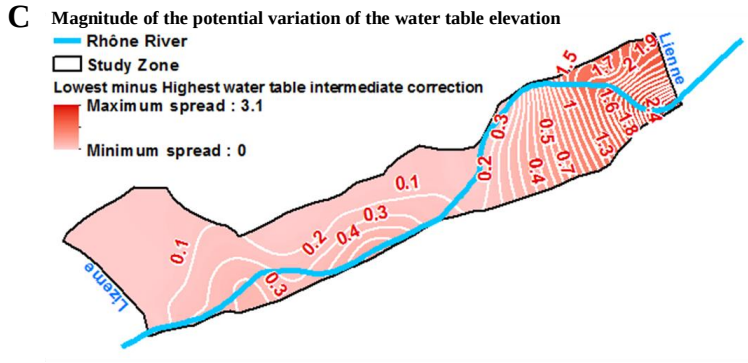

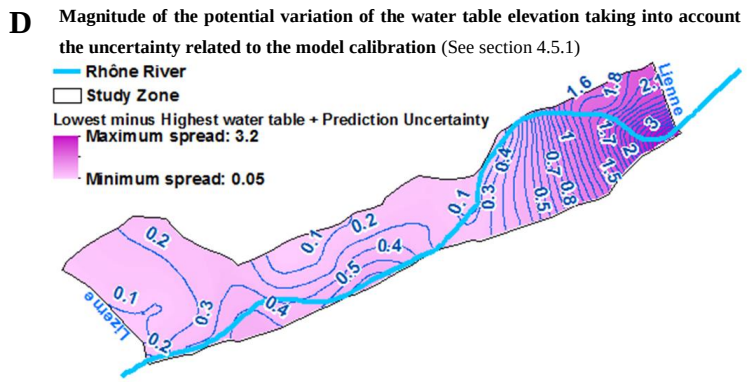

Figure 4.51: A and **B** show the maximum and minimum water table elevation variations compared to the current elevation for an increase in the future conductance of the Rhône riverbed (within the limit of the simulated values. **C** shows the difference between the maximum and minimum elevation variations, i.e. **B** − **A**. **D** shows the addition to **C** of the uncertainty related to the calibration of the model previously estimated using linear uncertainty analysis.

4.6. Conclusions

The 3rd Rhône River Correction project will modify the Rhône riverbed and increase its discharge capacity in order to protect the population from overflows and inundations of the alluvial plain. This report provided forecasting and related uncertainty of the water table elevation in the area of Sion (Capital of Valais, Switzerland) in the framework of the modifications projected by the 3rd Rhône River Correction.

First, a conceptual model of the study area was developed using historical research data and results, geological maps, climatic data, as well as analysis of the flow system based on head observation dataset. From the conceptual model, hard and soft knowledges were synthesized in a finite element numerical model and flow was simulated using the governing equation for unconfined saturated flow.

A base model has been parameterized with values for the aquifer, the Rhône riverbed and tributaries beds, and the drainage network beds in order to serve as an initial condition for the calibration of a two-dimensional zonal steady-state and a three-dimensional heterogeneous transient model. Then the calibrated model has been used to assess the uncertainty of the future elevation of the water table.

The uncertainty of the predictions related to model calibration has been estimated using linear uncertainty analysis. In addition, scenario modeling based on the uncertainty in the future hydraulic and geomorphologic properties of the Rhône riverbed have been carried out.

The analysis of the impact on the prediction uncertainty of the water table elevation of decrease in the Rhône riverbed conductance turned out to be the major source of uncertainty compared to the uncertainty related to the model calibration and the geomorphology of the Rhône riverbed. Over the study zone, the response of the water table elevation to the different scenarios is not homogeneous. Four zones have been identified:

- The upper part of the study zone is more sensitive to the evolution of the Rhône riverbed hydraulic properties. Potentially, this zone is susceptible to incurred increase or decrease of the water table elevation.
- The urban area of Sion could undergo a decrease of the water table elevation ranging from 1 to 1.5 m with an uncertainty of 0.3 m
- The upper part of the airport domain and of the commune of Conthey and Vétroz should be less affected by the modification of the Rhône riverbed, in particular, due to the current control of the water table elevation by the drainage network that already maintains the water table elevation at a lower level than the natural one.
- The area downstream the commune of Sion and riparian to the Rhône River should undergo a relatively small decrease of the water table if the current hydraulic properties of the Rhône riverbed bed are not altered (less than 0.5 m). However, for an increase in the riverbed conductance, increases of the water table elevation could occur (until 1 m).

These conclusions are dependent on the validity of the model to represent the complex geometries, hydraulic and hydrogeological properties and the dynamics of the study zone. Therefore, the results of the analysis could be put into question if model structural errors affecting the predictions of interest are identified. Moreover, the predictions and the related uncertainties are based on hydraulic forecasts of the Rhône River stage as well as the potential evolution of the Rhône riverbed. Consequently, errors in these parameters and predictions, as well as scenarios not taken into account and other unknown unknowns, could be the reason for which the water table variations that will actually occur may not be in accordance with the forecasts presented in this document.

4.7. References

Anderson, M. P., W. W. Woessner, and R. J. Hunt (2015), *Applied Groundwater Modeling*, Second ed., 563 pp., Elsevier.

Besson, O., R. Marchant, A. Pugin, and J.-D. Rouiller (1993), Campagne de sismique-réflexion dans la vallée du Rhône entre Sion et St-Maurice: Perspectives d'exploitation géothermique des dépôts torrentiels sous-glaciaires, *Bulletin du Centre d'Hydrogéologie, Université de Neuchâtel*, *12*, 39-58.

Brunner, P., and C. T. Simmons (2012), HydroGeoSphere: A Fully Integrated, Physically Based Hydrological Model, *Ground Water*, *50*(2), 170-176.

Calver, A. (2001), Riverbed permeabilities: Information from pooled data, *Ground Water*, *39*(4), 546-553.

Canton du Valais (2010), BD-for, Borehole database.

Darcy, H. (1856), Les Fontaines Publiques de la ville Dijon, *Dalmont, Paris*.

Devlin, J. F., and P. C. Schillig (2017), HydrogeoEstimatorXL: an Excel-based tool for estimating hydraulic gradient magnitude and direction, *Hydrogeol J*, *25*(3), 867-875.

Diersch, H.-J. G. (2014), *FEFLOW Finite Element Modeling of Flow, Mass and Heat Transport in Porous and Fractured Media*, Springer.

Doherty, J. (2003), Ground water model calibration using pilot points and regularization, *Ground Water*, *41*(2), 170-177.

Doherty, J. (2015), *Calibration and Uncertainty Analysis for Complex Environmental Models*, first ed., 227 pp., Watermark Numerical Computing.

Doherty, J., and R. J. Hunt (2010), *Approaches to Highly Parameterized Inversion: A Guide to Using PEST for Groundwater-Model Calibration*, 70 pp.

Dupuit, J. (1863), Étude théoriques et pratiques sur le mouvement des eaux dans les canaux découverts et à travers les terrains prerméable, *Dunod, Paris*.

Fetter, C. W. (2001), Applied Hydrogeology, *Person Education International*, 598 p.

Forchheimer, P. (1886), Ueber die Ergiebigkeit von Brunnen-Anlagen und Sickerschlitzen., *Zeitschrift des Architekten und Ingenieur Vereins zu Hannover*, *32*, 539-563.

Forchheimer, P. (1898), Grundwasserspiegel bei brunnenanlagen, *Zeitschrift des österreichischen Ingenieur und Architekten Vereins*, *44*, 629-635.

Franke, O. K., T. E. Reilly, and G. D. Bennett (1987), Definition of Boundary and Initial Conditions in the Analysis of Saturated Ground-Water Flow Systems - An Introduction, *U.S. Geological Survey*, *03-B5*, 15.

Geometres Center SA (2013), Gravières des Iles, plan de situation, estimation du solde à excaver., *Canton du Valais, Sion*.

GéoVal Ingénieurs-Géologues SA (1986), Rapport après 3 ans d'observation - Palier 1-7. Sion: Hydro-Rhône.

Gianni, G., J. Richon, P. Perrochet, A. Vogel, and P. Brunner (2016), Rapid identification of transience in streambed conductance by inversion of floodwave responses, *Water Resour Res*, *52*(4), 2647-2658.

Glenz, D. (2013), Inverse Modeling of Groundwater Flow in Rhone Alluvial Aquifer, Impact of the Third Rhone Correction, 172 p.

Gomez-Hernandez, J. J., A. Sahuquillo, and J. E. Capilla (1997), Stochastic simulation of transmissivity fields conditional to both transmissivity and piezometric data - I. Theory, *J Hydrol*, *203*(1-4), 162-174.

Grindat, S., G. Gianni, and P. Brunner (2014), Modelling of Gravel Pits Lakes in the region of Sion (Valais, Switzerland), 77 p.

Haitjema, H. (1995), *Analytic Element Modeling of Groundwater Flow*, Academic Press, Inc., San Diego, CA.

Haitjema, H. (2006), The role of hand calculations in ground water flow modeling, *Ground Water*, *44*(6), 786-791.

Heath, R. C. (1983), Basic Ground-water Hydrology, *U.S. Geological Survey Water Supply Paper 2220*, 84.

Hill, M. C., and C. R. Tiedeman (2007), *Effective groundwater model calibration: with analysis of data, sensitivities, predictions, and uncertainty*, xviii, 455 p. pp., Wiley-Interscience, Hoboken, N.J.

Kasahara, T., and A. R. Hill (2008), Modeling the effects of lowland stream restoration projects on stream-subsurface water exchange, *Ecol Eng*, *32*(4), 310-319.

Kuchovsky, T., A. Ricka, and J. Cervenkova (2008), Impact of Gravel Pits on Ground water: Case Study of Gravel Pits near the Mohelnice City, Czech Republic, *VŠB - Technical University of Ostrava*.

Landry, O. (1986), Rapport après 3 ans d'observation (1983-1985) - Vernayaz: Étude hydrogéologique, *Hydro-Rhône SA*.

Morris, D. A., and A. I. Johnson (1967), Summary of Hydrologic and Physical Properties of Rock and Soil Materials as Analyzed by the Hydrologic Laboratory of the U.S, *Geological Survey 1948e1960. U.S. Geological Survey Water Supply Paper 1839-D*, 42.

Niederer et Pozzi (2010), Modèle HEC-RAS du Rhône à l'amont du Léman.

Ramarao, B. S., A. M. Lavenue, G. Demarsily, and M. G. Marietta (1995), Pilot Point Methodology for Automated Calibration of an Ensemble of Conditionally Simulated Transmissivity Fields .1. Theory and Computational Experiments, *Water Resour Res*, *31*(3), 475-493.

Richon, J., A. Vogel, C. Badertscher, and A. Parriaux (2010), Modélisation hydrogéologique d'un renforcement de digue : cas du Rhône à Sion, *Master en Sciences et Ingénierie de l'Environnement, EPFL*.

Rosenberry, D. O., J. W. LaBaugh, and Geological Survey (U.S.) (2008), *Field techniques for estimating water fluxes between surface water and ground water*, iv, 128 p. pp., U.S. Geological Survey, Reston, Va.

Rovina + Partner AG (2009), Beurteilung der GW-Beeinträchtigungen auf Stufe Generelles Projekt, 48 p.

Sartori, M., M. Burri, J.-L. Epard, H. Masson, and J.-B. Pasquier (2011), Geological Map 1:25'000 - Sion (LK 1306), *Swiss Geological Atlas, GeoCover*.

Swisstopo (2012), SwissALTI3D - Modèle numérique d'altitude haute précision de la Suisse, *Office fédéral de topographie*.

US Army Corps of Engineers (2010), HEC-RAS River Analysis System, *Hydrologic Engineering Center*.

Vogel, A. (2003), Relation entre le lac de la gravière des Épines et la nappe phréatique de la plaine alluviale du Rhône (Valais, Suisse), *Centre d'hydrogéologie de Neuchâtel*.

Zarn, B. (1997), Einfluss der Flussbettbreite auf die Wechselwirkung zwischen Abfluss, Morphologie und Geschiebetransportkapazität, *Mitteilung Nr. 154, Versuchsanstalt für Wasserbau, Hydrologie und Glaziologie, ETH-Zürich*, 240

Chapter 5

5. Conclusions and recommendations

A comprehensive understanding of surface water-groundwater dynamics must support sustainable management of the water resources. Current hydrogeological modeling codes generally have the capacity to simulate such processes, the most recent ones can simulate both surface, and groundwater flows [*Brunner and Simmons*, 2012]. They are therefore essential tools to analyze and improve our understanding on the interaction between surface water and groundwater. Furthermore, synthesizing site conceptualization and field measurements within the framework of mathematical models is essential to consolidate the understanding of the interaction between rivers and their alluvial aquifers and thus to improve their management. As stated by *Anderson et al.* [2015] *"a model is the most defensible description of a groundwater system for informed and quantitative analyses as well as forecasts about the consequences of proposed actions"*. From this perspective, the motivation for modeling has grown with the increasing number of questions related to the consequences of previous, ongoing and future management strategies on local and regional water resources as well as future climatic conditions. However, an environmental forecast is often subject to some uncertainty and this uncertainty must be quantified in order to support decisions. To this end and through proper utilization of datasets, field investigations, adequate mathematical models, such as process-based codes, and uncertainty analysis theory, the predictive uncertainty can be bounded. The present research showed an analysis of the uncertainty in forecast resulting from unknowns and assumptions related to the imperfect knowledge of present and future underground structures and hydraulic properties, and its reduction using steady-state and transient head targets.

- The uncertainty related to imperfect knowledge of the current model parameters and stresses is, prior to the calibration process, delimited by expert knowledge (i.e. ranges of values commonly accepted for the study site) and, posterior to the calibration process, minimized by the information content of the calibration targets. The reduction of the uncertainty of the prediction of management interest will depend on the sensitivity of the predictions to the estimated parameters and the post-calibration uncertainty of the parameters. Using solely head targets, the results showed that transient simulations further constrain the uncertainty of water table elevation prediction.
- The uncertainty related to future conditions, such as the hydraulic conductance and morphology of the riverbed, has been tackled by scenario modeling that tends to frame the potential future properties of the hydrogeological system having an influence on the forecasting of management interest and calculate its maximal and minimal values. The results of the present study showed that uncertainty on the future clogging state of the Rhône riverbed dominates the uncertainty in the prediction of the water table elevation.
- The uncertainty related to so-called "unknown unknowns", i.e. the system characteristics that we do not know we do not know, is often the source of model defects, for which the consequences on the sensitive predictions of interest is not evaluated. In the case of alluvial aquifers, the impact on the quantification of the predictive uncertainty of the water table elevation of neglecting aquifer horizontal anisotropy has been investigated. The results support specific calibration approaches and characteristics, such as interpolation methods based on an anisotropic variogram and variations of the angle of anisotropy controlled by the river flowing direction in order to better simulate the geometry of alluvial hydrofacies. More generally, hydrogeological models should comprise all parameters and an appropriate discretization of these parameters, as well as including the relevant processes, that may have an influence on the value of the forecast deriving from the question of management interest.

In summary, the main goal of this Ph.D. thesis has been to search and analyze different approaches that will allow a better identification of key parameters and processes related to river-aquifer interaction. In particular, the investigations focused on:

- The temporal evolution of the hydraulic properties of the riverbed.
- The influence of alternate bars morphology in the riverbed onto the river-aquifer interaction and water table elevation at a local and regional scale.
- The influence of model defect, related to wrong assumption about aquifer horizontal anisotropy, onto predictive uncertainty.
- The identifiability of aquifer and riverbed hydraulic parameters using only head targets and the reduction of the predictive uncertainty by using transient head targets instead or together with steady-state head targets.
- The transient calibration of a three-dimensional heterogeneous anisotropic alluvial aquifer of the Rhône River in the area of Sion based on averaged and transient head targets. The estimation of the values and uncertainties of the water table elevations after the 3rd Rhône River Correction project achievements.

5.1. About riverbed physical properties transience identification

Streambed conductance controls the interaction between surface and groundwater. However, the streambed conductance is often subject to transience related to erosion and sedimentation processes. Directly measuring hydraulic properties in a river yields only point values, is time-consuming and therefore not suited to detect transience of physical properties. A method to continuously monitor the transience in streambed conductance was presented in *Chapter 2*. Input data are time series of stream stage and near stream hydraulic heads. The method is based on the inversion of floodwave responses. To apply the method, time series of river stage and water table data are required, as well as a transience in the river. The estimation can be done on very large or fast flowing rivers where direct measurements of the streambed hydraulic properties are virtually impossible.

The method has been successfully employed in a field case, and a clear transience in the streambed conductance was identified and related to seasonal and exceptional climatic events. Therefore, the identification of this transience within a period of interest can allow a better calibration of a model by allowing the calibration process to estimate different values of the riverbed hydraulic properties at different times. Subsequently, this transience should be considered in predictive modeling approaches when it can influence the predictions of management interest. Finally, the method could be employed for an adaptive management approach and for quantification of the impact of the 3rd Rhône River Correction on the broad scale hydraulic properties of the Rhône riverbed.

5.2. About calibration and forecasting in horizontally anisotropic alluvial aquifer

Physical properties of alluvial environments are typically featuring a high degree of anisotropy and are characterized by dynamic interactions between the surface and the subsurface. Hydrogeological models are often calibrated using isotropic hydraulic conductivity fields and steady-state conditions. An analysis of the information content provided by averaged, steady-state hydraulic data, compared to transient data with respect to the determination of aquifer hydraulic properties was presented in *Chapter 3*. It was showed that assuming isotropy or fixed anisotropy may generate biases in the prediction of water table elevation and underestimate its uncertainty. Also, the information contained in average or point in time hydraulic heads is insufficient to inform the values of aquifer and streambed hydraulic conductivity as well as the anisotropy, essentially due to correlations between these parameters arising during the

calibration process. Therefore, we further explored the information content of transient data to achieve a better estimation of the hydraulic parameters in order to reduce bias in the predictive uncertainty of the water table elevation. The results of the synthetic analysis supported the calibration of a dynamic and anisotropic alluvial aquifer system in Switzerland (the Rhône River). The results of the synthetic and real-world modeling and calibration exercises provided insight on future data acquisition, modeling and calibration strategies for these environments. It was demonstrated that the estimability of the riverbed and aquifer parameters can be increased when aquifer responses to river stage variations are used as calibration targets during the calibration process.
Essentially, the analysis demonstrated the potential underestimation of predictive uncertainty and suggest that where one or more parameters cannot be estimated uniquely, the problem of their non-uniqueness should not be addressed by fixing some and estimating others.

5.3. About scenario modeling and linear uncertainty analysis of the impact of the 3rd Rhône River Correction

The water table of the Rhône River alluvial aquifer is essentially controlled by the interaction between the groundwater and the surface water. However, the fluctuations of the water table imposed by the Rhône River stage variations is also constrained by the important drainage network crisscrossing the floodplain.
Through the calibration of a three-dimensional transient model of the Rhône River alluvial aquifer system, an estimation of the hydraulic properties of the riverbed and the aquifer have been pursued. Based on the information content of steady-state and transient heads, the estimation of predictive uncertainty standard deviations provided values ranging from 0 and 25 cm. This uncertainty related to the insensitivity and non-uniqueness of certain parameters in the calibration process is largely dominated by the predictive uncertainty arising from the uncertainty in the future hydraulic properties of the Rhône riverbed which range from -0.8 to 1.6 m (positive values corresponding to a decrease of the water table elevation). Therefore, the main source of uncertainty influencing the state of the post 3rd Rhône River Correction water table is the future hydraulic properties of the Rhône riverbed.

5.4. Recommendations and perspectives

The outcomes of this study provide methods and approaches to identify and estimate the temporal variations of the hydraulic properties of the riverbed (*Chapter 2*) and the characteristics of the aquifer hydraulic properties (*Chapter 3*). The research focused mainly on the large-scale influence of these properties, according to the first purpose of the work that was to determine the influence of the 3rd Rhône River Correction on the water table elevation distribution (*Chapter 4*). The following recommendations concern modeling approaches and the relative necessity to include the different spatial and temporal characteristics in the numerical simulations and uncertainty analysis of the alluvial river-aquifer system of the Rhône Valley.

5.4.1. Two-dimensional vs. Three-dimensional models

The advantage of a two-dimensional approach compared to three-dimensional models is the gain in time and cost of developing the numerical model, calibrating it and performing the prediction and uncertainty analysis. However, natural system, such as the Rhône alluvial valley, are three-dimensional, and therefore, three-dimensional modeling approach may appear to be more appropriate. Nevertheless, given that the Rhône aquifer is much longer (dozens of kilometers) and larger (1 to 2 kilometers) than deep (around 40 m in the area of Sion), the two-dimensional Dupuis-Forchheimer theory (valid for both confined and unconfined aquifer) is

applicable [*Anderson et al.*, 2015]. Furthermore, although three-dimensional flow is likely to occur at the nearby of partially penetrating hydraulic features, such as rivers and drains, it is worth noting that, although vertical head gradient are neglected for two-dimensional areal models, the curvature of the water table is to a certain extent well reproduced [*Kirkham*, 1967; *Polubarinova-Kochina*, 1962]. Additionally, the applicability of the two-dimensional approach is also supported by the fact that the prediction of interest is the water table distribution and not three-dimensional flows of the system. Also, the present work showed that no significant improvement of the calibration of the model, in terms of discrepancies between the observed and simulated values, relatively to the assume measurement error, is achieved by the three-dimensional model compared to the two-dimensional model (*Chapter 4*).
In summary, the two-dimensional modeling approach is applicable in the case of the Rhône alluvial system and for the prediction of interest, namely the water table elevation distribution.

5.4.2. Steady-state vs. Transient simulations

Two kinds of transience in the Rhône alluvial system have been defined: The transience of the Rhône River stage and the surrounding water table; and the transience in the hydraulic properties of the Rhône riverbed. Both are related to climatic events and human activities.

5.4.2.1. Transience of the Rhône River stage and the surrounding water table

The transience of the Rhône River and its surrounding aquifer has been considered in the calibration of the three-dimensional model (*Chapter 4*). It has been observed that the identifiability of certain parameters, especially of the Rhône riverbed hydraulic conductivity has been increased by the information content provided by transient targets. Nevertheless, the transient calibration results, in terms of discrepancies between the observed and simulated values, relatively to the assume measurement error, did not show significant improvement compared to the steady-state model. Furthermore, the prediction of interest being the future average (pseudo steady-state) water table elevation, the transient calibration did not provide more information, regarding these particular predictions, than the steady-state simulations.

5.4.2.2. Transience of the hydraulic properties of the Rhône riverbed

The transience in the hydraulic properties of the Rhône riverbed was identified and estimated (*Chapter 2*) [*Gianni et al.*, 2016]. It was shown that its conductance value varies over the time, depending on climatic events and human activities. Furthermore, the scenario modeling approach (*Chapter 4*) showed that variations in its hydraulic properties may lead to significant variations of the water table elevation, in the absence of drainage control measures. In order to identify such potential variations of the water table, it may be important to take into account the transience in the hydraulic properties of the Rhône riverbed. Finally, if a transient calibration is to be done, the identification of the transience of the riverbed (*Chapter 1*) within the period of interest can allow a better calibration of a model by allowing the calibration process to estimate different values of the riverbed hydraulic properties at different times.

5.4.3. Isotropic vs. Horizontally anisotropic aquifer

The influence of the horizontal anisotropy of the aquifer hydraulic conductivity on the uncertainty of the prediction has been analyzed in *Chapter 3*. Generic modeling showed that the assumption of a wrong anisotropy may lead to an error in the estimation of the hydraulic parameters and an underestimation of the predictive uncertainty. Nevertheless, the estimation of this uncertainty for a model of the study zone showed that this uncertainty is negligible in that case. Therefore, the consideration of a pervasive horizontal anisotropy of the aquifer hydraulic conductivity in the case of the Rhône alluvial aquifer appears to not be essential for the predictions of interest.

5.4.4. Flat bottom vs. Alternate bars riverbed

On a regional scale, the comparison of the simulations of the interaction between the Rhône River and its alluvial aquifer for alternate bars riverbeds and flat bottom riverbeds under real flow conditions did not show significant variations (centimeters scale) of the water table elevation. Therefore, the approximation of the Rhône River flow over a flat bottom riverbed under real flow conditions appears to be appropriate to estimate the elevation of the water table in hydrogeological models.

On a local scale, i.e. close to the Rhône River, the succession of riffles and pools encountered in alternate bars riverbeds will tend to generate variations, in terms of magnitude and direction, of the hydraulic gradient between the river stage and the surrounding water table. Therefore, local simulations should consider this dynamics.

5.4.5. Modeling perspectives

Finally, given that the most important uncertainties are related to the variations of the riverbed hydraulic properties, which may occur following modifications of the Rhône River dynamics and riverbed morphology, future research could be dedicated to the development of modeling codes coupling riverbed sedimentology, hydrology and hydrogeology [*Partington et al.*, 2017] in order to better constrain hydrogeological model predictions.

5.5. References

Anderson, M. P., W. W. Woessner, and R. J. Hunt (2015), *Applied Groundwater Modeling*, Second ed., 563 pp., Elsevier.

Gianni, G., J. Richon, P. Perrochet, A. Vogel, and P. Brunner (2016), Rapid identification of transience in streambed conductance by inversion of floodwave responses, *Water Resour Res*, *52*(4), 2647-2658.

Brunner, P., and C. T. Simmons (2012), HydroGeoSphere: A Fully Integrated, Physically Based Hydrological Model, *Ground Water*, *50*(2), 170-176.

Kirkham, D. (1967), Explanation of paradoxes in Dupuit-Forchheimer seepage theory, *Water Resour Res*, *3*(2), 609-622.

Partington, D., R. Therrien, C. T. Simmons, and P. Brunner (2017), Blueprint for a coupled model of sedimentology, hydrology, and hydrogeology in streambeds, *Rev Geophys*.

Polubarinova-Kochina, P.Y. (1962), Theory of Groundwater Movement, Princeton University Press, Princeton, NJ 613 p.